BMI1-BMP Connection in Medulloblastoma Pathogenesis

Merve, Ashirwad J.

For additional information about this publication click this link.
http://qmro.qmul.ac.uk/jspui/handle/123456789/8304

BMI1-BMP Connection in Medulloblastoma Pathogenesis

Thesis submitted for the degree of Doctor of Philosophy

Ashirwad J. Merve

Primary Supervisor: Prof. Silvia Marino,
Centre for Neurosciences and Trauma, Blizard Institute;

Second Supervisor: Prof. Nick Lemoine,
Centre for Experimental Cancer Medicine, Barts Cancer Institute

Queen Mary University of London

2014

ABSTRACT

Medulloblastoma (MB) is the commonest intracranial childhood malignancy and despite recent advances, current therapeutic approaches are still associated with high morbidity and mortality. A novel molecular classification has recently been proposed for these tumours – WNT Group (best prognosis), SHH Group (intermediate prognosis), Group 3 (worst prognosis) and Group 4 (intermediate prognosis). BMI1, a transcriptional repressor of the Polycomb group genes, is overexpressed in MB, most significantly in those of Group 4 MBs. Bone Morphogenetic Proteins (BMPs) are morphogens belonging to TGF-β superfamily of growth factors, and are known to inhibit MB cell proliferation and induce apoptosis in vitro, and to inhibit tumour growth in vivo. Our team have recently demonstrated that Bmi1 regulates cell adhesion properties during cerebellar development through repression of the BMP pathway. The aim of this project is to assess whether BMI1 overexpression may contribute to MB pathogenesis through repression of the BMP pathway.

Here we demonstrate that BMI1 knock down derepresses BMP pathway, and using a novel xenograft model of human MB of Group 4, we show that BMI1 controls tumour volume and intraparenchymal invasion. In in vitro assays on MB cell lines we show that cell adhesion and motility is controlled by BMI1 in a BMP dependent manner and that deregulation of extracellular matrix proteins are key mediators of this effect. Furthermore, we demonstrate that BMP treatment to BMI1 overexpressing MB cells reduces cell proliferation and invasion, suggesting BMI1 as a possible biomarker for those tumours that could benefit from treatment with BMP agonist small molecules.

ACKNOWLEDGEMENTS

FINANCIAL SUPPORT

DECLARATION

The experiments reported in this thesis are the results of my own work, except where it has been clearly stated.

A manuscript describing the results of this project is in press.

Merve A, Dubuc AM, Zhang X, Remke M, Baxter PA, Li X, Taylor MD and Marino S. Polycomb group gene BMI1 controls invasion of medulloblastoma cells through inhibition of BMP-regulated cell adhesion.
Accepted for publication in *Acta Neuropathologica Communication.*

The data from this project were presented in the following conferences, and the abstracts were published in the journals mentioned.

Oral/Platform presentation:

Merve A, Marino S. BMI1 controls medulloblastoma invasion through inhibition of BMP-mediated cell adhesion
Conference: 114th Meeting of the British Neuropathological Society (BNS).
Held at: Institute of Child Health, London, 13-15 March 2013.
Abstract published in: *Neuropathology and Applied Neurobiology*. March 2013. Vol. 39 , SI 1, 21-21

Merve A, Zhang X, Marino S. BMI1 gene silencing influences cell adhesion and invasive properties of medulloblastoma cells via BMP pathway.
Conference: Conference of the British-Neuro-Oncology-Society (BNOS).
Held at: Homerton College, Cambridge, 29 June – 01 July, 2011
Abstract published in: *Neuro-Oncology*. 2011. Vol 13, Suppl 2, 8-8.
(Best oral-poster prize was awarded for this presentation)

Poster presentation:

Merve A, Zhang X, Marino S. Understanding the role of BMI1 gene in medulloblastoma pathogenesis using mouse models.
Conference: Mouse Models of Disease - linking in vivo observations to pathology endpoints.
Held at: Wellcome Trust Genome Campus, Hinxton, Cambridge, 1–3 February 2012.
(Second prize was awarded for this poster presentation)

Table of Contents

LIST OF ABBREVIATIONS

ABC	Avidin Biotin Complex
ALK	Anaplastic lymphoma receptor tyrosine kinase
APC	Adenomatous Polyposis Coli
ARF	Alternate Reading Frame
AT/RT	Rhabdoid/Atypical Teratoid
ATCC	American Type Culture Collection
Atoh1	Atonal Homologue 1 (gene)
Axl	Axl receptor tyrosine kinase
Bcl-2	B-cell leukemia/lymphoma 2
BDNF	Brain Derived Neurotrophic Factor
bHLH	Basic Helix Loop Helix
BMI1 or Bmi1	B Lymphoma Moloney Murine Leukemia Virus Integration site 1
BMI1KD	BMI1 knock down
BMP	Bone Morphogenetic Protein
BSA	Bovine Serum Albumin
BSE	Basement Membrane Extract
CBF1	CMP binding factor 1
CCG	Children's Cancer Group
CCND1	Cyclin D1
CCRG	Childhood Cancer Research Group
CCRK	Alias for Cyclin-dependent kinase 20
CD44	Alias for Indian Blood Group Antigen
cDNA	Complimentary Deoxyribonucleic acid
CGH	Comparative Genomics Hybridisation
cGy	Centigray (units)
ChIP	Chromatin Immunoprecipitation
c-Myc or MYC	v-myc avian myelocytomatosis viral oncogene homolog (gene)
CNS	Central Nervous System
COSSH	Control of substances hazardous to health
CRUK	Cancer Research UK
CSF	Cerebrospinal Fluid
CSL	Citrate Synthase like
csRT	Cranio-spinal Radiotherapy
CT	Computed Tomography
CTNNB1	Catenin (cadherin-associated protein), Beta 1
DAPI	4',6-Diamidino-2-Phenylindole
Dcc	Deleted in Colorectal Carcinoma
DDL	Deltalike (protein)
DKK1	Dickkopf1 (protein)
DMEM	Dulbecco's Modified Eagle medium
DMSO	Dimethyl sulfoxide

DNA	Deoxyribonucleic acid
dNTP	Deoxynucleotide
DPX	Distyrene, a plasticizer, and xylene Mounting medium
Dsh	Dishevelled (protein)
DTT	Dithiothreitol
E	Embryonic day
ECL	Enhanced Chemoluminescence
EDTA	Ethylenediaminetetraacetic acid
EFS	Event Free Survival
EGL	External Granular Layer
EMT	Epithelial Mesenchymal Transition
EMT	Epithelial Mesenchymal Transition
En	Engrailed (gene)
ERAS	ES cell expressed Ras
FAM	6-Carboxyfluorescein
FBN	Fibulin
FBS	Foetal Bovine Serum
FFPE	Formalin Fixed Paraffin Embedded
Fgf	Fibroblast Growth Factor
FILA	Filament A precursor
FISH	Fluorescent In situ Hybridisation
FITC	Fluorescein isothiocyanate
Frz	Frizzled (receptor)
FSTL-5	Follistatin like-5
GAB1	GRB2-associated binding protein 1
GABA	Gamma Amino Butyric Acid
Gbx	Gastrulation Brain Homeobox (gene)
GC	Golgi Candidate
Gdf	Growth Differentiation Factor
GEM	Genetically Engineered Mouse
GFP	Green Fluorescent Protein
Gli	Gliotactin
GNP	Granule Neuron Progenitor
GSK	Glycogen Synthase Kinase
H&E	Haemotoxylin and Eosin
HCL	Hydrochloric acid
HEK293	Human Embryonic Kidney 293
HIV	Human Immunodeficiency Virus
Hox	Homeobox (gene)
hpf	High Power Field
Hsp	Heat Shock Protein
i17q	Isochromosome 17q
ICD-O	International Classification of Disease for Oncology
ID	Inhibitor of DNA binding (gene)

IGF-1	Insulin Like Growth Factor 1
IgG	Immunoglobulin G
IGL	Internal Granular Layer
IHC	Immunohistochemistry
IMDM	Isocove's Modified Dulbecco's medium
INK4A or Ink4a	cyclin-dependent kinase inhibitor 2A
IO	Isthmic Organiser
IQ	Intelligence Quotient
JAG	Jagged (protein)
JC	John Cunningham (virus)
KCNA1	Potassium Voltage Gated Channel 1
Ki-67	Marker of Proliferation 67
LAMB1	Laminin Beta 1
LB	Luria Broth
LCA	Large Cell Anaplastic
LHX1	LIM homeobox protein 1
LM	Leptomeningeal
Lmx	Lim homeobox (protein)
M&M	Materials and Methods
MAPK	Mitogen-activated protein kinase
Math 1	Alias for Atonal Homologue gene Atoh1
MBEN	Medulloblastoma with Extensive Nodularity
Mer	Merlin
MIB1	Mindbomb E3 Ubiquitin Protein Ligase 1
ML	Molecular Layer
MMP	Matrix Metalloproteinase
MOI	Multiplicity of Infection
MRI	Magnetic Resonance Imaging
mRNA	Messenger Ribonucleic acid
Msx2	Muscle Segment Homeobox (gene)
NCI	National Cancer Institute
NDS	Normal Donkey Serum
NeuN	Alias for RNA binding protein, fox-1 homolog
Ng	Noggin
Ngf	Nerve Growth Factor
NGS	Normal Goat Serum
N-Myc or MYCN	v-myc avian myelocytomatosis viral oncogene neuroblastoma
NOD-SCID	Non-obese diabetic Severe Combined Immunodeficiency
NRSF	Alias for RE1 silencing factor or REST
NST-1	Alias for heat shock protein 14
OCS	Organotypic Cerebellar Slice
OCT	Optimum Cutting Temperature
Otx	Orthodenticle (gene)
P	Postnatal day

p21	Alias for Cyclin-Dependent Kinase Inhibitor 1A or CDKN1A
p27	Alias for Cyclin-Dependent Kinase Inhibitor 1B or CDKN1B
Pax	Paxillin (gene)
PcG	Polycomb Gene
PCR	Polymerase Chain Reaction
PDGFRA	Platelet Derived Growth Factor Receptor Alpha
Petf	pancreas specific transcription factor
PFA	Paraformaldehyde
pGIPZ	Empty Lentiviral Vector
PL	Purkinje Layer
PLL	Polylysine
PNET	Primitive Neuroectodermal Tumour
PRC	Polycomb Repressive Complex
PS	Phosphatidylserine
Ptch	Patched (receptor)
PTEN	Phosphatase and Tensin homologue
RAS	Resistance to Audiogenic Seizures (gene)
Rb	Retinoblastoma (gene)
RIPA	Radio-immunoprecipitation Assay
RL	Rhombic lip
RNA	Ribonucleic acid
Ror	RAR-related orphan receptor
RT	Room Temperature
RU49	Zscan 21, a zinc finger protein
Scr	Scrambled
SD	Standard Deviation
SEER	Surveillance, Epidemiology and End Result
SFRP1	Secreted Frizzled-Related Protein 1
SHH or Shh	Sonic Hedgehog (gene/protein/pathway)
shRNA	Small hairpin RNA
siRNA	Short interfering RNA
SMAD	Homologue of Mother Against Decapentaplegic
SMC3	Structural maintenance of chromosomes 3
Sufu	Suppressor of Fused Homolog (gene)
TAE	Tris Acetate EDTA buffer
Tag 1	Tubulin Associated Glycoprotein 1
TAMRA	6-Carboxytetramethylrhodamine
TBST	Tris Buffered Saline with Tween
TGF-β	Transforming Growth Factor - beta
THBS	Thrombospondin
TMA	Tissue Micro Array
TP53	Tumour Protein 53
Tyro3	TYRO3 protein tyrosine kinase 3
VSVG	Vesicular Stomatitis Virus

WHO	World Health Organisation
WM	White Matter
WNT or Wnt	Wingless
YAP	Yes-associated protein
Zic	Zinc Finger Protein of the Cerebellum

LIST OF FIGURES

Fig. 7.4 Correlation analysis of pSMAD2 expression and MB subgroups in TMA II241

LIST OF TABLES

CHAPTER 1 Introduction

1.1 Development of the cerebellum

1.1.1 Overview of the normal cerebellum:

Cerebellum (Latin: 'little brain'), contains more than half of the total neurons of the brain, and plays an important role in our daily living (Wang and Zoghbi 2001). It primarily controls motor activity, regulating movements, co-ordination, muscle tone and balance; and integrates sensory and motor data from brain stem, spinal cord and cerebral cortex. Grossly, the cerebellum is divided along the medial-lateral axis into vermis (located along the midsagittal plane), intermediate zones (directly lateral to vermis), and the two lateral hemispheres (located lateral to intermediate zones) [Fig 1.1 A]. The two fissures namely posterolateral fissure and primary fissure, divide the cerebellar cortex along the anterior-posterior axis into flocculonodular lobe, posterior lobe and anterior lobe respectively (Fig 1.1 A). These lobes are further divided along the anterior-posterior axis into ten lobules at the vermis and eight lobules at the heimspheres (Fig 1.1 B). All the above divisions of the cerebellum bear functional relevance. Histologically, the mature cerebellar cortex has three layers – 1) the Molecular Layer (ML), containing Stellate and Basket neurons, 2) the Purkinje Layer (PL) containing Purkinje cells and Bergman glia (a type of radial glial cells), and 3) the Internal Granular Layer (IGL), containing granule neurons, Golgi cells and glial cells (Fig 1.1 C). The Purkinje cells, Golgi cells, Stellate cells and Basket cells are inhibitory neurons (GABAergic, releasing γ-aminobutyric acid) and the granule neurons are excitatory (glutamatergic, releasing glutamate). While Golgi cells provide inhibitory feedback to granule neurons, Stellate and Basket cells modulate

Purkinje cells which provide the primary output from the cerebellar cortex to the deep

cerebellar nuclei. The axons of the granule cells are projected to the ML where they

bifurcate in opposite directions to form Parallel fibres, which make excitatory

synapses with Purkinje cells (Fig 1.1 C). In addition to the above cells, the cerebellar

cortex contains Mossy fibres and Climbing fibres (Fig 1.1 C). The former originate

from the spinocerebellar, pontocerebellar and vestibulocerebellar pathways and

make excitatory synapses onto the granule cells (and the cerebellar nuclei). The

latter originate in the inferior olive and make excitatory synapses onto the Purkinje

cells (and the cerebellar nuclei).
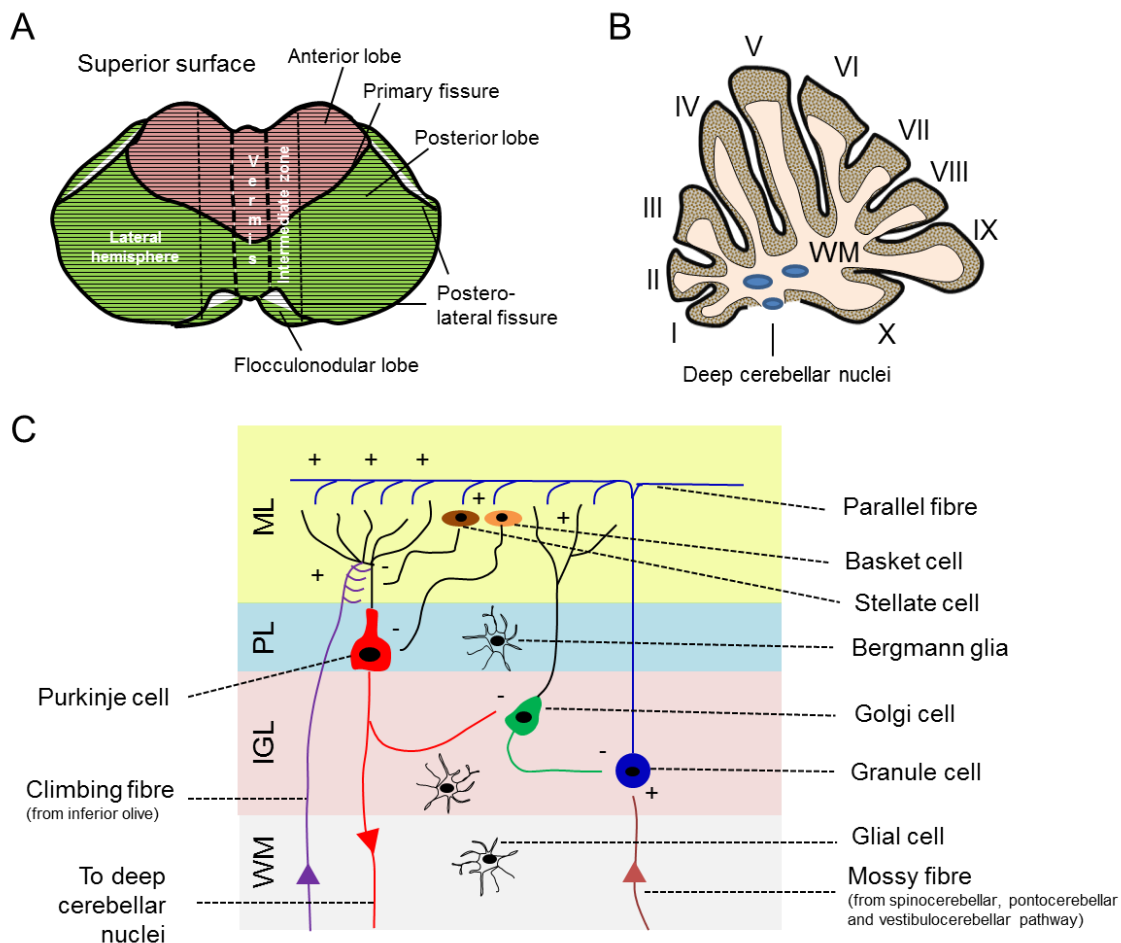
Fig. 1.1 Morphology of normal cerebellum.

(A) Gross anatomy of the cerebellum. **(B)** Diagrammatic representation of sagittal section at the vermis, showing division of cerebellar cortex into 10 lobules, I – X (there would be 8 lobules in the lateral hemispheres). Approximate locations of the deep cerebellar nuclei are represented in the white matter (WM). **(C)** Diagram representing the cells of the cerebellar cortex. Outer molecular layer (ML)

containing interneurons Basket and Stellate cells, middle Purkinje cell layer (PL) with Purkinje cells which has extensive dendritic arborisations, and the inner granule cell layer (IGL), containing granule neurons which send their axons to the molecular layer. In addition, there are Mossy and Climbing fibres entering into the cortex, and their connections are shown in brown and purple respectively. The glial cells are present in the WM and in the PL. The glial cells in the PL are called Bergmann glia. The excitatory synapses are marked with +, and inhibitory with -.

The cerebellar white matter contains fibre tracts, along with astrocytes, oligodendrocytes and neurons of the deep cerebellar nuclei (Altman J 1997; Behesti and Marino 2009). The deep cerebellar nuclei are - the fastigial nucleus (most medially located), the interposed nuclei (situated lateral to the fastigial nucleus), the dentate nucleus (largest nucleus, located lateral to the interposed nuclei) and functionally connected vestibular nuclei (actually located in the medulla). Three fibre bundles carry the cerebellar inputs and outputs, connecting the cerebellum to other parts of the brain and spinal cord, namely - the inferior cerebellar peduncle, the middle cerebellar peduncle and the superior cerebellar peduncle.

Although historically the cerebellum has been known to mainly coordinate motor functions, its role in cognition, memory and language functions has been postulated based on neuropsychiatric manifestations in patients with cerebellar disorders (Timmann and Daum 2007). However despite several study models, no concrete circuitry evidence has been established so far, and the consensus is that the role of cerebellum in the above functions are inferential (Koziol, Budding et al. 2013).

1.1.2 Cerebellar development

The development of the cerebellum begins in humans from an early embryonic stage and extends until the first postnatal years. Due to this protracted period of development, the cerebellum is susceptible to a spectrum of complex developmental disorders including genetic/sporadic syndromes (hypoplasia of cerebellar vermis in

Dandy-Walker syndrome), non-genetic abnormalities (cerebellar hypoplasia secondary to congenital cytomegalovirus infection), metabolic abnormalities (cerebellar atrophy secondary to pyruvate dehydrogenase deficiency) and neoplasia (Ramaekers, Heimann et al. 1997). There is considerable evidence that the origin of medulloblastoma is intimately related to the development of the cerebellum (reviewed in (ten Donkelaar, Lammens et al. 2003; Marino 2005; Gilbertson and Ellison 2008). Therefore it is relevant to first discuss the normal cerebellar developmental process in order to understand the pathogenesis of medulloblastoma.

The mouse has been extensively used as a model of human CNS development because it has close anatomic, physiologic and genetic similarity to humans. Moreover the ease of genetic manipulation of gene expression which can be achieved in mouse models is also very appealing. Hence, mouse models to study the molecular mechanisms of cerebellar development and medulloblastoma pathogenesis have been extensively used due to the high degree of conservation of cerebellar anatomy and function between mouse and human (Chizhikov and Millen 2003; Kho, Zhao et al. 2004). A word of caution is however warranted because of the inherent limitations of any experimental models. In the following cerebellum development sections, the process of mouse development is mainly discussed, and where available, processes and time points in human development is mentioned.

1.1.2.1 Early embryogenesis

In vertebrates, the central nervous system (CNS) is derived from the neural plate (epithelial structure arising from the dorsal ectoderm of the gastrula) during embryogenesis. The neural plate subsequently closes to form the neural tube; and the brain develops from the rostral (head end) part of the neural tube. The neural

tube soon forms flexures giving rise to three primary brain vesicles – the prosencephalon (forebrain), the mesencephalon (midbrain) and the rhombencephalon (hind-brain). The prosencephalon acquires further lateral extensions to form the telencephalon which is connected at the midline with the diencephalon. The mesencephalon remains as a single structure. The rhombencephalon is separated from the mesencephalon by the cephalic flexure and the cervical flexure separates it from the spinal cord. The pontine flexure divides the rhombencephalon into the metencephalon and the myelencephalon at embryonic day 9 (E9) in mouse. In vertebrates the rhombencephalon is known to arise from seven segments of the neural tube called rhombomeres 1-7 (Garel, Fallet-Bianco et al. 2011).

The cerebellum develops from the roof of metencephalon (dorsal rhombomere 1), with contributions from the mesencephalon (Hatten and Heintz 1995). The cerebellar development occurs in several interconnected stages, controlled by multiple genetic events which can be categorized into four categories – 1) establishing cerebellar territory, 2) specification of cerebellar cell types, 3) proliferation, differentiation and migration of the cells and, 4) formation of the cerebellar circuitry.

1.1.2.2 Establishment of the cerebellar territory (cerebellar anlage):

The anterior-posterior boundaries of the developing cerebellum are determined by Fgf8 (fibroblast growth factor 8) and Wnt1 (wingless homologue 1) signals from the Isthmic Organizer (IO), which is located at the junction of mesencephalon and metencephalon (Sato, Joyner et al. 2004). In turn IO is formed as a result of expression of two main genes - *Otx2* (mouse homologue of Drosophilia gene *orthodenticle)* and *Gbx2* (mouse homologues of the Drosophilia gene and

unplugged) which are expressed at E8, in mesencephalon and in metencephalon respectively

Some of the other genes that are important for establishing IO include *En1* and *En2* (homeobox genes engrailed 1 & 2), *Pax2* and *Pax5* (paired box genes), *Hoxa2* (homeobox A2) and Lmx1b (Lim homeobox 1b). The mechanisms controlling the dorsal – ventral patterning of the developing cerebellum are not well established, but there is suggestion that it may be controlled by Bone morphogenetic proteins (BMPs), Sonic Hedgehog (Shh) and the expression of Lmx1a (Lim homeobox 1a) (Chizhikov and Millen 2003). The cerebellar anlage is formed between E10 and E11. Further to this, the cerebellum continues to develop for the rest of the embryonic period undergoing extensive morphological changes. Subsequently, from the alar plates two germinal centers are formed – 1) the Ventricular zone – a mouth-like structure at the roof (dorsal) of the 4th ventricle, adjacent to cerebellar anlage, and 2) the Rhombic lip – a specialised region of ventricular zone, adjacent to the roof of the 4th ventricle (Fig 1.3 A). In contrast to most other brain regions, the cells of the cerebellum originate from these two distinct germinal zones (Fig 1.3 B).

1.1.2.3 Morphogenesis of the cerebellum:

Under this subheading, the next two stages of cerebellar development, namely the specification of the cerebellar cell types, and the proliferation/differentiation/migration of the cells, will be discussed. By fate mapping it is known that the cerebellar cell types arise at different developmental stages and from different locations (Hatten and Heintz 1995) and their development will be discussed below.

1.1.2.3.1 Purkinje cells and interneurons originate from the ventricular neuroepithelium:

The cells of the deep cerebellar nuclei, Purkinje cells, and later Golgi cells, Stellate cell, Basket cells develop from multipotent precursor cells called the ventricular neuroepithelium (Hallonet and Le Douarin 1993) which express bHLH (basic helix loop helix) factor Ptf1a (pancreas specific transcription factor 1a). The ventricular neuroepithelium is located in the ventricular zone in the roof of the 4th ventricle as discussed above, which is also known as the primary germinal zone. Purkinje cells are specified at E13, when they exit the cell cycle and start to migrate along the radial glial cells towards the cerebellar primordium. From E14-E17 they migrate over the already formed deep cerebellar nuclei. In humans, the generation of the deep cerebellar nuclei and Purkinje cells are estimated to occur at around 5th – 6th week of gestation (ten Donkelaar, Lammens et al. 2003). These cells then arrest and await the inward migration of the granule neurons. This timely arrest of migration is driven by the reelin pathway (Hatten 1999). Purkinje cells rely on signalling from granule neuronal precursors for their migration, but their differentiation is thought to be independent of them. Towards late embryogenesis, the Climbing fibres from the inferior olive begin to connect to the Purkinje cells, which are thought to promote their development. At this stage, they express markers such as NST-1 (Hsp70-4, heat shock protein). Purkinje cells develop extensive arborisation towards their final maturation phase and start to establish synapses with granule neurons. Wnt3 is thought to influence this phase of development (Salinas, Fletcher et al. 1994). Earlier we learnt the role of Wnt1 signals from IO in the development of the cerebellar anlage. Furthemore, Wnt signaling is implicated in early CNS development (Salinas and Zou 2008) and in the regulation of growth and

differentiation of the developing cerebellum both in the embryonic and early postnatal stages (Schuller and Rowitch 2007). Mutations in the WNT pathway have a well-established role in human medulloblastoma development (discussed later in section 1.2.4). Therefore it is relevant to discuss **Wnt signalling pathway** briefly at this stage (other molecular pathways of relevance are discussed in the sections below).

In the absence of Wnt signalling, intracellular β-catenin is phosphorylated by casein kinase Iα (CK1α) and/or CKIε at Ser45. In turn this enables glycogen synthase kinase 3β (GSK3β) to phosphorylate serine/threonine kinase residues 41, 37 and 33, which triggers ubiquitylation and proteasomal degradation of β-catenin. Phosphorylation and eventual degradation of β-catenin takes place in a multiprotein complex containing the axin (the scaffold protein), adenomatous polyposis coli (APC, the tumour suppressor gene product) and GSK3β. Wnt signalling is activated by the binding of Wnt ligands (which are secreted glycoproteins) to the transmembrane receptor Frizzled (Frz). In the presence of Wnts, dishevelled (Dsh, the activity of which is modulated by the kinase PAR1) blocks β-catenin phosphorylation by inhibiting GSK3 (α- and β-isoforms). The exact mechanism of GSK3 inhibition by Wnts is unclear and has been the focus of intensive research (Metcalfe and Bienz 2011). Recently, a cell-biological model was proposed (Taelman, Dobrowolski et al. 2010): Wnt proteins induce the uptake of GSK3 into multivesicular bodies (MVBs), an event that sequesters the enzyme away from newly synthesised β-catenin substrate in the cytoplasm, thus blocking its phosphorylation. The unphosphorylated (stabilised) β-catenin enters the nucleus and associates with LEF/TCF transcription factors, which leads to the transcription of Wnt-target genes. Some of the Wnt-target genes are c-MYC, CCND1 (cyclin D1), and NRSF/REST (RE1-silencing transcription

factor), which are involved in the proliferation, inhibition of apoptosis, and differentiation of cells (Huelsken and Behrens 2002; Ille and Sommer 2005; Rossi, Caracciolo et al. 2008). An overview of the Wnt signalling pathway is represented in Fig. 1.2A.

In addition to the above, various growth factors are thought to influence the development of the Purkinje cells such as Ngf (nerve growth factor), acetylcholine, BDNF (brain-derived neurotrophic factor) and ciliary neurotrophic factor. Similarly, Rorα (RAR-related orphan receptor α) and Bcl2 (B-cell leukemia/lymphoma 2) genes are thought to play a role in this process (Wang and Zoghbi 2001).

1.1.2.3.2 Granule neurons originate from the rhombic lip:

In contrast to other cells of the cerebellum, which are derived from the ventricular zone, the granule neurons are derived from the rhombic lip, also known as second germinal zone. As mentioned before, the rhombic lip is the dorsolateral part of the alar plate formed at E9 – E10, between the 4th ventricle and the roof plate in the metencephalon, which forms the proliferative zone along the hindbrain (Wingate 2001). Granule neurone progenitor cells (GNPs) from the rostral (upper or head end) part of the rhombic lip cells start to migrate outwards at about E13. Three members of TGF-β family, namely Bmp6, Bmp7 and Gdf7 expressed in the roof plate are known to play an important role in GNP specification (Alder, Lee et al. 1999). These cells populate the cerebellar anlage, reaching the superficial part, which form the external granular (or germinal) layer [EGL] by the end of embryonic period, which is known as secondary germinal zone. In humans, the EGL persists from several post natal months up to 1 or 2 years of age (Lemire RJ 1975). *Math1 (atonal homologue 1*

or Atoh1), which is expressed in the mid to hind brain region at about E9 – E10, is considered essential for the genesis of cerebellar GNPs (Ben-Arie, Bellen et al. 1997) and its expression persists in the rhombic lip and its derivatives. At this stage the GNPs also express Nestin and other markers such as zinc finger proteins RU49/Zipro1, Zic1 and Zic 3.

The Notch1 activity is known to prevent the induction of Math1 by antagonising the BMP signalling pathway at the level of Msx2 expression, thereby balancing between neural induction and maintenance of neural progenitors in the embryonic development of the rhombic lip (Machold, Kittell et al. 2007). Furthermore, postnatally Notch 2 is shown to inhibit differentiation and maintain cerebellar granule cell precursor proliferation (Solecki, Liu et al. 2001). As **Notch signalling pathway** mutations are associated with medulloblastoma development (reviewed in (Hatten and Roussel 2011)), it is briefly discussed at this stage. Notch receptor acts as a membrane-tethered transcription factor, which is activated by Jagged (JAG) or Delta-like (DDL) family members, cleaving the extracellular domain and releasing intracellular domain of Notch, which translocates to the nucleus (Fig 1.2 B), where it interacts with CBF1 [or other CSL family members such as Su(H) or Lag-1] of transcriptional regulators, leading to activation of target genes namely, Myc, p21, and the HES-family members (Ehebauer, Hayward et al. 2006).
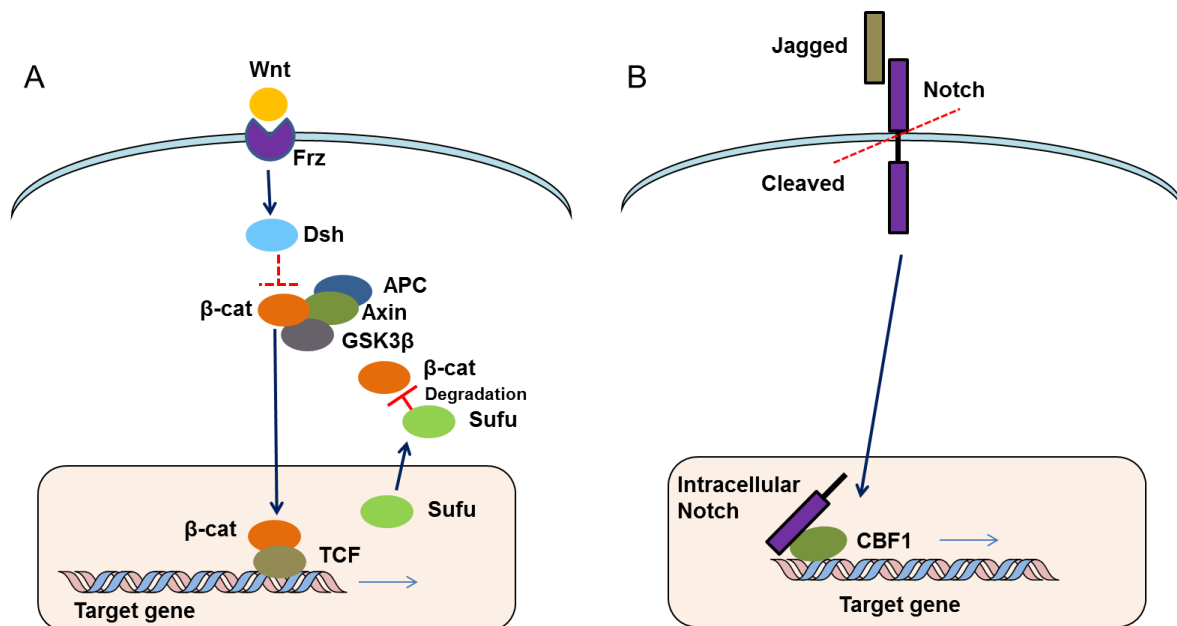
Fig. 1.2 Diagrammatic representation of Wnt and Notch signalling pathways.

(A) Wnt pathway. **(B)** Notch pathway.

Once the GNPs form the EGL, they continue to proliferate in the outer EGL, driven by RU49/Zipro1, Zic1 and Math1. Cell proliferation in the outer EGL at this stage also requires input from Purkinje cells through secretion of Shh (Wechsler-Reya and Scott 1999). As Shh pathway mutations are associated with medulloblastoma development (discussed later in section 1.2.4), due to its effects on GNP proliferation, this pathway is briefly discussed here.

The **Shh pathway** (Fig 1.6) is maintained in an 'off' state by Ptch (patched transmembrane protein) which inhibits smoothened protein (Smo). Upon ligand binding of Shh (secreted by Purkinje cells), Ptch-mediated repression is alleviated and a signal is transduced to the nucleus to promote the proliferation of granule cells via Gli (GLI-Kruppel) 1 and Gli 2, and possibly N-Myc mediated signalling cascade [Fig 1.6] (Marino 2005). The evidence that Shh pathway plays a role in GNP proliferation is strengthened by the association of Ptch (patched) mutation [leading to activation of Shh pathway] with Gorlin's or naevoid basal cell carcinoma syndrome

and medulloblastoma (Wechsler-Reya and Scott 2001). Expression of Gli1 and Gli 2 which mediate Shh pathway, is shown to be in turn modulated by Zic proteins, suggesting that Zic proteins control GNP proliferation by affecting Shh pathway (Mizugishi, Aruga et al. 2001). Furthermore, Bmi1 (a Polycomb gene) is shown to be expressed in EGL precursor cells (at E16.5 & P8 in mouse and 26th gestational week and post natal 8 months in humans) and it is thought to promote clonal expansion of GNPs (Leung, Lingbeek et al. 2004). The role of Bmi1 gene, which is thought to be a downstream target of Shh pathway, in cerebellar development and in medulloblastoma pathogenesis is discussed in detail later (section 1.3.2). In addition, GNP proliferation in the outer EGL is also dependent on genes involved in cell cycle such as Cyclin D2.

The GNPs then cease to proliferate and migrate from outer EGL into the inner EGL. This change from a proliferative to a postmitotic phase involves cell-cycle inhibitors such as p27/Kip1 (cyclin dependent kinase inhibitor 1b), which is expressed in the inner EGL (Miyazawa, Himi et al. 2000). In the inner EGL, GNPs lose their Math1 expression, and begin to express other bHLH transcription factors NeuroD1 (Miyata, Maeda et al. 1999) and NSCL1 (Duncan, Bordas et al. 1997). The cell number at this stage is controlled by trophic factors such as BDNF and IGF1 (insulin-like growth factor 1) which modulate apoptosis (Goldowitz and Hamre 1998).

Next, the GNPs differentiate (forming axons, the Parallel fibres) and migrate inwards along the Bergmann glia at around 16 – 25 weeks of postnatal age in humans. They migrate into their definitive site, the internal granular layer (IGL), under a single layer of Purkinje cells (Fig 1.3 C) separated by a transient layer, lamina dissecans. The cells at this stage mainly express Tag1 (tubulin-associated glycoprotein 1) and Tuj1

(class 3 β-tubulin), which are mature neuronal markers. They also express Dcc (deleted in colorectal carcinoma) and components of Dcc/netrin pathway, Unc5h2 and Unc5h3, which are involved in cell migration and axonal projection. Several other genes have been implicated in the migration and differentiation of GNPs such as *Pax6* (paired box homeotic gene 6) expressed in EGL, Girk2 (encoding inward-rectifying K$^+$ channel) and Grid2 (encoding δ2 glutamate receptor subunit). Several extracellular proteins that are known to be important at this stage are – astrotactin, thrombospondin, tenascin and neuregulin.

The final stages of GNP cells maturation to form the granule neurons take place in the IGL, at which point they express mature markers such as GC5 (golgin candidate 5) and GABA receptors (Raetzman and Siegel 1999). At this stage, the Mossy fibres (from the precerebellar nuclei) develop contact with the granule neurons, which is partly mediated by *Wnt7a* released by granule neurons (Hall, Lucas et al. 2000), and the granule neurons extend connections to the Golgi cells, which is mediated by a protein, called contactin (Stoeckli 2010).
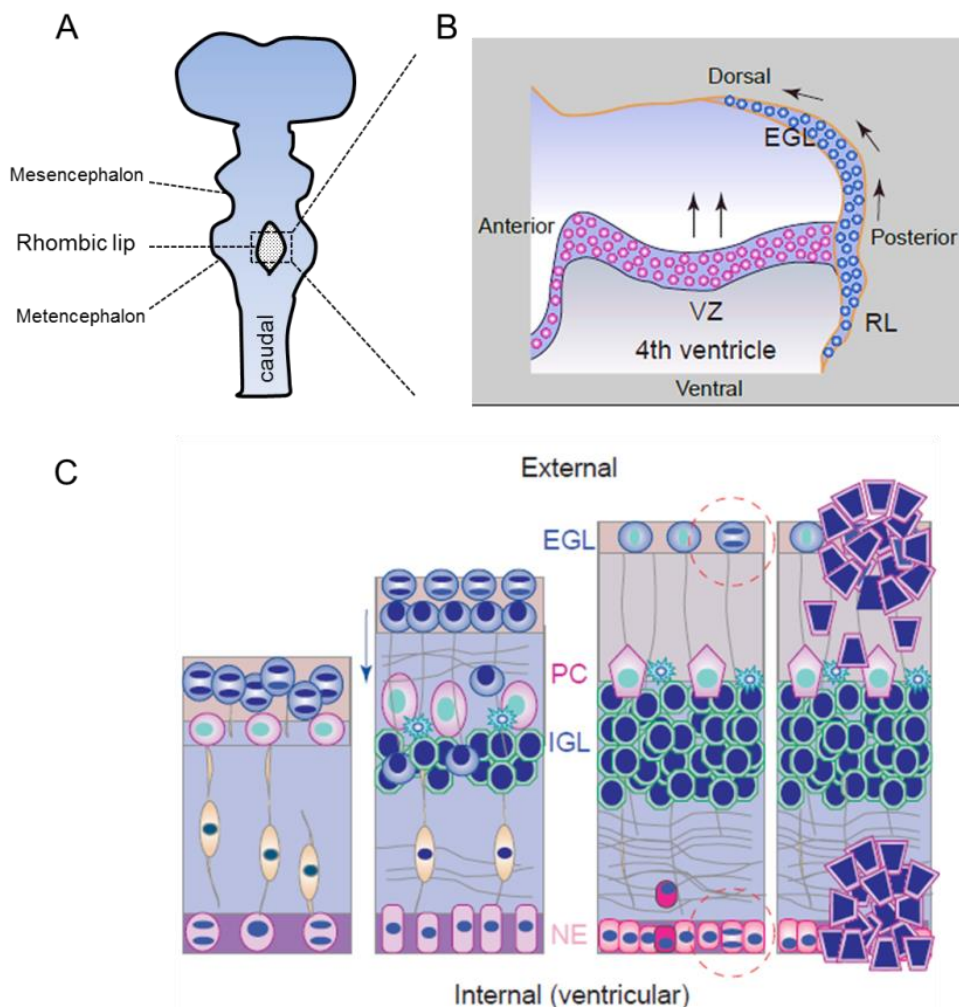
Fig. 1.3 Schematic representation of cerebellar development*

(A) & (B) Embryonal development of the cerebellum. (A) The cerebellar anlage is formed in the roof of the metencephalon with contribution from the mesencephalon, subsequently giving rise to two germinal centres – the ventricular zone or primary germinal zone and the rhombic lip adjacent to 4th ventricle. (B) Represents the boxed germinal centres from (A) and depicts migration of the precursor cells. The cells originating from neuroepithelium of the ventricular zone (VZ) migrate radially to give rise to Purkinje cells, Golgi cells, Basket cells and Stellate neurons. Granule neuron progenitor cells (GNPs) located in rhombic lip (RL) migrate dorsally to populate the external germinal layer (EGL) or the secondary germinal zone. **(C)** Late embryonic and postnatal development, showing clonal expansion of GNPs in the EGL which will then become postmitotic, differentiate and migrate inwards to generate the internal granular layer (IGL) under the Purkinje cells (PC). On the right hand side, the putative sites of origin of medulloblastoma, namely EGL and Neuroepihelium (NE) of VZ is shown.
* This picture is adapted from Marino S, *Trends in Mol Med,* 2005.

Apart from the granule neurons, the rhombic lip also generates cells of the

precerebellar nuclei, namely pontine nucleus, lateral reticular nucleus, external

cuneate nucleus, reticulotegmental nucleus (origin of Mossy fibres) and inferior olive

nucleus (origin of Climbing fibres), as demonstrated by the expression of *Math1* during their development (Ben-Arie, Bellen et al. 1997).

1.1.2.4 Formation of cerebellar circuitry and completion of morphological development.

As a final step in cerebellar development, there is the formation of the intricate neuronal circuitry which is crucial for cerebellar functions. This process is associated with terminal differentiation of the cerebellar neurons (Hatten and Heintz 1995). The main aspects of the development of the cerebellar circuit have been discussed in the relevant sections above, and an overview of the circuitry is depicted in Fig 1 C. Although these connections are present across the cerebellum, it is important to note that cerebellum is functionally highly compartmentalised (term coined following cell lineage experiments in *Drosophila)* into distinct modules (Herrup and Kuemerle 1997). The morphological development of the cerebellum is completed by about post natal day 15 (P15) in mice (Millen, Wurst et al. 1994) and second postnatal year in the human. The post natal proliferation of progenitor cells in the EGL and the subsequent migration of granule neurons and ingrowth of cerebellar afferents results in a significant growth and foliation of the cerebellum.

The origins and fates of different precursor cells and the molecular mechanisms that regulate their development are summarised in Table 1.1.

Table 1.1 Summary of the main genes and pathways regulating the different stages of cerebellar development.

Stage of development	Genes/proteins/molecules implied*
Cerebellum anlage	Otx2, Gbx2, Fgf8, Wnt1, En1/2, Pax2/5, BMP and Smad pathway**, Shh**, Hoxa2
Purkinje cell development	Ngf, BDNF, Ciliary neurotropic factor, acetyl choline, Nt4/5, Rorα, Reelin pathway (migration)
Granule neuron development	For generation/proliferation - Math1, Shh pathway**, Bmi1**, Ccnd2, p27, NeuroD1, NSCL1, TGF-β pathway**, Notch pathway. For migration - Tag1, Tuj1, Pax6, Dcc/netrin pathway, Unc5h2/3, Girk2, astrotactin, Thrombospondin**, tenascin, neuregulin.

* Ref: Wang and Zoghbi, *Nature Reviews* 2001; Tong and Kwan, *Mol. Cell. Biol.* 2013.
**These genes/pathways/molecules are relevant for this current study.

1.1.2.5 Cells of origin of medulloblastoma

Medulloblastoma is traditionally thought to arise from the granule cell progenitors located in the EGL (Kadin, Rubinstein et al. 1970; Reddy and Packer 1999; Marino, Vooijs et al. 2000), and possibly from precursor cells located in the ventricular neuroepithelium (Marino 2005; Gilbertson and Ellison 2008). Stem cells have also been isolated from post natal cerebellar white matter by means of sorting for the stem cell marker CD133 (Lee, Kessler et al. 2005)**.** There is a shifting paradigm from viewing medulloblastoma as a single entity to different distinct subtypes, based on their genetic profiles and cell of origin (discussed later in section 1.2.6). There is evidence that MB subtypes demonstrate distinct anatomical differences in their origin and development (Gibson, Tong et al. 2010); such as - WNT tumours are related to 4th ventricle close to dorsal brain stem and SHH tumors within the cerebellar hemispheres. While the cellular origin for WNT and SHH Group have been implicated as dorsal brainstem progenitors and cerebellar GNPs respectively, the origin of more aggressive Group 3 is thought to be from cerebellar stem cells

(reviewed in (Eberhart 2012)). The exact cellular origin for Group 4 remains to be elucidated.

1.2 Medulloblastoma

Medulloblastoma (MB, medulloblastoma cerebelli), was first described as a primitive neuroectodermal tumour (PNET) by Bailey and Cushing in 1925 (Bailey and Cushing 1925). Prior to that, MB were theoretically grouped under divergent tumours such as sarcomas, neuroblastomas, spongioblastomas (poorly differentiated gliomas including astrocytic, ependymal and oligodendroglia) and primitive tumours with capacity for multi-lineage differentiation (Rorke 1994). The WHO (World Health Organisation), ICD-O (International Classification of Disease for Oncology), recognised MB as one of the PNET and classified them under embryonal tumours [ICD-O code 9470/3] (Louis, Ohgaki et al. 2007). Other tumours of the central nervous system that are merged under PNET umbrella, primarily due to their histological similarity, are ependymoblastoma and supratentorial PNET. Medulloblastoma is defined as a malignant, invasive embryonal tumour of the cerebellum, occurring preferentially in children, with predominantly neuronal differentiation, and tendency to metastasize via CSF pathways (Giangaspero, Binger et al. 2000).

WHO working group recognise four escalating grades in CNS tumours depending on histological severity – grade I (low proliferative potential, predicting good outcome) to grade IV (highly malignant, predicting worst outcome). Medulloblastoma corresponds histologically to WHO grade IV.

Medulloblastoma in children are known to commonly arise within the vermis (>75%), whereas in adults it is more common to originate in the cerebellar hemispheres (Bourgouin, Tampieri et al. 1992; Tortori-Donati, Fondelli et al. 1996).

1.2.1 Epidemiology

Brain and CNS cancers are the second most common cancers in the childhood, following leukemia, accounting to >27% of all cancers in 0-14 years age, with approximately 410 cases diagnosed each year in the UK (CRUK 2008-2010). Medulloblastoma is the commonest solid tumour in children, and is also the commonest brain malignancy, accounting to approximately 19 – 22% of all brain tumours (CCRG 2010). Age adjusted annual incidence rates for MB are 0.5 - 0.7 per 100,000 children (Stevens, Cameron et al. 1991; McKean-Cowdin, Razavi et al. 2013). National Cancer Institute's SEER (Surveillance, Epidemiology and End Results) data (1973 - 2009) analysis by McKean et al. predicts that the combined incidence of MB-PNET shows an increasing trend as compared to previous decades, although this may be due to the changes in the classification of these tumours (McKean-Cowdin, Razavi et al. 2013).

The peak incidence of MB is between 4 – 9 years of age (41%), followed by 0 - 3 years (32%), 10 – 14 years (18%) and 15 – 19 years [9%] (McNeil, Cote et al. 2002). In general, childhood MB show a bimodal distribution, peaking at 3-4 years of age and then at 8-9 years. Collins' law highlights the importance of age at diagnosis to predict the outcome which is based on the period of risk for recurrence (PRR), defined as age at diagnosis plus 9 (Brown, Tavare et al. 1995; Zhang and Zhou 1999). More than 70% of medulloblastoma occur in patients younger than 16 years of age. It is rare in adults, accounting to less than 1% of all adult malignancies. In adults, the majority (80%) of medulloblastoma occurs before the age of 40 years, and is very rare beyond the fifth decade of life (Giordana, Schiffer et al. 1999).

This decrease in incidence with increasing age is well in agreement with the embryonal nature of MB and favours genetic factors as etiology rather than environmental factors. Occasional reports attempting to associate parental exposure/contact with chemicals (such as pesticides, hydrocarbons, and N-nitroso compounds) and metals with development of MB have been published , although none of which is conclusive (Bunin, Kuijten et al. 1993; Colt and Blair 1998; Zahm and Ward 1998). A study has reported detection of low frequency simian virus (SV40)- like sequences in MB samples, without detection of large T antigen (Weggen, Bayer et al. 2000). Another study has shown detection of John Cunningham (JC) virus genome in significant proportion of MB samples, with presence of JC Virus T antigen in tumour cells (Krynska, Del Valle et al. 1999). However, an aetiological role of the above polyomaviruses in medulloblastoma pathogenesis has not been established (Huang, Reis et al. 1999; Giangaspero, Binger et al. 2000).

MB has a higher predilection in males, with approximately 65% of patients being male and 35% female. SEER data showed an annual incidence of combined MB-PNET of 0.84 and 0.58 per 100,000 for males and females respectively (McKean-Cowdin, Razavi et al. 2013). Based on ethnic background, MB-PNET was noted to be common in Caucasian population (82%) compared to African-Caribbean (9%) or other backgrounds [9%] (McNeil, Cote et al. 2002).

The prognosis of MB depends on several factors such as age at diagnosis, stage of the tumour/presence of metastasis, histological and/or molecular subtype, and treatment received. However, overall survival rate for MB is 50 – 60 % (Verlooy, Mosseri et al. 2006; Rutkowski, von Hoff et al. 2010) and the median survival rate is better in females compared to males (McNeil, Cote et al. 2002). There are

conflicting evidence reported regarding survival figures in adults, but the overall data does not suggest a significant difference in survival outcomes in adults compared to children (Davis, Freels et al. 1998; Smoll 2012)

1.2.2 Clinical features

The presenting clinical symptoms are: 1) Cerebellar, due to the primary tumour, namely – ataxia and disturbed gait (in children where the majority of tumours are in the vermis) and ispilateral dysmetria (in adults where most of the tumours are in the hemisphere). 2) Secondary to hydrocephalus, such as headache, lethargy, vomiting and other symptoms of raised intracranial pressure. In younger children with no verbal communication, behavioral changes and decreased social interactions are noted. Visual disturbances may also occur due to cranial nerve compression. 3) Rarely related to leptomeningeal dissemination, such as weakness, due to spinal cord or nerve root compression [radiculopathy] (Giangaspero, Binger et al. 2000; Jallo and A. 2012). Spinal cord metastasis via leptomeningeal route at the time of presentation is seen in up to 33% of cases (Hsieh, Wu et al. 2008). In addition, there may be symptoms due to associated supratentorial metastases (14 - 15%), spontaneous haemorrhage (5-6%) or systemic metastases [9%] (Park, Hoffman et al. 1983).

Common differential diagnoses based on clinical features include brain stem gliomas, cavernous sinus syndrome, cerebellar haemorrhage, cerebral aneurysms and craniopharyngioma. Clinical evaluation combined with radiological (CT/MRI scans) examination and CSF cytology aid in detection of the extent and spread of the disease, which helps stratify patients for appropriate treatment scheme, which may or may not include craniospinal irradiation (Jakacki, Burger et al. 2012).

Furthermore, the extent and dissemination of MB are classified based on Chang's

staging system (Table 1.2) which guides the treatment strategies and outcomes

(Chang, Housepian et al. 1969; Dufour, Beaugrand et al. 2012).

Table 1.2 Chang's Staging System for Medulloblastoma*

Variable	Greatest tumour dimension and disease spread
Tumour classification	
T1	<3 cm
T2	>3 cm
T3a	>3 cm with spread into the aqueduct of Sylvius and/or foramen of Luschka, cerebral subarachnoid space, third or lateral ventricles
T3b	>3 cm with unequivocal spread into the brainstem; for T3b, surgical staging maybe used in the absence of involvement at imaging
T4	>3 cm with spread beyond the aqueduct of Sylvius and/or the foramen magnum
Metastasis classification	
M1	Microscopic tumour cells in CSF
M2	Gross nodular seeding in cerebellum
M3	Gross nodular seeding in spinal subarachnoid space
M4	Metastasis beyond cerebrospinal axis

*Ref. Chang et al. *Radiology*, 1969.

Although the above clinical variables are essential for patient stratification,

classification of MB based on histology must not be underestimated. Histological

classification has been and still remains the mainstay in neuropathology diagnosis,

and proves to be a useful combination tool to tailor the treatment and predict

prognosis (Davis, Freels et al. 1998; Packer, Rood et al. 2003; von Hoff, Hartmann

et al. 2010).

1.2.3 Histological classification

The latest morphological classification of medulloblastoma (WHO classification of

tumors of the CNS, 2007) lists the following subtypes (Ellison, Love et al. 2004;

Louis, Ohgaki et al. 2007; Gilbertson and Ellison 2008): 1) Classic, 2) Desmoplastic, 3) Medulloblastoma with extensive nodularity (MBEN), 4) Anaplastic, and 5) Large-cell MB.

Classic MB is the commonest type of histology observed in more than 70% of MB (Burger and Scheithauer 1994). They are composed of uniformly arranged, small round to oval tumour cells with hyperchromatic nuclei and indistinct cytoplasm (Fig 1.4 A). Nuclear molding (denting the neighboring) may be a marked feature due to the dense population of tumour cells. Neuroblastic (Homer-Wright) rosettes, which are tumour cells arranged in a circular fashion tangled around cytoplasmic processes, are observed in about 40% of classic MB. A high proportion of tumours show nuclear polymorphism, high mitotic activity and individual cell apoptosis (in the form of nuclear pyknosis or karyorrhexis as opposed to generalised geographic necrosis). Mitoses are seen in about 25% of the cases (Burger, Grahmann et al. 1987) in keeping with the notion that MB are predominantly proliferative tumours. Occasional features include nuclear gigantism, multinucleate giant cells and atypical mitosis. A minority of cases have pseudopalisading necrosis, vascular proliferation or neovascularisation, calcification and massive haemorrhage. MB with classic histology has an intermediate prognostic risk, i.e., the outcomes are shown to be better than that of anaplastic/large cell variants, but worse than that of desmoplastic/MBEN variants [Fig 1.4 E] (Rutkowski, von Hoff et al. 2010).

Desmoplastic MB constitutes about 7% of MB, and are typically characterised by the presence of nodular architecture with desmoplasia (increased reticulin/collagen) within the inter-nodular areas (Fig 1.4 B). The cells outside the nodules (within the desmoplasia) often show increased pleomorphism while the cells within the nodules are less pleomorphic and usually have a neuronal (neurocytic) phenotype with

positivity for neuronal markers such as synaptophysin and NeuN (McManamy, Pears et al. 2007). Desmoplasia may also occur in other types of MB as reaction to leptomeningeal invasion, and hence should be interpreted with caution (Gilbertson and Ellison 2008). The molecular and cytogenetic abnormalities in nodular/desmoplastic MBs are distinct compared to other subtypes (McManamy, Pears et al. 2007), and have a significantly better outcome compared to other subtypes. In adults, desmoplastic MB is the commonest variant observed, compared to children (Abacioglu, Uzel et al. 2002).

Medulloblastoma with extensive nodularity (MBEN) represent about 3% of MB, and as the name suggests, they are extremely nodular giving a 'grape-like' appearance on imaging. The uniformly round intranodal cells are arranged in a streaming fine fibrillary background and due to their resemblance to neurocytes of central neurocytoma, this subtype have been previously termed as cerebellar neuroblastoma (Pearl and Takei 1981). These tumour subtype predominantly occur in children less than 3 years of age, and have a favourable outcome (Giangaspero, Perilongo et al. 1999).

Anaplastic MB represent upto 15% of all MB and are characterised by large cells, and more striking nuclear pleomorphism, mitoses (with a high Ki-67 labelling index) and nuclear molding as compared to the classic type. They also have increased atypical mitoses, apoptotic bodies and show a distinctive cell wrapping phenomenon [Fig 1.4 C, wrapping of one cell around another] (Ellison, Love et al. 2004).

Large cell MB accounts for about 3-4% of all MB, and histologically resembles the anaplastic type. They are composed of large cells with prominent nucleoli and more abundant cytoplasm (Fig 1.4 D) and they contain large areas of necrosis and display a high mitotic count. They are thought to resemble rhabdoid/atypical teratoid (AT/RT)

tumours of cerebellar origin, although they differ from these tumours in their immunophenotype and cytogenetic features (Giangaspero, Rigobello et al. 1992).

Anaplastic and large cell variants are thought to form a continuum, and they have been grouped together for prognostic purposes and referred to as **large-cell/anaplastic (LCA) MB**. LCA is biologically very aggressive and have the worst prognosis compared to other subtypes [Fig 1.4 E] (Giangaspero, Rigobello et al. 1992; Ellison 2002; McManamy, Lamont et al. 2003).

Rare forms of MB, such as medullomyoblastoma and melanotic MB are recognised. Medullomyoblastoma show rhabdomyoblast (immature skeletal muscle cell) differentiation, which may show formation of crude skeletal muscle fibrils or scattered large globular cells with desmin immunoreactivity (Smith and Davidson 1984). Melanotic MB, which otherwise has the histological appearance of classic MB, contains melanin pigment in a proportion of the cells, occasionally forming epithelioid, tubular or papillary pattern (Dolman 1988). The biological behavior of these rare variants have been thought to be similar to classic MB, however the rarity of these cases has limited a thorough assessment (Ellison 2002).

The common features that any of the subtypes may display are i) invasion of the tumour cells into the cortex, deep white matter or the deep cerebellar nuclei, ii) extension into the subarachaoid space (4th ventricle), iii) leptomeningeal tumour deposits iv) supratentorial dissemination and v) metastasis outside of neural axis.

Although the morphological differentiation of MB can be diverse, it mainly tends to occur along the neuroepithelial lines with the neuronal differentiation being the commonest. In keeping with this, immunoreactivity for synaptophysin is a characteristic feature of medulloblastoma and it is the most prominent in the nodules

and in the centre of neuroblastic rosettes. Other neuronal lineage markers such as nestin and vimentin show variable expression. Glial differentiation is rare, and when present, may form small groups of cells with astrocytic phenotypes, with GFAP (glial fibrillary acidic protein) immunoreactivity. Other than synaptophysin and GFAP, other markers such as S100 (marker of neural crest derivatives including glial cells), MIB-1 (a proliferation marker, similar to Ki-67), Bcl-2 (B-cell lymphoma 2) and TP53 (tumour protein 53) have also been associated with a minority of MB, the clinical significance of which is yet to be established (McLendon, Friedman et al. 1999). Ependymal differentiation is extremely rare, and if present raises possibility of other tumour diagnosis. In about 5% of the cases, mature ganglion cells are present (Burger, Grahmann et al. 1987).
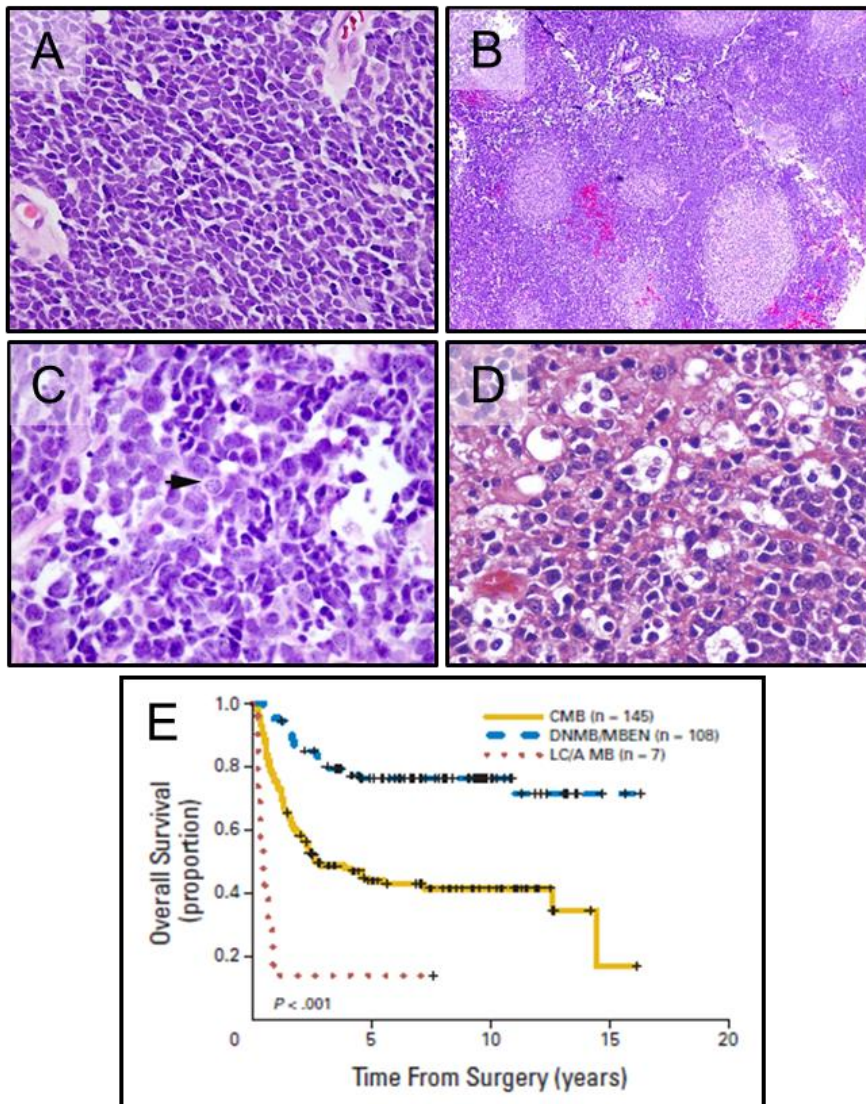
Fig. 1.4 Histological variants of medulloblastoma and their predicted prognosis

(A) Classic type, showing densely arranged small round to oval cells with hyperchromatic nuclei and indistinct cytoplasm. Also seen is nuclear molding. Classic type is the commonest histological MB variant. **(B)** Desmoplastic type, with nodular tumour architecture. **(C)** Anaplastic type, showing large cells with more striking nuclear pleomorphism and nuclear molding, Arrow pointing to an example of cell wrapping phenomenon. **(D)** Large cell type comprising large cells with prominent nucleoli and more abundant cytoplasm. **(E)** Kaplan-Meier plot showing overall survival for different subtypes. Classic histology (yellow line) is associated with intermediate prognosis as compared to desmoplastic/nodular type (blue interrupted line, best prognosis) and large cell anaplastic type (red dots, worst prognosis). This picture is reproduced with permission from Rutkowski et al. *JCO* 2010. JCO copyright clearance licence no. 3254311484547

1.2.4 Genetic abnormalities in the pathogenesis of MB:

Chromosomal aberrations:

Common cytogenetic abnormalities in MB include isochromosome 17q (i17q), deletions of 17p and aberrations of chromosome 1. The most common specific abnormality, associated with more than 50% of the cases, is i17q (Bigner, Mark et al. 1988) which mainly has a dicentric (with two centromeres) structure, similar to i17q occurring in leukemia. Although i17q is the most common mechanism for loss of 17p in MB, in minority of cases, partial or complete loss of 17p can occur by interstitial deletion, unbalanced translocation or monosomy 17 (Biegel, Burk et al. 1992). The types of aberrations of chromosome 1 found in MB are variable, and include unbalanced translocations, deletions and duplications (Griffin, Hawkins et al. 1988). Using comparative genomic hybridisation (CGH), further genomic imbalances in MB such as loss of chromosome 10q, loss of chromosome 11, and gain of chromosome 7 (Reardon, Michalkiewicz et al. 1997) were identified. Isolated examples of deletions of 6q, 9q, 10q and 16q and gain of 4p, 5p, 7q, 8q and 9p have also been reported (Avet-Loiseau, Venuat et al. 1999; Giangaspero, Binger et al. 2000).

These alterations are not distributed equally among the histologic variants. Presence of i17q in tumours has been associated with a poor clinical outcome, suggesting that this cytogenetic alteration may contribute to the development of aggressive variants of medulloblastoma. In contrast, monosomy 6 has recently been shown to occur exclusively in tumour with favourable prognosis, mainly in classic medulloblastomas. (Thompson, Fuller et al. 2006). Recently, gain of 6q and 17q were shown to be associated with poor prognosis, raising the possibility that they could be used as

independent markers of disease progression and survival (Pfister, Remke et al. 2009).

Gene amplification

MYC (c-Myc) amplification (detected by fluorescent in-situ hybridisation/FISH) is the most common gene amplification found in MB containing double minutes (fragments of extrachromosomal DNA), followed by *MYCN* (N-myc) amplification which is found less often, together occurring in 6-8% of all MB (Badiali, Pession et al. 1991; Tomlinson, Jenkins et al. 1994). In particular the large cell histological variant which is associated with poor prognosis, carries a high incidence of *MYC* amplification (Brown, Kepner et al. 2000), which renders the tumour resistant to chemotherapy, resulting in fatal outcomes (Scheurlen, Schwabe et al. 1998). Further studies have confirmed the association of *MYC* and *MYCN* amplification with aggressive MB types (Aldosari, Bigner et al. 2002). Pfister et al. have shown that *MYC/MYCN* amplification is associated with poor outcome in MB (hazard ratio for death = 2.75, reference being 1.00), suggesting their possible use as independent prognostic markers (Pfister, Remke et al. 2009).

Mutations of tumour suppressor genes:

Mutations of *TP53* (P53, located on 17p13) have been identified in a subset of 5-10% of MB (Adesina, Nalbantoglu et al. 1994; Batra, McLendon et al. 1995). Some studies have reported high association of *TP53* mutation with large cell/anaplastic type of MB carrying a poor prognosis, hence suggesting that alterations within the TP53-ARF tumour suppressor pathway contribute to the development of aggressive types of MB (Frank, Hernan et al. 2004). Marino et al. have shown that somatic inactivation of *Rb* (retinoblastoma) gene in the EGL precursor cells of the developing

cerebellum in the p53-null mouse, induced high incidence of medulloblastoma formation of large cell anaplastic type (Marino, Vooijs et al. 2000), through acquisition of additional genetic mutations affecting N-Myc and Ptch2 (Shakhova, Leung et al. 2006).

PTEN (phosphatase and tensin homolog, located on chromosome 10q) mutations although found to be common in high grade gliomas, are rare in MB (Rasheed, Stenzel et al. 1997). However, a recent study has shown *PTEN* homozygous deletion to be present in 33% of MB (Inda, Mercapide et al. 2004). Also, Castellino et al. have demonstrated that heterozygosity for *Pten* promotes tumorigenesis in a mouse model of medulloblastoma and that *PTEN* expression is a marker of favourable prognosis (Castellino, Barwick et al. 2010).

DMBT1 [deleted in malignant brain tumour 1, a member of scavenger receptor cysteine-rich (SRCR) superfamily, located on chromosome 10q] deletion, first cloned in a MB cell line, was identified and implicated in pathogenesis of small subset of MB (Mollenhauer, Wiemann et al. 1997).

Familial syndromes and their genetic pathway mutations:

Of particular importance, loss/mutations of tumour suppressor genes associated with two familial syndromes (Huang, Mahler-Araujo et al. 2000; Zurawel, Allen et al. 2000) have been shown to predispose to MB – 1) Gorlin's syndrome, and 2) Turcot syndrome. These syndromes are caused by the deregulation of the SHH and WNT signalling pathway and they will be discussed in parallel, as this should be useful to understand the novel molecular classification of MB which will be discussed later.

Gorlin's syndrome [or naevoid basal cell carcinoma syndrome (NBCCS)] is a rare autosomal dominant condition with skeletal abnormalities, facial dysmorphism, large body size, ectopic calcifications, multiple basal cell carcinoma (Lo Muzio 2008). Medulloblastoma arising in Gorlin's syndrome are known to have desmoplastic histology (Ellison 2002). As mentioned previously (section 1.1.2.3.2), Gorlin's syndrome is characterised by germ line mutations of the *PTCH* (Patched) gene. As MB are thought to originate from GNPs of the EGL in developing cerebellum, deletion of *PTCH* in these cells result in malignant transformation leading to medulloblastoma. *PTCH1* mutations have also been identified in about 9% of sporadic medulloblastoma (Thompson, Fuller et al. 2006). The function of Ptch1 as tumour suppressor was proved when 15% of mice with heterozygous deletion for Ptch1 developed medulloblastoma (Goodrich, Milenkovic et al. 1997). Mutations or deletions of Suppressor of Fused (SUFU) locus, a downstream molecule in the SHH signalling (Fig 1.6), have also been associated with sporadic MB (Taylor, Liu et al. 2002), indicating that SUFU also acts as a tumour suppressor gene. Mutations of SMO (Smoothened) have also been reported in a significant proportion of MB (Zurawel, Allen et al. 2000).

Turcot's syndrome (Turcot, Despres et al. 1959) is a rare heritable disorder, associated with colonic cancer and malignant neuroepithelial brain tumours such as gliomas, and medulloblastoma. The syndrome is characterised by mutations of the *APC* (Adenomatous Polyposis Coli, located on chromosome 5q) gene (Huang, Mahler-Araujo et al. 2000). Since its first description, this syndrome has been refined to also include brain tumour polyposis (BTP) syndrome type 2, with *APC* mutation, which mainly develop medulloblastoma as their brain tumour component (Paraf, Jothy et al. 1997). *APC* is a component of the wingless (WNT) pathway (Ille and

Sommer 2005), which regulates various developmental processes including the

proliferation and the fate of neural progenitor cells (WNT pathway has been

described in section 1.1.2.3.2, Fig 1.2 A). Mutations in a range of WNT pathway

members have been identified in sporadic medulloblastoma. They include *CTNNB1*

(β-catenin 1, 8%), *APC* (3%) and *AXIN* [2%] (Zurawel, Chiappa et al. 1998; Huang,

Mahler-Araujo et al. 2000; Yokota, Nishizawa et al. 2002). Compared to SHH

pathway mutations, WNT pathway mutations are less frequent. In an analysis of

childhood MB (from children entered in the International Society of Pediatric

Oncology/United Kingdom Children's Cancer Study Group) PNET3 trial, those cases

with positivity for nuclear CTNNB1 showed better survival [5 year event free survival

(EFS) of 89%], compared to CTNNB1 nuclear negative cases [5year EFS of 60%]

(Ellison, Onilude et al. 2005). Another study from St Jude MB trial showed similar

results, but importantly this study also demonstrated that CTNNB1 nucleopositive

tumours and those tumour with Gli and SFRP1 positivity (indicative of SHH pathway

activation) are mutually exclusive, and have significantly different survival rates

favouring CTNNB1 nucleopositive tumours (Gajjar, Chintagumpala et al. 2006).

Although SHH and WNT mutations appear mutually exclusive, these are only found

in 30-40% of the MB (Thompson, Fuller et al. 2006).

In keeping with the notion that mutations in signalling pathways regulating cerebellar

development lead to medulloblastoma, there is evidence that also mutations leading

to activation of the NOTCH pathway are involved in MB tumorigenesis (Gilbertson

and Ellison 2008). Notch signalling, discussed before (in section 1.1.2.3.2, Fig 1.2

B), is known to play a multifaceted role in the differentiation, morphogenesis and

functioning of the vertebrate nervous system (Louvi and Artavanis-Tsakonas 2006)A

study has shown that activation of *NOTCH2* in embryonal brain tumour cell lines

accelerated their proliferation and *in vivo* growth; this study also observed NOTCH2 to be expressed at high levels in some MBs and to be occasionally amplified at DNA level (Fan, Mikolaenko et al. 2004). Other syndromes where MB may develop include i) Li Fraumeni syndrome, with germ-line *TP53* mutation (Tabori, Baskin et al. 2010), and ii) Ruenstein-Taybi syndrome, with germ-line *CREBBP* (CREB binding protein) deletion, which is the first syndrome identified for non-WNT/non-SHH MB. (Bourdeaut, Miquel et al. 2013).

Mutations in RAS signalling pathway are known to be associated with certain syndromes such as Noonan syndrome with multiple lentigines [or Leopard syndrome, with skin, facial and cardiac defects] (Sarkozy, Digilio et al. 2008). Recently Rankin et al., have reported an adult patient with clinical and molecular features of Leopard syndrome with *PTPN11* mutation to have had MB as a child, indicating that MB may be an association with RAS associated mutations (Rankin, Short et al. 2013).

Alternative splicing:

Alternative splicing is a controlled mechanism for generating protein diversity, and refers to a primary transcript being spliced in more than one pattern to generate multiple, distinct mRNAs (Koscielny, Le Texier et al. 2009). Previous studies have reported alternative splicing of individual genes in human MB (Ferretti, Di Marcotullio et al. 2006; Li, Shu et al. 2007). A more recent, genome wide analysis of alternative splicing in paediatric MB and normal cerebellum by Menghi et al., have identified eleven validated splicing events associated with MB (Menghi, Jacques et al. 2011). Three of the eleven genes (*DAAM1, EHBP1 and TRRAP*) were shown to have characteristics for Sonic Hedgehog-driven MBs. Furthermore, they demonstrate that

some of the tumour associated splicing patterns were observed in the GNP cell

cultures, suggesting that abnormal alternative splicing during cerebellar

development may lead to failure of neuronal differentiation and MB development

(Menghi, Jacques et al. 2011). The main genes known to participate in

medulloblastoma pathogenesis, are summarised in Table 1.3 (de Bont, Packer et al.

2008).

Table 1.3 Differentially expressed genes in medulloblastoma*

Genes	Change type	Approximate % of tumour association (where known)	Genes	Change type	Approximate % of tumour association (where known)
SHH signalling			**IGF signalling continued**		
PTCH1	Mutation	4 – 13	IGF-1R	Phosphorylation	80
PTCH2	Overexpression		IRS-1	Overexpression	
SUFU	Mutation	0 – 9	IGF-2	Overexpression	
Smo	Mutation	0 – 10	AKT/PKB	Phosphorylation	
Gli	Overexpression	30	Erk-1	Phosphorylation	
BMI1**	Overexpression	67	Erk-2	Phosphorylation	
RENKCTD 11	Deletion	39	IGFBP-2	Overexpression	
Wnt signalling			CXCR4	Overexpression	51
Axin 1	Mutation	1 – 6	PDGFRB	Overexpression	
	Deletion	12 – 41	OTX2	Overexpression	>70
Axin 2	Mutation	3		Amplification	33
APC	Mutation	1 – 4	ATOH1	Expression	
β-catenin	Mutation	1 – 63	P75	Expression	
Survivin	Overexpression	5 – 50		Overexpression	
SOX4	Overexpression		TrkA	Overexpression	67
SOX11	Overexpression		TrkC	Overexpression	29 - 73
Cyclin D1	Overexpression		Heparanase	Expression	62 - 88
Cyclin D2	Overexpression		NEUROG1	Expression	55
Lef1	Overexpression		Calbindin	Expression	41
Notch signalling			P53	Mutation	0 - 11
HES1	Overexpression	<46	PAX5	Overexpression	70
HES5	Overexpression	<71	MDM2	Overexpression	0 - 20
JAG1	Overexpression		CDK6	Overexpression	30
Notch1	Overexpression	75	HIC1	Hypermethylation	70
Notch2	Overexpression	12 – 15	EEF1D	Overexpression	
Notch3	Overexpression		RPL30	Overexpression	
FOXG1	Overexpression	>90	RPS20	Overexpression	
Musashi	Overexpression		STMN1	Overexpression	
ErbB signalling			hTERT	Overexpression	42
ErbB4	Overexpression	66	SGNE1/7B2	Hypermethylation	70
ErbB2	Overexpression	70 - 86	RASSF1A	Hypermethylation	80 - 90
CIC	Overexpression		CASP8	Hypermethylation	90
NRG-1β	Overexpression	87	ZIC2	Hypermethylation	
c-Myc	Amplification	5 – 10	P14-ARF	Hypermethylation	4 - 50
	Overexpression	42			
Mnt	Underexpression	43	P16INK4A	Hypermethylation	2 - 14
JPO2	Overexpression		TIMP3	Hypermethylation	0 - 11
N-Myc	Ampification	5	CDH1	Hypermethylation	8
IGF signalling			P18INK4C	Hypermethylation	20
MCJ	Hypermethylation	33	S100A6	Hypermethylation	12
RB1	Hypermethylation	18	S100A10	Hypermethylation	12
DKK1	Histone acetylation		S100A4	Hypomethylation	17

* Ref. De Bont et al. *Neuro Oncol* 2008. ** In this study we are primarily interested in the role of *BMI1*.

1.2.5 Current treatment strategies:

Following patients' clinical, radiological and pathological evaluation, a multidisciplinary team makes the treatment recommendation. The treatment options are based on patient stratification into average, intermediate and high risk groups, which takes into account several factors including age of the patient, associated co-morbidities, stage of the tumour/extent of resection, histological tumour type and associated genetic markers (Packer, Cogen et al. 1999). The criteria for patient risk stratification may further evolve owing to advances in understanding the tumour biology (Packer, Rood et al. 2003). Generally, the main modalities of treatment are surgical excision, radiotherapy and chemotherapy; mostly a combination of all the three. Rarely (especially in recurrent cases) stem cell/bone marrow transplantation may be recommended. In advanced or terminal cancer, palliative care/support may be the only appropriate management option.

Surgery

Surgery is considered as the gold-standard treatment, which remove/reduce tumour bulk and provides tumour material for histologic confirmation of tumour type. It is crucial to maximally resect the primary MB tumour, and therefore aggressive surgical approaches are undertaken to always excise the tumour as much as possible (Albright, Wisoff et al. 1996). In most cases of MB in children, the tumour is located at the midline in the posterior fossa, and can be accessed via sub-occipital craniotomy, in a prone (face down) position (Cogen and Donahue 1999). It may necessitate partial resection of the cerebellar vermis to access the tumour, but the floor of IV ventricle needs to be protected. Neuronavigation using stereotactic guidance and operating microscope to carefully identify crucial neural structures are

used. Associated hydrocephalus is treated by ventriculostomy [shunt catheter] (Lee, Wisoff et al. 1994), which may have to be left in place permanently in a proportion of the patients; the likelihood of which is increased in infants and those children with leptomeningeal dissemination. Common postoperative complications include diplopia (sixth-nerve palsies), ataxia (due to vermis dissection) incoordination (if cerebellar peduncles are resected), and rarely (5-15%) mutism-associated pseudobulbar signs (Pollack, Polinko et al. 1995). Most of these findings tend to resolve over a few weeks post operatively (Packer, Cogen et al. 1999). Post operatively MRI scan is done routinely, to ensure that 'total' or 'near total' resection has been achieved. If not, a second operation to remove the residual tumour is undertaken in non-metastatic disease (MacDonald, Rood et al. 2003).

Radiation treatment

Adjuvant radiation therapy is usually given 4-6 weeks after surgery, and remains the single most effective means of postoperative treatment for children with MB (Packer, Cogen et al. 1999; Taylor, Bailey et al. 2004). Prophylactic craniospinal radiotherapy (csRT, covering entire craniospinal axis) is administered routinely to the newly diagnosed patients, independent of radiological or cytological (CSF) evidence of spinal metastasis, as this is shown to maximise survival (Bouffet, Bernard et al. 1992). In children less than 3 years of age, conventionally, 3600 cGy and 5400-5960 cGy is given to entire neuraxis and the posterior fossa (total dose) respectively (Landberg, Lindgren et al. 1980; Hershatter, Halperin et al. 1986)(Hershatter et al., 1982; Landberg et al., 1980). It is of note that use of next generation radiotherapy such as proton therapy and intensity modulated radiotherapy (IMRT) are emerging (St Clair, Adams et al. 2004).

Chemotherapy

Untoward neurocognitive and endocrine effects resulting from irradiation of the developing neuraxis in children poses a great obstacle for this treatment, prompting clinical trials using adjuvant chemotherapy. These clinical trials showed variable benefits (Bailey, Gnekow et al. 1995; Deutsch, Thomas et al. 1996; Kuhl, Muller et al. 1998), including preserved intellectual or neurocognitive ability (Ris, Packer et al. 2001) compared to those of conventional radiotherapy alone. Chemotherapy, is a standard component of the treatment in older children (> 3 years of age), and is usually given during and after radiation therapy (for about 12 months following radiotherapy).In younger children (< 3 years of age), chemotherapy is used to delay or sometimes to avoid the need for radiotherapy in localised MB. As the treatment regime differs depending on the age of the patient and their risk group, this will be discussed under different headings (NCI 2013).

Children aged 3 years or younger: The main principle in this age group is to achieve adequate cure with chemotherapy alone, removing the need of adjuvant radiotherapy. Several studies have observed that desmoplastic and MBEN histology, which is common in younger children, have favourable outcome even with chemotherapy alone (Geyer, Sposto et al. 2005; von Bueren, von Hoff et al. 2011), while other histologic subtypes fare less well (Grill, Sainte-Rose et al. 2005), necessitating adjuvant radiotherapy. Newer regime using higher dose chemotherapy (marrow ablative) followed by autologous bone marrow/stem cell rescue, has been shown to ablate the need of radiotherapy in a subgroup of patients younger than 3 years of age (Chi, Gardner et al. 2004; Dhall, Grodman et al. 2008).

Children older than 3 years, with average-risk MB: Prospective randomised and single-arm trials have demonstrated that adjuvant chemotherapy during and after radiotherapy improve overall survival in children with average-risk MB. (Bailey, Gnekow et al. 1995; Kortmann, Kuhl et al. 2000; Carrie, Grill et al. 2009). A prospective multi-centre trial shows a favourable outcome (5-year overall survival of 85%) when risk-adapted radiotherarpy, followed by a short (4-month) dose-intensive chemotherapy supported by stem cell rescue was used (Gajjar, Chintagumpala et al. 2006). This study also showed a poor survival associated with large cell/anaplastic type of MB, compared to other histological subtypes.

Children older than 3 years with high-risk MB: The drugs that are used for average-risk patients have been used extensively in high-risk (Jakacki, Burger et al. 2012). Post radiation, short, dose-intensive chemotherapy supported by stem cell rescue study mentioned above, also showed favourable outcome in high-risk MB ([5-year overall survival and 5-year progression free survival of ~70%] (Gajjar, Chintagumpala et al. 2006). Innovative drug delivery system and decreased neurotoxicity of chemoradiotherapy are major directives for future clinical trials.

Adults: Because of the rarity of MB in adults, prospective comparative chemotherapy trials are limited. Adolescents and young adults tolerate chemotherapy relatively poorly (Tabori, Sung et al. 2005). Several studies have shown no benefit of addition of chemotherapy to radiotherapy (Carrie, Lasset et al. 1994; Prados, Warnick et al. 1995; Chan, Tarbell et al. 2000), but the studies have been small and underpowered, suggesting that further comparative studies are needed.

Shortfalls of current therapy: Despite recent advances and multimodality in treatment MB is still associated with high morbidity and mortality. Approximately 40% of childhood tumours are treatment refractory, leading to recurrence, and about 30% of the patients die because of the tumour. Those who survive the treatment often have a significantly impaired quality of life (Jones, Jager et al. 2012). Novel therapies targeting specific molecular pathway and improved classification are necessary to improve patient stratification and response to less toxic therapies. Therefore understanding different molecular and genetic pathway giving rise to this heterogeneous tumour is crucial.

1.2.6 Recent advances in molecular classification of medulloblastoma (molecular subgroups)

As discussed previously (section1.2.5), clinical prognostication and stratification in patients with MB include clinical factors, histological type and expression of certain molecular markers. However, it is increasingly clear that MB is not a single disease entity. Based on their gene expression profiles, DNA copy number aberrations, and analysis of transcriptional profiles, several research studies (Pomeroy, Tamayo et al. 2002; Thompson, Fuller et al. 2006; Kool, Koster et al. 2008; Fattet, Haberler et al. 2009; Northcott, Nakahara et al. 2009; Al-Halabi, Nantel et al. 2011; Cho, Tsherniak et al. 2011; Northcott, Korshunov et al. 2011) have provided evidence to suggest that MB can be classified into multiple molecular subgroups. Furthermore, it has been suggested that the tumours belonging to each subgroup differ in their demographics and clinical outcomes. A consensus conference, which took place in 2010 in Boston, USA, came to a consensus that the overall evidence supported the distinction of MB into four main non overlapping molecular subgroups, namely, WNT, SHH, Group 3

and Group 4 (Taylor, Northcott et al. 2012). Two groups, characterized by activation of WNT and SHH pathways respectively, are better characterized molecularly, while the molecular signatures underlining Groups 3 and 4 are less well defined. There was evidence that further subtypes existed within each of these groups (decided to be named with Greek letters - α, β, γ etc.). The participants of the consensus agreed that molecular classification will continue to evolve in the future, as larger cohorts are analysed in greater depth (Northcott, Korshunov et al. 2011). .

1.2.6.1 WNT subgroup

WNT subgroup has a very good long term prognosis compared to other subgroups (Clifford, Lusher et al. 2006; Ellison, Dalton et al. 2011). Due to their good prognosis, the possibility to undertake a clinical trial to de-escalate therapy (to avoid morbidities associated with treatment) is being discussed for this group of patients. The gender ratio for this subgroup is equal in males and females, and they can occur in all ages, but are uncommon in infants. Genetic abnormalities that define tumours in this subgroup (Hamilton, Liu et al. 1995; Zurawel, Chiappa et al. 1998) are: i) germline mutations of WNT pathway inhibitor *APC* (that predisposes to Turcot's syndrome), and ii) somatic mutations of *CTNNB1* encoding β-catenin (Fig 1.5). The tumours in this group showed monosomy 6 (92.6% of cases as opposed to 7.4% in SHH subgroup) as the predominant cytogenetic abnormality, and one of the genetic abnormality associated with monosomy 6 is serum/glucocorticoid regulated kinase 1 [*SGK1*] (Ellison, Dalton et al. 2011). However occasional reports of cases with WNT transcriptional signature without monosomy 6 (Northcott, Korshunov et al. 2011), and those with mutations in both *CTNNB1* and *PTCH* together (Parsons, Li et al. 2011), complicate the definition of this subgroup. Immunohistochemical marker DKK1

(dickkopf WNT signalling pathway inhibitor 1) has been found to be strongly associated to this subgroup of tumours (Northcott, Korshunov et al. 2011; Remke, Hielscher et al. 2011). The majority of the tumours in this group have classic histology; and although tumours with large cell/anaplastic histology have been reported, this does not seem to affect the prognosis negatively (Ellison, Kocak et al. 2011). A mouse model of Wnt group has been established, which suggest that the tumours from this subgroup arise from lower rhombic lip of the cerebellum (Gibson, Tong et al. 2010).

1.2.6.2 SHH subgroup

The SHH subgroup MB have an intermediate prognosis, similar to Group 4 patients, worse than WNT (good) and better than Group 3 (poor). There is no difference in gender ratio, and they show a dichotomous age distribution, being common in infants (0-3 years) and in adults (> 16 years), but less common in children (3-16 years) [Fig 1.5]. Genetic abnormalities that define this subgroup of tumours (Bale, Falk et al. 1998; Brugieres, Pierron et al. 2010; Northcott, Hielscher et al. 2011; Northcott, Korshunov et al. 2011) are i) germline mutations in Shh receptor *PTCH* (predisposing to Gorlin syndrome), ii) germline mutations in SHH inhibitor *SUFU* (particularly in infantile MB), iii) somatic mutations of SHH pathway members such as *PTCH, SMO* and *SUFU*, and, amplifications of *GLI1* and *GLI2,* and iv) deletion of chromosome 9q (where PTCH gene is located). Although this MB subgroup can be identified on the basis of transcriptional profiling (Taylor, Liu et al. 2002; Northcott, Fernandez et al. 2009), other approaches (Al-Halabi, Nantel et al. 2011; Ellison, Dalton et al. 2011; Northcott, Korshunov et al. 2011) to identify this subgroup by immunohistochemical staining for SFRP1(secreted frizzled-related protein 1) or

GAB1 (GRB2-associated binding protein 2) have been described. The most common histology type associated with SHH is nodular/desmoplastic MB, although this is considered not be an effective marker as up to 50% of MB in SHH subgroup are not of the nodular/desmoplastic type. The majority of the mouse models for MB established so far belong to Shh subgroup of tumours and they have been shown to originate from Math1-positive granule cell progenitors (Hatten and Roussel 2011).

1.2.6.3 Group 3

Group 3 MB is characterized by the worst prognosis as compared to all other subgroups (Taylor, Northcott et al. 2012). They are more common in males than in females, and are found in children and infants, but almost never in adults (Fig 1.5). Although no specific molecular pathway characterises this subgroup, their main genetic abnormalities include i) *MYC* amplification/overexpression (Cho, Tsherniak et al. 2011; Hatten and Roussel 2011), ii) amplification/overexpression of *OTX2* (de Haas, Oussoren et al. 2006; Adamson, Shi et al. 2010), iii) overexpression of several genes that are associated with retinal development [although the role of these genes in Group 3 MB pathogenesis is yet to be completely understood] (Kool, Koster et al. 2008) and iv) gain of chromosome 1q, loss of chromosome 5q and chromosome 10q (more likely to have these compared to Group 4).

There is a high association of Group 3 MB with c-*MYC* (or *MYC*) overexpression; and *MYC* amplification appears to be almost always limited to Group 3 (Northcott, Korshunov et al. 2011). In fact, Group 3 patients are being subdivided into different subgroups based on *MYC* amplification status namely, 3α (harbor) and 3β (do not harbor), where the latter show similar prognosis as Group 4 patients (Cho, Tsherniak

et al. 2011). The gold standard for diagnosis of Group 3 tumours is by means of transcriptional profiling , but immunohistochemistry for the marker NPR3 (natriuretic peptide receptor 3) has been suggested as a reliable Group 3 marker (Northcott, Korshunov et al. 2011). Group 3 MB mostly show classic and large cell/anaplastic type histology, and are frequently metastatic (Northcott, Korshunov et al. 2011). There is a need to focus on further understanding of underlying pathogenesis, establish practical biomarkers, and develop accurate mouse models for MB of this subgroup in particular, as they bear the worst prognosis. Recently however, Pei et al. have described a novel model of Myc expressing and mutant p53 bearing cerebellar stem cell orthotopic xenograft as a representative model of Group 3 (Pei, Moore et al. 2012).

1.2.6.4 Group 4

Group 4 MB are characterised by an intermediated prognosis as discussed above. They are prototypical MBs, arising in young boys (i.e. Common in children with male preponderance) and displaying a classic histology, and with isochromosome 17q (Fig 1.5). However this subgroup has a diverse molecular pathogenesis, and currently tumours belonging to this subgroup are identified through transcriptional profiling (Cho, Tsherniak et al. 2011; Taylor, Northcott et al. 2012). Isochromosome 17q is also seen in Group 3 tumours, but its association with Group 4 tumours is much stronger [26% vs 66%] (Northcott, Korshunov et al. 2011). Isolated deletion of 17p is seen Group 3 and Group 4, but not in SHH or WNT subgroups. The other notable genetic alteration in Group 4 tumours is loss of X chromosome in females. Multiple studies have identified over-representation of genes involved in neuronal differentiation and development in Group 4 MB (Kool, Koster et al. 2008; Cho,

Tsherniak et al. 2011; Northcott, Korshunov et al. 2011), although their clinical relevance is not yet clear. The Polycomb group gene *BMI1* (the gene that we are interested in our study, which will be discussed in details in the next section below) is also more prominently overexpression in Group 4 MB (or Northcott Group D) MBs (Behesti, Bhagat et al. 2013; Manoranjan, Wang et al. 2013). .

KCNA1 (potassium voltage-gated channel, shaker-related subfamily, member 1) has been suggested as the immunohistochemical marker for Group 4 MB, but requires further validation (Northcott, Korshunov et al. 2011). In addition FSTL5 (follistatin-like 5) has been suggested as an effective marker indicative of poor prognosis for non-WNT/non-SHH group of MBs (Remke, Hielscher et al. 2011) . The immunohistochemical markers currently suggested for the identification of the various subgroups (Taylor, Northcott et al. 2012) are listed in Table 1.4. However, at the consensus conference it was felt that until definitive immunohistochemical markers are established, histopathological classification (discussed in section 1.2.3) continues to play an important role in the diagnosis and risk stratification of medulloblastoma. Currently no mouse model for Group 4 MB has been reported. Although Group 4 tumours make >30% of all MBs, the molecular pathogenesis of this tumour subtype is the least understood, highlighting the need of further studies to clarify the pathogenesis of this subgroup.

1.2.6.5 Adult MB

SHH tumours make up to two-thirds of cases in adults, while Group 3 tumours are exceptionally rare (Remke, Hielscher et al. 2011). SHH MBs are extensively studied, and small molecules (GDC-0449) targeting smoothened (SMO) have been shown to be temporarily highly effective against SHH MBs (Rudin, Hann et al. 2009; Yauch,

Dijkgraaf et al. 2009). As the cerebellar development in adults is complete, targeting the molecular pathways involved in the normal cerebellum development may cause less toxicity in adults, making them an attractive cohort for molecular-targeted therapies. However there are still doubts about the degree of molecular and clinical similarities between adult and paediatric MBs. Some studies suggest a distinct molecular profiles and clinical behavior between the two tumour groups (Tabori, Sung et al. 2005; Tabori, Sung et al. 2006; Korshunov, Remke et al. 2010) . The transcriptomic differences between adult and paediatric patients defined under same subgroups have yet to be studied in detail.
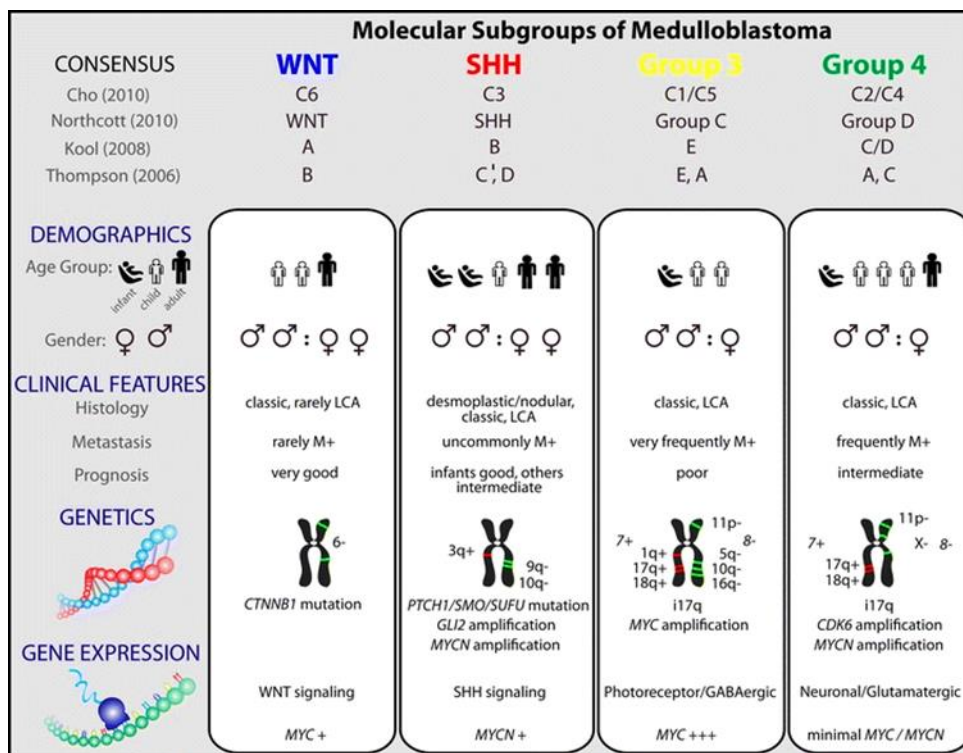
Fig. 1.5 Comparison of different molecular subgroup of MB

Comparison of demographics, clinical features, genetics and expression profiles of the four major MB subgroups defined by the consensus conference. The affiliations of previously published papers on MB molecular subgrouping (prior to consensus) is mentioned on top. The terminology used to classify the subgroups by respective publication is mentioned (Eg. Consensus Group 4 was referred to as Group D by Northcott et al, 2010). This picture is reproduced from an open access article from Springerlink.com, with licence permitting any non-commercial use. Ref: Taylor M.D et al. *Acta*

Table 1.4 List of immunohistochemical markers being defined for different MB subgroup association*

Subgroup	Immunohistochemical marker suggested (pending further validation).
WNT	CTNNB1 (nuclear), DKK1
SHH	SFRP1, GLI1, GAB1
WNT/SHH	FILA, YAP1
Group 3	NPR3
Group 4	KCNA1
Group 3/Group 4	FSTL5

* Ref. Taylor et al. *Acta Neuropathol*, 2011.

1.3 BMI1 gene

The *BMI1* (B lymphoma Moloney murine leukaemia virus Insertion region 1) gene was first isolated as an oncogene that cooperates with c-*myc* in the generation of mouse lymphomas through repression of tumour suppressor Cdkn2a or ink4a/Arf (Haupt, Alexander et al. 1991; van Lohuizen, Verbeek et al. 1991). Subsequently *Bmi1* was identified as a transcriptional repressor belonging to the Polycomb group of genes in the vertebrates (van Lohuizen, Frasch et al. 1991; Alkema, van der Lugt et al. 1995; Jacobs, Kieboom et al. 1999; Jacobs, Scheijen et al. 1999). The gene (located on chromosome 10p in humans and 2 A3 in mice) encodes for a highly conserved nuclear protein with 326 amino acid sequence (mass of 37 kD) that contains a zinc-finger motif, and is closely related to other zinc-finger proteins such as *Mel-18* (Tagawa, Sakamoto et al. 1990). BMI1 (protein) is a component of the Polycomb group (PcG) multi-protein complex and is also known as Polycomb group RING finger protein 4 (PCGF4).

1.3.1 Polycomb group (PcG) proteins

The PcG proteins are chromatin-modifying complexes that are essential for embryonic development. They were originally identified in the fruitfly *Drosophila melanogaster*, as a repressor of Hox (homeobox) genes (Ringrose and Paro 2004), which define the position of structures and appendages along the anterior-posterior axis of the adult body. The name 'Polycomb' was introduced as mutation in these genes led to additional sex combs in the developing *Drosophila* embryo (Sparmann and van Lohuizen 2006). This function of PcG proteins is essentially conserved in vertebrates (including humans), with mutations leading to skeletal malformations (Akasaka, Kanno et al. 1996). At molecular level, PcG proteins are classified into two groups, termed Polycomb repressive complexes (PRCs) – 1) PRC 2 initiation complex (E.g. EED, EZH1), and 2) PRC1 maintenance complex, which contain core components such as Polycomb (PC), Polyhometoic (PH), really interesting new gene (RING) and Posterior sex combs (PSC). The best characterised members of the PRC1 complex in humans are BMI1 and RING1 (containing RING finger protein domain), CBX2 (containing chromodomain), and EDR1 (containing Zinc finger SPM domain). PRC2 is responsible for trimethylation of lysine 27 and lysine 9 of histone H3 (H3K27 and H3K9me^3 respectively) and deletion of PRC2 member genes in mice has shown to result in early embryonic lethality, highlighting their importance in development (Schumacher, Faust et al. 1996; O'Carroll, Erhardt et al. 2001). PRC1 acts via chromatin remodelling and modification of histones, and is able to recognise H3K27me^3 mark through the chromodomain of PC. In addition, PRC1 possesses ubiquitin E3 ligase activity that targets H2AK119 (monoubiquitinates nucleosomal histone H2A at lysine 119), which is associated with gene repression (Wang, Wang et al. 2004). However the PRC core components are thought to assemble into

various distinct sub-units depending on the cellular functional context (Otte and Kwaks 2003). Although the role of PRCs in epigenetic gene silencing is well recognised, the precise molecular mechanisms of PRC-mediated repression are still poorly understood (Sparmann and van Lohuizen 2006).

1.3.1.1 Role of PcG in cancer

The first association of PcG with cancer came from functional characterisation of BMI1 (discussed below), which is one of PcG protein most strongly associated with neoplastic development (Sparmann and van Lohuizen 2006). Other PcG members associated with cancer are SUZ12 (overexpression) in colon and breast cancer (Kirmizis, Bartley et al. 2003), and EZH2 (overexpression) in lymphoma, prostate and breast cancer (van Kemenade, Raaphorst et al. 2001; Varambally, Dhanasekaran et al. 2002; Kleer, Cao et al. 2003). Interestingly, an extranuclear/cytosolic role of EZH2, influencing cell adhesion and migration, thereby contributing to the metastatic capacity of the tumour cells has been described (Su, Dobenecker et al. 2005). Bracken et al. have shown [by chromatin immunoprecipitation (ChIP) and genome-wide screenings to identify PcG target genes in human fibroblast cells] that the PRC complex could contribute to cancer development by specifically silencing tumor-suppressor genes by DNA methylation (Bracken, Dietrich et al. 2006). In relation to this, they have also found an inverse correlation between the expression levels of the PcGs, *EZH2, SUZ12,* and *BM11,* and the target genes *MT1G, HOXA5,* and *RARB* in breast cancer.

Stem cells are defined as cells that have the ability to extensively self-renew and to differentiate into progenitors. In addition to transcriptional repression of tumour suppressor genes, there is evidence that PcGs might influence tumour development

through modulation of stem cells (Valk-Lingbeek, Bruggeman et al. 2004). This is strengthened by the results demonstrating that PcGs maintain stem cell state (or stemness) by repression of alternative lineages genes necessary for differentiation (Boyer, Plath et al. 2006; Lee, Jenner et al. 2006). Moreover, there are results highlighting that stem cell fate is in part governed by the PcG genes, one of the first indications coming from *Bmi1*-deficient mice, which show loss of hematopoietic cells and cerebellar neurons (van der Lugt, Domen et al. 1994). An RNA expression signature associated with 'stemness', based on BMI1-driven transcriptional changes was predicted to have poor treatment outcome in patients with different types of cancer (Glinsky, Berezovska et al. 2005).

1.3.2 Bmi1 in cerebellar development

Bmi1 is essential for maintenance and self-renewal of haematopoietic and neural stem cells (Richie, Schumacher et al. 2002; Molofsky, Pardal et al. 2003). In fact, targeted deletion of *Bmi1* in a mouse model (null mutant) causes severe neurological and haematopoietic defects (van der Lugt, Domen et al. 1994). Origin and fate of cerebellar granule cell precursors (GNPs) during the development of the cerebellum have been discussed before (section 1.1.2.3.2). Leung et al. have shown that Bmi1 is expressed in the EGL precursors during embryonic (E16.5 in mouse and 26 gestational week in human) and early postnatal (P8 in mouse, 2 months in human) development of the cerebellum (Leung, Lingbeek et al. 2004). In addition, they demonstrated that postnatal mice with targeted Bmi1 deletion (Bmi1-/-) showed reduced brain mass and developed cerebellar signs/symptoms (ataxia, balance disorders and behavioural changes) due to phenotypic changes in cerebellum. The cerebellar phenotypes included reduced cellularity in the granular and molecular

layers, reduced Math-1 positive EGL precursors and wider expression of postmitotic marker p27 at P1. There was also reduction in BrDU incorporation (indicating reduced proliferation), and an increase in apoptosis in the EGL at P8. They also noted reduction in cell density and size of the internal granular layer (IGL) at P15 (Leung, Lingbeek et al. 2004). Bmi1 is expressed in the EGL as well as in the ventricular zone neuroepithelium from E16.5 onwards, but it has been shown to be involved mainly in postnatal GNP proliferation.

There is a peak of proliferation of GNPs in the EGL during early post-natal development, induced by Shh secreted by Purkinje neurons (Dahmane and Ruiz i Altaba 1999; Wechsler-Reya and Scott 1999). The GNPs later differentiate and migrate inwards past the molecular layer (ML) to reach their final destination, IGL (Wang and Zoghbi 2001). Studies have demonstrated that addition of Shh *in vitro* induced proliferation in cerebellar granule cells [CGCs] (Dahmane and Ruiz i Altaba 1999; Wechsler-Reya and Scott 1999). Leung et al. have further shown that Bmi1 is upregulated in response to Shh treatment in CGCs in a similar fashion as Gli1, Sufu and cyclin D2, indicative of Shh pathway activation (Leung, Lingbeek et al. 2004).

1.3.2.1 Bmi1 is a downstream target of Shh pathway

The results described above suggest that Bmi1 is a downstream target of Shh pathway. The pathway has been briefly discussed in section 1.1.2.3.2 and is diagrammatically represented in Fig 1.6. Further evidence supporting this is discussed here.

Bruggeman et al. have later confirmed that the process of GNP proliferation in the EGL is linked to Bmi1 as a downstream target of the Shh pathway (Bruggeman, Valk-Lingbeek et al. 2005). They show that Ink4a and to a lesser extent Arf

expression is increased in Bmi1-/- GNPs and cerebella. The Ink4a/Arf locus is located on chromosome 9, comprising two genes with overlapping reading frames, encoding tumour suppressors p16INK4a (inhibitor of cyclin dependent kinase 4) and p19ARF (alternate reading frame, p14ARF in humans), both of which play an important role in regulating cell, growth, survival and senescence (reviewed in Sharpless and DePinho 1999). They demonstrated that stimulation of GNPs with Shh led to Bmi1 protein expression, and a concomitant down-regulation of both Ink4a and Arf mRNA expression. This was consistent with the notion of Bmi1 mediates regulation of Ink4a/Arf by Shh. Jacobs et al. have demonstrated that removal of Ink4a/Arf partly rescued the cerebellar (and lymphoid) defects seen in Bmi1-/- mice (Jacobs, Kieboom et al. 1999), indicating that ink4a/Arf is a critical in vivo target for Bmi1. This also connects transcriptional repression role of Bmi1 (a PcG protein) with cell-cycle control and senescence.

Kenney et al. have shown that N-Myc is a direct downstream target of the canonical Shh pathway regulating GNP proliferation (Kenney, Cole et al. 2003). They demonstrate that Shh stimulation directly induces *N-myc* in GNPs and that *N-myc* is expressed in proliferating GNPs. They also observed that when N-myc is upregulated in GNPs, Cyclin D1 protein expression was maintained (which was abolished by Shh inhibitor cyclopamine treatment), despite treatment with the Shh inhibitor cyclopamine. Other studies have also shown that proliferation of GNPs in vitro can be induced by Shh and that it induced *N-myc and cyclin D1* [and cyclin D2] (Ciemerych, Kenney et al. 2002; Knoepfler, Cheng et al. 2002). In keeping with the above results, Bruggeman et al. show that Bmi1-/- GNPs are only partially responsive to Shh (Bruggeman, Valk-Lingbeek et al. 2005), and propose a model in

which Shh controls proliferation in these cells via an alternate, i.e. N-Myc/Cyclin D2 mediated route.

Valk-Lingbeek et al reviewed the potential link between Shh signalling and Bmi1 suggesting a novel regulatory pathway of external morphogen interacting with cell-intrinsic epigenetic pathway controlling cell fate programs (Valk-Lingbeek, Bruggeman et al. 2004). In this model, Bmi1, induced by Gli1, negatively regulates the Ink4a/Arf locus. This locus encodes the cell cycle regulators/tumor suppressors p16Ink4a and p19Arf (p14ARF in humans). p16Ink4a impacts on Rb (retinoblastoma) regulation via inhibition of cyclin D/cyclin dependent kinase complexes. The pRb (hypophosphorylated Rb) sequesters E2F transcription factors and repress their target genes - leading to a cellular context dependent cell cycle arrest, senescence or apoptosis (reviewed in (Sharpless and DePinho 1999)). p19Arf binds MDM2 and inhibits p53 transcription factor degradation which results in activation of its target genes - leading to cell cycle arrest and apoptosis (reviewed in (Lowe and Sherr 2003)).
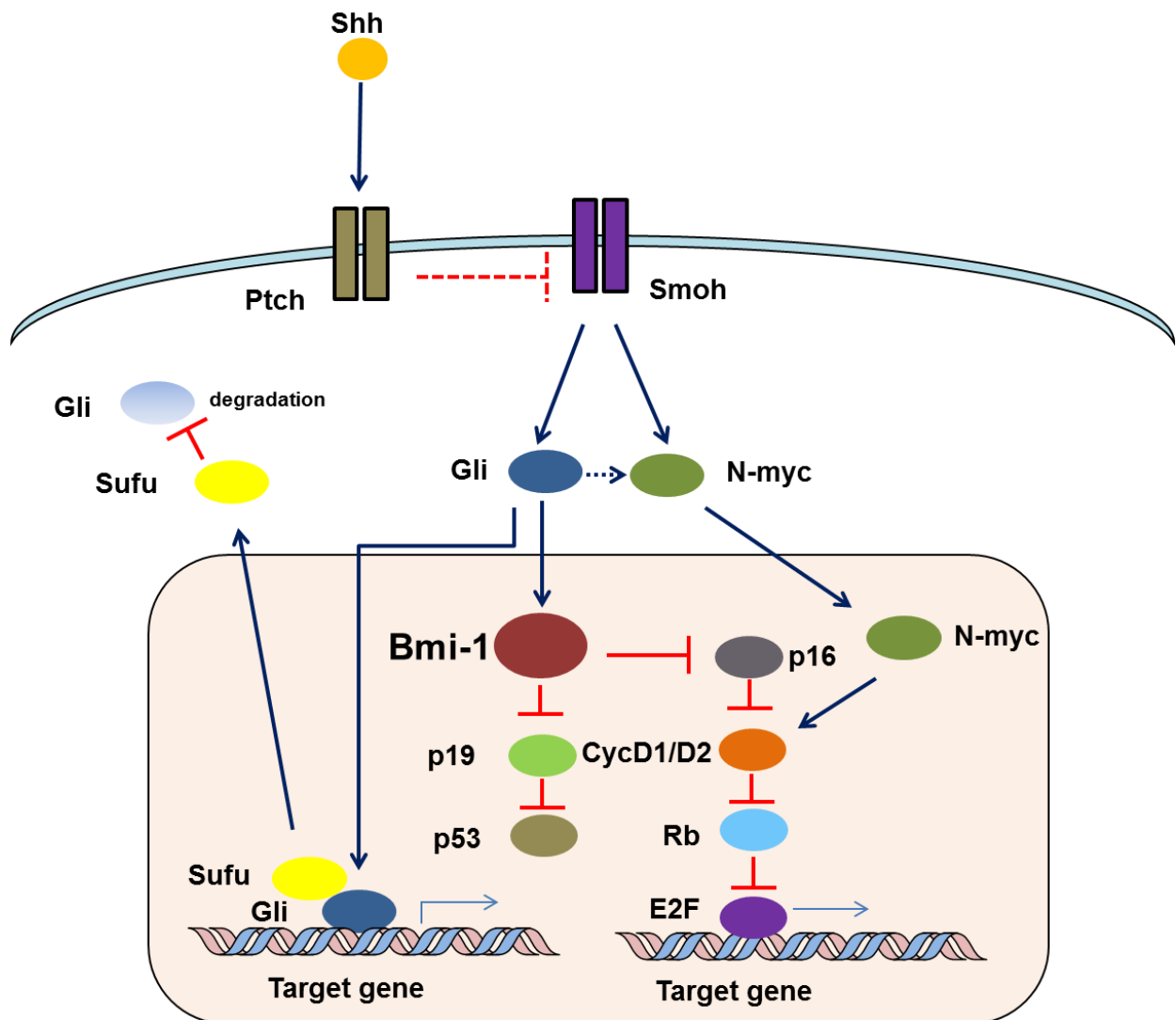
Fig. 1.6 Diagrammatic representation of Shh pathway in cerebellar granule cell progenitor development.

Bmi1 as a downstream effector of Shh signalling is highlighted here, thus indicating that Bmi1 is required for proliferation and/or self-renewal of cerebellar progenitor cells, in association with N-myc. Abbreviations: Shh, Sonic Hedgehog; Ptch, Patched; Smoh, Smoothened.

1.3.3 The role of Bmi1 in medulloblastoma pathogenesis

In agreement with Bmi1 being associated with GNP proliferation during cerebellar development as discussed above, there is ample evidence that Bmi1 is implicated in pathogenesis of medulloblastoma. Leung et al., demonstrated higher BMI1 expression in three human MB cell lines and twelve primary human medulloblastoma

samples, when compared to normal cerebellum (Leung, Lingbeek et al. 2004). Furthermore, in their study, BMI1 overexpression correlated well with overexpression of PTCH and SUFU, suggesting that there is SHH pathway activation in BMI1-overexpressing MB. As they also observed BMI1 overexpression in the fraction overexpressing N-MYC, they suggest that BMI1 is not a target for N-MYC. In another study, Northcott et al. observed greater than two fold BMI1 expression in more than 80% of the MBs as compared to normal foetal cerebellum (Northcott, Nakahara et al. 2009).

Michael et al., have demonstrated 100% MB formation between P14 and P26 in a transgenic mouse model, SmoA1, expressing an oncogenic Hedgehog effector, (Michael, Westerman et al. 2008). However, they did not detect MB in any of the SmoA1 crossed to Bmi1-/- mice, but only small ectopic cell collections in the regions, suggesting that the tumours were initiated but did not undergo expansion. They also detected alterations in proliferation and apoptosis in the ectopic cells of SmoA1;Bmi1-/-, which were associated with reduced Cyclin D1 and elevated expression of p19Arf. These results suggest that Bmi1 is required for progression and maintenance of MB and implicate Bmi1 as a key factor in SHH pathway driven tumour pathogenesis (Michael, Westerman et al. 2008)

Wiederschain et al., have demonstrated in a human MB cell line that shRNA-mediated BMI1 (and Mel-18) knock down resulted in their inhibition of proliferation, loss of clonogenic survival and anchorage-independent growth in vitro (Wiederschain, Chen et al. 2007). They also show that BMI1 knock down led to suppression of tumour formation in vivo. Furthermore, gene expression analysis identified a number of cancer-relevant pathways that may be controlled by BMI1

(and Mel-18). Altogether, this study highlights the importance of BMI1 (and Mel-18) in cancer cell growth (Wiederschain, Chen et al. 2007).

Recently, Wang et al. have demonstrated the functional relevance of BMI1 as downstream target of SHH pathway in human medulloblastoma context (Wang, Venugopal et al. 2012). They show that BMI1 expression positively correlated with SHH ligand concentrations when stem cell-enriched populations from medulloblastoma cell lines and primary medulloblastoma samples were treated with SHH ligand and SHH antagonist, cyclopamine. By Chromatic Immunoprecipitation (ChiP) assay they show that SHH pathway affector GLI1 preferentially binds to the *BMI1* promoter, and that *BMI1* transcript levels increased or decreased when *GLI1* was overexpressed or downregulated respectively. Furthermore, by knockdown experiments of *BMI1* in vitro and in vivo, they demonstrated that Shh signalling not only drives BMI1 expression, but a feedback mechanism exists wherein downstream effectors of BMI1 may, in turn activate SHH pathway genes. These data implicate SHH and BMI1 as mutually indispensable pathways in medulloblastoma maintenance, and correlates well with the previous evidence of Bmi1 as a downstream effector of Shh pathway seen in the context of GNP proliferation.

Manoranjan et al., have shown that BMI1 is essential for self-renewal and tumorigenicity of MB stem cells. In addition to demonstrating that BMI1 knock down reduced in vitro self-renewal capacity, they show that overexpression of BMI1 (and FOXG1) in CD15+ MB stem cells, generated much larger and more infiltrative tumours *in vivo*, compared to controls xenografts (Manoranjan, Wang et al. 2013).

1.3.3.1 The role of Bmi1 in Group 4 medulloblastoma

Bmi1 is expressed at high levels in human and mouse proliferating GNPs, and at low levels in postmitotic granule cells and in adult cerebellum. As Bmi1 is viewed as a downstream effector of Shh pathway in relation to GNP proliferation and MB pathogenesis (as discussed above), it can be hypothesised that BMI1 expression would be enriched in MB tumours driven by SHH pathway mutation (i.e. SHH subgroup). However contrary to this expectation, emerging evidence show that although BMI1 overexpression is found across all subgroups, it is most highly expressed in Group 3 and Group 4 (i.e. Non-SHH/WNT subgroup) tumours.

Wang et al., having analysed the MB dataset derived from exon array profiling (Northcott, Korshunov et al. 2011), show that BMI1 is overexpressed across all MB subgroups (compared to normal foetal and adult cerebellum) , but their levels were highest in the aggressive subtypes – Group 3 and Group 4 MB (Wang, Venugopal et al. 2012). Similarly, Manoranjan et al., having probed four of the existing transcriptional databases [Boston (Cho, Tsherniak et al. 2011), Amsterdam (Kool, Koster et al. 2008), Toronto (Northcott, Korshunov et al. 2011), and Memphis (Thompson, Fuller et al. 2006)), of MB for differential stem cell gene expression patterns in the subgroups identified BMI1 (and FOXG1) as being preferentially expressed in non-Shh/Wnt MBs.

Behesti et al. analysed BMI1and TP53 expression in a data set derived from 103 primary human MBs and 14 normal cerebella. They observed BMI1 overexpression in 54% of tumours, relative to median foetal cerebellar levels of expression, which occurred across all subgroups of MB. However, BMI1 was found to be most highly expressed in Group 4 (with >3-fold compared to median of foetal cerebellar expression), followed by Group 3 (>1.93-fold), SHH (>1.92-fold) and WNT (>1.60-fold) subgroups (Behesti, Bhagat et al. 2013). They also observed a statistically

significant enrichment of Group 4 MB across tumours expressing higher levels of BMI1 and low levels of TP53. These results are interesting as it was seen that MB formation could not be initiated by Bmi1 overexpression alone in mice, and raises the possibility that this combination of mutations plays a role in the pathogenesis of Group 4 human MBs.

1.3.4 The role of Bmi1 in systemic carcinogenesis

Bmi1 is ubiquitously expressed in almost all tissues, but it is higher in the brain, spinal cord, kidney, gonads, lungs and placenta. Many studies have shown that Bmi1 is frequently upregulated in various types of human cancers, including lung cancer, ovarian cancer, acute myeloid leukemia, nasopharyngeal carcinoma, breast cancer, neuroblastoma and gliomas (reviewed in (Jiang, Li et al. 2009)). As with MB, BMI1 is generally associated with aggressive human cancers. Its association is known for its principal role in regulating cancer cell proliferation and senescence via suppression of p16Ink4a/p19Arf tumour inhibitor pathways (Jacobs, Kieboom et al. 1999; Jacobs, Scheijen et al. 1999; Meng, Luo et al. 2010). However, studies investigating the role of Bmi1 in cancer cell migration and invasive properties have also emerged. Bmi1 is shown to induce epithelial-mesenchymal transition (EMT) in human nasopharyngeal carcinoma (Song, Li et al. 2009). Suppression of endogenous Bmi1 has been shown to reduce cell motility and invasive properties in breast cancer cells (Guo, Feng et al. 2011) and in gliomas cells (Jiang, Wu et al. 2012). Due to its role in cancer stem cell maintenance and self-renewal (Park, Qian et al. 2003), Bmi1 has attracted attention as a potential target for cancer therapy.

BMI1 has been associated with other mechanisms essential to promote EMT and tumour initiating capabilities such as Twist1 (Yang, Hsu et al. 2010) and PTEN

(Song, Li et al. 2009). BMI1 is known to be transcriptionally regulated by a number of factors including SALL4, c-Myc, E2F-1, HDAC, Mel-18 and FoxM1 (reviewed in (Cao, Bombard et al. 2011)).

1.4 Bone Morphogenetic Proteins and their role in medulloblastoma pathogenesis

Bone Morphogenetic Proteins (BMPs) are multi-functional growth factors that belong to and form the largest group of the Transforming Growth Factor Beta (TGF-β) superfamily. TGF-β family of polypeptides are known to control cellular functions that underwrite embryonal development and tissue homeostasis, which act by modifying the expression of their target genes (reviewed in (Massague and Chen 2000)). BMP and TGF-β signaling pathways seem to act synergistically on various biological processes (Miyazono, Maeda et al. 2005). The activity of BMPs was first identified in 1960s while studying the process of bone induction (Urist 1965), but it was not until they were purified and sequenced in 1980s that they were recognised as proteins responsible for bone induction [and hence the nomenclature] (Wozney, Rosen et al. 1988; Luyten, Cunningham et al. 1989).

1.4.1 BMP signalling pathway

Around twenty different members of BMP family have been characterised in humans so far (reviewed in (Chen, Zhao et al. 2004)). Due to their association with medulloblastoma (discussed below), BMPs that are important and relevant to this project are BMP-2 (gene encoding this, *BMP2* is located on chromosome 20p), BMP-4 (chromosome 14q) and to some extent BMP-7 (chromosome 20q). The BMP signal is mediated through serine/threonine kinase receptors, which are Types I and II, with further subtypes. Three Type I receptors have been shown to bind to BMP ligands – i) BMPR (BMP receptor) IA, also known as ALK-3, ii) BMPR-IB or ALK-6, and iii) ActR-IA (type IA activin receptor) or ALK-2 (ten Dijke, Yamashita et al. 1994). Three Type II receptors have also been identified which bind to BMPs, namely i)

BMPR-II, ii) ActR-II, and iii) ActR-IIB (Rosenzweig, Imamura et al. 1995). While BMPR-IA, IB and II are specific to BMP ligands, the rest of the receptors bind to Activins too. Both Type I and II receptors are essential for signal transduction, and these receptors are expressed differentially in various tissues. Following ligand binding, they form a heterotetrameric, transphosphorylated (activated) receptor-complex comprising pairs of Types I and II receptors [Fig 1.7] (Moustakas, Pardali et al. 2002).

The signalling cascade is mediated through SMAD (homologue of mothers against decapentaplegic, MAD) proteins. Briefly, SMAD family members are intracellular proteins involved with TGF-β signal transduction, and comprise of Receptor – regulated SMADs (R-SMADs, SMAD2/3 and SMAD1/5/8), common partner SMADs (co-SMADs, SMAD4) and inhibitory SMADs [I-SMADs, SMAD6/7] (reviewed in (Miyazono, ten Dijke et al. 2000)). R-SMADs are anchored to the cell membrane. Upon BMP receptor complex activation, R-SMADs are phosphorylated (pSMADs) and form oligomeric complexes with co-SMADs (SMAD4).

The BMP receptors phosphorylate SMAD1, 5 and 8 (to form pSMAD1,5,8) in a ligand-dependent manner, and this is thought to be a reliable indicator of BMP pathway activation (Hoodless, Haerry et al. 1996; Chen, Bhushan et al. 1997; Nishimura, Kato et al. 1998; Grimmer and Weiss 2008). The pSMAD and SMAD4 oligomeric complexes then translocate into the nucleus, where they regulate the transcription of their target genes by direct binding to DNA, interaction with various DNA-binding proteins, and recruitment of transcriptional co-activators or repressors. The BMP signalling pathway is represented in Fig 1.7.
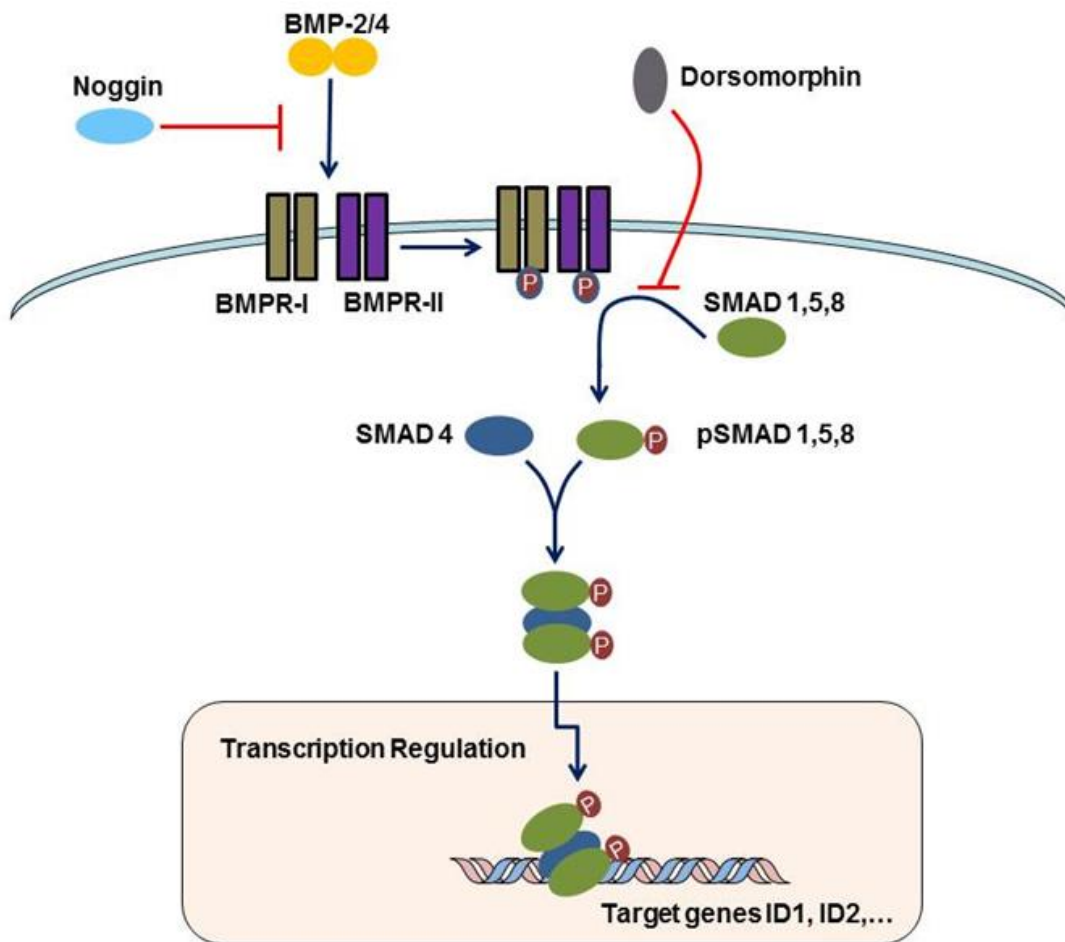
Fig. 1.7 BMP - SMAD signalling pathway.

Upon BMP ligand stimulation, the BMP receptors (BMPR Types I and II) are activated by phosphorylation. In turn, these receptors phosphorylate intracellular receptor-regulated SMAD proteins (pSMADs). The pSMADs form a complex with SMAD4 (co-SMAD) and the complex translocates into the nucleus to act as transcriptional regulators on target genes. Noggin and Dorsomorphin are some of the BMP pathway inhibitors. This is a simplified structure of the pathway and highlights only BMP-2/4 mediated signalling via SMAD1,5,8.

The target genes of BMP pathway are numerous and variable (reviewed in (Miyazono, Maeda et al. 2005)). Among the target genes, *Id* (inhibitor of differentiation or inhibitor of DNA binding, Id1-4) are known to be one of the most important targets of BMP (Ogata, Wozney et al. 1993). Peng et al. have revealed by expression profiling analysis, that the most significantly upregulated (target) genes

upon BMP-2 (and BMP-6 or BMP-9) stimulation are *Id1, Id2*, and *Id3* (Peng, Kang et al. 2004). Other target genes induced by BMP-2/BMP-4 include *TEIG-1* (TGF-B-early inducible gene 1), *Msx1*, *GATA2* and *Snail* (Miyazono, Maeda et al. 2005). Since the I-SMADs, induced by the TGF-beta superfamily proteins, inhibit the BMP receptor mediated signalling, they are thought to have an auto-inhibitory signalling role. The functions of SMADs can also be regulated by other signalling pathways, such as the MAP kinase pathway. SMADs interact with and modulate the functions of various transcription factors which are downstream targets of other signalling pathways.

1.4.2 Functional relevance of the BMPs/BMP pathway

BMPs play an important role in embryonic development as well as in regulation of post-natal cellular functions. Their best characterized roles include regulation of lineage commitment, differentiation, proliferation, patterning or morphogenesis, cellular maintenance/survival and apoptosis (Hogan 1996). With regards to bone development, they are known to be involved in intramembranous and endochondral bone formation, as well as cartilage formation (Reddi 1981; Wozney and Rosen 1998). BMPs are known to have broad roles in regulating the biology of stem cells and in maintaining embryonic stem cells (Varga and Wrana 2005). With regards to the role of BMPs in cancer, there are contradictory reports in different cancers. Thawani et al., have published a literature review after evaluating MEDLINE, EMBASE and Cochrane databases, and conclude that there is no definitive association between BMPs and the promotion of tumorigenesis or metastasis (Thawani, Wang et al. 2010). Few examples of the contradictory reports on the role of BMPs in cancers include: BMP-2 and/or BMP-4 were shown to promote

tumorigenesis and metastasis in breast carcinoma (Raida, Clement et al. 2005), lung carcinoma (Langenfeld, Calvano et al. 2003), prostate cancer (Ye, Lewis-Russell et al. 2007), ovarian cancer (Shepherd, Theriault et al. 2008), osteosarcoma (Arihiro and Inai 2001) and medulloblastoma (Iantosca, McPherson et al. 1999) but they were also shown to have the opposite effects on same cancers, in different studies [using different models of study] (Soda, Raymond et al. 1998; Zhao, Ayrault et al. 2008). Similarly the roles of other BMPs such as BMP-6, BMP-7 and BMP receptors (BMPR Types I/II) are also shown to have contradictory roles in different cancers (reviewed in (Thawani, Wang et al. 2010).

From the above evidence, we feel that the role of different BMPs in each cancer should be considered and interpreted individually.

1.4.3 BMPs in cerebellar development

During cerebellar development the BMPs, in particular, BMP-2 and BMP-4 inhibit SHH-induced GNP proliferation, resulting in GNP differentiation, whereas BMP7 has the opposite effect (reviewed in (Behesti and Marino 2009)).

It is shown that BMPs induced Math1 expression and that BMP-treated GNPs formed mature granule neurons upon transplantation into early postnatal cerebellum (Alder, Lee et al. 1999). The above evidence highlights the role of BMPs in fate specification of GNPs. Expression of BMP-4 and Smad1 have been demonstrated in the EGL of rat cerebellum at early postnatal stages, and BMP-4 was shown to promote neuronal and astroglial differentiation of cerebellar cell cultures, suggesting that BMP-4 (via SMAD1 signalling) participate in regulating postnatal cerebellar differentiation (Angley, Kumar et al. 2003). Rios et al. have shown using mouse and chick embryos, that BMP-4 (in EGL), to a lesser extent BMP-2 (in IGL) and BMP-7

(in Purkinje cells, which also produces Shh) are expressed in the developing cerebellar cortex (Rios, Alvarez-Rodriguez et al. 2004) . Furthermore they demonstrate that BMP-2 and BMP-4, significantly antogonised Shh-induced GNP proliferation *in vitro* and *ex vivo*, with a slightly opposite effect with BMP-7, and that BMP-2 mediated GNP differentiation via Smad5 signalling. Later in a separate study they also showed that BMP-2 antagonizes Shh-dependent proliferation by expressing TIEG-1 which directly represses *N-myc* transcription (Alvarez-Rodriguez, Barzi et al. 2007). Zhao et al. have shown that BMPs antagonize Shh-dependent proliferation and induce differentiation of GNPs (Zhao, Ayrault et al. 2008). Furthermore they demonstrate that BMP treatment led to downregulation of Atoh1/Math1 protein, and that this occurred in a post transcriptional manner.

Recently, our group have demonstrated that Bmi1 controls cellular interactions between granule and glial progenitors during cerebellar development through repression of the BMP pathway (Zhang, Santuccione et al. 2011).

1.4.4 BMPs are potential targets for medulloblastoma treatment

In keeping with the above discussion regarding the role of BMPs in inhibiting GNP proliferation and induction of differentiation, there is emerging evidence to suggest that BMPs, in particular BMP-2 and BMP-4, inhibit medulloblastoma growth (reviewed in (Roussel and Hatten 2011)).

Math1/Atoh1 has been demonstrated to be essential for MB development (Flora, Klisch et al. 2009), and has been shown to collaborate with Gli1 to transform normal GNPs into tumor initiating cells (Ayrault, Zhao et al. 2010). Gene profiling of mouse and human MBs with a constitutively activated SHH pathway revealed that most

genes within the BMP signalling pathway are downregulated in tumours compared to proliferating GNPs and neurons, whereas Math1/Atoh1 levels were high (Zhao, Ayrault et al. 2008). Moreover, in addition to showing that BMPs inhibit (Shh-dependent) proliferation and induction of differentiation of GNPs and GNP-like MB cells, they show that BMP-2 and BMP-4 suppress primary murine MB cell growth *in vivo* (Zhao, Ayrault et al. 2008). GNP-like tumour cells from the murine MBs were infected with retroviral vectors co-expressing human *BMP4* and tumour allografts were generated using athymic mice. They observed a smaller tumour size among *BMP4* co-expressing tumours compared to controls. Importantly, they also observed that the tumour allografts failed to grow when the cells were pre-treated *in vitro* with BMP-4 (for 3 days), whereas allografts of untreated cells grew quickly. In this study they also go on to demonstrate that BMP-4 and cyclopamine (Shh inhibitor) treatment in combination, achieved tumour inhibition at lower concentrations as compared to treatment with either method alone, suggestive of potential therapeutic role of BMP agonists.

Hallahan et al., have demonstrated that retinoids [all-*trans* retinoic acid (ATRA), RAR-α agonist (AGN195183) or RAR-β/γ agonist (tazarotene)] induced a significant apoptosis in seven of nine (77%) primary human medulloblastoma cells compared to vehicle only treatment. The two with no significant apoptosis were of large cell type and showed neuronal differentiation in response to retinoids (Hallahan, Pritchard et al. 2003). Gene expression array of human MB cell lines treated with retinoids revealed that BMP-2 was one of the small set of genes (related to apoptosis) that were induced in retinoid-sensitive cells only. BMP-2 is known to be a mediator of retinoid-induced apoptosis in several developmental paradigms

(Rodriguez-Leon, Merino et al. 1999) and it is known to induce apoptosis in myeloma cells (Kawamura, Kizaki et al. 2000). Retinoid treatment (ATRA) increased BMP-2 expression in primary MB cells, and furthermore, addition of BMP-2 resulted in significant apoptosis of primary MB cells and cell lines in a time and dose dependent manner. The above observations support the notion that BMP-2 mediates retinoid-induced apoptosis in medulloblastoma (Hallahan, Pritchard et al. 2003). In this study they also show that BMP antagonist noggin blocked both retinoid and BMP-2 induced apoptosis and that BMP-2 induced p38 mitogen-activated protein kinase (MAPK), which may be necessary for BMP-2 and retinoid-induced apoptosis in MB. This was the first study to show that BMP-2, as a secreted protein mediates apoptosis in medulloblastoma cells that express or do not express BMP-2

Similar to the above study, Spiller et al., used human MB cell lines and genetically engineered mouse models to show that 13-cis Retinoic acid in combination with suberoylanilide hydroxamic acid (SAHA, a histone deacetylase inhibitor), induced BMP-2 mediated MB apoptosis (Spiller, Ditzler et al. 2008). They observed a 3-fold increase in BMP-2 transcription when Retinoic acid (RA) was added to the MB cell (D283) culture and 7-fold with both agents. Although the induction of p38 MAP kinase partially blocked the apoptotic activity of RA alone, there was no inhibition of RA + SAHA activity, indicating a separate mechanism for SAHA mediated apoptosis. Furthermore, the tumour cell graft in athymic mice showed a slower growth when orally treated by RA + SAHA, compared to single drug controls. In addition, tumours arising in the background of ND2:SmoA1 mice treated with RA + SAHA + cisplatin showed a 4-fold increase in apoptosis over controls. Retinoic acid acts by transcriptionally activating BMP-2 and SAHA facilitates transcriptional activity

through chromatin accessibility. Both drugs cross the blood brain barrier, have been given safely to children, and achieve brain concentrations that are at or near therapeutic levels (Miller 1998; Spiller, Ravanpay et al. 2006).

In the context of a different aggressive brain tumour, but related to BMPs, Piccirillo et al., show that BMPs, amongst which BMP4 had the strongest effect, trigger a significant reduction in the stem-like, tumour-initiating precursors of human glioblastomas [GBMs] (Piccirillo, Reynolds et al. 2006). Even transient *in vitro* exposure to BMP-4 rendered the GBM cells incapable of generating *in vivo* tumours. Importantly, in vivo delivery of BMP-4 effectively blocked the tumour growth in intracerebral grafted mice. They demonstrate that BMPs acted through SMAD signalling cascade and in vitro they led to reduced proliferation, increased differentiation and reduced clonogenic ability.

The above evidence is suggestive that BMPs (or BMP analogues/ agonists/activators) could represent therapeutic targets in the development of novel drugs for the treatment of aggressive brain tumours including medulloblastoma. In a recent study, Vrijens et al., have reported identification of small molecule activators of BMP signaling (Vrijens, Lin et al. 2013). Using a BMP-responsive clone C33A-2D2, they have screened a bioactive library containing approximately 5,600 small molecules. They have identified four small molecules of the flavonoids family, two of which (isoliquiritigenin and 4'hydroxychalcone) induced phosphorylation of SMAD1/5 and Id1/Id2 expression in a dose-dependent manner. Although the suitability of these molecules for treatment is yet to be established, they support the notion that

BMPs/BMP pathway could be targets for the treatment of MB in the foreseeable

future.

1.5 Hypothesis and aims of the study

1.5.1 Hypothesis

In this project, we want to test the hypothesis that:

Repression of the BMP signalling pathway through BMI1 is an essential event in human medulloblastoma pathogenesis, potentially through deregulation of cell adhesion and of cell-cell or cell-extracellular matrix interactions, and that BMI1 expression could be a potential bio-marker for the identification of MB which could profit from treatment with BMP analogues.

1.5.2 Aims

This aims of this study are:

i) To analyse the impact on the BMP pathway of *BMI1* downregulation in MB cell lines and in primary human MB cells of Group 4,

ii) To study any functional changes in particular those related to cell adhesion or cell migration properties *in vitro* and in an ex vivo organotypic cerebellar co-culture model

iii) To study the effects of *BMI1* downregulation in primary human MB cells on BMP pathway *in vivo* in a xenograft model

iv) To use primary human MB tumour samples to assess any correlative expression of BMI1 and BMP pathway activation

CHAPTER 2 General Materials and Methods

2.1 Production of lentivirus vector for shRNA delivery

Stable BMI1 gene silencing (knock down) in MB cells was achieved by short hairpin RNA (shRNA) technology (Brummelkamp, Bernards et al. 2002; Yu, DeRuiter et al. 2002) using a lentivirus-based delivery system (Rubinson, Dillon et al. 2003) . The glycerol stock of human GIPZ lentiviral shRNAmir *BMI1* constructs (Open Biosystems) containing a CMV-driven GFP reporter and seven clones of target sequences of human Hs BMI1 (NM_005180) was used. The glycerol stocks of pGIPZ scrambled, HIV1 and VSVG, also containing GFP reporter, were a gift from Dr Paolo Salomoni's group in UCL. The latter vectors were used to package BMI1 shRNA construct.

2.1.1 Purification of Plasmids:

First, plasmids were purified from the above mentioned glycerol stocks using QIAfilter maxikit (Qiagen) to yield low-copy plasmids.

Luria broth (LB) (Invitrogen) which contains peptone 140, yeast extract and sodium chloride, was diluted in sterile H_2O to prepare 200 ml of LB solution in each of 4 glass flasks. The flasks were autoclaved and after cooling, ampicillin (Sigma) 100 µg/ml was added to each of the flasks to allow selection of ampicillin resistant bacterial growth. A small amount of each bacterial glycerol stock was scraped with a 20 µl pipette and added into separate LB containing flasks and labelled. The openings of the flasks were sealed with paraffin film and were incubated at 37^0C overnight on a rocker set at 220 rpm, ensuring vigorous shaking until the broth turned turbid due to bacterial proliferation. The broth containing the respective

bacterial culture were transferred to labelled large centrifuge tubes and centrifuged at 6000 rpm for 15 min at 4^0C. After removal of the excess broth medium by careful suction, the pellets were either temporarily stored (for up to 2 weeks) at -20^0C or used immediately for plasmid purification.

The bacterial pellets of the respective vectors were resuspended in each tube with 10 ml Buffer PI (after adding RNase A to Buffer P1) at room temperature. The tube containing the pellet is vortexed and pipetted thoroughly and ensured that no clumps remained. 10 ml of Buffer P2 was added to each tube, mixed by vigorously inverting the tubes 4-6 times and incubated at room temperature for 5 min. The resulting cell suspension after adding Buffer P2 turned blue homogeneously. The tubes were not vortexed at this stage to avoid DNA damage. 10 ml of pre chilled lysate Buffer P3 was added and mixed immediately by vigorous inverting 4-6 times until the blue colour disappeared. The resulting lysate was poured into QIAfilter cartridge (with capped outlet nozzle) and incubated at room temperature for 10 min. A precipitate (containing proteins, genomic DNA, and detergent) formed as a layer on top of the solution. Qiagen-tip 500 was equilibrated with 10 ml of Buffer QBT and the column was allowed to empty by gravity flow. The cap from the QIAfilter cartridge was removed from the outlet nozzle and the plunger was gently inserted into the cartridge to filter the cell lysate into the previously equilibrated Qiagen-tip. Approximately 25 ml of cell lysate was recovered. The cleared lysate was allowed to enter the resin by gravity flow. The Qiagen-tip was washed with 30 ml Buffer QC twice (using gravity flow). The DNA was eluted with 15 ml Buffer QF, and the elute was collected in 50 ml falcon tube. The elute was either stored temporarily at 4^0C overnight or used immediately to precipitate the plasmid DNA. 10.5 ml of isopropanol was added to the elute and mixed to precipitate the plasmid DNA. The tube was centrifuged at 15000

rmp for 30 min at 4^0C. The supernatant was carefully removed. The DNA pellet was washed with 5 ml of 70% ethanol (to remove precipitated salt and to replace isopropanol) and centrifuged at 15000 rpm for 10 min at 4^0C. The supernatant was carefully removed without disturbing the pellet. The site of the pellet was marked on the outside of the tube and the pellet was air dried for 5-10 min. The pellet was then dissolved with 200 µl of filtered sterile water and temporarily stored in labelled eppendorfs at -80^{0}C. The process of purification of plasmid DNA is summarised in Fig 2.1 A.

2.1.2 Determination of yield:

The concentration of the plasmid DNA was determined both qualitatively and quantitatively by agarose gel analysis and by spectrometry respectively.

Agarose gel 0.8% was prepared by heat dissolving 0.48 g of Agarose gel powder (Starlab) with 60 ml of 1 X TAE buffer (Qiagen) and adding 4.8 µl of ethidium bromide. The gel solution was poured into the electrophoresis chamber and allowed to set for 10 – 15 min. The 4 DNA samples (10 µl each) were mixed with 3 – 4 µl of dye and loaded into the wells along with 1Kb ladder (10 µl). The electrophoresis was performed at 80 – 100 V for 30 min. The gel was photographed in the UV chamber to detect the bands – pGIPZ, BMI1 and HIV vectors at ~ 8000 bp and VSVG at ~ 6000 bp (Fig 2.1 B).

The yield of DNA was quantitated using NanoDrop spectrometry (Thermo scientific) by selecting Nucleic Acid DNA-50 measurement after normalising with distilled water (blank). The measurements are shown in Fig 2.1 B.

2.1.3 Packaging:

The purified plasmids were then packaged (Chang, Marran et al. 2013) using

HEK293T cells (discussed in section 2.2.4) to produce lentiviral particles. The

procedure is categorised as Class II biohazard level and was therefore carried out in

Genetic Modification Organisms (GMO) suite after appropriate risk assessment

under GMO regulations 2000 (Project Ref. no 774/0801/07). On day 1, HEK293T

cells were plated at a density of $5 - 6 \times 10^6$ cells in 20 ml of IMDM medium (Gibco)

enriched with glutamate, 10 % FBS and 1% penicillin/streptomycin (sigma) in 15 cm

culture dish. Two culture dishes for each virus were prepared. The cells were

incubated for 12 – 24 hr at 37^0C with 5% CO_2. On day 2, the transfection mix was

prepared in a falcon tube with quantities mentioned in Table 2.1.

Table 2.1 Preparation of transfection mix for lentiviral packaging.

Contents	Quantity for one 15 cm dish
Transfer vector pGIPZ (with or without shRNA)	28 µg
pCMV-G (VSV-G)	8.4 µg
pCMV-HIV1	18.1 µg
2.5M $CaCl_2$	140 µl
Filtered H_2O	To make up to 1 ml
2X HBS (NaCl, HEPES, Na_2HPO_4, pH 7.12)	1 ml (added drop wise while vortexing the rest of the mix)

The transfection mix (2 ml) was immediately added to the cell culture dish gently

along the side wall of the dish. The dish was gently shaken several times in all

directions to ensure thorough mix. The cell culture medium was replaced with 25 ml

fresh medium 8 – 16 hr after transfection. On day 3, the transfected cells were

checked under UV microscope and showed HEK293T cells positive for GFP

fluorescence (Fig 2.1 C). On day 4 (48 hr post transfection), the supernatant from the

cell culture dish (2 dishes per each virus) was collected in 50 ml falcon tube and

centrifuged at 3000 rpm for 5 min to remove cells and cell debris. The resulting

supernatant was filtered through a 0.45 µm PVDF filter to further eliminate cellular

debris. The filtered supernatant was transferred to a sterile falcon tube and the viral particles were precipitated by adding cold 5X polyethylene glycol (PEG) solution. The PEG solution was prepared by mixing polyethylene glycol (Sigma), NaCl, Tris 1M, pH 7.5 and H_2O. The tubes were stored overnight at 4^0C.

On day 5, the supernatant and PEG mixture was centrifuged at 1500 g for 30 min at 4^0C to obtain the viral pellet. The supernatant was aspirated and the tube was centrifuged again at 1500 G for 5 min to remove any traces of residual PEG solution. The supernatant was carefully removed by aspiration. The lentiviral pellet was diluted with 1000 µl (1:50 dilution compared to original volume which was 50 ml) of cold sterile PBS and resuspended to dissolve the pellet. The lentiviral suspensions were aliquoted in labelled cryovials and stored at -80^0C until further use.

2.1.4 Titration:

0.5×10^5 HEK293T cells were plated in each well of a 12 well plate with 1 ml IMEM medium and incubated for 24 hr at 37^0C, 5 % CO_2. Six wells were prepared per viral stock to be titrated (including one well as negative control) ensuring that the cells were uniformly distributed within the well. It was estimated that the cell number is doubled after 24 h in culture. Five serial dilutions of each viral stock were prepared as follows – dilution 1 (1:10): 110 µl of virus to 990 µl of medium, dilution 2: (1:100) 100 µl from dilution 1 to 900 µl of medium, dilution 3 (1:1000): 100 µl from dilution 2 to 900 µl of medium, dilution 4 (1:10,000): 100 µl from dilution 3 to 900, dilution 5 (1:100,000): 100 µl from dilution 4 to 900 µl of medium. The medium in the five cell culture wells were replaced with 1 ml of corresponding serial dilution and labelled. 1 ml of media without virus was added to the sixth well (negative control). The infected cells were incubated for 12 – 24 hr at 37^0C, 5 % CO_2 The media was replaced with

fresh media after 12 – 24 hr. After 96 hr post infection, the cells were collected in FACS tubes for flow cytometry to analyse the percentage of lentivirus infected cells which would be GFP positive. Following the flow cytometry analysis, the titre of viral stock in calculated as transducing units/ml (TU/ml) as per the formula:

[(% GFP positive cells) x (number of cells infected)] / [(volume of virus in ml) x (dilution)]

The final titre of the lentivirus prepared ranged 2.5 – 11 x 10^8 TU/ml.
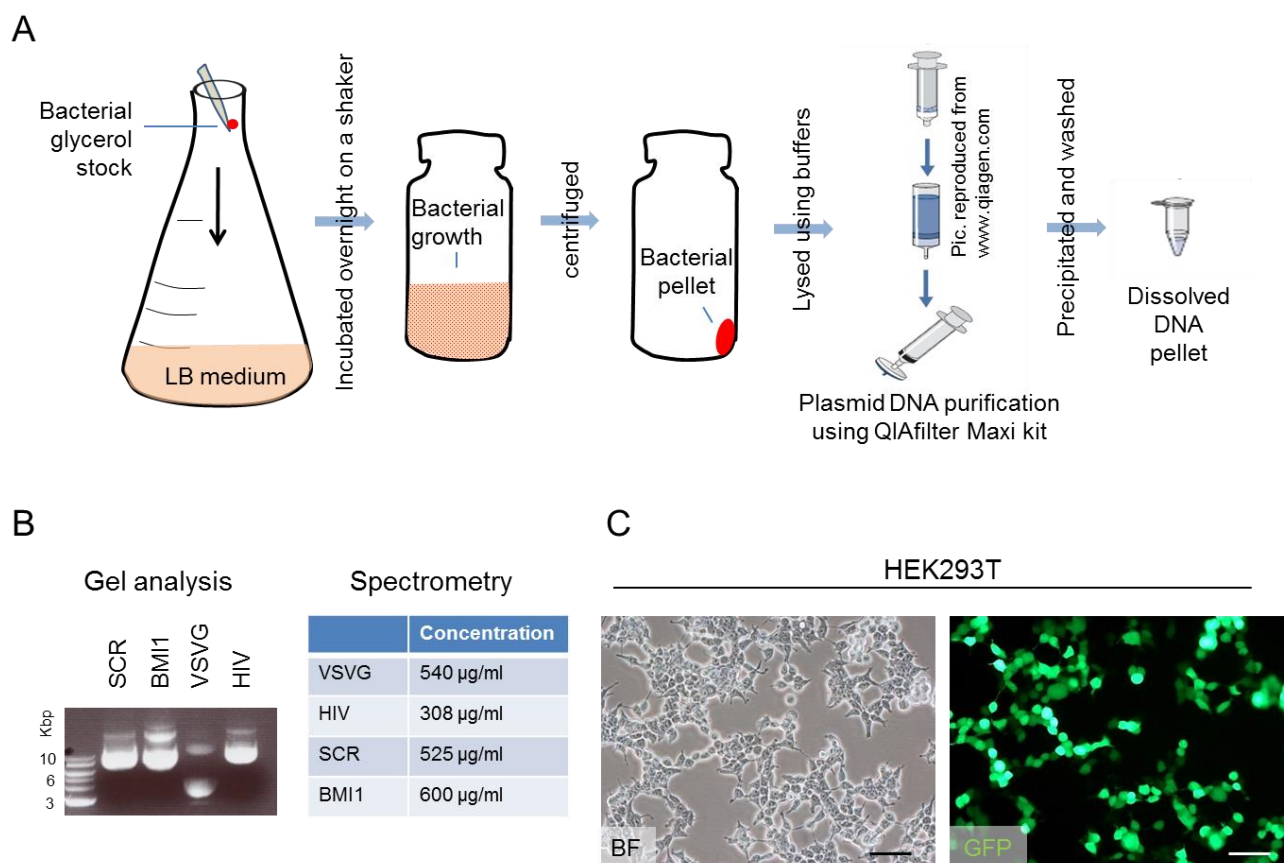
Fig. 2.1 Lentivirus production and packaging.

(A) Schematic of plasmid purification using QIAfilter maxikit. **(B)** The yield of plasmids determined qualitatively by agarose gel analysis (left panel) which shows plasmid bands at 6-8 Kbp, and quantitatively (right panel) showing the concentration of each plasmid. **(C)** Packaging of lentiviral particles using HEK293T cells which show marked GFP positivity 24 hr after treating them with the transfection mix. Scale bars in C = 100 µm

2.2 Cell culture

2.2.1 General methodology

2.2.1.1 Thawing:

The frozen aliquots of cells stored in liquid nitrogen were transported on dry ice and incubated in the 37^0C water bath. The vials were gently shaken during the incubation until the cells were completely thawed. The thawed cells were immediately transferred to 15 ml falcon tubes containing 10 ml pre-warmed media and centrifuged at 1000 rpm for 5 min. The resulting supernatant was carefully discarded and the cells were resuspended in 1-2 ml of appropriate media and pipetted to dissociate the cell pellets. While the cell lines were pipetted using standard 1 ml pipette tip, the primary cells were pipetted using 200 µl fine tip pipettes to achieve adequate dissociation. The dissociated cells were transferred to a 10 cm tissue culture dish (cell lines) or a 6 well plate (primary cells) containing appropriate media for culture. The cell culture plates were incubated at 37^0C, and were replaced with fresh media after 12 - 24 h.

2.2.1.2 Sub culture:

The cells were sub cultured (split or passaged) when > 90% confluence was reached – which was 3-4 days for the cell lines and 5-7 days for the primary cells. The non-adherent or loosely adherent (primary cells, D-458) cells were gently scraped off the culture dish using a cell scraper. The adherent (DAOY and HEK293T) cells were first washed with PBS and detached using pre-warmed 1% trypsin EDTA solution (Sigma) followed by neutralization of trypsin by serum containing medium. The cells were collected in a 15 ml falcon tube, centrifuged and resuspended as above. The

cells were sub cultured at a ratio of 1:3 to 1:8 dilutions. The cell culture plates were incubated at 37^{0}C, and were replaced with fresh media after 12 - 24 h. The primary cells were maintained in *in vitro* culture for a limited number of passages, up to 4-5 weeks.

2.2.1.3 Cell count:

The cell count was performed using Neubauer haemocytometer. A glass coverslip was placed over the haemocytometer chamber and 10 µl of dissociated cell suspension was introduced under the coverslip. Using an inverted bright field microscope (X20 mag.) the number of cells in the peripheral 4 squares of the chamber was counted. The average cell count from the total count was calculated which gives the cell count per ml. The average count was multiplied by the original volume of the media (number of ml) to obtain the final cell count. Non-viable cells were excluded from the counting by the Trypan blue method (Strober 2001), where the cells were treated with 0.4% trypan blue solution at 1:5 dilutions for 5 min, and only the viable clear (unstained) cells were counted using haemocytometer as above.

2.2.1.4 Screening for Mycoplasma contaminants:

The cell were checked for any Mycoplasma contamination using Mycoalert™ detection kit (Lonza) which is a biochemical test to detect the Mycoplasma enzymatic activity in the cell culture supernatants. The reagent and buffer were reconstituted with 600 µl of buffer and incubated for 15 min at RT according to manufacturer's instructions. The supernatant from the cell culture media were collected and spun at 1500 rpm for 5 min. 100 µl of clear supernatant were placed in Brand 96 well plates and 100 µl of reagent was added to each well, incubating for 5 min at RT. The

luminescence (referred to as A) was measured using microplate reader. 100 µl of substrate was added to each sample and incubated for 10 min at RT. The luminescence (referred to as B) was detected. The ratio B/A was calculated. If the ratio was > 1 then the test was considered to be positive and the cells were discarded. If the ratio was < 1 it was considered negative for contamination and the cells were cultured for further studies.

2.2.1.5 Cryopreservation:

The cells were harvested from culture, counted, and centrifuged as described above. $1 – 5 \times 10^6$ cells were diluted in 1 ml freezing medium containing 10% DMSO and 20% FBS in DMEM medium. The cells were then transferred in to labelled Nunc® cryovials (Thermo Scientific) and the vials were gradually cooled by placing them in Mr Frosty freezing container (Thermo Scientific) which was filled with isopentane along the lining of the container and kept -80^0C freezer for 24 hr. The frozen cells were transported on dry ice and stored in liquid nitrogen.

2.2.2 Medulloblastoma cell lines

Established human MB cell lines UW228-2, D-425, D-458, D-341 and DAOY were obtained from American Type Culture Collection (ATCC). DAOY and D-458 were used for functional studies in this project. The DAOY cell line was originally established by P.F Jacobsen from Royal Perth Hospital in 1985 (Jacobsen, Jenkyn et al. 1985). It was derived from desmoplastic medulloblastoma originating in cerebellum from a 4 year old boy. Although the original tumour exhibited neuronal and glial differentiation, the cell line did not retain either of them. They are polygonal cells which grow as adherent monolayer cultures *in vitro* (Fig 2.2 A). D-458 is known to have predominantly neuronal phenotype (He, Wikstrand et al. 1991) and grow in

suspension mainly as multicellular aggregates with some cells also adhering to the bottom of the dish (Fig 2.2 B). All MB cell lines were cultured and maintained in Improved MEM media (Gibco) containing L-lysine and Glutamate, supplemented with 10% FBS (Gibco), 1 % penicillin/streptomycin (Sigma). Prior to passaging, DAOY cells were detached using 1% trypsin EDTA (Gibco) and D-458 were gently scraped off the culture dish.

2.2.2.1 Small interfering RNA (siRNA) transfection:

Transient *BMI1* gene silencing (knock down) was achieved by siRNA technology (McManus and Sharp 2002; Schutze 2004) in which transfection was carried out using cationic and neutral lipid based transfection method. FlexiTube siRNA (Qiagen) specific for *BMI1*, containing a mix of *Hs BMI1 1, Hs BMI1 2 and Hs BMI1 3* (also known as *Polycomb Ring Finger 4, PCGF4)* was used. All Stars Negative siRNA (Qiagen), referred to as scrambled (Scr) was used as control. The transfection mix in combination with HiPerFect Transfection Reagent (Qiagen) was prepared as detailed in Table 2.2. DAOY or D-458 (0.5 – 1 x 10^5 cells in 420 µl of media) were plated in each well of a 24 well plate. After 12 – 24 h incubation, and when 70-80% confluence was achieved, the cells were treated with siRNA transfection mix (~83 µl/well) at a final concentration of 30 nM and gently mixed. The transfected cells were incubated for 48 hr prior to functional studies for maximum knock down efficiency, as assessed by Western blot and qRT-PCR analysis.

Table 2.2 BMI1 siRNA transfection mix preparation*.

Reagent	Scrambled (per well)	Bmi1 SiRNA (per well)
Medium	80 µl	80 µl
Hi Perfect Transfection reagent	3 µl	3 µl
Negative	0.72 µl	-
SiRNA kit (Quiagen) 1. Hs BMI1 1 2. Hs BMI1 2 3. Hs BMI1 3	-	0.24 µl 0.24 µl 0.24 µl (Total of 0.72 µl)
Total volume	83.72 µl	83.72 µl

*To obtain a final concentration of 30 nM.

2.2.3 Primary human medulloblastoma cells

Primary human MB cells ICb-1299, were obtained from Dr Xiao-Nan Li, Baylor College of Medicine, Texas Children's Cancer Centre, USA. These cells were isolated from primary MB tumours arising in cerebellum in a 2.8 year old girl who underwent surgery at the Texas Children's Hospital. The tissue was obtained in regulation with local institutional review board policy and appropriate consent. The original tumour was diagnosed as an anaplastic MB, stage M3. The tumour cells were maintained as intracerebellar xenografts in mice after orthotopic transplantation of fresh tumour (Shu, Wong et al. 2008). Genetic profiling of the original tumour and of the primary cells has classified them as Group 4 (Northcott Group D) MB (Zhao, Liu et al. 2012). For expansion and knock down studies, these cells were cultured in Dulbecco's Modified Eagle Medium (D-MEM) with high glucose (Gibco) supplemented with 10% FBS (Gibco) and 1% Penicillin/Streptomycin (Sigma). The cells grew in suspension mainly as multicellular aggregates (tumour spheres) with some cells also adhering to the bottom of the dish (Fig 2.2 C).
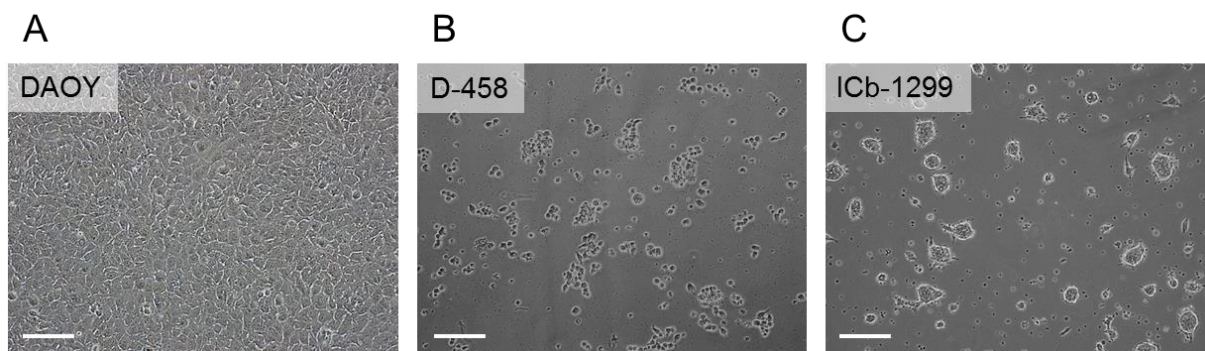
Fig. 2.2 Cells in culture.

(A) DAOY cells which grow as an adherent monolayer. Relatively larger size and polygonal shape of the cells is evident. **(B)** D-458 growing in suspension mainly as multicellular aggregates but also showing some adherence to the floor of the dish **(C)** short term cultures of ICb-1299 which grew in suspension mainly as tumour spheres. Scale bars in A,B and C = 200 μm.

2.2.3.1 Infection with lentivirus shRNA and stable selection

Stable BMI1 silencing was achieved by shRNA technique using lentiviral vectors. Both DAOY and ICb-1299 were infected with shRNA BMI1 lentivirus, and a separate cohort of cells were infected with shRNA scrambled (Scr) lentivirus to be used as controls. Multiplicity of infection (MOI) is defined as the number of virions that are required to infect each cell.

The formula to calculate MOI = [μl of viruses used X titration in TU/μl]/no. of cells transduced.

Having calculated the titres of each virus group (after packaging, described in section 2.1.4), we decided to carry out infection at high MOI (based on Poisson distribution) in order to achieve adequate infection. First, the cells were harvested from cultures, mechanically dissociated and plated at a density of 1×10^6 cells on a 10 cm culture dish. Having calculated the titres of each virus group, the cells were infected at MOI of 12.5 for DAOY and MOI of 25 for ICb-1299, and incubated at 37^0C for 24 hr. The media was then replaced with fresh media and the cells were

incubated for a total of 72 hr from the time of infection. The cells were then checked for GFP expression under UV microscope. There were > 90% cells showing GFP positivity. The cells were harvested 72 hr post infection and the GFP positive (infected) cells were selected for stable culture.

Initially, stable selection by Puromycin was attempted. 1×10^5 cells in 1 ml media were plated in each well of 24 well plate and Puromycin (Sigma) was added to the wells at increasing concentrations – 1 µg/ml, 2 µg/ml, 3 µg/ml, 4 µg/ml and 5 µg/ml. The cells in all the wells including that of the lowest concentration failed to survive possibly due to drug toxicity. Therefore this method for stable selection was discontinued.

The lentivirus treated cells were selected for stable cultures by fluorescent activated cell sorting (FACS) by flow cytometry. The procedure was carried out with the help of Dr Gary Warnes, manager of the flow cytometry core facility, Blizard Institute, Barts and the London school of Medicine and Dentistry. The procedure was carried out as per the COSSH biohazard risk assessment protocol. The lentiviral infected cells were harvested from their cultures (in sterile PBS at density of 5×10^6 cells/ml sterile PBS) and collected in FACS tubes through a filter to remove any debris. The cells were passed through the flow cytometer machine BD FACS Canto II analyser aided by FACS Diva™ v6.1.3 software (BD Biosciences) set for 488 nm excitation and 509 nm emission FITC fluorochrome gate (Fig 2.3). The GFP positive cells were collected, washed with PBS and incubated at 37^0C in complete medium. The cells were incubated for at least 96 hr prior to expansion or use for further studies.

The efficacy of knock down was assessed by western blot and qRT-PCR analysis at multiple time points after passaging.

BMI1 knock down studies on DAOY and D-458 MB cell lines to investigate BMP

pathway activation by immunofluorescence and to demonstrate cell aggregate

formation were performed using siRNA method. All other knock down experiments

were conducted following lentiviral mediated shRNA method.
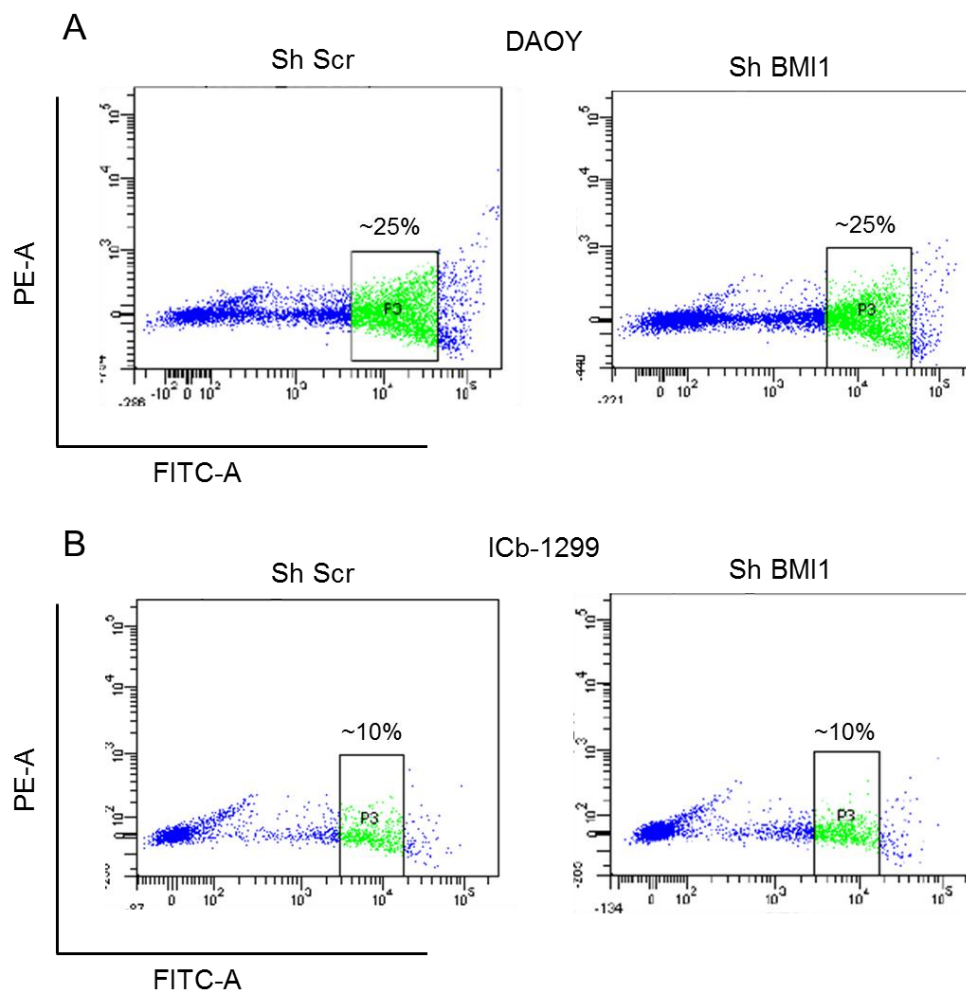
Fig. 2.3 Selection of stable shRNA transfected cells by FACS.

The FITC gate (P3) was set to select only lentivirus shRNA infected cells which expressed GFP. Approximately 25% of the cells were selected from **(A)** DAOY population, and approximately 10% of the cells were selected from **(B)** ICb-1299 population. In each, left panel is for shRNA Scr and right panel is for BMI1 shRNA. The selected cells were allowed to recover for at least 96 hr prior to expansion or use for further studies.

2.2.4 HEK293T cells

HEK293T (human embryonic kidney) cell lines used for packaging of lentiviral vectors were obtained from Denise Sheer's group in our institute (Jones, Ogunkolade et al. 2011). HEK293T cells were chosen for packaging because compared to HEK293 cells, HEK293T cells constitutively express SV40 large T antigen, are neomycin resistant and have better transfectability (Pear, Nolan et al. 1993).

These cells were cultured using IMDM media enriched with 10% FBS, and 1% penicillin/streptomycin and passaged when they reached confluence of >90%. Prior to passaging, they were detached using 1% Trypsin EDTA.

2.3 Activation and inhibition of BMP pathway

To assess if the functional effects of BMI1 silencing were BMP signalling dependent, we concomitantly used BMP pathway inhibitor (for DAOY and D-458) or recombinant BMPs (for DAOY) in *in vitro* studies.

2.3.1 Recombinant BMP-4

Use of recombinant BMP-2 and/or BMP-4 for BMP pathway activation is well established (Iantosca, McPherson et al. 1999; Hallahan, Pritchard et al. 2003; Piccirillo, Reynolds et al. 2006; Zhao, Ayrault et al. 2008). Use of BMP ligands is justified in DAOY cells as they are shown to express BMP receptors - BMPRI isoforms and BMPRII - which activate phosphorylation of SMAD1,5,8 proteins (Iantosca, McPherson et al. 1999; Fiaschetti, Castelletti et al. 2011). To induce BMP signaling pathway in our study, we used recombinant human BMP-4 (R&D systems) on DAOY. The lyophilized form was reconstituted with 4 mM HCl and 0.1% BSA as recommended by the manufacturer. Aliquots of 10 μg/ml were prepared and stored at -20^0C. 1×10^5 cells (with or without prior treatment with shRNA lentivirus) were plated in 2 ml medium in each well of a 6 well plate and treated with BMP-4 at a concentration of 100 ng/ml for 24 – 36 hr. The BMP signaling activation was assessed by the increased pSMAD1,5,8 expression by Western Blot analysis. The BMP-4 treated cells were used in Transwell migration and cell proliferation assays.

2.3.2 Noggin

Noggin is a well characterised BMP signalling inhibitor (Zimmerman, De Jesus-Escobar et al. 1996) and has been used previously in medulloblastoma studies as a BMP antagonist (Hallahan, Pritchard et al. 2003).

To inhibit BMP signaling pathway in our study, we used recombinant Noggin/Fc Chimera (Sigma). The lyophilized form was reconstituted with sterile PBS containing 0.1% BSA as recommended by the manufacturer. Aliquots of 50 µg/ml were prepared and stored at -20^0C. 1×10^5 cells (with or without prior treatment with siRNA or shRNA lentivirus) were plated in 2 ml medium in each well of a 6 well and treated with Noggin at a concentration of 1µg/ml for at least 24 hr prior to functional analysis. The BMP signaling inhibition was assessed by reduction of pSMAD1,5,8 expression by immunocytochemistry and Western blot. Noggin was used in all *in vitro* functional studies using DAOY or D-458 cells.

2.4 Western Blot

Semi-quantitative assessment of BMI1 and pSMAD1,5,8 protein expression in MB cells and in mouse MB tumour tissue samples was performed using Western Blot.

2.4.1 Sample preparation:

MB cells: $10^5 - 10^6$ cells were harvested from the culture, washed with sterile PBS to remove medium containing serum, and centrifuged to obtain cell pellets in eppendorf tubes. The pellets were either temporarily freeze-stored or used immediately for protein extraction.

Tumour tissue: The frozen tumour tissue was thawed and weighed. About 80 - 100 mg of tissue was collected for protein extraction and the rest was re-frozen and stored at -80^0C. The collected sample was homogenised using a tissue chopper prior to protein extraction.

2.4.2 Protein extraction and protein measurement

The samples were resuspended in Radioimmunoprecipitation assay (RIPA) buffer (Table 2.3) containing a freshly added solution of protease inhibitor (Complete Mini, Roche, 1 tablet added to 1ml of d. H_2O to make 10X solution). The amount of RIPA buffer + protease inhibitor (1%) solution was proportional to the size of the cell pellet – as a guide100 µl of RIPA buffer was used for a cell pellet containing 0.5 - 1 x 10^6 cells and 200 µl for 80 – 100 mg of tissue homogenate.

Table 2.3 Preparation of RIPA buffer for Western blot.

Contents	Quantity
Igepal CA-630 or NP40	1 ml
2M Tris HCl (2M), pH 8.0	2.5 ml
Sodium deoxycholate	0.5 g
20% Sodium dodecyl sulphate (SDS)	500 μl
0.5M Ethylene diamine tetraacetic acid (EDTA)	400 μl
1M Sodium chloride (NaCl, 1M)	15 ml
Distilled water	Total up to 100 ml

The sample suspension was sonicated for 4 - 5 brief spells using Soniprep 150 ultrasonic disintegrator (MSE UK Ltd.) at amplitude of ~ 20 μ. The cell suspension was kept on ice for 20 – 60 min, and then spun at 13,000 rpm for 15 min at 4^0C to collect the supernatant containing total proteins.

The protein concentration was measured using Pierce BCA protein assay kit (Thermoscientific). First, Parts A and B were mixed at 50:1 ration to obtain the working reagent. Five dilutions of albumin standards were prepared – 0.125 mg/ml, 0.25 mg/ml, 0.5 mg/ml, 1 mg/ml and 2 mg/ml. Each albumin standard is then diluted with the working reagent at ratio of 1:20 in a 72 well plate and gently mixed. The same amount of test protein supernatant is added with working reagent in separate wells. Blank wells containing RIPA buffer with working reagents are also prepared. The 72 well plates is incubated at 37^0C for 15 min, and then cooled to room temperature, while the solution is protected from the light. The absorbance is measured @ 562 nm using NanoDrop photospectrometer (Thermo Scientific). The standard albumin curve is first obtained using the 5 prepared dilutions of albumin, followed by blank solution and then the test solutions. The readings are obtained in triplicates and the average reading is calculated.

2.4.3 Gel electrophoresis and ECL detection

25 µg of each protein sample was taken in an eppendorfs, mixed with 2.5 µl loading buffer (final concentration of 25%) and diluted with RIPA buffer to make a final working volume of 12.5 µl. The samples were boiled at 99^0C on eppendorf thermo mixer for 5 min. The boiled samples were quickly spun and kept on ice until electrophoresis.

The running and stacking gel were prepared as in Table 2.4. After polymerisation of the gels, 10 µl working solution of protein samples were loaded on to the gel along with the 10 µl standard ladder (Bio-Rad), in an electrophoresis chamber filled with 1X running buffer. Electrophoresis was carried out at 80 V first (until the proteins passed through the stacking gel) and then at 100 V for 90 – 120 min.

Table 2.4 Western blot gel preparation.

Contents	Running gel (10%)	Stacking gel
30% Acrylamide mix	3.3 ml	0.5 ml
1.5M Tris HCl	2.5 ml (pH 8.8)	0.38 ml (pH 6.8)
10% SDS	0.1 ml	0.03 ml
10% Ammonium persulfate (APS)	0.1 ml	0.03 ml
Tetramethylethylenediamine (TEMED)	0.004 ml	0.003 ml
Distilled water	4 ml	2.1 ml

Following separation, the proteins were transferred on to Nitrocellulose membrane (Protran) by electrophoresis. The immunoblot sandwich for the transfer was in the order – Negative charge (black side) – sponge – Whatman paper - gel with separated proteins – nitrocellulose membrane – Whatman paper – sponge – positive charge (red side). The sandwich was carefully inserted into electrophoresis chamber filled with pre-chilled 1X transfer buffer and an ice tray was placed in the chamber to

keep the temperature low. Transfer electrophoresis was carried out at 32 V in the

cold room overnight. The contents of running and transfer buffer are listed in Table

2.5.

Table 2.5 Contents of electrophoresis buffers

Running buffer (10X)	Transfer buffer (10X)
248 mM Tris 300g 1.918M glycine 1440 g 1% SDS 100 g d.H$_2$O add to total 10 L	1.2M glycine 90 g 156 mM Tris 18.9 g 0.25% SDS 2.5 g d.H$_2$O add to total 1 L

Following overnight transfer, the nitrocellulose membrane was treated with Ponceau

S solution (Sigma) to confirm protein transfer. The membrane was washed

thoroughly with 1X TBST solution and treated with 5% non-fat milk solution for at

least 1 hr at room temperature to block unspecific binding of antibodies to antigens.

The membrane was incubated with appropriate primary antibody for the desired

duration (see Table 2.6) and rinsed with 1X TBST 2 x 5 min on a rocker. The

membrane was treated with the appropriate secondary antibody (Table 2.6) at a

concentration of 1:3000 for 1 hr at RT, and then rinsed with 1X TBST for 3 x 5 min

on a rocker. The HRP conjugated protein was detected by Enhanced

Chemoluminiscence (ECL) substrate (supersignal west PICO, Thermo Scientific).

The solutions 1 and 2 were mixed in equal ratios and added on to the membrane,

followed by incubation at room temperature for 5 min. The ECL treated membrane is

wrapped in cling film, fixed in lead cassette and exposed to a film. The exposure time

varied between 1 – 10 min for different protein band detection. The film was

processed using the developer in the dark room. The nitrocellulose was soaked in

TBST and stored at 4^{0}C. For repeat immuboblotting, the membrane was treated with

Piercenet stripping buffer (Thermo Scientific) for 5 – 15 min at RT and washed with

TBST. The immunoprobing procedure was repeated from blocking antigen step onwards.

Table 2.6 Primary and secondary antibodies used in WB

Primary antibody	Company	Incubation conditions	Secondary antibody used
Mouse monoclonal anti-Bmi1	Millipore (05-657)	1:500, overnight at 4^0C.	ECL peroxidase anti-mouse IgG from sheep (GE Healthcare, NA931VS)
Mouse monoclonal anti-alpha-tubulin	Sigma (T6199)	1:5000, 2 hr at RT.	
Rabbit polyclonal anti-pSMAD1,5,8	Cell Signaling (9511)	1:500, overnight at 4^0C.	HRP anti-rabbit IgG (Santa Cruz Biotechnology, sc-2030)
Rabbit polyclonal anti-SMAD1,5,8	Santa Cruz Biotechnology (sc-6031-R)	1:400, 6 hr at RT	HRP anti-rabbit IgG (Santa Cruz Biotechnology, sc-2030)

2.5 Quantitative Real-Time PCR (qRT-PCR).

The efficiency of siRNA/shRNA induced BMI1 gene silencing was determined in MB cell lines and primary MB cells by qRT-PCR TaqMan Assay. The expression levels of Bmi1 in MB tumours arising from transgenic mouse model Math1Cre;Smo (comparing to the expression level of wild type mouse cerebellum) was also tested with this method. To evaluate the downstream targets of BMP pathway in MB cells, *ID* (inhibitor of differentiation) gene expression, namely, *ID1* and *ID2* expression was analysed by qRT-PCR SYBR Green method.

2.5.1 Sample preparation:

MB cells: $10^5 - 10^6$ were harvested from the culture, washed with sterile PBS and centrifuged to obtain cell pellets in eppendorf tubes. The pellets were either temporarily freeze-stored or used immediately for RNA extraction.

Tumour tissue – The frozen tumour tissue was thawed and weighed. About 80 - 100 mg of tissue was collected for RNA extraction and the rest was re-frozen and stored at -80^0C. The collected sample was homogenised using a tissue chopper and transferred to RLT lysis buffer containing eppendorf tube and pipetted using a 21G needle to ensure thorough mixing.

2.5.2 RNA extraction:

Total RNA was extracted using RNeasy minikit (Qiagen). First, lysis buffer was prepared by adding 30 µl of β-mercaptoethanol to 2970 µl of guanidine-isothiocyanate containing RLT Buffer. 80% ethanol and 70% ethanol solutions were prepared by diluting absolute alcohol in RNase free water. 350 µl of lysis buffer was added to the eppendorfs containing cells/tissue sample and vortexed to homogenise the sample. 350 µl of 70% ethanol was added and mixed by inverting the tube. The lysate was then transferred to gDNA eliminator mini elute spin column and centrifuged at 10,000 rpm for 15 sec at room temperature (RT). 75 µl of DNase solution (prepared by mixing DNase in Buffer RDD) was added to the lysate and incubated at RT for 15 min. The column was centrifuged at 10,000 rpm at RT for 15 sec and the filtered liquid was discarded. 500 µl of RPE Buffer with ethanol was added and centrifuged at 10,000 rpm at RT for 15 sec. The above process eliminated genomic DNA. Then, 500 µl of 80% ethanol was added to provide appropriate binding conditions for RNA and was centrifuged at 10,000 rpm at RT for 2 min and again at 13,000 rpm for 5 min. The filtered liquid was discarded at all

stages. RNA was then eluted with 30 µl of RNase free water by spinning at 13000 rpm at RT for 1 min. The RNA yield was determined by NanoDrop photospectrometry.

2.5.3 Reverse Transcription:

cDNA synthesis was performed using Quantitect kit (Qiagen). The RNA samples, 1 µg each were first treated with 2 µl of gDNA wipe out buffer and totalled to 14 µl of working volume. The mix was incubated at 42^0C for 2 min to remove any DNA contamination. The samples were then placed on ice. Reverse Transcriptase III (RT III) mix was prepared by adding 1 µl of Quantiscript RT, 4 µl Quantiscript Buffer and 1 µl of RT primer mix. 6 µl of prepared RT III mix was added to each sample and gently shaken. The samples are then incubated at 42^0 C for 15 min and at 95^0 C for 3 min – to synthesise respective cDNA. The cDNA samples were stored at -80^0C until further analysis.

An alternative method to synthesise cDNA using SuperScript III Reverse Transcriptase kit (Invitrogen) was also used. First, 1 µg of RNA was annealed with 2 µl of random primers(Invitrogen) to give a final volume of 14 µl, for 5 min at 65^0C. The master mix was prepared by mixing 4 µl of first strand buffer 5X, 1ul of DTT 0.1M, 1 µl of dNTP 10 mM, 0.5 ul of Reverse Transcriptase III and 3.5 ul of RNase free water. The master mix was then added to the annealed primers to give a total volume of 24 µl. Reverse transcription was carried out at 25^0C for 5 min, 50^0C for 1 hr and 72^0C or 10 min cycle. The resulting cDNA was stored at -80^0C until further analysis.

2.5.4 Polymerase chain reaction (PCR):

To evaluate ID1 and ID2 expression in MB cells, we performed qRT-PCR using ID primer sequences. Prior to qRT-PCR, we checked for primer functionality by performing PCR. The RNA was extracted from MB cells and cDNA was prepared as above. The primers (Table 2.7) were designed using PRIMER3 software – frodo.wi.mit.edu/primer3/. The primers were validated for specificity using NCBI primer-Blast - http://www.ncbi.nlm.nih.gov/tools/primer-blast/. Forward and reverse primer templates were ordered and obtained from Sigma and reconstituted with Milli-Q® water to achieve the recommended working dilution. The PCR was performed using the cDNA samples. The PCR mix was prepared as in Table 2.8 and PCR amplification was carried out at 65^0C for 40 cycles. Dimethyl sulfoxide (DMSO) was added to increase specificity. RNA or genomic DNA was used as controls to exclude contamination. The samples were then loaded on 1.2% agarose gel for electrophoresis for 45 min at 200V. The gel was photographed for band analysis. Clean bands for *ID1* were identified at ~ 193 bp and for *ID2* at ~ 347 bp (Fig 2.4), confirming that the primers were suitable for qRT-PCR.

Table 2.7 Primer sequences of *ID* genes

Gene	RefSeq	Primer sequence
ID1	NM_002165.3	*Forward 5'-CCCCAGAACCGCAAGGTGAGC-3'* *Reverse 5'-CAGGAACGCATGCCGCCTCG-3'*
ID2	NM_002166.4	*Forward 5'- TCTCGCCTTCCCTCGCGGTC-3'* *Reverse 5'- CGTGTTGAGGGTGGTCAGCGG-3'*

Table 2.8. Preparation of PCR mix

Contents	Volume
Buffer 10X	2.5 µl
dNTP	2.5 µl
Forward Primer (working solution)	2.5 µl (10 µM)
Reverse Primer (working solution)	2.5 µl (10 µM)
TaqMan Polymerase	0.35 µl
cDNA (100 ng) or RNA (100 ng)	2 µl
DMSO	0.1 µl
Sterile dH$_2$O	Make up to 25 µl
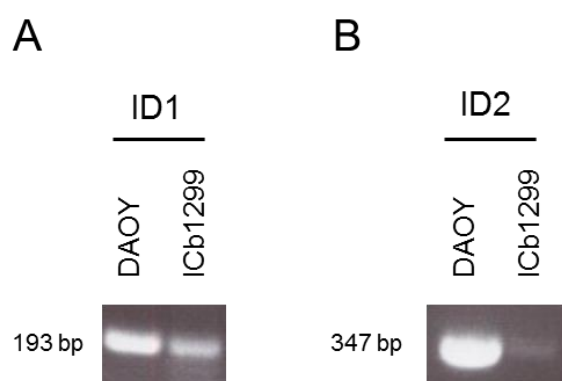
Fig. 2.4 PCR for *ID1* and *ID2* genes.

DAOY and ICb-1299 cDNA were screened for **(A)** ID1, and **(B)** ID2 gene expression. Clean bands were noted on PCR indicating their suitability for qRT-PCR analysis.

2.5.5 qRT-PCR and data analysis:

2.5.5.1 TaqMan assay:

To briefly describe, in TaqMan probe-based assay (Maeda, Fujimoto et al. 2003), reporter dye and a quencher are attached to the 5' and 3' ends of a TaqMan probe. When the probe is intact, the reporter dye emission is quenched. During the extension cycle, DNA polymerase cleaves the reporter dye from the probe and once separated from the quencher the reporter dye emits its characteristic fluorescence. TaqMan based system is known to have a high specificity as compared to SYBR

Green method (Applied Biosystems). Here TAMRA dye was used as the quencher

dye, and the methodology is discussed below.

Triplicates of cDNA templates (~ 25 ng each) were mixed with TaqMan gene

expression master mix (Applied Biosystems), TaqMan gene expression assay and

RNase free H_2O (to a working volume of 25 µl) to prepare the qRT-PCR samples (as

in Table 2.9) in MicroAMP optical 96 well plate (Applied Biosystems). The gene

expression assays used are listed in Table 2.10.

Table 2.9 qRT-PCR Master mix preparation for TaqMan Assay.

Contents	Volume per well
Master Mix 2X	12.5 µl
TaqMan Assay Mix 20X (Bmi1 or β-actin primer)	1.25 µl
cDNA	1 µl
RNAase free H2O	10.25 µl

Table 2.10. Details of TaqMan gene expression Assay.

Gene	Assay ID	Reference sequence	Exon boundary	Amplicon length (bp)
BMI1 (human)	Hs00180411_m1	NM_005180.8	3-4	105
Bmi1 (mouse)	Mm00776122_gH	NM_007552.4	6-7	150
ACTB (human β-actin)	Hs99999903_m1	NM_001101.3	1-1	171
Actb (mouse) β-actin	Mm00607939_S1	NM_007393.3	6-6	115

The samples along with negative controls were run on the SDS 7500 system

(Applied Biosystems) set for the detection of the FAM reporter and the TAMRA

quencher. The expression levels of the Bmi1 gene was determined by calculating the

∆CT ratio between this gene and the house-keeping gene beta-actin. Mean

expression (fold change) with standard deviation relative to controls were calculated using Excel spread sheet.

2.5.5.2 SYBR Green assay:

In SYBR Green assay (Maeda, Fujimoto et al. 2003), the SYBR Green dye fluoresces when bound to double-stranded DNA. When the DNA is denatured, the SYBR Green dye is released and the fluorescence is drastically reduced. During extension, primers anneal and PCR product is generated and when polymerisation is complete, SYBR Green dye binds to the double-stranded product resulting in a net increase in fluorescence detected by PCR machine. The specificity of this method depends on the template quality and primer optimisation. The methodology used is described below.

Triplicates of cDNA templates (~ 25 ng each) were mixed with SYBR Green master mix as stated in Table 2.11.

Table 2.11 Preparation of Master mix for qRT-PCR by SYBRgreen method

Contents	Volume
SYBR Green JumpStart Taq ReadyMix	5 µl
Forward Primer (10 uM)	0.5 µl
Reverse Primer (10 uM)	0.5 µl
Reference dye	0.1 µl
cDNA	1 µl
RNAase free H2O	Make up to 10 µl

The samples along with negative controls were analysed in microAMP optical 96 well plate, run on a Rotor Gene machine (Corbett Research). The cycling profile was as follows: 95^0C for 10 min, 60^0C for 30 sec, 72^0C for 30 sec for 40 cycles. The expression levels of ID1 and ID2 genes were determined by calculating the ΔCT ratio between these genes and house-keeping gene GAPDH. Mean expression (fold

change) with standard deviation relative to controls were calculated using Excel

spread sheet.

2.6 Cell migration assays

To assess the effects of *BMI1* silencing on MB cell migration/motility and cell

invasion *in vitro*, we used wound healing assay and Transwell[®] migration assay.

2.6.1 Wound healing assay using time lapse videomicroscopy

Wound healing assay allows studying cell migration and cell interactions. The

experiment was performed as per published protocols from literature (Hu and

Verkman 2006; Kurayoshi, Oue et al. 2006) and was modified and optimised

according to our requirements. First, shRNA lentivirus treated cells were plated in a

24 well plate (2 cm^2 growth area per well) at a constant density of 0.5 x 10^5 cells/well

in 0.5 ml serum free media. The culture plates were not plated with ECM substrates

to maintain uniform culture conditions. No growth factors were added to the medium

to exclude any effect due to a potential proliferation difference. At this stage, Noggin

was added to the cultures, if required and labelled. The cells were incubated at 37^{0}C

for 24 hr ensuring they attain >90% confluence. Using a 20 µl pipette tip, three

different linear wounds (scratches) were incised in each to remove ~80 µm wide strip

of cells. The wounded monolayer was washed with medium to remove floating cells

and cell debris. Fresh medium containing 10% FBS was added and the cells were

incubated in dark time lapse chamber at 37^0 C, 5% CO_2 flow. The time lapse stage

was set to acquire images from three areas from each well, a total of 9 areas for

each group. The images were acquired using phase contrast inverted microscope

(Nikon), 10X magnification, every hour, for 12 hr. Three sets of wells were analysed

for each condition tested. The images were compiled and a movie was created using Metamorph software (Molecular Devices, Sunnyvale, California). The healed wound area or the area of migration was analysed and tabulated as mean ± SD. The relative area of migration was compared to controls. The experiments were conducted in triplicates.

2.6.2 Time lapse videomicroscopy to assess cell motility (without wound)

Time lapse videomicroscopy is also used to track and study individual cell characteristics (Simpson, Selfors et al. 2008). This experiment was performed to confirm that the area of migration that was assessed by wound healing assay was not confounded by cell proliferation. Individual cells were tracked and distance of motility was analysed in this experiment, to complement the wound healing assay. shRNA lentivirus treated DAOY cells (36 hr after transfection) were plated in 24 well plate at a density of 0.5 x 10^5 cell/well in 0.5 ml serum free medium for 12 hr at 37^0C. Fresh medium containing 10% FBS was replaced and the cells were incubated in dark time lapse chamber at 37^0 C, 5% CO_2 flow. The time lapse stage was set to acquire images from five random areas in each well. The images were acquired using phase contrast inverted microscope (Nikon), 20X magnification, every 30 min, for 6 hr. Three sets of wells were analysed for each condition tested. The images were compiled and a movie was created using Metamorph software (Molecular Devices, Sunnyvale, California). Ten cells in each movie were tracked and the distance of migration was calculated and expressed as mean ± SD. The distances were compared with controls. The experiments were conducted in triplicates.

2.6.3 Transwell migration assay

In contrast to cell motility assay, cell invasion assay requires cell to migrate through a basement membrane extract (BME) or extracellular matrix (ECM) barrier by enzymatic digestion of the barrier to reach the new location. Transwell® inserts (Corning); 24mm diameter wells with polycarbonate membrane of pore size 8 μm and base area of 4.5 cm^2 were used for this assay. Transwell migration assay is a well-established method to assess cancer cell invasion *in vitro* (Hu and Verkman 2006; Moskovits, Kalinkovich et al. 2006). The procedure was performed according to manufacturer's protocol and was modified or optimised according to our requirements. First, shRNA lentivirus treated cells were plated in a 6 well plate (10 cm^2 growth area per well) at a constant density of 4 x 10^5 cells/well in 2ml serum free media to starve the cells (to synchronise them prior to migration assay). Noggin or BMP was added to the cultures at this stage, if required, and the cultures were labelled. The cells were incubated for 24 hr at 37^{0}C ensuring less than 80% confluence. The Transwell$^®$ inserts were simultaneously coated with 1 ml/well of ECM extract – either type I Collagen (First Link) 20 μl /ml, laminin (Sigma) 20 μl /ml or BD Matrigel$^™$ (BD Biosciences) 100 μg/ml - and incubated overnight at 37^{0}C. Excess ECM solution was then carefully removed by aspiration. The cells were harvested from their cultures, dissociated, resuspended in serum free medium and plated on top surface in Transwell insert wells at a constant number of 4 x 10^5 cells in 2 ml serum free medium per well. Noggin or BMP was added in to the cultures at this stage, if required, and the cultures labelled. 2 ml complete media containing 10% FBS was added in the reservoir or base of each well which acted as a chemo attractant for cells to migrate. The cultures were incubated for 12 hr (overnight) at 37^{0}C to allow invasion. Following 12 hr incubation, the medium was removed from the reservoir well by careful suction at the periphery, the wells were rinsed with PBS

and the cells were fixed with 4% PFA for 10 min. The wells were washed with 0.5%

Triton to increase cell permeabilization, and stained with 1 ml Gill's Haematoxylin on

both top and bottom of the membrane. The non-migrated cells from the top surface

of the insert membrane were gently scraped off using a wet cotton bud and washed

with PBS, preserving only the migrated cells on the bottom surface of the membrane.

Five random images from each insert membrane were acquired using light

microscopy at 20X magnification. The number of cells migrated (stained nuclei) were

counted using ImageJ software. The average number of cells per group was

calculated, values were expressed as mean ± SD, comparing to controls. Three

wells per each group of cells were prepared. The experiments were conducted in

technical and biological triplicates.

2.7 Proliferation assays

The effect of BMI1 silencing on cell proliferation was assessed in DAOY cells by

three independent methods – growth curve analysis, CyQuant NF assay and EdU

assay.

2.7.1 Growth curve analysis

The proliferation of cells was assessed by time course experiment to produce a

growth curve (Horiuchi, Huskey et al. 2012). The DAOY cells were plated at a

constant density of 1×10^5 cells per well in a 6 well plate and incubated for 3 days

until they reached confluence. They were then collected by trypsinisation, and the

number of live cells were counted using Neubauer chamber. Multiplication factor (f)

was generated where f = no. newly counted cells/no. of originally plated cells.

Estimated number of cells (e) was calculated during each passage where e = f x previous e. During each passage, 1×10^5 cells were plated, for a total of 7 passages, P1 to P7, corresponding to day 0, 3, 5, 7, 10, 12 and 14. Triplicates of each group of cells were prepared and counted. The experiment was done in three biological replicas. The estimated number of cell counts (e) for each passage was tabulated and the growth curve graph was generated using Excel spread sheet.

2.7.2 CyQuant NF assay

The CyQUANT® NF proliferation assay kit (Hong, Jiang et al. 2007) [Invitrogen] was used. This assay is based on the measurement of cellular DNA content by fluorescent dye binding capacity. The cells were plated in Costar® 96 well plate (Corning Inc.) at a constant density of 1×10^3 cells per well in 100 µl medium and were incubated at 37^0C overnight to achieve cell adherence. Initially, 11 ml of 1X Hank's balanced salt solution (HBSS buffer) was prepared by diluting 2.2 ml of 5X HBSS buffer (Component C) with 8.8 ml of deionized water. 1X Dye Binding solution was prepared by mixing 1X Hank's balanced salt solution (HBSS buffer) with Dye Reagent (Component A, containing digitonin and dimethylsulfoxide), as per manufacturers protocol. Following overnight incubation, the medium from the cultures were removed and replaced by 100 µl of 1X Dye Binding solution in each well. The plate was incubated at room temperature for 30 min in the dark to allow equilibration of the dye-DNA binding. After a stable fluorescence endpoint was reached, the fluorescence intensity (excitation set at 480 ±10 nm, and emission detection at 530 ± 10 nm) of each sample was measured by Synergy HT microplate reader (BioTek) supported by KC4™ v3.4 software (BioTek). Three independent experiments with three technical replicas each were performed.

2.7.3 EDU assay:

The Click-iT® EdU Alexa Fluor® 594 Imaging kit (Life Technologies) was used for this assay. This assay is based on detecting newly synthesised DNA by EdU (5-ethynyl-2′-deoxyuridine) that is incorporated into new DNA by quick click chemistry reaction. 0.5×10^5 cells (lentivirus treated) per well in 0.5 ml media were plated in each well of a 24 well plate over Polylysine (PLL) coated coverslips, and incubated overnight to obtain adherence. 250 µl 2X working solution of EdU (Component A) was replaced in to each well by removing 250 µl of the media and added to each well to achieve a 1X concentration (10 µM). The EdU was pulsed for 3 hr at 37^0C. The cells were fixed with 4% PFA for 15 min at RT and washed with 3% BSA in PBS for 5 min x 2. The cells were permeabilised using 500 µl 0.1% triton in PBS for 20 min at RT. Alexa Fluor® azide working solution was prepared by diluting it (component B) with 70 µl DMSO (component C). 1X Click-iT reaction buffer was prepared by diluting 10X solution (component D) with water. 1X Click-iT reaction buffer additive was prepared by freshly diluting 10X solution (component F) with deionised water. Click-iT cocktail was prepared by mixing 430 µl of reaction buffer, 20 µl CuSO4 (component E), 2 µl Alexa Flour® azide working solution and 50 µl reaction buffer additive to make a final volume of ~ 500 µl per coverslip. The cocktail was added into each well and incubated for 30 min in dark at RT. The coverslips were then placed on the glass slide for imaging and analysis. The fluorophore used in this experiment was Alexa Flour® 594 which was detected at excitation 590 nm and emission 615 nm.

2.8 Apoptosis assay

The effect of BMI1 silencing on apoptosis was assessed in DAOY cells by Annexin V assay and by Cleaved Caspase-3 assay.

2.8.1 Annexin V and flow cytometry

Annexin V is a Ca^{2+} dependent phospholipid binding protein that has a high affinity for phospholipid phosphatidylserine (PS). PS is translocated from the inner to outer leaflet of the plasma membrane in early apoptotic cells. Annexin V conjugated with fluorochrome could be used to detect early apoptotic cells without compromising its affinity for PS (Vermes, Haanen et al. 1995). PE Annexin V Apoptosis Detection Kit I (BD Pharmingen™, BD Biosciences) was used with Alexa Fluor 647 Annexin V conjugate (Invitrogen) as per manufacturer's protocol. Initially, 1X binding buffer was prepared by diluting 1 part of 10X Annexin V binding buffer with 9 parts of distilled water. The cells were collected from cultures and washed with sterile cold PBS twice and resuspended using 1X binding buffer. $1x10^5$ cells in 100 µl of 1X binding buffer per group were collected in FACS tube. 5 µl of Annexin V conjugate was added to each tube along with 10 µl of 1:1000 DAPI. The samples were gently mixed and incubated at room temperature in the dark for 15 min. 400 µl of 1X binding buffer was then added to each tube and the samples were kept on ice until flow cytometry. Three controls (DAPI only, Annexin V only, green fluorescent cells only) were prepared along with the test sample for each cohort to facilitate optimisation of flow cytometer detection probes. The cells were run through the flow cytometer machine (BD FACS Canto II analyser) set at 633 nm excitation and 660 nm emissions for Annexin V conjugate. The percentage of early apoptotic cells was determined using

FACS Diva™ v6.1.3 software (BD Biosciences). Average percentage of three independent experiments was used for analysis.

2.8.2 Cleaved Caspase-3 assay:

This assay is based on detection of cleaved caspase-3 which is responsible for photolytic cleavage of several key proteins and is a measure of apoptosis. Cleaved Caspase-3 rabbit monoclonal antibody (Cell Signaling) was used for this assay. 0.5×10^5 cells (lentivirus treated) were plated with 0.5 ml media in each well of a 24 well plate over Polylysine (PLL) coated coverslips, and incubated overnight to obtain adherence. The cells were fixed with 4% PFA for 15 min at RT and blocked with 3% BSA in PBS for 30 at RT. The cells were permeabilised using 500 µl 0.1% triton in PBS for 20 min at RT. 250 µl per well of antibody was added at a concentration of 1:200 diluted in PBS and incubated in the dark for 3 hr at RT. The coverslips were washed with PBS for 5 min x 2. Secondary antibody 1:500 Alexa Fluor® goat anti-rabbit 647 (Invitrogen) diluted in PBS was added and incubated for 1 hr at RT. The coverslips were then placed on the glass slide, mounted with DAPI medium and used for imaging and analysis.

2.9 Animal procedures

All animal procedures were carried out as per the Animals Scientific Procedures Act 1986, under the Home Office approval licences – Project licence PPL 70/7275 and Personal licence PIL – 70/23444. The mice were housed at the Biological Services Unit (BSU) Whitechapel Campus, Queen Mary University of London. The mice were temporarily transferred to the BSU Charter House Square Campus, Barts Cancer Institute for *in vivo* imaging. Nonobese diabetic –severe combined immunodeficiency (NOD-SCID) mice were used for intracranial injection to generate MB xenografts, and C57/BL6 mice were used to isolate cerebellum for organotypic cerebellar slice and MB tumour spheres co-culture assay. The animals were humanely killed as per Schedule 1 procedures.

2.9.1 Anaesthesia:

The mice were anesthetised using standard protocols (Wixon 1997; Arras, Autenried et al. 2001). For intracranial xenografts, the adult mice were anaesthetised by injectable anaesthetics Ketamine (Ketanest®, Chemdex) 50 – 120 mg/kg and Xylazine (Rompun®, Bayer) 5 – 10 mg/kg. The anaestheic mix was prepared by diluting 1 ml of Ketanest® and 0.5 ml of Rompun® in 5.7 ml distilled water making a total volume of 7.2 ml. Each mouse was weighed, and the anesthetics mixture was administered by intraperitoneal (IP) injection at the dose of 7.2 μl per gram of body. This provided an anaesthesia time of 15 – 30 min. For *in vivo* imaging the adult mice were anaesthetised using inhalational anaesthetic isoflurane. The gas was delivered using face mask at 4.5% for induction and 1-2% for maintenance, for anaesthesia time of 15 – 20 min.

The neonatal mouse pups were anaesthetised by hypothermia method. The pups were held in crushed ice for 2-4 min, with precautions taken to avoid freeze injuries to the skin. This provided an anaesthesia time of 10 – 15 min.

Following the procedure, the mice were allowed to recover on a heated mat for 10 – 30 min until they were alert and mobile before transferring them to their respective cages.

2.9.2 Stereotaxic intracranial transplantation:

Intracranial injections for xenograft tumour generation in mice were performed using SR6M Stereotaxic instrument (Narishige). The stereotactic frame was sterilized and a 25 µl Hamilton syringe/ 26G needle filled with the cell suspension was fixed to the frame. The anaesthetized mouse was then mounted on to the frame (Fig 2.5). First, the ear bar was fixed anchoring it to the ears of the mouse, and then the bar was fixed to the frame, supporting the snout (keeping the nostrils patent) and slightly tilting the head forward to expose the cerebellum landmarks. The area of procedure was sterilized and an incision was made to expose the skull. The lambda suture was identified and the needle was adjusted using the frame scales to necessary co-ordinates. The co-ordinates used to inject MB cells for intracerebellar xenograft were 1 – 2 mm posterior, 1 – 2 mm lateral from the lambda suture (Shu, Wong et al. 2008). The needle was inserted at 10^0 – 15^0 angles to a depth of 2 - 3 mm and 2 – 5 µl of cell suspension, containing 1 x 10^5 cells was slowly injected into the right hemisphere with gradual retraction of the needle. Prior to completely withdrawing the needle, a skin suture was placed to cover the scalp wound. After completion of injection the mouse was dismounted from the frame, and allowed to recover on a

heated mat. The position of the mouse was changed every 10 - 15 minutes during the recovery phase to ensure adequate circulation.
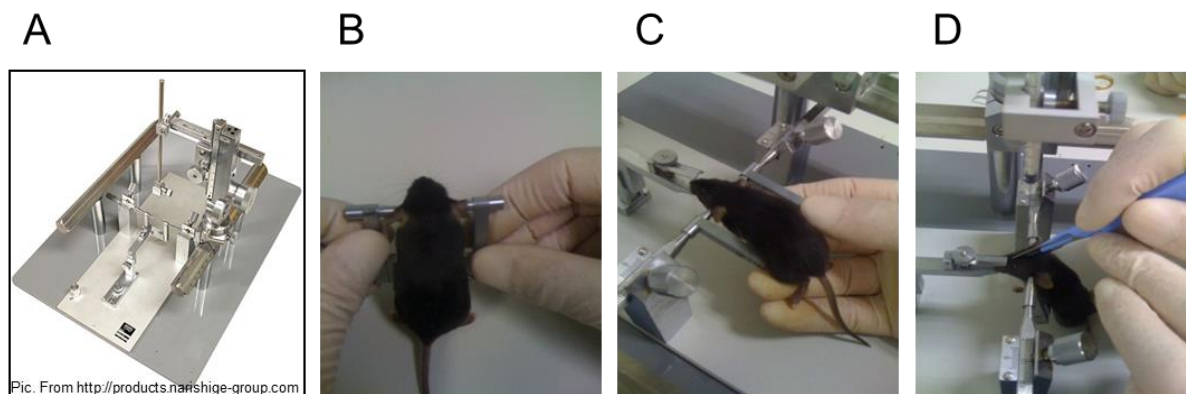
Fig. 2.5 Use of stereotaxic frame.

(A) Picture of Narishige Stereotaxic instrument used. **(B)** Fixation of the mouse to the ear barto keep the head stable during the procedure. **(C)** The mouse is mounted on the bars of the frame and the snout is supported. **(D)** Mid-line incision of scalp to expose the skull prior to injection.

2.9.3 In vivo fluorescence imaging

Following intracranial MB cell transplants, the mouse brains were imaged *in vivo* using Xenogen IVIS® Lumina II imaging system (Caliper Life Sciences). The procedure was carried out in collaboration with Dr Julie Foster from Prof. Steve Mather's group at Barts Cancer Institute. The anaesthetised mice were labelled by tail tipping or tail marker and imaged in IVIS chamber for GFP fluorescence. As the transplanted MB cells were GFP labelled, we expected to detect GFP emission which would enable us to monitor the tumour growth. But due to inadequate penetration of fluorescence signalling through the skull bones, the acquired images did not show any GFP detection (Fig 2.6). As positive controls, vials of lentivirus infected cell pellets were used.
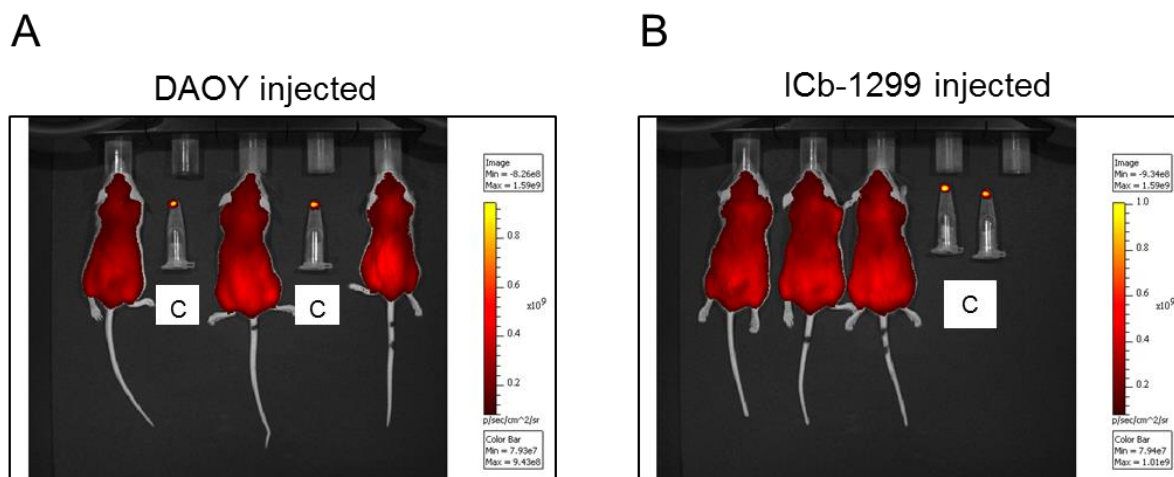
Fig. 2.6 Attempt to acquire *in vivo* fluorescence images using IVIS system.

The overlay images show GFP radiance (yellow) in lentivirus infected control cells in vials 'C'. However the xenografted mice show no GFP radiance in both **(A)** DAOY or **(B)** ICb-1299 transplants 6-8 weeks after injection. This is thought to be due to non-penetrance of GFP emission through the skull. The capture (red) on the body of the animals is auto fluorescence from the coats of the animals. Eventually it was decided to analyse the xenografts by an alternative method - to harvest the xenografts and examine by fluorescent microscopy.

Because no in vivo fluorescence could be detected due to non-penetrance, we decided to harvest the brain at the end of the experiment and study the invasive properties of the transplants by *in vitro* fluorescence imaging as described in chapter 6.

2.9.4 Organ harvest:

2.9.4.1 Brain harvest for organotypic co-culture assay:

The cerebellum was isolated from C57/BL6, P4 – P6 neonates. The pups were sacrificed by decapitation and the brain was collected on ice cold dissecting buffer. The cerebellum was isolated and the meninges were carefully peeled off the surface. Freshly isolated cerebellum was then sectioned using McIlwain tissue chopper (The

Mickle Lab. Engineering Co. Ltd.) to obtain cerebellar slices for *ex vivo* studies as described in chapter 5.

2.9.4.2 Brain harvest following xenograft generation:

Following MB tumour cell engraftment, the animals were sacrificed when they developed neurological symptoms or at the end of the experiment by exposure to raising concentrations of CO_2 gas. The brain and spinal cord from each mouse were harvested immediately. The brain was fixed in 4% PFA in view of cryopreservation of tissue and examination of GFP positive (lentiviral infected) MB cells using fluorescent microscopy. The spinal cords were fixed in 10% formalin and embedded in paraffin in view of further morphological examination to study any tumour burden as described in chapter 6.

The brain samples were incubated in 4% PFA for 2 hr at 4^0C for initial fixing. The forebrain was then separated from the cerebellum and brain stem pedicle. The latter was bisected coronally and fixed in 4% PFA at 4^0C for further 24 hr. The bisected samples were then transferred to 30% sucrose solution (30 g sucrose in 100 ml 0.1 M phosphate buffer) for 24 – 48 hr at 4^0C (until the tissues sank) for cryoprotection and avoidance of crystal formation. After dehydration, each bisected sample was placed cut side down in 15 x 15 x 15 mm tissue moulds (Tissue-Tek), labelled and filled with Optimum Cutting Temperature (OCT) compound (VWR) until total immersion at room temperature . The moulds were kept in cooled isopentane (on dry ice) to gradually freeze the tissue. Once the OCT hardened the moulds were stored in – 80^0C until cryostat sectioning.

2.9.4.3 Spinal cord dissection for tumour burden analysis

The spinal cords of the xenografted animals were harvested to assess the spread of the tumour. The mice were prepared by shaving their dorsum. A long incision was made along the mid-line extending from head to hip. The skin was retracted to adequately expose the vertebral column. The vertebral column was disarticulated just below the skull and at the hip level and the cross section of the spinal cord at the upper and lower end of the disarticulation sites were identified. Starting from the tail end of the vertebral column (because the spinal foramen is larger at this end), the vertebral bones were cut on either sides of the spinal cord using a small dissecting scissors. The blood was rinsed away with PBS in order to see the cord. The bony vertebrae along the lateral aspect were cut on both sides from below upwards (ie. lumbar to cervical). Care was taken to avoid damaging the spinal cord which is identified as a white and glistening structure (with dural covering). Once the whole length was dissected, the bone was removed from the dorsal side to expose the spinal cord. The spinal cord was gently peeled with blunt forceps by disconnecting the nerve roots/chords and fixed in formalin for at least 48 hr. It was then sectioned in to 4-5 pieces along its longitudinal axis and embedded in paraffin blocks. The blocks were sectioned at 4-5 μm thickness and were stained with H&E for morphological analysis of tumour burden. The sections from all the samples were screened for presence of tumour deposits in the spinal cord, identified by morphological characteristics of medulloblastoma. The rate of tumour positivity in shRNA BMI1 silenced xenografts were compared with control xenografts.

2.9.4.1 Cryostat sectioning:

The cerebellum and brain stem samples, fixed and frozen in OCT compound, were sectioned in their entirety using Leica CM1850 cryostat (Leica) to study the invasive properties of the xenografted tumour. The cryostat chamber was maintained at -20^0C. Each half of the bisected sample was fixed on to the cryostat tissue holder using OCT compound and sectioned at 20 μm thickness. The sections from each sample were transferred to 12 SuperFrost® Plus glass slides (VWR) serially (ie. 1-12 sections to slides 1-12 and 13 – 24 sections to slide 1 – 12 again etc.), to ensures that each slide would be representative of the entire sample. The slides were labelled and left to dry overnight. The dried sections were stored at -80^0C until stereology and confocal microscopy analysis was performed as described in chapter 6.

2.10 Histology and immunohistochemistry

2.10.1 Haematoxylin and eosin (H&E) staining

The tissue morphology was examined histologically using conventional H&E staining on the tissue sections. The sections were dewaxed (if FFPE) or thawed (if cryopreserved) and were rehydrated with PBS for 5 min. The slides were then incubated in PBS + 0.1% Triton X for 10 min followed by immersion in haematoxylin for 2-3 min and washed with distilled water briefly and tap water for 5 min. They were then immersed in eosin for 2 min and briefly washed with distilled water followed by tap water for 5 min. The stained sections were dehydrated in 70% alcohol for 30sec, 100% alcohol for 30sec and in Xylene for 30 sec in succession. The sections were mounted using DPX (mixture of distyrene, plasticizer, and xylene), covered with coverslips and left drying for 2-3 hr.

2.10.2 Immunohistochemistry by Avidin-biotinylated Complex (ABC) method:

The Formalin fixed paraffin embedded (FFPE) tissue and cell block sections were stained by avidin-biotinylated complex (ABC) method of immunohistochemistry. The slides were dewaxed by incubating them in the oven at 60^0C for 20 min. The sections were then deparaffinated by treating them in xylene for 10 min x 2 followed by 100% ethanol for 5 min x 2 and 90% ethanol for 5 min x 2. They were then treated with H_2O_2 solution (1% hydrogen peroxidase, H_2O_2, in cold methanol) for 20 min to block endogenous peroxidase and rehydrated in 70% ethanol for 5 min followed by rinsing in dH_2O for 5 min x 2. Antigen retrieval was done by the heat method – the slides were immersed in 10 mM citrate buffer (2.1 g of citric acid monohydrate dissolved in 1 L dH_2O), pH 6 and microwaved (Panasonic apparatus) for 1 min at high power and 15 min at medium power. The slides were allowed to cool and rinsed with PBS for 5 min x 3. The block to prevent unspecific binding of antibodies to antigens was carried out using appropriate serum (Table 2.13) diluted in 0.2% triton + 0.1% sodium azide solution at room temperature for 1 hr. After blocking, the sections were treated with the primary antibody diluted in 0.2% triton + 0.1% sodium azide solution and incubated overnight at room temperature in a moist chamber. The primary antibodies used with the respective concentration are listed in Table 2.12. After primary antibody treatment, the sections were washed with PBS + 0.1% tween 20 solution for 5 min x 3 and appropriate biotinylated secondary antibody (Table 2.13) was applied at room temperature for 1 hr. The sections were washed with PBS + 0.1% tween 20 solution for 5 min x 3 and incubated with avidin/biotinylated enzyme complex using Vecstatin ABC reagent (Vector labs) for 30 min. They were washed again with PBS + 0.1% tween 20 solution for 5 min x 2 and

enzymatic detection was carried out with 3,3'- diaminobenzidine tetrahydrochloride (DAB solution,Sigma). Working solution of DAB was prepared by mixing 1 ml of DAB liquid chromogen with 9 ml of DAB liquid buffer as per manufacturer's instructions. The duration of DAB incubation varied for different antibodies – the reaction was stopped when brown staining appeared – which was between 1 – 10 min. The slides were rinsed in dH$_2$O to stop the reaction, and counterstained with haematoxylin for 30 sec. The slides were washed with dH$_2$O to remove the excess dye and dehydrated with 50% ethanol for 5 min, 70% ethanol for 5 min, 90% ethanol for 5 min x 2, 100% ethanol for 10 min x 2 and xylene for 10 min x 2 successively. The sections were then mounted using DPX, covered with coverslips and allowed to dry for 2-3 hr at RT. For membrane antigen detection, PBS without Triton was used during the wash steps.

Table 2.12 List of primary antibodies used for immunohistochemistry using ABC method.

For antigen to be detected	Primary antibody used	Company	Concentration	Positive control
Bmi1 (mouse) or BMI1 (human)	Rabbit polyclonal anti-Bmi1	Abcam (ab38295)	1:100	Gastric carcinoma
pSMAD1,5,8	Rabbit polyclonal anti-phosphoSmad1/5/8	Millipore (AB3848)	1:100	Breast carcinoma
CD44	Rabbit polyclonal anti-CD44	Abcam (ab24504)	20 µg/ml	Glioblastoma
Thrombospondin (THBS)	Mouse monoclonal anti-thrombospondin	Abcam (ab1823)	1:25	Glioblastoma
MMP8	Goat polyclonal anti-MMP8	Santa Cruz (sc-8848)	1:50	Breast carcinoma
MMP10	Rabbit polyclonal anti-MMP10	Abcam (ab59437)	1:500	Breast carcinoma
Synatophysin	Rabbit polyclonal to synaptophysin	Abcam (ab14692)	1:500	Brain
GFAP	Rabbit polyclonal anti-glial fibrillary acidic protein	DakoCytomation (Z0334)	1:500	Brain
KCNA1 (Kv1.1)	Rabbit polyclonal anti-Kv1.1	Abcam (ab86211)	1:1000	Brain

Table 2.13 Biotinylated secondary antibody and blocking serum used

For primary antibody source	Secondary antibody used	Blocking agent
Rabbit or Mouse	Universal biotinylated anti-mouse/anti-rabbit IgG (Vector) raised from horse.	2.5% Normal horse serum (Vector)
Goat	1:400 Anti-goat IgG (Vector) raised from rabbit	5% Normal rabbit serum

OCT embedded tissue: Freshly frozen tissue sections (xenografts fixed with 4% PFA and embedded in OCT) were initially treated with cold methanol for 10 min followed by either 5% Normal Goat Serum or 10% Normal Donkey Serum for 1 hr. They were then incubated with either goat polyclonal anti-BMI1 (Santa Cruz Biotechnology) 1:100 or rabbit polyclonal anti-pSmad1/5/8 (Cell Signalling) 1:100 primary antibody overnight at room temperature. Appropriate secondary antibody was used: donkey anti-goat 568 (red, Invitrogen) 1:400 or goat anti-rabbit 546 (red, Invitrogen) 1:400 for 2 hr at room temperature. The sections were counterstained with DAPI and examined using Confocal 710 microscope (Zeiss).

2.10.3 Immunofluorescence

2.10.3.1 Cell preparation:

DAOY or D458 were plated at a concentration of 0.5×10^5 cells (with or without siRNA transfected) in 0.5 ml medium in each well of 24 well plate, containing Poly-lysine (PLL) coated coverslips. The PLL coated coverslips allowed cells to adhere better and contributed to better fluorescent imaging because the coverslips could be transferred on to a glass slide. After 24 – 48 hr in culture, the cells were fixed using 4% PFA for 15 min at RT. The antigen block was carried out using 5% Normal Goat Serum (NGS), and incubated with primary antibodies for 2 hr at RT (Table 2.14).

Appropriate fluorescent secondary antibodies were used at a concentration of 1:400 for 2 hr at RT. The coverslips were counterstained with DAPI (blue, nuclear staining) and mounted on glass slides. Fluorescent imaging was carried out using a Leica DFC350 microscope (Leica) and the cell counts analysed as described in chapter 3.

2.10.3.2 Cryosections:

The tissue sections that were embedded in OCT compound were removed from -80^0C, thawed and washed in PBS for 5 min x 3 on a rocker. The sections were placed in cold methanol for 5-10 min at RT to enable penetration of antibodies into the sections and to optimal staining. The slides were placed in 0.1% Tween in PBS for 5 min at RT. The edges of the slides were dried and the section areas were marked with PAP pen to limit the antibody usage. The sections were incubated with blocking solution – either 5% normal goat serum (NGS) or 10% normal donkey serum (NDS) diluted in PBS + 0.2% Triton + 0.1% NaAzide, for 1hr at RT in a humidified chamber. The sections were then incubated with theprimary antibody pre-diluted in PBS + 0.2% Triton + 0.1% NaAzide overnight at RT in a humidified chamber. The primary antibody was removed and sections were washed in PBS for 5 min x 2 and then with PBS/0.1%Tween for 5 min x 1. The sections were incubated with appropriate prediluted fluorescent secondary antibody in PBS + 0.2% Triton + 0.1% NaAzide for 2 hr in a humidified chamber. The sections were washed in PBS for 5 min x 2 and in PBS/0.1%Tween for 5 min x 1. The sections were coverslipped and mounted with Vectashield Mounting Medium (Vector) contains DAPI nuclear stain. The slides were allowed to dry for 10-15 min and the coverslips were sealed with nail polish. The sections were stored in the dark at 4^0C until microscopic

examination. The sections were evaluated at the confocal microscopy and analysed
as described in chapter 6.

Table 2.14 List of primary antibodies used in immunofluorescence analysis.

For antigen to be detected	Primary antibody used	Company	Concentration	Alexa Fluor® secondary antibody (Invitrogen)
Cell preparation				
BMI1	Mouse monoclonal anti-Bmi1	Millipore (05-637)	1:500	Goat anti-mouse 546 (red) IgG, A11003
Synaptophysin	Mouse monoclonal anti-synaptophysin	DakoCytomation (M0776)	1:50	
GFAP	Rabbit polyclonal anti-glial fibrillary acidic protein	DakoCytomation (Z0334)	1:1000	Goat anti-rabbit 488 (green) IgG, A11008
Cryosections				
BMI1	Goat polyclonal anti-Bmi1	Santa Cruz Biotechnology (sc-8906)	1:200	Donkey anti-goat IgG 568 (red) A11057
pSMAD1,5,8	Rabbit polyclonal anti-phosphoSmad1/5/8	Cell signalling (9511)	1:100	Goat anti-rabbit 546 (red) IgG A11035
CD44	Rabbit polyclonal anti-CD44	Abcam (ab24504)	1:100 (20 µg/ml)	
Laminin β-1 (LAMB1)	Rabbit polyclonal anti-Lamb1	Abcam (ab65986)	1 µg/ml	
Thrombospondin (THBS)	Mouse monoclonal anti-Thsb	Abcam (ab1823)	1:25	

2.11 Statistical analysis

All *in vitro* and *ex vivo* experiments were performed at least in triplicates unless
otherwise stated. Minimum of 6 *in vivo* xenograft models in each group were used for
tumour volume and invasion analysis, and three xenograft tumours from each group
were used for pSMAD1,5,8 expression analysis. The statistical significance of the
quantitative data was calculated using student's *t test*, and presented as mean ± SD.
The statistical significance was set at $P < 0.05$. Spearman non parametric tests and
cross-tabulations were used for correlation analysis on TMA data using SPSS®

statistical package version 20 (IBM$^®$). Kaplan-Meir survival estimation among xenograft mice were also done using SPSS, where statistical significance was calculated using Log-Rank analysis.

CHAPTER 3 BMI1 represses the BMP signalling pathway in MB cell lines and in primary MB cells of Group 4.

3.1 Introduction

BMI1 plays a role in the pathogenesis of several human cancers (Sparmann and van Lohuizen 2006) including brain tumours such as gliomas (Bruggeman, Hulsman et al. 2007) and MBs. (Leung, Lingbeek et al. 2004). Recently, using genome-wide expression analysis, MB has been classified into four distinct molecular subgroups – SHH, WNT, Group 3 (Consensus Group 3 or Northcott Group C) and Group 4 (Consensus Group 4 or Northcott Group D) (Northcott, Korshunov et al. 2011; Taylor, Northcott et al. 2012). Using a genetically engineered mouse model, our group have recently demonstrated that Bmi1 critically influences cell-cell interactions during cerebellar development, and more importantly it does so through specific inhibition of BMP signalling (Zhang, Santuccione et al. 2011). In this study, we hypothesise that BMI1 represses BMP pathway also in human medulloblastoma. BMP signalling is deregulated in MB cells (Zhao, Ayrault et al. 2008), hence the system seemed appropriate to study whether Bmi1 contributed to its deregulation. To test our hypothesis, we used well characterised MB cell lines with high BMI1 expression and checked for BMP signalling status. BMI1 overexpression is known to be more significantly associated with aggressive MB subtypes – most significantly with Group 4 tumours (Behesti, Bhagat et al. 2013). Because of the known association of Group 4 MB with high BMI1 expression, we decided to validate the findings obtained in cell lines on primary human MB cells belonging to Group 4 (or Northcott Group D) specifically.

3.2 Experimental design and methodology

3.2.1 BMI1 gene silencing by RNA interference (RNAi):

Transient *BMI1* gene silencing (knock down) in DAOY and D-458 was achieved by siRNA technology. FlexiTube siRNA (Qiagen) specific for *BMI1*, containing a mix of Hs BMI1 1, Hs BMI1 2 and Hs PCGF4 3 was used. All Stars Negative siRNA (Qiagen), referred to as scrambled (Scr) was used as control. The transfection mix was prepared and added to the cell cultures as described in Materials and Methods (M&M, chapter 2, section 2.2.2.1). To obtain maximum knock down efficiency, the transfected cells were incubated for 48 hr with the transfection mix prior to any functional study. The efficiency of BMI1 knock down was assessed by Western blot and immunofluorescence (explained in section 3.3, Fig 3.2).

Stable BMI1 silencing in DAOY cell lines and in ICb-1299 primary cells was achieved by shRNA technique using GFP labelled lentiviral vectors. Production and packaging of lentivirus is described in M&M (chapter 2, section 2.1). The cells were infected with either shRNA *BMI1* or shRNA scrambled (Scr) lentivirus at a Multiplicity of Infection (MOI, formula stated in chapter 2, section 2.2.3.1) of 12.5 for DAOY and 25 for ICb-1299. After 72 hr incubation, they were sorted by FITC gated flow cytometry (FACS) for stable selection. The cells were incubated for at least 96 hr prior to expansion or use for further studies. The efficacy of knock down was assessed by Western blot and qRT-PCR analysis at multiple time points after passaging.

Stable *BMI1* knock down (in DAOY cell lines and in primary cells ICb-1299), using the above method was used for all of the knock down experiments, except for i) investigation of BMP pathway status (section 3.3, Fig 3.5 and Fig 3.6), and ii) investigation of cell adhesion phenotype (chapter 4, section 4.3.1, Fig 4.2), where

transient BMI1 knock down (in DAOY and D-458 cell lines), using siRNA method was used.

3.2.2 BMP pathway inhibition:

To inhibit BMP signalling in DAOY or D-458 cell cultures, recombinant Noggin (Sigma) was used at a concentration of 1µg/ml (which showed low cell toxicity and efficient BMP pathway inhibition, explained in section 3.3.2.1 (Fig 3.4). Noggin was used either alone or concomitantly with siRNA *BMI1* knock down. The cultures were incubated for at least 24 hr prior to assessment of BMP signaling inhibition by reduction of pSMAD1,5,8 expression. Where the cultures had to be incubated for longer than 24 hr, they were supplemented with Noggin every 24 hr.

3.2.3 Immunocytochemistry:

The cells treated with siRNA/shRNA BMI1 for knock down studies were cultured on Poly-lysine (PLL) coated coverslips and were treated concomitantly with Noggin where appropriate to inhibit BMP signaling. Following incubation for 48 hr they were fixed using 4% Paraformaldehyde (PFA) and antigen blocked with 5% Normal Goat Serum. They were treated with BMI1 and pSMAD1,5,8 antibodies (details below) for 2 hr at RT, followed by fluorescent secondary antibodies (details below) for 2 hr at RT. The coverslips were transferred to glass slides and mounted using DAPI medium. Five random fluorescent micrographs (20X magnification) were obtained using Leica Confocal microscope DFC350 set with Y3 (red), A4 (blue) and L5 (green) filters. The number of cell nuclei staining for DAPI (blue, representing total number of cells present) and the number of cells positive only for pSMAD1,5,8 (green) was counted using ImageJ software and expressed as percentage of cells

expressing pSMAD1,5,8. The results were tabulated under scrambled and BMI1 siRNA group for both DAOY and D458.

Primary antibodies used are:

1) Mouse monoclonal anti-Bmi1, (Millipore, 05-637), 1:500

2) Rabbit polyclonal anti-phosphoSmad1/5/8, (Cell signalling, 9511), 1:100

Secondary antibodies used are (incubated at 1:400 for 2 hr at RT):

1) Alexa Flour® goat anti-mouse 546 (red) IgG (Invitrogen, A11003), 1:400

2) Alexa Fluor® goat anti-rabbit 488 (green) IgG (Invitrogen, A11008), 1:400

3.2.4 Western blot:

This method was used:

i) To screen MB cell lines for BMI1 expression levels,

ii) To confirm efficacy of BMI1 knock down in DAOY and ICb-1299, and

iii) To study pSMAD1,5,8 and SMAD1,5,8 expression levels following BMI1 silencing in DAOY and ICb-1299.

The results were normalised against expression of α-tubulin. The procedure was carried out as explained in M&M (chapter 2, section 2.4). Briefly, total protein extraction, gel separation and transfer to nitrocellulose membrane by electrophoresis were carried out. The membrane was blocked with 5% fat free milk solution and incubated with primary followed by secondary antibodies. The complex was exposed to ECL detection system and processed using film developer. The protein bands

were compared for semi-quantitative expression analysis. The antibodies used are as follows -

Primary antibodies:

1) Mouse monoclonal anti-Bmi1 (Millipore, 05-657), 1:500, ON at 4^0C.

2) Mouse monoclonal anti-alpha-tubulin (Sigma, T6199), 1:5000, 2 hr at RT.

3) Rabbit polyclonal anti-pSMAD1,5,8 (Cell Signalling, 9511), 1:500, ON at 4^0C.

4) Rabbit polyclonal anti-SMAD1,5,8 (Santa Cruz Biotechnology, sc-6031-R), 1:400. 6 hr at RT.

Secondary antibodies:

1) ECL peroxidase anti-mouse IgG from sheep (GE Healthcare, NA931VS), 1:3000, 1 hr at RT.

2) HRP anti-rabbit IgG (Santa Cruz Biotechnology, sc-2030), 1:3000, 1 hr at RT.

3.2.5 qRT-PCR:

The efficacy of BMI1 silencing following lentiviral shRNA treatment in DAOY and Icb-1299 was tested using TaqMan Assay. Expression analysis of *ID1* and *ID2* (Inhibitors of DNA binding 1 & 2 respectively) genes to check for activation of downstream targets of BMP-pSMAD1,5,8 signalling was done by SYBR Green assay. The details of qRT-PCR is explained in M&M (chapter 2, section 2.5.5).

ID1 and *ID2* primers were designed using PRIMER3 software and validated using NCBI primer-BLAST system. The forward and reverse primers were obtained from Sigma. RNA was extracted from the cells and cDNA was prepared by reverse transcription. qRT-PCR was carried out using the following primers -

TaqMan Assay (Applied Biosystems):

1) BMI1 (human), Hs00180411_m1, NM_005180.8

2) ACTB (human β-actin), Hs99999903_m1, NM_001101.3

SYBR Green method:

1) ID1 (transcript variant 1) NM_002165.3

   Forward 5'-CCCCAGAACCGCAAGGTGAGC-3'

   Reverse 5'-CAGGAACGCATGCCGCCTCG-3'

2) ID2, NM_002166.4

   Forward 5'- TCTCGCCTTCCCTCGCGGTC-3'

   Reverse 5'- CGTGTTGAGGGTGGTCAGCGG-3'

3) GAPDH, NM_002046.4

   Forward - GCACAGTCAAGGCCGAGAAT

   Reverse- GCCTTCTCCATGGTGGTGAA

The expression levels of required genes were determined by calculating their ΔCT values and were normalised to that of house-keeping gene, GAPDH expression. Mean expression (fold change) with standard deviation relative to controls were calculated.

3.3 Results

3.3.1 Efficient BMI1 knock down was achieved by RNAi methods in human medulloblastoma cell lines known to express high levels of BMI1

To test our hypothesis that BMI1 overexpression suppressed BMP signalling pathway in human medulloblastoma, we set out to study the BMP pathway status in those MB cell lines which had high BMI1 expression. Five human MB cell lines - UW228-2, D-425, D-458, D-341 and DAOY (obtained from ATCC) were screened for BMI1 protein expression by Western Blot (test carried out by Xinyu Zhang, Department of Neurosciences, Blizard Institute, Barts and the London School of Medicine and Dentistry). BMI1 expression in these cell lines was observed (Fig 3.1A), and the expression levels were comparable to that previously observed by Leung et al. Fig 3.1B) (Leung, Lingbeek et al. 2004), and in majority of the 12 primary human tissue samples analysed (Fig 3.1C) (Leung, Lingbeek et al. 2004).
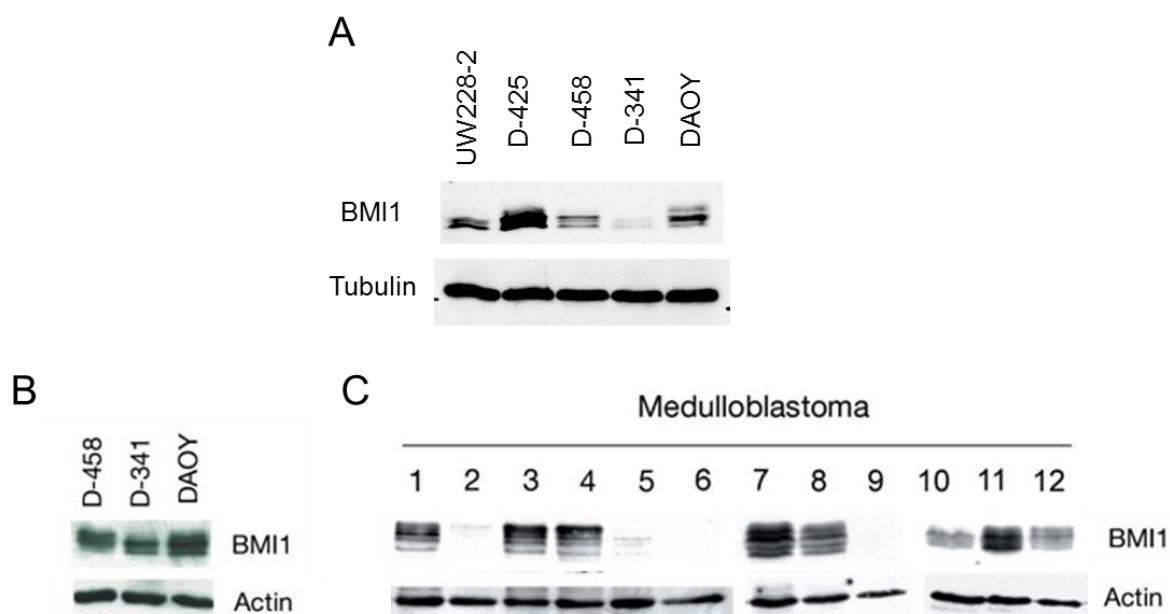
Fig. 3.1 Western blot analysis of BMI1 expression in human MB cell lines and primary tumour samples.

(A) BMI1 is expressed in the fiveMB cell lines screened – UW228-2, D-425, 4-458, D-341 and DAOY. The expression levels of the cell lines is estimated by means of Western blot compared to previous

results **(B),** and twelve primary human primary MB tissue samples **(C),** from Leung et al. study (Leung et al. 2004, Nature). Similar BMI1 expression levels were observed with a slightly lower expression in D-341. DAOY and D-458, which had stable BMI1 expression levels were further used in our study,

Having established that BMI1 was highly expressed in the above cell lines, we chose DAOY and D458 for further studies. We chose these cell lines because i) they are extensively characterised, and ii) stable BMI1 expression levels were detected. *BMI1* knock down was carried out using both transient lipofection-mediated siRNA delivery and stable lentiviral-mediated shRNA delivery. To assess efficiency of knockdown immunocytochemistry for BMI1 antibody was performed. Five fields in each well were imaged and the experiments were conducted in triplicates. Although the number of cells expressing BMI1was not quantified, optical imaging suggested consistently reduced BMI1 expression (number and/or intensity) in both DAOY (Fig 3.2A) and D-458 (Fig 3.2B) cultures upon BMI1 knock down.

To confirm the above finding, a semi-quantitative assessment using the Western Blot method was performed. Total protein was extracted from siRNA treated cells cultures and immunoblot was performed against BMI1 antibody. There was a reduced BMI1 protein expression noted in BMI1 siRNA treated DAOY and D-458 extracts as compared to siRNA Scr and untreated controls (Fig 3.2C), thus corroborating the immunocytochemistry results. It is noted that the BMI1 bands in Fig 3.2C appear different for DAOY and D458. The possible reason for this could be partial degradation of BMI1 protein in the DAOY lysates used, giving a smear like appearance. Other possible influencing factors could be the exposure time, and quality of primary and/or secondary antibody used.
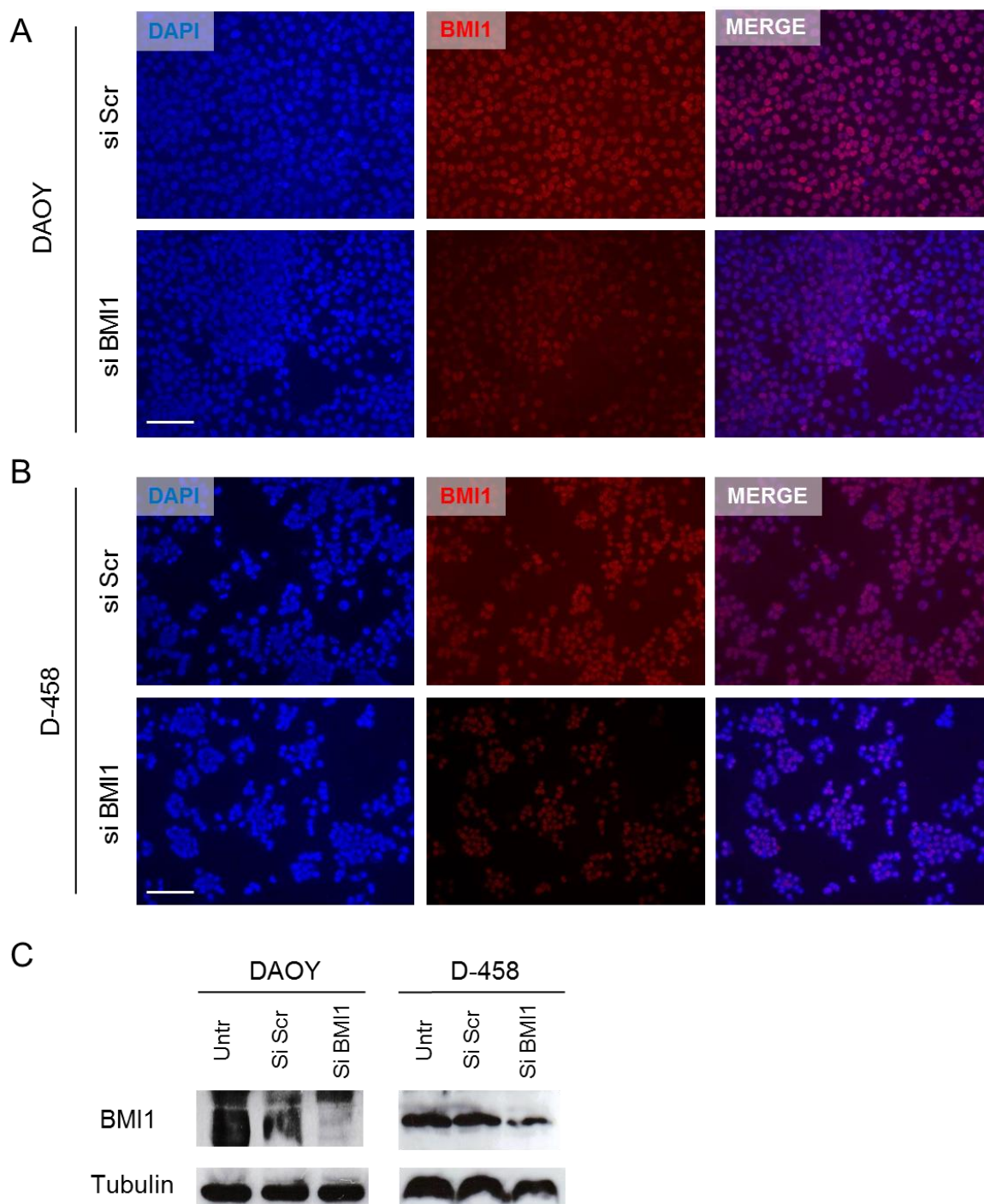
Fig. 3.2 Immunofluorescence and Western blot demonstrating an effective siRNA mediated BMI1 knock down in MB cell lines.

Transient *BMI1* knock down was carried out using lipofection-mediated siRNA delivery. Immunohistochemistry suggested an effective BMI1 knock down 48 hr of transfection in both **(A)** DAOY and **(B)** D-458, where a reduction in number and intensity of BMI1 expression was observed in all five representative fields (n=3). Left panel showing DAPI channel with total number of cell nuclei; middle panel showing BMI1 positive cells; and right panel showing merged image. **(C)** Western blot analysis confirming a reduction in BMI1 protein expression in siRNA BMI1 treated DAOY (left) and D-458 (right) cells, as compared to untreated and siRNA scrambled treated controls. Scale bar in both **(A)** and **(B)** = 50 μm.

The procedure for stable BMI1 knock down using lentivirus mediated shRNA constructs is detailed in section 3.2.1 and in M&M (chapter 2, section 2.2.3.1). Briefly, DAOY cells were infected with shRNA lentivirus at an MOI of 12.5, incubated for 72 hr and stable selection was achieved by FACS-mediated enrichment for GFP positive cells, which were expanded for further studies. The efficacy of knock down in the cultures was assessed by qRT-PCR analysis at three different time points after passaging. The average of relative fold change in shRNA BMI1 treated cells as compared to shRNA Scr treated cells was calculated. There was an average of five fold reductions in *BMI1* mRNA levels in DAOY cells confirming an effective *BMI1* knock down (Fig 3.3 A). Reduction in BMI1 protein levels was also demonstrated by Western Blot analysis (Fig 3.3 B) using protein extracts from cells collected 96 hr after FACS selection following shRNA lentiviral infection.

This shows that lentivirus mediated shRNA-technique is suitable for BMI1 knock down in DAOY; and was used for further experiments. From here on shRNA Scr treated DAOY cells will be referred to as DAOY^{Scr} and shRNA BMI treated cells as DAOY^{BMI1kd}.
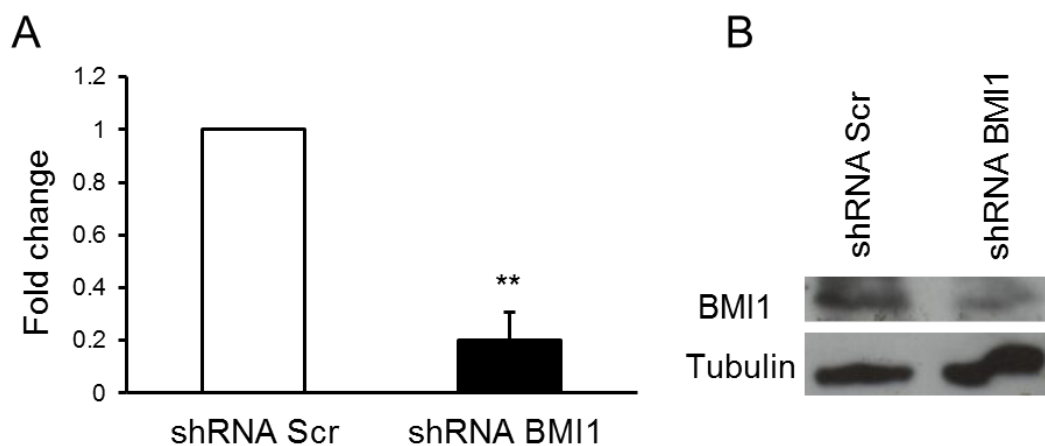
Fig. 3.3 Successful reduction of BMI1 expression in DAOY cells upon lentivirus shRNA-mediated knock down.

(A) qRT-PCR showing an average (n=3) of five-fold relative reduction in *BMI1* expression (normalised against *β–actin* expression) in shRNA BMI1 treated cells as compared to shRNA Scr treated cells. **(B)** Western blot confirming reduction in BMI1 protein expression 96 hr after FACS sorting of shRNA BMI1 Treated cells. Error bar represents SD (n=3). **, P<0.01.

3.3.2 BMI1 silencing leads to aberrant activation of BMP signalling pathway in MB cell lines.

3.3.2.1 Efficacy of Noggin as BMP pathway inhibitor was demonstrated in DAOY and D-458

Having established efficient BMI1 knock down techniques, the next step was to identify a method to efficiently inhibit BMP pathway to enable us to study if any functional impact observed upon BMI1 silencing was mediated by a putative BMP pathway activation.

Noggin is a 26 kd secreted protein that was first described as a neural inducer in Xenopus, required for normal dorsal development (Smith and Harland 1992). Noggin is an established inhibitor of BMP pathway (Zimmerman, De Jesus-Escobar et al. 1996) which acts by competitively binding to BMP-2 and BMP-4 preventing ligand activation of BMP receptors and SMAD1,5,8 mediated signalling. Noggin has been previously used as a BMP inhibitor in medulloblastoma cells (Hallahan, Pritchard et al. 2003).

DAOY and D-458 were plated in a density of 0.5 x 10^5 cells in 0.5 ml media/well in triplicates. Noggin was added to the cultures at 1µg/ml and incubated for 24 hr. The cells were then fixed and immunocytochemistry for pSMAD1,5,8 was performed to assess BMP pathway inhibition. Phosphorylation of SMAD1/5/8 proteins (pSMAD 1/5/8) via activated BMP receptors (BMPR) is the main functional indicator of BMP

pathway activation (Grimmer and Weiss 2008), and its detection is commonly used to assess pathway status (see Fig 1.7 in chapter 1). The number of cells expressing pSMAD1,5,8 was assessed by fluorescence imaging and compared to that of untreated cells. Five fields in each coverslip were imaged at 20X magnification, and the experiments were conducted in triplicates. The average number of cells expressing pSMAD1,5,8 among Noggin treated cells were reduced compared to the untreated cultures – 57.88% (± 2.85) vs. 77.05% (± 3.25) in DAOY (p=0.0007) [Fig 3.4 A and C] and 23.69% (± 7.19) vs. 36.06% (± 5.19) in D-458 (p=0.036) [Fig 3.4 B and D].

Western blot was also performed using DAOY protein lysates, which showed that pSMAD1,5,8 expression was reduced in relation to total SMAD1,5,8 among Noggin treated cells as compared to the untreated control cells (Fig. 3.4 E).

We concluded that Noggin behaved as a BMP signalling inhibitor in our cell lines, in keeping with existing literature (Hallahan, Pritchard et al. 2003). Noggin was therefore used in further experiments to study if functional changes induced upon BMI1 knock down were BMP pathway related.
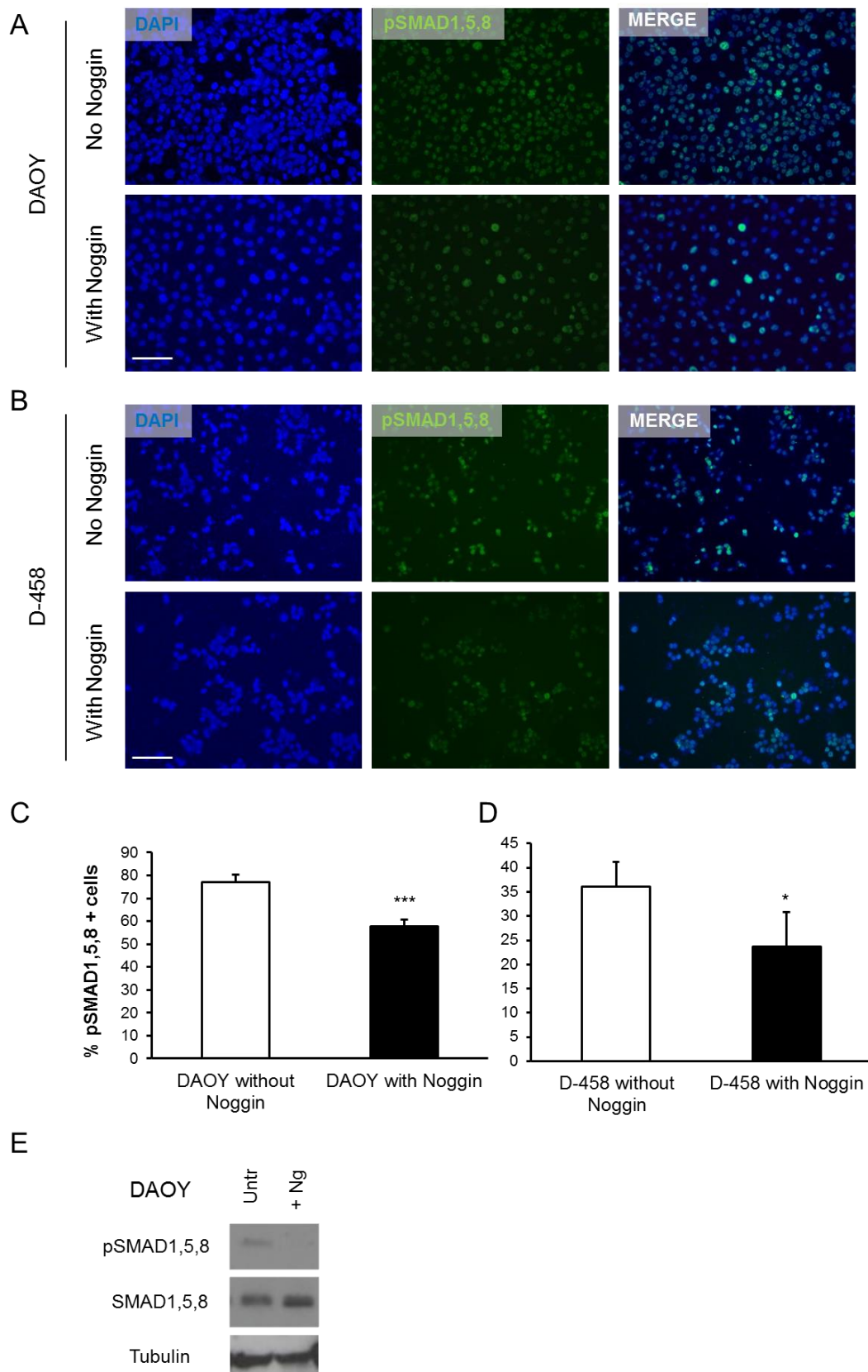
Fig. 3.4 Noggin treatment reduces the pSMAD1,5,8 expression in MB cell lines.

After 24 hr of Noggin treatment at 1 μg/ml, a reduction in the number of cells expressing pSMAD1,5,8 as well as a reduction in the staining intensity was noted in both **(A)** DAOY and in **(B)** D-458 cells,

suggestive of inhibition of BMP pathway. Left panel showing DAPI channel with total number of cell nuclei; middle panel showing pSMAD1,5,8 positive cells; and right panel showing merged images. **(C and D)** Quantification of the percentage of pSMAD1,5,8 positive cells (per 20x field), from three independent experiments shows a significant reduction in the number of positive cells in Noggin treated DAOY **(C)** and D-458 **(D)** cells as compared to corresponding untreated counterparts. **(E)** Western blot showing a reduction of pSMAD1,5,8 expression upon Noggin (Ng) treatment in DAOY cells, as compared to total SMAD1,5,8 expression and Tubulin expression as a loading control. Scale bar in both **(A)** and **(B)** = 50 μm. Error bars in **(C)** and **(D)** represent SD (n=3). *, p<0.05; ***, P<0.001.

3.3.2.2 Increased pSMAD1,5,8 expression upon BMI1 knock down in DAOY and D-458 cell linesis reversed by Noggin.

Next, the effect of BMI11 knock down on BMP pathway in MB cell lines was assessed by checking pSMAD1,5,8 expression upon Bmi1 knock down in these cell lines.

DAOY and D-458 were plated in a density of 0.5×10^5 cells in 0.5 ml media/well in 3 wells of 24 well plates. The cells were transfected with BMI1 siRNA using lipid based transfection agent and incubated for 48 hr. Negative siRNA (Scramble or Scr) treated cells were used as controls. The cells were then fixed and immunocytochemistry for pSMAD1,5,8 was performed . The number of cells expressing pSMAD1,5,8 was assessed in DAOY^{BMI1kd} and D-458^{BMI1kd} cultures as compared to that of DAOY^{Scr} and D-458^{Scr}. Five fields in each well were imaged and the experiments were conducted in triplicates. The average number of cells expressing pSMAD1,5,8 among DAOY^{BMI1kd} and D-458^{BMI1kd} was increased when compared to those with DAOY^{Scr} and D-458^{Scr} cultures respectively - 86.63% (+/- 2.41) vs. 77.05% (+/- 3.25) in DAOY (p=0.017) [Fig 3.5 A and C] and 51.17% (+/- 1.74) vs. 36.06% (+/- 5.19) in D-458 (p=0.004) [Fig 3.5 B and D].

In parallel, DAOY cells were treated with lentivirus mediated BMI1 shRNA to achieve stable knock down (DAOY^{BMI1kd}). As controls DAOY cells infected with empty vector

(Scrambled or Scr) lentivirus (DAOY^{Scr}) were used. After FACS sorting cells were collected and total protein was extracted. Western blot was performed to assess pSMAD1,5,8 expression in comparision to SMAD1,5,8 (α-tubulin used for loading control). In keeping with above findings, there was an increase in pSMAD1,5,8 expression in DAOY^{BMI1kd} as compared to DAOY^{Scr} control (Fig. 3.5 E).

To assess if the above differential expression is indeed related to BMP pathway, we assessed the pSMAD 1,5,8 expression in cultures concomitantly treated with Noggin. Noggin treatment in DAOY and D-458 significantly reduced the pSMAD1,5,8 expression in both DAOY and D-458 (Fig 3.4) thereby confirming its efficacy as a BMP signalling inhibitor in our experimental setting. Noggin was further added concomitantly to siRNA BMI1 treated cultures at 1µg/ml, incubated for 48 hr and immunofluorescence was performed as above. The average number of pSMAD1,5,8 positive cells were reduced as compared to siBMI1 only treated cells – 78.47% (+/- 1.69) vs. 86.63% (+/- 2.4) in DAOY (p=0.006) [Fig 3.5 A and C] and 39.67% (+/- 1.35) vs. 51.17% (+/- 1.74) in D-458 (p=0.0004) [Fig 3.5 B and D]. These results support the notion that BMI1 mediated repression of pSMAD1,5,8 is BMP pathway related.

To exclude any non-specific effect of the Noggin treatment on BMI1 expression, qRT-PCR was performed on DAOY^{Scr} or DAOY^{BMI1kd} cells. BMI1 expression levels (normalised to β-actin) were unchanged upon Noggin treatment (Fig 3.5 F).
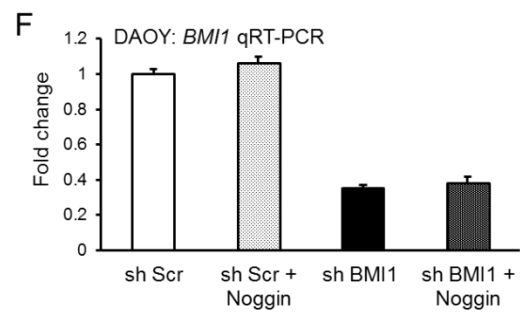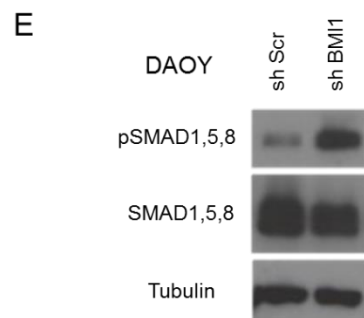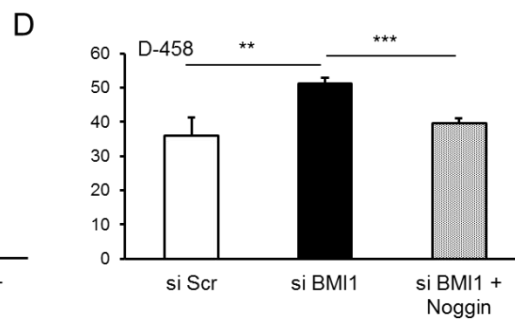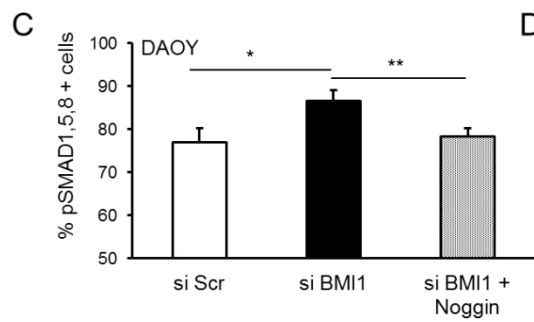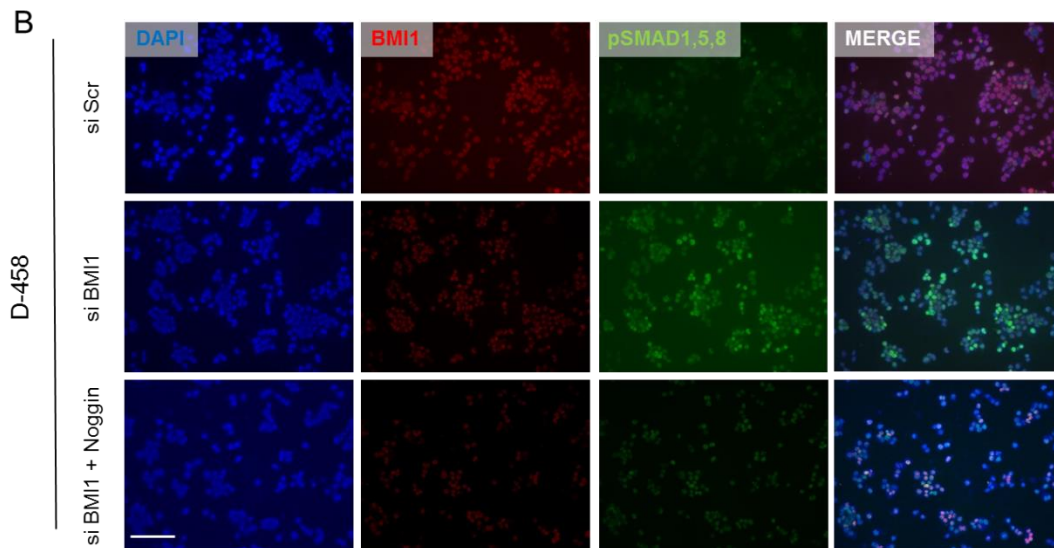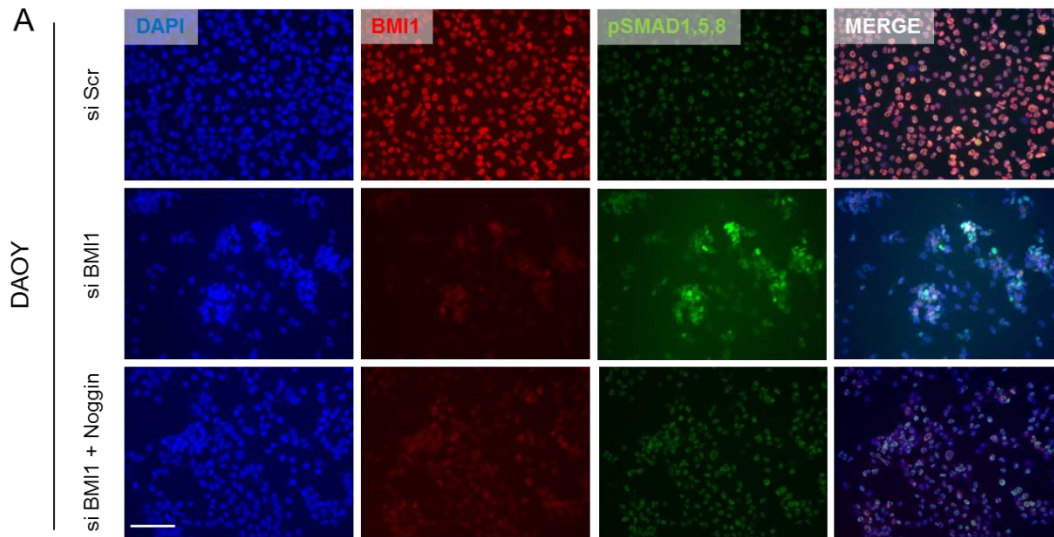
Fig. 3.5 Aberrant activation of BMP pathway upon *BMI1* knock down in MB cell lines is reversed by Noggin treatment.

(A and B) Immunohistochemistry showing an increase in the average number (and intensity) of cells expressing pSMAD1,5,8 between siRNA BMI1 treated **(A)** DAOY or **(B)** D-458 cells, and siRNA Scr treated controls. This finding is indicative of BMP pathway activation. Concomitant addition of Noggin to BMI1 knock down cultures shows a decrease in pSMAD1,5,8 expression, to levels similar to that seen in siRNA Scr treated cultures. Left panel showing DAPI channels with total number of cell nuclei; middle panel showing pSMAD1,5,8 positive cells; and right panel showing merged images. **(C and D)** Quantification of percentage of pSMAD1,5,8 positive cells (per 20x field) from three independent experiments shows a significant increase in siRNA BMI1 treated cells compared to corresponding siRNA Scr treated counterparts. There is a significant reduction in pSMAD1,5,8 levels when Noggin is concomitantly added to BMI1 knock down cells. **(E)** Western blot confirming an increase in pSMAD1,5,8 expression (in relation to total SMAD1,5,8 expression) in protein extracts of shRNA BMI1 treated cells compared to shRNA Scr treated control. Tubulin expression is used for loading controls. **(F)** qRT-PCR showing no difference in BMI1 expression levels when Noggin is added to either shRNA Scr or shRNA BMI1 treated cells, excluding any non-specific actions of Noggin on BMI1 expression. Scale bar in both **(A)** and **(B)** = 50 μm. Error bars in **(C)**, **(D)** and **(F)** represent SD, n=3. *, $p<0.05$; **, $p<0.01$; ***, $p<0.001$.

3.3.3 Primary human medulloblastoma cells isolated from a Group 4 tumour show high BMI1 expression and BMI1 knock down confirms activation of BMP signalling.

Having observed BMP signalling pathway repression by BMI1 in MB cell lines, we wanted to validate the findings on primary human MB cells. We obtained different lines of primary cells from our collaborator Dr Xiao-Nan Li, Baylor College of Medicine, Texas Children's Cancer Centre, USA. These primary short term cultures have previously been shown to give rise to MB mimicking the tumour of origin in murine xenografts (Shu, Wong et al. 2008; Zhao, Liu et al. 2012) . Our Group have recently reported that *BMI1* is most highly expressed in Group 4 MB (Behesti, Bhagat et al. 2013). Among the cultures established by our collaborator, ICb-1299 was derived from a group 4 MB and was shown to stably retain this expression profile (Zhao, Liu et al. 2012). Therefore we used short term cultures of ICb-1299 cells for our experiments. First we checked BMI1 expression in these cells. Total protein was extracted and Western blot was performed to assess BMI1 expression. We observed BMI1 protein expression (normalised to α-tubulin) in ICb-1299 at even higher levels compared to that in DAOY (Fig 3.6 A).

Next, we set out to check BMP signalling status upon BMI1 silencing in the primary cells. Due to the nature of growth of these cells as tumour spheres siRNA mediated knock down would be unsuitable. Therefore lentivirus shRNA mediated stable knock down method was used. The cells were infected with shRNA *BMI1*, and GFP positive cells were enriched for by FACS. Following short term cultures, the cells were collected to extract total RNA and protein. shRNA scrambled (Scr) lentivirus treated cells were used as controls. qRT-PCR analysis normalised to β–actin showed an approximately 4-5 fold reduction in *BMI1* expression (Fig 3.6 B). Western Blot analysis normalised to α-tubulin demonstrated a significantly reduced BMI1 protein expression in shRNA BMI1 treated cells (Fig 3.6 C).

These findings demonstrated an effective BMI1 knock down achieved by lentiviral mediated BMI1 shRNA delivery in these cells (ICb-1299^{BMI1kd}) as compared to scrambled shRNA treated cells (ICb-1299^{Scr}).

Prior to functional studies using the primary cells, it was essential to check for BMP pathway status following BMI1 silencing. Western blot analysis using total protein extracts from these short term cultures was performed. Negligible pSMAD1,5,8 protein expression was noted in ICb-1299^{Scr} as compared to SMAD1,5,8 expression, whereas a significant increase in its expression was detected in ICb-1299^{BMIkd} (Fig 3.6 D). This is indicative of increased phosphorylation of SMAD1,5,8 proteins and BMP pathway activation and it is keeping with a scenario where BMI1 represses BMP pathway in human MB cells.
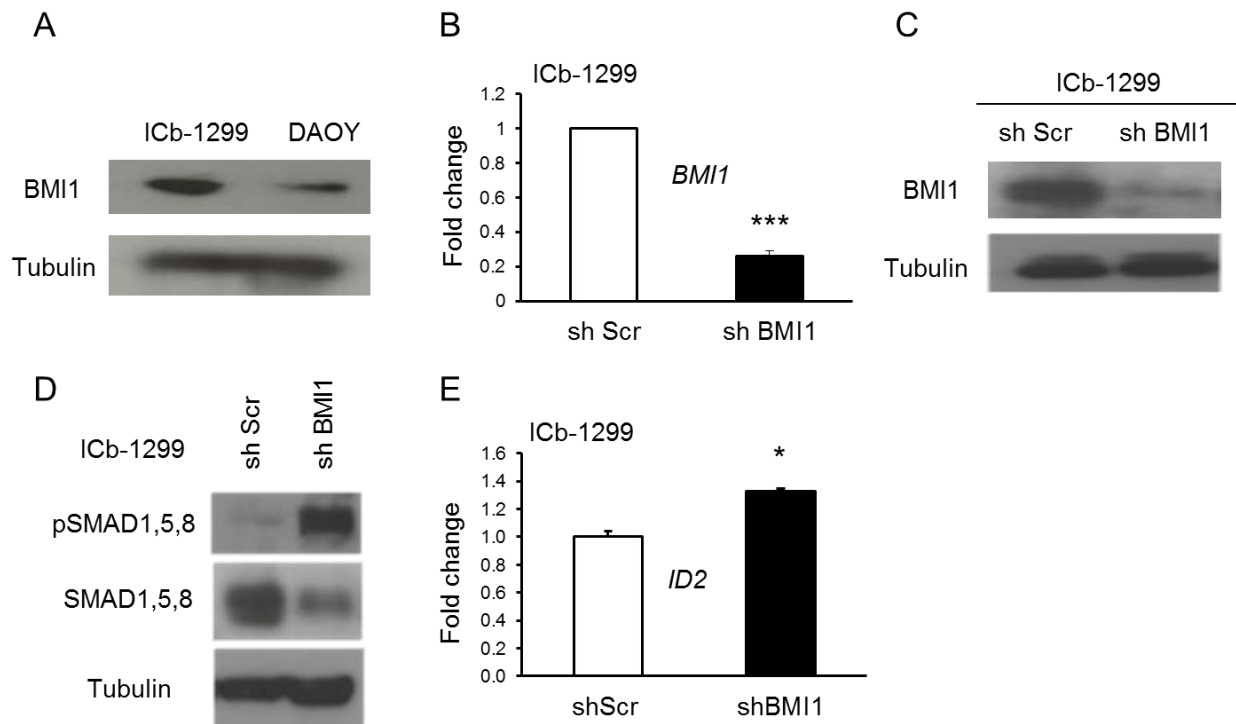
Fig. 3.6 BMP pathway activation upon BMI1 knock down in primary Group 4 MB cells.

(A) Western blot showing BMI1 expression in ICb-1299 to be even higher than that seen in the DAOY cell line. **(B and C)** Efficient BMI1 knock down is established in primary cells ICb-1299 following lentivirus shRNA-mediated transfection, as demonstrated by qRT-PCR analysis **(B),** and by Western blot analysis **(C)**. **(D)** Western blot analysis shows an increase in pSMAD1,5,8 expression in relation to total SMAD1,5,8 (Tubulin as loading control) following BMI1 knock down in ICb-1299 cells. This is similar to the observation made in DAOY and D-458 cell lines and implies activation of BMP pathway. **(E)** qRT-PCR showing an increase in *ID2* (a downstream target of BMP-SMAD pathway) expression in *BMI1* silenced cells as compared to controls. Error bars in **(B)** and **(E)** represent SD of three technical replicas. *, $p<0.05$; ***, $p<0.001$.

Having observed increased pSMAD1,5,8 levels upon BMI1 knock down, we asked if this could be confirmed by activation of known downstream targets of BMP signalling. To this end, we chose to check for *ID* (Inhibitors of DNA binding) mRNA transcript levels by qRT-PCR.

Briefly, Id proteins are dominant negative helix-loop-helix (dnHLH) transcription factors that do not have DNA binding capacity, but that can heterodimerize with basic helix-loop-helix (bHLH) proteins and inhibit transcriptional activity of the latter (Sun, Copeland et al. 1991). Four distinct members (Id1 – Id4) have been identified

in mammals and they are involved in control of cell growth, differentiation and tumorigenesis [Reviewed in (Ruzinova and Benezra 2003)]. *ID* genes are well established downstream targets of BMP – SMAD signalling pathway (Katagiri, Imada et al. 2002; Korchynskyi and ten Dijke 2002; Lopez-Rovira, Chalaux et al. 2002). Exogenous BMPs are shown to increase *ID1* and *ID2* expression in a time dependent fashion in human bone marrow stromal cells (Locklin, Riggs et al. 2001). Moreover, BMP-2 and BMP-4 treatment is shown to increase ID1 and ID2 protein levels along with pSMAD1,5,8 protein levels in primary medulloblastoma cells in vitro (Zhao, Ayrault et al. 2008). We optimised conditions for *ID1* and *ID2* and performed qRT-PCR, normalising the expression to GAPDH. There was no significant increase in *ID1*, but we noted an increase in *ID2* expression in ICb-1299[BMI1kd] as compared to ICb-1299[Scr] (Fig. 3.6 E).

3.4 Discussion

BMI1 overexpression is strongly associated with aggressive MB subtypes with poor prognosis (Wang, Venugopal et al. 2012). *BMI1* is essential for self-renewal of haematopoietic and neural stem cells [reviewed in (Valk-Lingbeek, Bruggeman et al. 2004)] and its targeted deletion in a mouse model (null mutant) causes severe neurological and haematopoietic defects (van der Lugt, Domen et al. 1994). As targeted deletion of BMI1 is incompatible with life, it is conceivable that its targeted suppression as a therapeutic option could be associated with important side effects. BMP-2 is shown to induce apoptosis in a dose and time dependent fashion in primary human MB cells (Hallahan, Pritchard et al. 2003). Moreover, BMP-2 and BMP-4 are shown to suppress primary murine MB cell growth *in vitro* and *in vivo* (Zhao, Ayrault et al. 2008), and BMP-2 inducing agents such as retinoic acid have been shown to reduce human MB cell growth *in vitro* and *in vivo* (Spiller, Ditzler et al. 2008). Therefore BMPs or BMP agonists could be developed as therapeutic options for MB treatment. We hypothesise that, if repression of the BMP signalling pathway by BMI1 is an essential event in human medulloblastoma pathogenesis, then BMI1 expression could be a potential bio-marker for MB which may respond to BMP analogues.

In this chapter we demonstrate that in human MB cell lines DAOY and D-458, which are known to express BMI1, pSMAD1,5,8 expression is negligible. But upon BMI1 silencing, pSMAD1,5,8 expression is increased - indicative of a derepression of the BMP signalling pathway. Moreover, we observe that pSMAD1,5,8 expression is increased following *BMI1* silencing also in primary human MB cells, thereby validating our findings of cell lines. We have used two independent methods -

immunohistochemistry (for DAOY and D-458) and Western Blot (for primary cells Icb-1299 and DAOY) to demonstrate repression of BMP pathway by BMI1 in MB cells. Similar results were observed when *BMI1* silencing was carried out using either transient siRNA technique (for DAOY and D-458) or protracted shRNA method (in primary cells Icb-1299 and in DAOY again), allowing us to exclude technical artefacts even more robustly. The experiments carried out in DAOY and D-458 after concomitant inhibition of BMP signalling by noggin provided further support to the notion that the effect seen upon BMI1 knock down in human MB cells was BMP mediated.

One of the downstream targets of BMP-SMAD signalling, ID2 gene expression was found to be increased following *BMI1* silencing, providing additional support to the notion that BMI1 overexpression suppresses BMP signalling. Id proteins are implicated in several cancers (Lasorella, Uo et al. 2001) and a recent study has shown that although Id expression in normal cerebellum is absent or minimal there is a differential expression of Id proteins observed in human medulloblastoma tumour cells and in the endothelial cells of the tumour (Snyder, Dulin-Smith et al. 2013). Therefore the association between BMI1 and Id genes could be further explored in future studies.

In summary, we demonstrate here that BMI1 constitutively represses BMP signaling in both MB cell lines and in primary group 4 MB cells. To understand the relevance of BMI1 silencing on BMP signalling, we set out to investigate the BMP-dependency of the functional changes seen upon BMI1 knock down in MB cells.

CHAPTER 4 Cell migration of medulloblastoma cell lines is regulated by BMI1 in a BMP dependent fashion in vitro.

4.1 Introduction

The role of Bmi1 in human cancers has been primarily associated to the regulation of cell proliferation and senescence via suppression of p16Ink4a/p19Arf cell cycle inhibition pathways. (Jacobs, Kieboom et al. 1999; Jacobs, Scheijen et al. 1999; Meng, Luo et al. 2010). Studies investigating its role in cancer cell migration and invasive properties have also emerged. Bmi1 is shown to induce epithelial-mesenchymal transition (EMT) in human nasopharyngeal carcinoma (Song, Li et al. 2009). Suppression of endogenous Bmi1 has been shown to reduce cell motility and invasive properties in breast cancer cells (Guo, Feng et al. 2011) and in gliomas cells (Jiang, Wu et al. 2012). This is suggestive that Bmi1 regulates other cell signalling pathways, more relevantly, those regulating extracellular matrix and cell adhesion properties. BMP pathway is known to regulate EMT and hence cancer cell motility and invasion (Reviewed in (Yang and Weinberg 2008)). Furthermore, TGF-β/BMP pathways are known to cross talk with other signalling pathway related to EMT such as Notch, Wnt and Shh pathways thereby influencing cancer invasion and metastasis (Reviewed in (Bailey, Singh et al. 2007) and (Guo and Wang 2009)).

Using a genetically engineered mouse model, our team have demonstrated that cell-cell interactions between granule and glial progenitors are critically affected by Bmi1 during cerebellar development, through specific inhibition of BMP signalling (Zhang, Santuccione et al. 2011). As BMP signalling is known to regulate cell-cell and/or cell-extracellular matrix (ECM) interactions, thereby controlling cell motility

(reviewed in (Guo and Wang 2009)), our team have also analysed whether Bmi1 could regulate the expression of cell-cell and cell-matrix interaction genes in granule cell progenitors (GCPs). GCPs were isolated from P7 cerebella of $Bmi1^{-/-}$ mice and control littermates, total RNA was extracted at DIV1 and real time PCR expression arrays were used to analyse the expression of 84 genes related to cell adhesion (RT^2 Profiler^{TM} PCR Array Mouse Extracellular Matrix and Adhesion Molecules). The analysis was performed on three independent preparations, fold changes were calculated and significance was analysed by Student's t-test. 18 cell-cell/matrix interaction genes were expressed at significantly higher level in $Bmi1^{-/-}$ GCPs ($p<0.05$) (Table 4.1), of which 12 showed more than 2-fold increase in their expression level (range 2.11-5.68). These genes included Thrombospondin1, 2 and Fibronectin, Fibulin, Collagens -type I, IV, V and VI, Laminin 1 as well as CD44 and MMP 2, 8, 10.

Next, it was assessed whether BMP pathway inhibition would affect the expression of Bmi1-regulated cell adhesion and extracellular matrix genes. Cultures were prepared from P7 cerebella of $Bmi1^{-/-}$ and control littermates in triplicates and were treated with Noggin prior to expression analysis. Noggin (Ng) is a well characterised inhibitor of BMP signalling which acts by competitively binding to the BMP cell surface receptors (Zimmerman, De Jesus-Escobar et al. 1996). We identified 4 Bmi1-regulated cell adhesion genes whose expression was significantly ($p<0.05$) downregulated upon Noggin treatment are listed in Table 4.1. These genes were Thrombospondin 2, CD44, MMP10 and Collagen 6a1.

Table 4.1. Cell adhesion and extracellular matrix genes whose expression is significant upregulated in Bmi1-/- mCGC and expression profile after Noggin treatment*

Genes	Accession	KO/WT-Fold	P value	Ng-KO/WT-Fold	P value
Thrombospondin 1, mRNA	NM_011580	4.72	0.0005	5.92	0.189343
Elastin microfibril interfacer 1, mRNA	NM_133918	2.54	0.0012	2.8	0.303034
Matrix metallopeptidase 2, mRNA	NM_008610	2.97	0.0014	9.47	0.185114
Thrombospondin 2, mRNA	NM_011581	**1.65**	**0.0047**	**-1.15**	**4.98E-05**
Collagen, type IV, alpha 1, mRNA	NM_009931	1.9	0.0058	2.59	0.057293
Laminin, alpha 1	NM_008480	3.67	0.0062	2.83	0.168255
A disintegrin-like and metallopeptidase (reprolysin type) with thrombospondin type 1 motif, 8, mRNA	NM_013906	1.74	0.0071	3.08	0.182631
Matrix metallopeptidase 10, mRNA	NM_019471	**4.32**	**0.0091**	**-1.22**	**0.007599**
Collagen, type VI, alpha 1	NM_009933	**1.69**	**0.0115**	**1.02**	**0.028593**
Collagen, type I, alpha 1, mRNA	NM_007742	2.61	0.0124	5.56	0.128066
Collagen, type V, alpha 1, mRNA	NM_015734	3.19	0.0133	1.01	0.158273
CD44 antigen	NM_009851	**1.73**	**0.0160**	**-1.13**	**0.037609**
Selectin, lymphocyte, mRNA	NM_011346	-2.36	0.0190	-2.5	0.49582
Matrix metallopeptidase 8, mRNA	NM_008611	5.68	0.0201	3.47	0.227461
Tissue inhibitor of metalloproteinase 2, mRNA	NM_011594	2.69	0.0289	1.96	0.106224
Fibronectin 1	NM_010233	3.18	0.0310	4.08	0.331714
Secreted acidic cysteine rich glycoprotein, mRNA	NM_009242	2.11	0.0452	1.67	0.220898
Fibulin 1	NM_010180	3.91	0.0495	1.51	0.109213

* Statistically significant genes are highlighted in bold.

These data suggest that a subset of cell adhesion genes may be regulated by Bmi1 through BMP pathway repression during cerebellar development, which forms the basis for our further experiments described in this chapter.

Having established that BMI1 represses BMP signalling in human MB cells (chapter 3), we set out to assess whether Bmi1 could control cell adhesion and cell motility properties through suppression of BMP signalling. To this end we studied cell adhesion and cell motility of MB cells upon BMI1 knock down. To assess whether

BMI1 could regulate these properties of MB cells via BMP pathway, cells were

concomitantly treated with Noggin and the results were analysed comparatively.

4.2 Experimental design and methodology:

4.2.1 Assessment of multicellular aggregate formation:

The cells treated with siRNA/shRNA BMI1 for knock down studies were cultured on PLL coated coverslips in 24 well plates (3 wells per group) and concomitantly treated with Noggin where appropriate to inhibit BMP signaling. Following incubation for 48 hr they were fixed and immunohistochemistry was performed for BMI1 and pSMAD1,5,8 antibodies as described in the previous chapter. The coverslips were transferred to glass slides and mounted using DAPI medium. Five random fluorescent micrographs (20X magnification) were obtained using Leica Confocal microscope DFC350 set with Y3 (red), A4 (blue) and L5 (green) filters. The DAPI pictures were used to quantify the multicellular clusters using ImageJ software. Number of clusters of 10 cells or more were counted in five random fields in each well (3 wells per group) and averaged. The results were tabulated under scrambled and BMI1 siRNA group for both DAOY and D458. The experiment was conducted in triplicates. Student's t-test was used to calculate the significance of differences.

4.2.2 Cell migration assays

To assess the effects of *BMI1* silencing on MB cell migration/motility and cell invasion *in vitro*, Transswell® migration and wound healing assays were used.

4.2.2.1 Wound healing assay using time lapse videomicroscopy

Wound healing assay allows studying cell migration and cell interactions. The experiment was performed following published protocols (Hu and Verkman 2006; Kurayoshi, Oue et al. 2006). The procedure is detailed in M&M (chapter 2, section 2.6.1).

Wound healing assay could not be conducted using D-458 cells as they grew as partial tumour spheres in suspension and showed minimal adhesion. Therefore wound healing assay was carried out using DAOY cells only.

4.2.2.2 Time lapse videomicroscopy to assess cell motility (without wound)

Time lapse videomicroscopy is used to track and study individual cell characteristics (Simpson, Selfors et al. 2008). This experiment was performed to confirm that the area of migration that was assessed by wound healing assay was not confounded by cell proliferation. Individual cells were each tracked and distance of motility was analysed in this experiment, to compliment wound healing assay. The procedure is described in M&M (chapter 2, section 2.6.2).

4.2.2.3 Transwell® migration assay

In contrast to cell motility assay, cell invasion assay requires cell to migrate through a basement membrane extract (BME) or extracellular matrix (ECM) barrier by enzymatic digestion of the barrier to migrate to the new location. Transwell® inserts (Corning); 24mm diameter wells with polycarbonate membrane of pore size 8 µm and base area of 4.5 cm^2 were used for this assay. Transwell® migration assay is a well-established method to assess cancer cell invasion *in vitro* (Hu and Verkman 2006; Moskovits, Kalinkovich et al. 2006). The procedure was performed according to the manufacturer's protocol. The details of the procedure are mentioned in M&M (chapter 2, section 2.6.3).

4.2.3 Proliferation assays

The effect of BMI1 silencing on cell proliferation was assessed by two independent methods – growth curve analysis and CyQuant NF assay.

4.2.3.1 Growth curve analysis

The proliferation of cells was assessed by time course experiment to produce a growth curve (Horiuchi, Huskey et al. 2012). The DAOY cells were quantified over a total of 7 passages, P1 to P7, corresponding to day 0, 3, 5, 7, 10, 12 and 14. The procedure is described in details in M&M (chapter 2, section 2.7.1).

4.2.3.2 CyQuant NF assay

The CyQUANT$^®$ NF assay (Hong, Jiang et al. 2007) was also used to assess proliferation. This assay is based on the measurement of cellular DNA content by fluorescent dye binding capacity. The procedure is detailed in M&M (chapter 2, section 2.7.2).

4.2.4 Annexin V Apoptosis assay

The effect of BMI1 silencing on apoptosis was assessed in DAOY cells by means of the Annexin V assay. Annexin V is a Ca^{2+} dependent phospholipid binding protein that has a high affinity for phospholipid phosphatidylserine (PS). PS is translocated from the inner to outer leaflet of the plasma membrane in early apoptotic cells. Annexin V conjugated with fluorochrome can be used to detect early apoptotic cells without compromising its affinity for PS (Vermes, Haanen et al. 1995). PE Annexin V Apoptosis Detection Kit I (BD Pharmingen™, BD Biosciences) was used with Alexa

Fluor 647 Annexin V conjugate (Invitrogen) as per manufacturer's protocol. The

complete procedure is described in M&M (chapter 2, section 2.8.1).

4.2.5 Immunohistochemistry:

The Formalin fixed paraffin embedded (FFPE) D-458 cell block sections were

stained by avidin-biotinylated complex (ABC) method of immunohistochemistry for

CD44, Thrombospondin, MMP8 and MMP10. The procedure is described in details

in chapter 2 (section 2.11). The list of primary and secondary antibodies and

blocking agents used is presented in Table 4.2.

Table 4.2 List of primary antibodies, secondary antibodies used for ABC IHC.

Primary antibodies				
For antigen to be detected	**Primary antibody used**	**Company**	**Concentration**	**Positive control**
CD44	Rabbit polyclonal anti-CD44	Abcam (ab24504)	20 µg/ml	Glioblastoma
Thrombospondin (THBS)	Mouse monoclonal anti-thrombospondin	Abcam (ab1823)	1:25	Glioblastoma
MMP8	Goat polyclonal anti-MMP8	Santa Cruz (sc-8848)	1:50	Breast carcinoma
MMP10	Rabbit polyclonal anti-MMP10	Abcam (ab59437)	1:500	Breast carcinoma
Biotinylated secondary antibody and blocking serum used				
For primary antibody source	**Secondary antibody used**		**Blocking agent**	
Rabbit or Mouse	Universal biotinylated anti-mouse/anti-rabbit IgG (Vector) raised from horse.		2.5% Normal horse serum (Vector)	
Goat	1:400 Anti-goat IgG (Vector) raised from rabbit		5% Normal rabbit serum	

4.2.6 Exogenous BMP treatment:

Use of recombinant BMP-2 and/or BMP-4 for BMP pathway activation is well

established (Iantosca, McPherson et al. 1999; Hallahan, Pritchard et al. 2003;

Piccirillo, Reynolds et al. 2006; Zhao, Ayrault et al. 2008). Use of BMP ligands is justified in DAOY cells as they are shown to express BMP receptors - BMPRI isoforms and BMPRII - which triggers phosphorylation of SMAD1,5,8 proteins (Iantosca, McPherson et al. 1999; Fiaschetti, Castelletti et al. 2011). To induce BMP signaling pathway in our study, we used recombinant human BMP-4 (R&D systems) on DAOY which was used at a concentration of 100 ng/ml for 24 – 36 hr. Further details of the procedure are described in M&M (chapter 2, section 2.3.1). The BMP-4 treated cells were used in Transwell® migration and cell proliferation assays.

4.3 Results

4.3.1 Increased multicellular cluster formation is observed upon BMI1 knock down in MB cell lines

Having previously established that BMI1 silencing led to aberrant BMP pathway activation; we asked whether the cell adhesion properties of MB cells may be affected. DAOY and D-458 were plated in a density of 0.5 x 10^5 cells in 0.5 ml media/well in 3 wells of 24 well plates. The cells were transfected with BMI1 siRNA using lipid based transfection agent and incubated for 48 hr. Negative siRNA (Scr) treated cells were used as controls. Noggin was added to the relevant wells at 1 µg/ml concentration. After 48 hr the cells were fixed and immunocytochemistry for pSMAD1,5,8 and BMI1 antibodies was performed. The cells were counterstained with DAPI nuclear stain. The pSMAD1,5,8 expression in BMI1 knock down and control cultures were quantified as described in chapter 3. While analysing these cultures we incidentally noticed a greater tendency to form multicellular aggregates in BMI1 knock down cultures. To quantify this observation, the number of multicellular aggregates as defined by cohesive clusters of 10 or more cells per 20x field was quantified in the DAPI staining. Five fields in each well were imaged and the experiments were conducted in triplicates.

The average number of cell aggregates per high power field (hpf, 20x) was found to be increased in DAOY^{BMI1kd} and D-458^{BMI1kd} as compared to DAOY^{Scr} and D-458^{Scr} respectively – 1.93 (+/- 0.31) vs. 0.07 (+/- 0.12) in DAOY (p=0.004), and 3 (+/- 0.6) vs. 1.2 (+/- 0.2) in D-458 (p=0.003) [Fig 4.1 A and B].

To assess whether cluster formation was dependent on aberrant BMP pathway re-activation after BMI1 knock down, DAOY and D-458 cultures were concomitantly

treated with Noggin. Previously we have demonstrated the efficacy of Noggin as BMP pathway inhibitor. Here we were interested to know if changes in adhesion seen upon BMI1 knock down are BMP pathway related. When Noggin was applied to DAOY^{Scr} or D-458^{Scr}, there were no discernible change in the cellular aggregates noted (Fig 4.1 A and B). However Noggin treated DAOY^{BMI1kd} and D-458^{BMI1kd} showed a reduced number of aggregates/hpf as compared to cultures without Noggin – 0.73 (+/- 0.30) vs. 1.93 (+/- 0.31) in DAOY (p=0.004), and 1.07 (+/- 0.30) vs. 3 (+/- 0.6) in D-458 (p=0.003) [Fig 4.1 A and B].
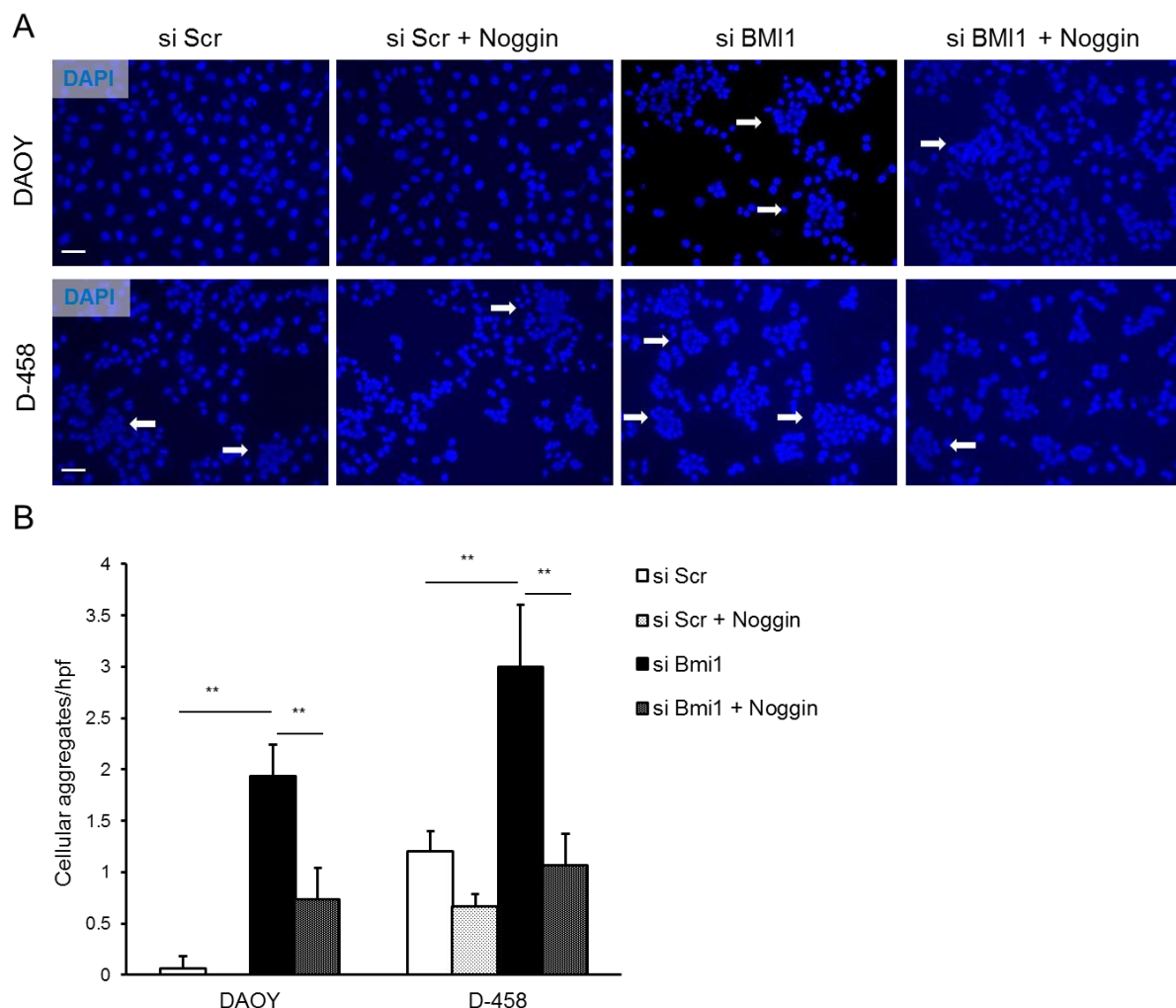
Fig. 4.1 Deregulation of cell adhesion properties in MB cell lines following BMI1 knock down.

(A) DAPI images demonstrating an increase in cell cluster formation upon BMI1 knock down in both DAOY (upper panel) and D-458 (lower panel) cells, which interestingly does not occur upon

concomitant addition of Noggin to BMI1 knock down cultures. The arrowheads show the cell clusters that were counted in each field, representing aggregates of 10 cells or more. There was no difference in cell cluster formation between Scr and Noggin treated Scr groups **(B)** Quantification of average number (from three independent experiments) of cell clusters per 20x hpf shows an increase in siRNA-mediated BMI1 knock down cultures as compared to Scr cultures in both DAOY (left) and D-458 (right). Furthermore, concomitant addition of Noggin to BMI1 knock down cultures shows a significant decrease in the number of cell clusters per field in both cell lines. Scale bar in **(A)** = 50 µm. Error bars in **(B)** represent SD (n=3). **,p<0.01.

From the above findings we can infer that BMI1 knock down affects the cell adhesion properties of MB cell lines. Epithelial-Mesenchymal transition (EMT) and Mesenchymal-Epithelial transition (MET) are known to be dependent upon change in the microenvironment and in stimulatory signals(reviewed in (Hugo, Ackland et al. 2007)). As concomitant BMP inhibition by Noggin significantly reduced cluster formation induced by BMI1 knock down, it is likely that this phenomenon is mediated by BMP pathway activation. These results prompted us to further assess its functional relevance in *in vitro* experiments to assess cell motility and invasiveness of MB cell lines.

4.3.2 BMI1 knock down affects MB cell migration in a BMP dependent fashion

A well characterised method that mimics *in vivo* cell migration is the Wound healing assay which is based on cell-cell interaction and directional migration of cells (Rodriguez, Wu et al. 2005). Only DAOY cells (and not D-458) were used for this assay as they suitably grew as an adhesive monolayer. Each group of shRNA lentivirus infected cells were plated in 3 wells of a 24 well plate at a constant density. At this stage, Noggin was added at 1 µg/ml to the appropriate cultures and labelled. Following further 24 hr incubation when >90% confluence was seen, ~80 µm wide wounds (linear scratches) were incised in each well. The cells were then incubated

in time lapse chamber and the stage was set to acquire images from three areas from each well. Three phase contrast images (10x maginification) per well were intermittently acquired over 12 hr and movies were created using Metamorph software. Using the same software, area of migration of cells in to the incited wound (healed area) was determined. Then, relative area of migration in percentage to the original wound area was calculated. The experiments were conducted in triplicates. The schematic of the wound healing experiment is shown in Fig 4.2 A.

We observed a significant reduction in the average relative wound area in the DAOY^{BMI1kd} cultures as compared to DAOY^{Scr} cultures – 29.08% (+/- 5.19) vs. 43.11% (+/- 6.47), p=0.0025 (Fig 4.3 B and C).

The above reduction in area of migration in DAOY^{BMI1kd} was observed to be reverted by concomitant treatment of with Noggin. The average area for DAOY^{BMI1kd} with Noggin as compared to DAOY^{BMI1kd} without Noggin were 40.18% (+/- 8.42) and 29.08% (+/- 5.19) respectively, p=0.048 (Fig 4.2 B and C). There was however no significant difference in wound closure noted upon DAOY^{Scr} additionally treated with Noggin as compared to DAOY^{Scr} only – 45.79% (+/- 12.59) vs. 43.11% (+/- 6.47), p=0.12 (Fig 4.2 B and C).
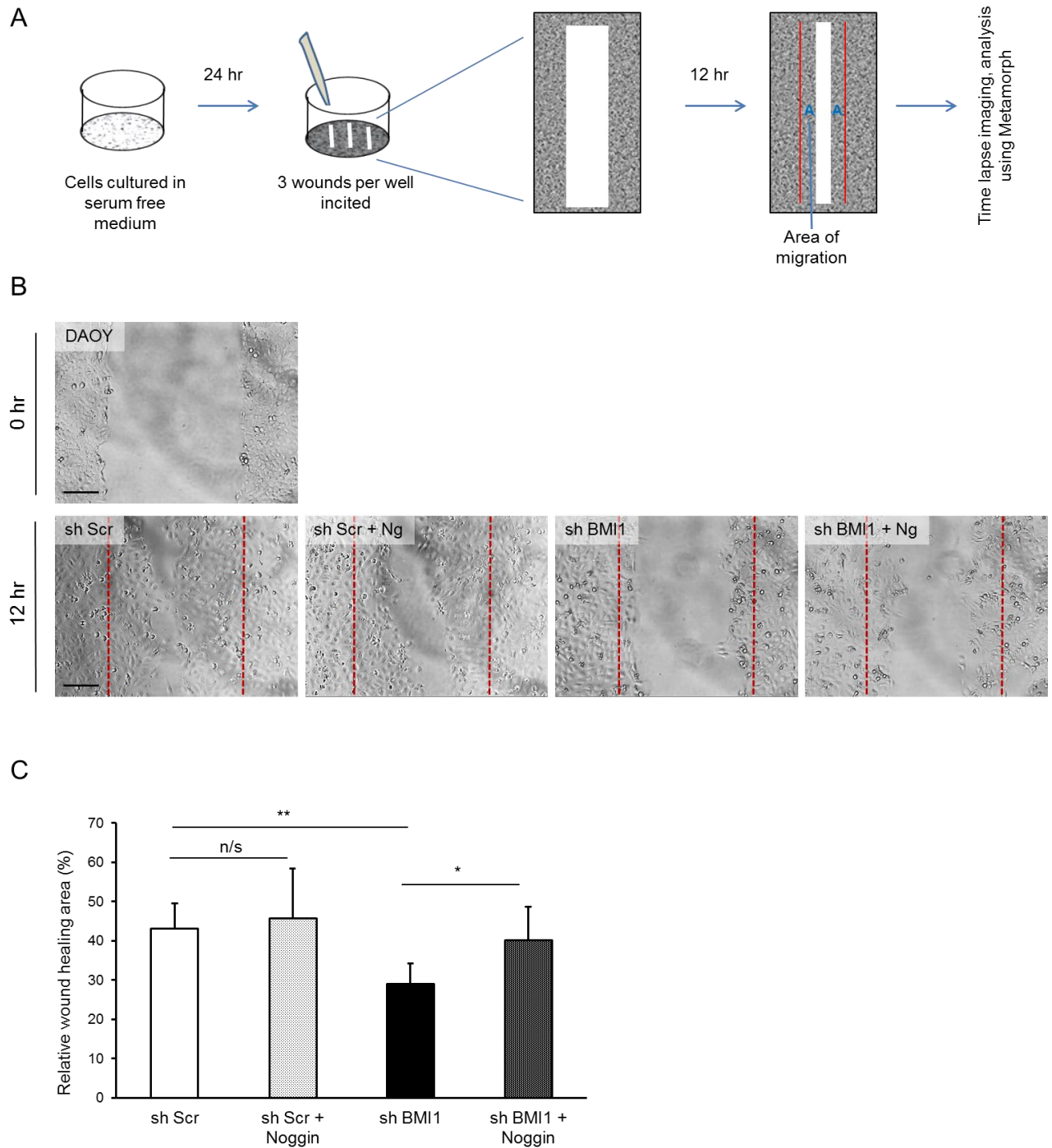
Fig. 4.2 Wound healing assay demonstrating that cell migration of MB cell line DAOY is regulated by BMI1 in a BMP pathway dependent fashion.

(A) Schematic diagram of the wound healing assay: Approximately 80 μm wound is incited in a confluent monolayer of cells and the cell migration is recorded on time lapse videomicroscopy to calculate relative area of wound or gap closure using Metamorph software at the end of 12 hr. **(B)** Top - representative picture of wound gap at 0 hr, Bottom row – representative pictures of wound gap closure (wound healing) following cell migration after 12 hr incubation, for shRNA Scr, shRNA Scr +

Ng, shRNA BMI1 and shRNA BMI1 + Ng treated cells, from left to right. There is a significant decrease in area of gap closure seen in shRNA BMI1 treated cells compared to shRNA Scr treated cells. Upon concomitant Ng addition, an increase (reversal) in the area of migration is noted. The red dotted lines mark the original gap at the start of the experiment at 0 hr. **(C)** Quantitation of average percentage of area of migration from three independent experiments. Scale bar in **(B)** = 20 µm. Error bars in **(C)** represent SD (n=3). *, p<0.05, **, p<0.01. Abbreviation: Ng, Noggin.

BMI1 knock down in DAOY cells not only causes changes in cell adhesion as observed previously, but also causes changes in cell migration properties. Interestingly these changes appear to be dependent on BMP signalling as reversal of phenotype was observed upon concomitant Noggin treatment.

4.3.3 BMI1 knock down affects individual cell motility.

As it was possible that the changes in wound healing observed could be due to the effects of BMI1 on cell proliferation, we performed individual cell motility assay using time lapse microscopy. Similar to wound healing assay shRNA lentivirus treated DAOY cells were plated in 3 wells for each group at constant densities and incubated in time lapse chamber with stage set to acquire images from five random areas in each well. Phase contrast (20x magnification) images were acquired intermittently for 6 hr and compiled using Metamorph software. Using the same software, ten cells in each field were tracked and the distance of migration of each cell to its origin was determined. The experiments were conducted in triplicates. The average distances were calculated for both groups and compared.

There was a significant reduction in the average distance travelled by the cells over 6 hr observed in DAOY^{BMI1kd} cultures as compared to DAOY^{Scr} cultures – 8.43 µm (+/- 1.61) vs. 11.41 µm (+/- 1.69), p=0.005 (Fig 4.3).
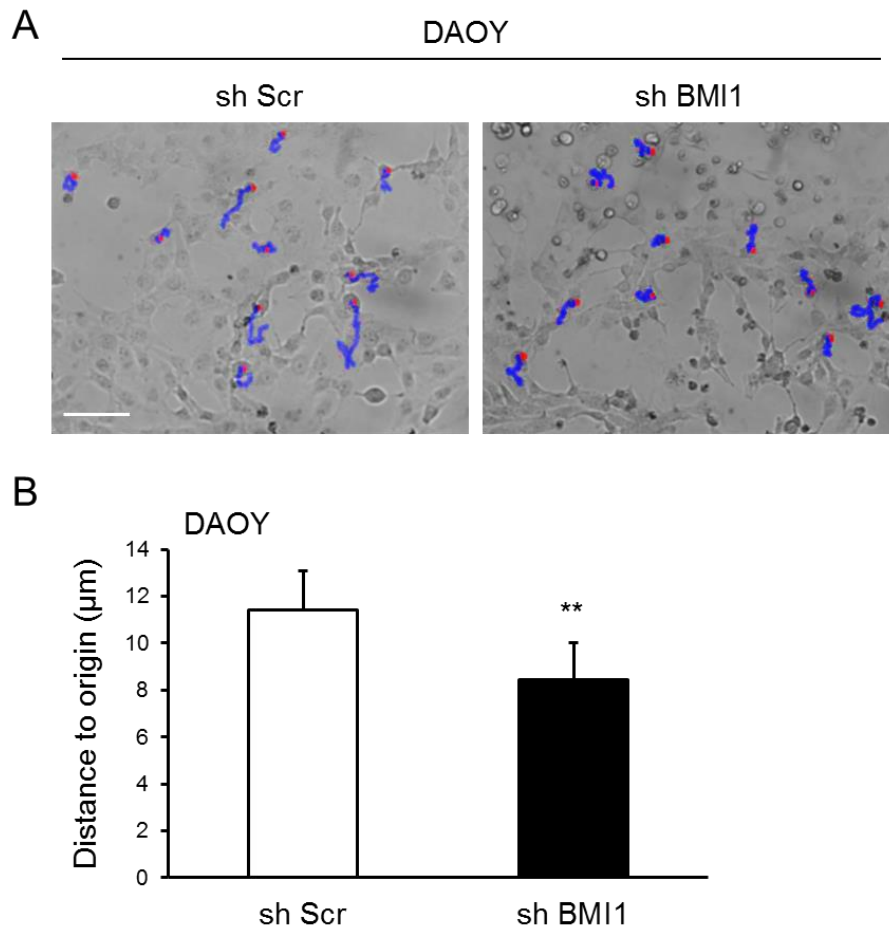
Fig. 4.3 Time lapse experiment tracing individual cells shows decreased cell motility following BMI1 knock down in DAOY.

(A) Representative pictures of time lapse tracing of DAOY cell migration comparing shRNA Scr treated (left) and shRNA BMI1 treated (right) cells. Blue lines are tracings of movement of ten random cells recorded over 6 hr, representing the distance moved from their origin (red dot). **(B)** Quantification of average distance of cell migration, from three independent experiments, showing a significant reduction in individual cell motility following BMI1 knock down. This makes it unlikely that the effects of BMI1 on cell proliferation confound the results of the wound healing assay. Scale bar in **(A)** = 20 µm. Error bars in **(B)** represent SD (n=3). **, $p<0.01$.

This reduction in individual cell migration upon BMI1 knock down support the

conclusion that the reduction in the wound healing area observed is due to the

effects of BMI1 on cell migration properties independently of its effects on cell

proliferation.

4.3.4 BMI1 knock down reduced *in vitro* cell invasion in a BMP mediated fashion

Having identified changes in cell-cell adhesion (multicellular aggregates/cluster formation) and cell motility (wound healing/migration) upon BMI1 knock down, we set out to investigate whether these could impact on the invasive properties of MB cells *in vitro.* As the above phenotypic changes were linked to BMP pathway, we also set out to investigate any dependency on BMP deregulation of the potential impact of BMI1 knock down on the invasive characteristics of MB cells. For this we used Transwell® migration assay – a method which to an extent simulates *in vivo* invasion, as it requires cells to migrate through a substrate barrier. MB are known to primarily metastasise via leptomeningel route (Chang, Housepian et al. 1969). The principal ECM components of the leptomeninges include laminin and collagens (Wikstrand, Friedman et al. 1991; Montagnani, Castaldo et al. 2000); including type I collagen (Hubert, Grimal et al. 2009). Therefore to mimic the leptomeningeal environment we used Matrigel™ (rich in laminin) and type I collagen as substrates barriers.

The D-458 cells proved to be unsuitable for Transwell® assay as they failed to adhere to the basement membrane extracts used. Therefore the experiments were performed using DAOY cells alone. Porous Transwell® inserts were lined with Matrigel or collagen substrates. Serum starved shRNA lentivirus or siRNA treated cells (with or without Noggin addition) were seeded at a constant density in the substrate coated insert wells (3 wells per group) and serum containing media was used in the bottom wells. The cells were incubated for 12 hr to allow migration through the substrate barrier. The cells were then fixed and stained with Haematoxylin. The non-migrated cells from the top surface of the insert membrane

were scraped and the migrated cells on the bottom surface of the membrane were imaged. Five random images from each insert were acquired using light microscopy at 20X magnification. The number of cells migrated were counted using ImageJ software and the average number of cells per group were compared to controls. The experiments were conducted in triplicates. The schematic of the wound healing experiment is outlined in Fig 4.4 A.

We observed a significant reduction in the number of migrating cells in DAOY^{BMI1kd} cultures, compared to DAOY^{Scr} through collagen type I substrate after 12 hr – 80.67 (+/- 55.51) vs. 176.07 (+/- 42.38), p=0.005 (Fig. 4.4 B,C).

Importantly, the number of migrating cells significantly increased upon Noggin treatment of DAOY^{BMI1kd} cultures as compared to DAOY^{BMI1kd} alone – 147.23 (+/- 46.63) vs. 80.67 (+/- 55.51), p=0.004 (Fig. 4.4 B,C). This reversal demonstrates that decreased migration of DAOY^{BMI1kd} cells was dependent on aberrant activation of BMP pathway. No statistically significant difference in cell migration was noted upon Noggin treatment of DAOY^{Scr} as compared to DAOY^{Scr} alone – 129.58 (+/- 72.56) vs. 176.07 (+/- 42.38), p=0.081 (Fig. 4.4 B,C).

There was no statistically significant difference in the number of migrated cells between the DAOY^{BMI1kd} and DAOY^{Scr} on Matrigel substrate – 87.22 (+/- 6.63) vs. 118.61 (+/- 15.93), p=0.061(Fig 4.4 D), although a trend toward decrease migration similar to what observed in the experiments using collagen substrates was observed. The laminin contained in Matrigel substrate is known to be isolated from Engelbreth-Holm-Swarm (EHS) mouse sarcoma cells (Kleinman, McGarvey et al. 1982), and hence Matrigel may not serve as an ideal physiological substrate for studies using MB cells. Furthermore, Collagen type 1 is shown to be expressed in leptomeninges

(Liang, Diehn et al. 2008), hence it could represent a more appropriate substrate for

MB cell invasion as compared to Matrigel.
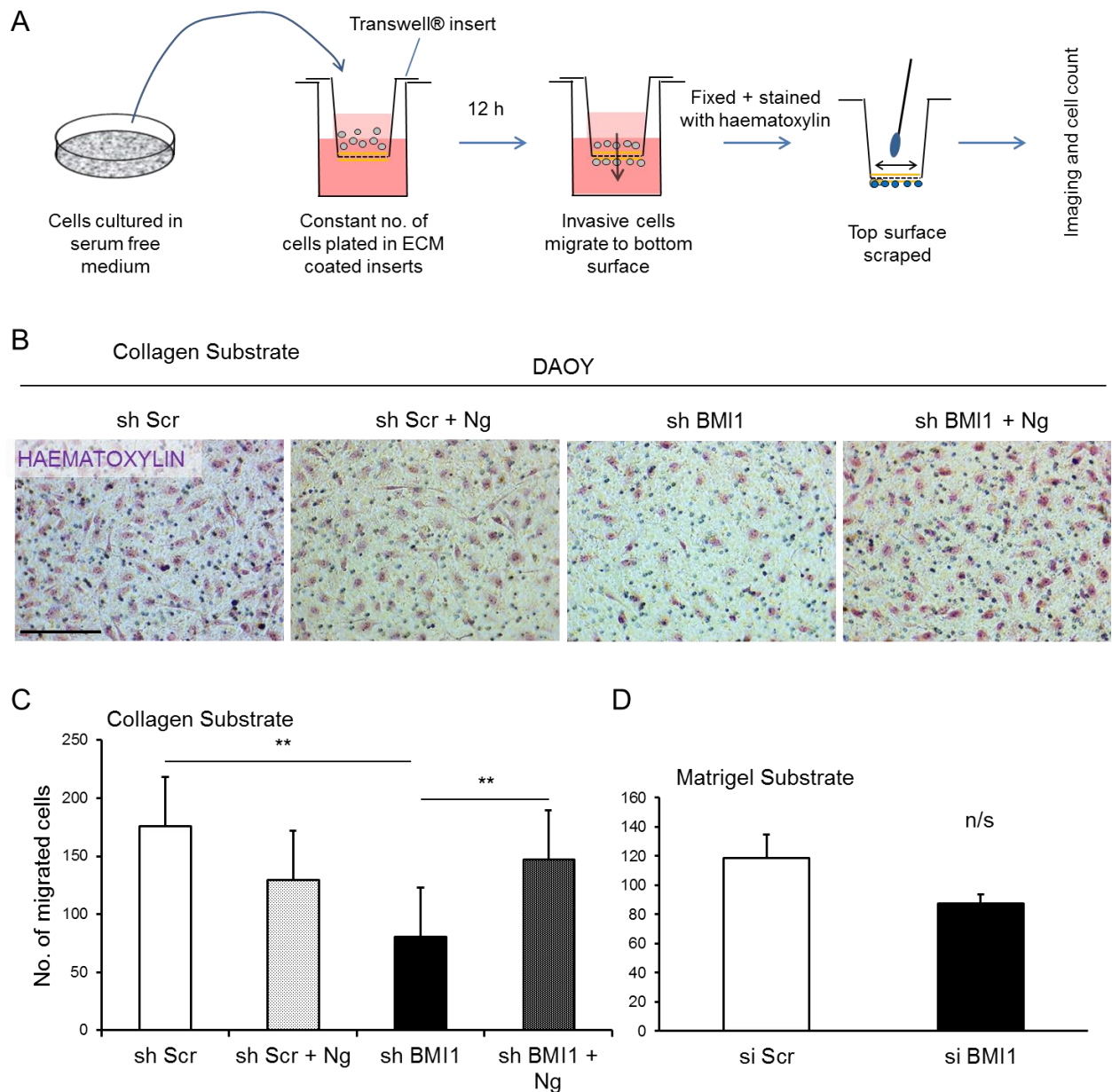
Fig. 4.4 Transwell® assay reveals a reduced DAOY cell invasion upon BMI1 knock down *in vitro*.

(A) Schematic diagram of the Transwell® assay: Constant number of cells was seeded in the upper chamber of substrate coated Transwell® inserts, and allowed to migrate for 12 hr, followed by fixation,

staining and counting. **(B)** Pictures of the bottom surface after scraping the cells from top surface, representing only the migrated (invaded) cells at end of 12 hr. From left to right - shRNA Scr, shRNA Scr + Ng, shRNA BMI1 and shRNA BMI1 + Ng treated cells. There is a significant decrease in the number of cell invasion/migration through collagen seen in shRNA BMI1 treated cells compared to shRNA Scr treated cells. Upon concomitant Ng addition, an increased   invasion is noted. **(C)** Quantitation of the average number of migrated cells through collagen substrate. **(D)** Quantitation of average number of migrated/invaded cells through Matrigel substrate. Scale bar in **(B)** = 20µm. Error bars in **(C and D)** represent SD (n=3). **, p<0.01. Abbreviation: Ng, Noggin.

These results raise the possibility that BMI1 overexpression increases invasiveness of MB cells. These observations prompted us to perform further validation experiments taking advantage of *ex vivo* and *in vivo* models. Importantly, the changes we observed here could be reverted upon BMP pathway inhibition hence supporting the notion that BMI1 may contribute to MB aggressiveness via repression of the BMP pathway.

4.3.5 BMI1 knock down leads to deregulation of cell adhesion/ECM molecules

From previous experiments conducted by our team (experiments conducted by Dr Xinyu Zhang, results in press), which were discussed in this chapter's introduction (section 4.1), four cell adhesion/ECM genes whose expression was significant upregulated in Bmi1-/- mCGC and reversed after Noggin treatment were identified (Table 4.1).

Here we analysed whether *BMI1* silencing would impact on the expression of these genes in MB cells. Immunohistochemistry for CD44, Thrombospondin 1&2 (THBS 1/2), MMP10 and additionally for MMP8 was carried out on DAOY and D458 cytoblocks that were previously generated in the Marino lab from cells treated with either *BMI1* siRNA or with scrambled siRNA (controls). There was no interpretable staining noted in DAOY cell blocks. However, we observed a diffuse and intensely

increased staining for CD44 antibody in D-458^{BMI1kd} cell blocks as compared to D-458^{Scr} (Fig 4.5 A,E). Conversely, THBS staining was seen to be uniformly reduced among D-458^{BMI1kd} cell blocks as compared to D-458^{Scr} (Fig 4.5 B,F). However there was no change in either intensity or extent of staining observed with MMP8 (Fig 4.5 C,G) and MMP10 (Fig 4.5 D,H) antibodies.
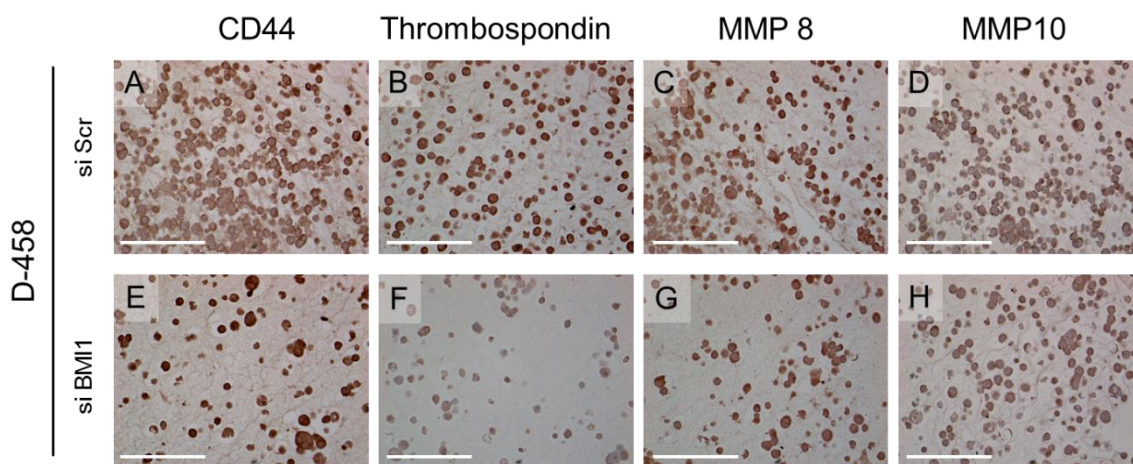
Fig. 4.5 Deregulation of certain cell adhesion/ECM molecules upon BMI1 silencing in D-458 cells.

D-458 cells were treated with siRNA BMI1 or siRNA Scr, fixed and embedded in paraffin blocks. Immunohistochemistry on the sections using CD44, Thrombospondin, MMP8 and MMP10 antibodies was performed. An increased (intensity) CD44 expression **(A and E)**, and a decreased Thrombospondin (intensity and number) expression **(B and F)** was noted upon BMI1 knock down as compared to Scr controls. There was no change in expression present for MMP8 **(C and G)** and MMP10 **(D and H)**. Scale bar in all = 20 μm.

The changes in the expression of ECM proteins could be in keeping with the *in vitro* observation of changes in cell adhesion and cell migration/invasion after *BMI1* downregulation in medulloblastoma cells. However, a note of caution is warranted because the staining intensity could not be reliably quantified as the immunostaining was performed with the chromogenic method and the results were somewhat variable among the different replicas. Also, the lack of a reliable staining in the

DAOY cytoblock prevented us from comparing the results with existing datasets (Wiederschain, Chen et al. 2007) to further validate the findings.

4.3.6 Decreased proliferation of MB cells upon BMI1 knock down is not BMP pathway dependent

Next, we set out to assess whether the changes in cluster formation and in cell migration/invasion upon BMI1 downregulation could be influenced by the Ink4a/Arf-mediated cell cycle control exerted by Bmi1 in various physiological and cancer-related contexts. Bmi1 downregulation was shown to cause reduced proliferation and early senescence in various cancer cells such as oral carcinoma cells (Kang, Kim et al. 2007) and gliomas cells (Godlewski, Nowicki et al. 2008). Wiederschain et al., have shown that shRNA mediated BMI1 knock down in DAOY cells causes reduced proliferation (Wiederschain, Chen et al. 2007). Here we performed proliferation and apoptosis assays in MB cells to check the dependency of these effects on BMP pathway deregulation.

We used two independent methods to quantify proliferation in MB cells in response to BMI1 downregulation – growth curve analysis and CyQuant assay.

To produce a time course growth curve shRNA transfected DAOY cells were plated at a constant density of 1×10^5 cells per well in a 6 well plate and after 3 days incubation the cells were re-counted. Multiplication factor (f) was generated where f = no. newly counted cells/no. of originally plated cells. Estimated number of cells (e) was defined at each passage as e = f x previous e. During each passage, 1×10^5 cells were plated, for a total of 7 passages, P1 to P7, corresponding to day 0, 3, 5, 7, 10, 12 and 14. Triplicates of each group of cells were prepared and counted. The

experiment was done in three biological replicas. Relevant DAOY cultures were supplemented with Noggin 1 µg/ml every 24 hr.

There was a significant reduction in proliferation of DAOY^{BMI1kd} cultures compared to DAOY^{Scr} for all passages (Fig 4.7 A,B). However there was no difference in proliferation in Noggin treated DAOY^{BMI1kd} compared to DAOY^{BMI1kd} only cultures (Fig 4.7 A,B). The average estimated number of cells (e) calculated during each passage for each group is tabulated in Table 4.3, and the respective p values are listed in Table 4.4.

Table 4.3 Growth curve assay with estimated number of DAOY cells 'e' at the end of each passage.

Passage (days)	Estimated cell number e with (std. dev.)		
	sh Scr	sh BMI1	sh BMI1 + Ng
P1 (0)	100000	100000	100000
P2 (3)	240333 (+/- 1247)	174333 (+/- 1700)	175000 (+/- 17795)
P3 (5)	386917 (+/- 6188)	209763 (+/- 1206)	218483 (+/- 34300)
P4 (7)	797090 (+/- 22719)	356499 (+/- 15077)	374355 (+/- 54713)
P5 (10)	199189 (+/- 110689)	774266 (+/- 76427)	871283 (+/- 113634)
P6 (12)	4648035 (+/- 329337)	1573638 (+/- 170055)	2023768 (+/- 443809)
P7 (14)	9417207 (+/- 352784)	2782843 (+/- 336752)	3947720 (+/- 771796)

Table 4.4 Statistical significance (p value) calculated in DAOY growth curve analysis for different passages.

Groups compared	p values generated by Student's *t-test*					
	P2 (3)	P3 (5)	P4 (7)	P5 (10)	P6 (12)	P7 (14)
sh Scr vs. sh BMI1	0.000001	0.000028	0.002644	0.033383	0.016736	0.023710
sh BMI1 vs. sh BMI1 + Ng	0.480233	0.305787	0.397628	0.075917	0.092425	0.092037

CyQUANT® NF proliferation assay, which is based on measurement of cellular DNA content by fluorescent dye binding capacity, was also performed using shRNA transfected DAOY cells. Each group of cells were plated in 3 wells in 96 well plates at a constant density and after 24 hr overnight incubation fluorescent dye binding solution was added to each wells and allowed equilibration for 30 min as per manufacturer's instructions. The fluorescence intensity (excitation set at 480 ±10 nm, and emission detection at 530 ± 10 nm) of each sample was measured. The experiments were conducted in triplicates and average readings were obtained.

The average fluorescence units (indicative of DNA content and hence proliferation, measured at a single time point) was significantly reduced among DAOY^{BMI1kd} as compared to DAOY^{Scr} – 280.55 (+/- 43.60) vs. 532.44 (+/- 51.60), p=0.003 (Fig 4.6 C). Importantly there was no significant difference in proliferation between Noggin treated DAOY^{BMI1kd} cultures and DAOY^{BMI1kd} alone – 203.56 (+/- 51.30) vs. 280.55 (+/- 43.60), p=0.09 (Fig 4.6 C).

Proliferation assay on ICb-1299 primary cells showed similar results to that observed in DAOY. The average fluorescence units was significantly reduced among ICb-1299^{BMI1kd} as compared to ICb-1299^{Scr} – 37.11 (+/- 2.08) vs. 56.56 (+/- 3.28), p=0.001 (Fig 4.6 D).
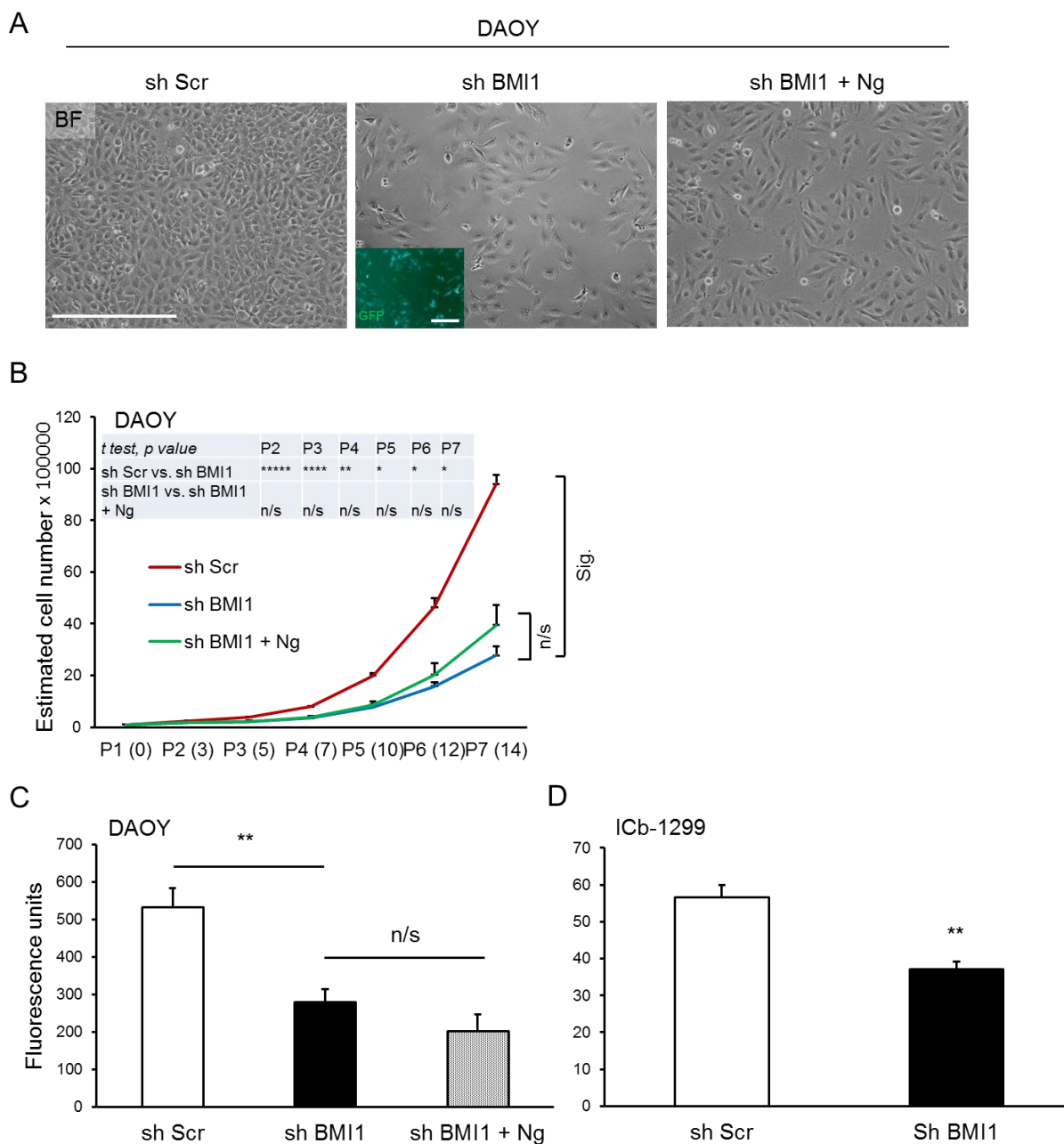
Fig. 4.6 BMI1 controls MB cell proliferation in a BMP pathway independent fashion.

(A) Representative pictures of DAOY cells in culture at P1 (day 3); demonstrating a reduced *in vitro* growth/proliferation in sh BMI1 treated cells (middle, inset – fluorescent channel of the same field showing GFP positive cells), compared to sh Scr treated cells (left), which does not change significantly upon concomitant addition of Ng (right). **(B)** Growth curve plotted against cell passages over seven passages (14 days), showing a significant reduction in proliferation among BMI1 knock down cells, with no significant difference upon addition of Ng. **(C)** CyQuant® NF assay confirming the results observed with the growth curve analysis in DAOY. **(D)** CyQuant® NF assay on ICb-1299 primary cells, showing a reduced proliferation in shRNA BMI1 treated cells as compared to shRNA Scr treated controls. The values on X-axis are fluorescence units corresponding to rate of proliferation (based on new DNA content). Scale bar in **(A)** = 50 μm. Error bars in **(C and D)** represent SD (n=3). *, p<0.05; **, p<0.01; ****, p<0.0001; *****, p<0.00001. Abbreviation: BF, bright field; Ng, Noggin; P, passage number with corresponding day in ().

The above results confirm the literature findings (Wiederschain, Chen et al. 2007) that BMI1 downregulation leads to reduced cell proliferation in both MB cell lines and primary cultures. However, concomitant treatment of DAOY^{BMI1kd} with Noggin did not affect proliferation as demonstrated by two independent methods. This is compatible with a model whereby BMI1-mediated regulation of proliferation is independent of BMP pathway, thus is not involved in the migration/invasion phenotype.

4.3.7 BMI1 knock down does not significantly affect apoptosis and remains uninfluenced by inhibition of the BMP pathway

Next, we set out to study if BMI1 knock down has any effects on apoptosis in MB cells. For this we used Annexin V assay with Alexa Fluor 647 conjugate as per manufacturer's protocol. $1x10^5$ lentivirus sh RNA transfected DAOY cells (with or without Noggin treatment) were collected in 100 µl of 1X binding buffer per group in FACS tube. 5 µl of Annexin V conjugate was added to each tube along with 10 µl of 1:1000 DAPI. The samples were gently mixed and incubated at room temperature in the dark for 15 min. 400 µl of 1X binding buffer was then added to each tube and the samples were run in a flow cytometer machine according to protocols optimised for DAPI, GFP and Annexin V channel detection. The percentage of total GFP positive cells was detected first. Then the gates were set to detect early apoptosis (Annexin V positive, DAPI negative), dead cells (DAPI positive, Annexin V positive) and live cells (Annexin V negative, DAPI negative) from the GFP only positive population (representing lentivirus infected cells only). The percentage of early apoptotic cells was determined using FACS Diva™ v6.1.3 software. Average percentage of four independent experiments was used for analysis.

11-23% of cells were detected to be viable cells for analysis (Fig 4.7 A), among them, 59-61% of the cells were GFP positive (Fig 4.7 B). Among the GFP positive cells, the average percentages of Annexin V only positive cells indicative of early apoptosis for DAOY^{BMI1kd} as compared to DAOY^{Scr} were 80.13% (+/- 11.15) vs. 85.65% (+/- 8.02), p=0.257 (Fig 4.7 C, 3rd and 1st pic from left). This difference for Noggin treated DAOY^{Scr} as compared to DAOY^{Scr} only were 81.50% (+/- 6.35) vs. 85.65% (+/- 8.02), p=0.254 (Fig 4.7 B, 2nd and 1st pics from left). The counts for concomitant Noggin treated DAOY^{BMI1kd} as compared to DAOY^{BMI1kd} only were 78.58% (+/- 10.77) vs. 80.13% (+/- 11.15), p=0.434 (Fig 4.7 B, 4th and 3rd pics). To summarise, there was no significant changes in apoptosis seen upon BMI1 knock down whether or not the BMP pathway was concomitantly inhibited (Fig 4.7 D).
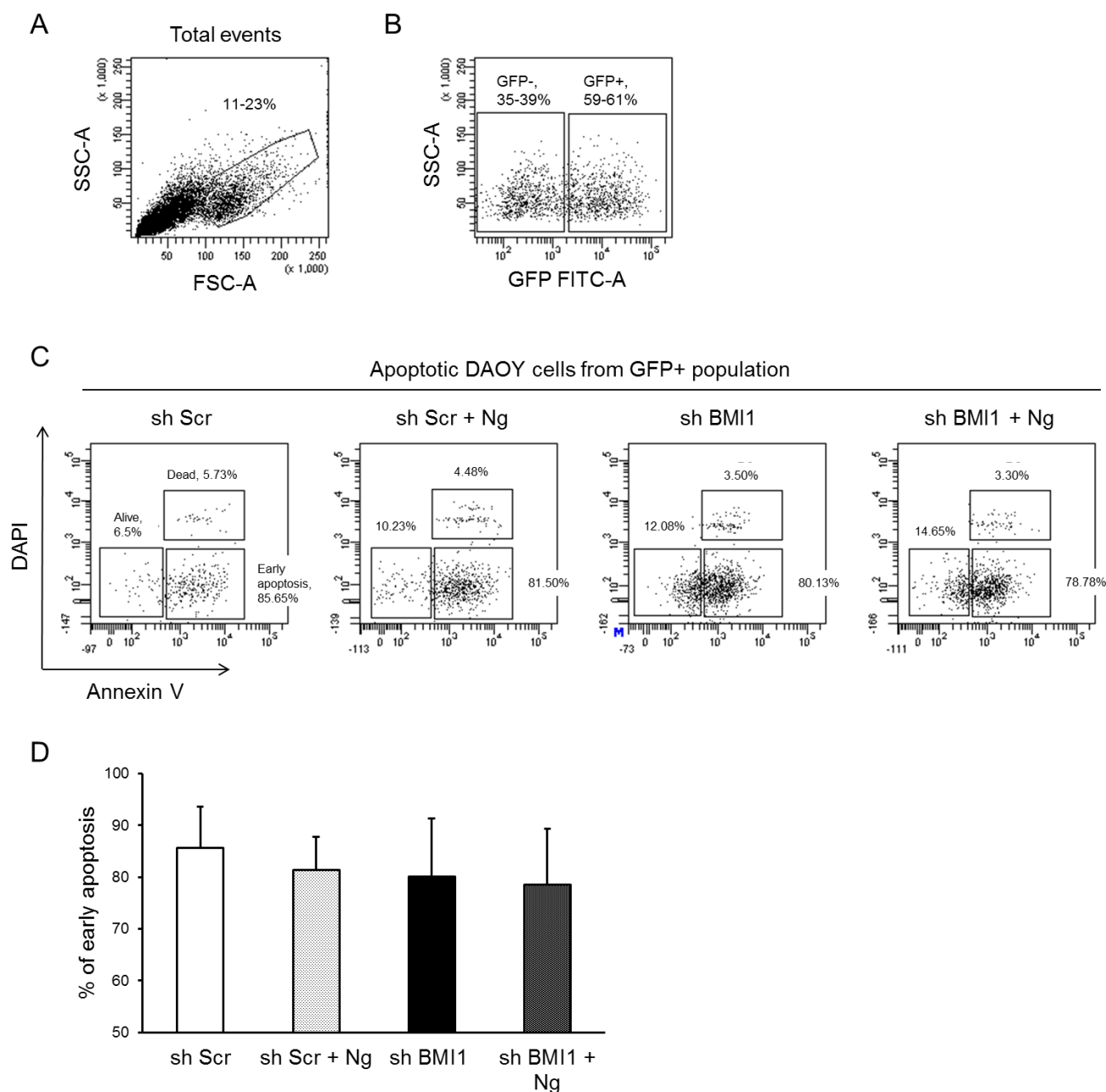
Fig. 4.7 BMI1 knock down does not affect apoptosis, and remain uninfluenced upon BMP pathway inhibition.

(A) Fluorescent activated cell sorting (FACS) flow cytometry, selecting suitable fluorescent labelled cells (11-23%) from the total cells. (**B**) Among the selected cells, approximately 59-61% of the cells were GFP positive representing efficiently infected with GFP-lentivirus. This population is selected for Annexin V apoptosis assay. **(C)** FACS analysis indicating the fractions of dead (DAPI only positive), early apoptotic (Annexin V only positive) and alive (DAPI and Annexin V negative) cells. There is no significant difference in early apoptosis between shRNA BMI1 or shRNA Scr treated cells. Furthermore, there is no difference in early apoptosis between shRNA BMI + Ng or shRNA BMI1 only treated cells. **(D)** Average of percentage of early apoptosis cells (Annexin V positive fraction) from three independent experiments, showing no significant difference in different cell groups as above. Error bars in **(D)** represent SD (n≥3). Abbreviation: Ng, Noggin; SSC, side scatter; FSC, forward scatter; FITC, green fluorochrome (480 nm) in flow cytometry; GFP, green fluorescent protein; DAPI, 4',6'-Diamindino-2-Phenylindole, staining nuclei of dead cells.

4.3.8 Exogenous BMP-4 treatment of MB cell lines affects in vitro cell invasion in a BMI1-dependent fashion

Next, we reasoned that if Bmi1 represses BMP pathway in MB cells, its expression could be an indicator of potential responsiveness of the cells to BMP treatment. Hence we set out to investigate whether changes in cell invasion could be exerted by treatment with exogenous BMP treatment and whether they were dependent on Bmi1 expression. .

First, we wanted to confirm BMP pathway activation upon treatment of DAOY cells with exogenous BMP. 1 x 10^5 DAOY cells were plated in 2 ml medium in each well of a 6 well and treated with BMP-4 at 100 ng/ml concentration for 24 – 72 hr. Protein expression analysis for pSMAD1,5,8 and SMAD1,5,8 was performed by Western blot. This demonstrated BMP pathway activation 24h and 48h after BMP-4 treatment (Fig.4.8).
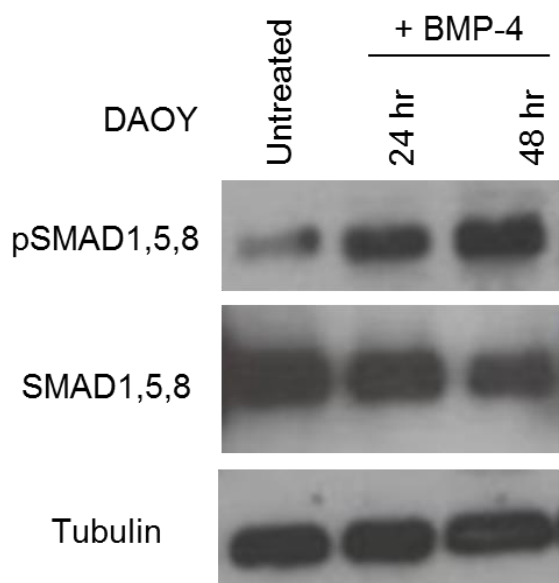
Fig. 4.8 BMP-4 activates BMP pathway in DAOY cells.

Western blot analysis showing an increase in phosphorylated SMAD1,5,8 (pSMAD1,5,8) protein in relation to SMAD1,5,8 expression in DAOY cells upon treatment with human recombinant BMP-4 100 ng/ml, indicative of BMP pathway activation. The pSMAD1,5,8 levels are increased at 24 - 48 hr time points. Tubulin expression is used as loading control. Abbreviation: BMP, Bone Morphogenetic Protein.

4.3.8.1 BMI1 expression is essential for BMP-4 mediated reduction of DAOY in vitro cell invasion

There is conflicting evidence in the literature on the effects of BMPs on cancer cells. BMP-2 is shown to enhance *in vitro* migration and invasiveness in a time and dose dependent fashion in gastric carcinoma cells (Kang, Kim et al. 2010) and breast carcinoma cells (Katsuno, Hanyu et al. 2008). Contrarily, BMP-4 treatment has been shown to effectively inhibit tumour growth in *in vivo* glioblastoma tumour transplants (Piccirillo, Reynolds et al. 2006). Here we investigate the effects of exogenous BMP on cell invasion in DAOY cells. For this we used previously established Transwell® migration assay (discussed previously in this chapter, section 4.3.4 and Fig 4.4 A.).

The timeline of BMP pathway activation observed in DAOY upon treatment with exogenous BMP4 was well within the requirements for the Transwell migration assay. Hence the assay was performed as previously described (section 4.2.2.3).

There was a significant reduction in the average number of cell migration/20X field noted in DAOY^{Scr} treated with BMP-4 as compared to untreated DAOY^{Scr} cells – 75.8 (+/- 14.78) vs. 142.85 (+/- 24.26), p=0.003 (Fig 4.9 A,B). As observed previously, reduction in migration was reproducible in DAOY^{BMI1kd} as compared to DAOY^{Scr} cultures – 65 (+/- 8.85) vs. 142.85 (+/- 24.26), p=0.001 (Fig 4.9 A,B). Notably there was no additional reduction of cell migration seen in DAOY^{BMI1kd} cultures treated with BMP-4 as compared to DAOY^{BMI1kd} without BMP4 treatment – 61.84 (+/- 9.07) vs. 65 (+/- 8.85), p=0.160 (Fig.4.9 A,B).

A

Collagen Substrate   DAOY

| sh Scr | sh Scr + BMP-4 | sh BMI1 | sh BMI1 + BMP-4 |

B
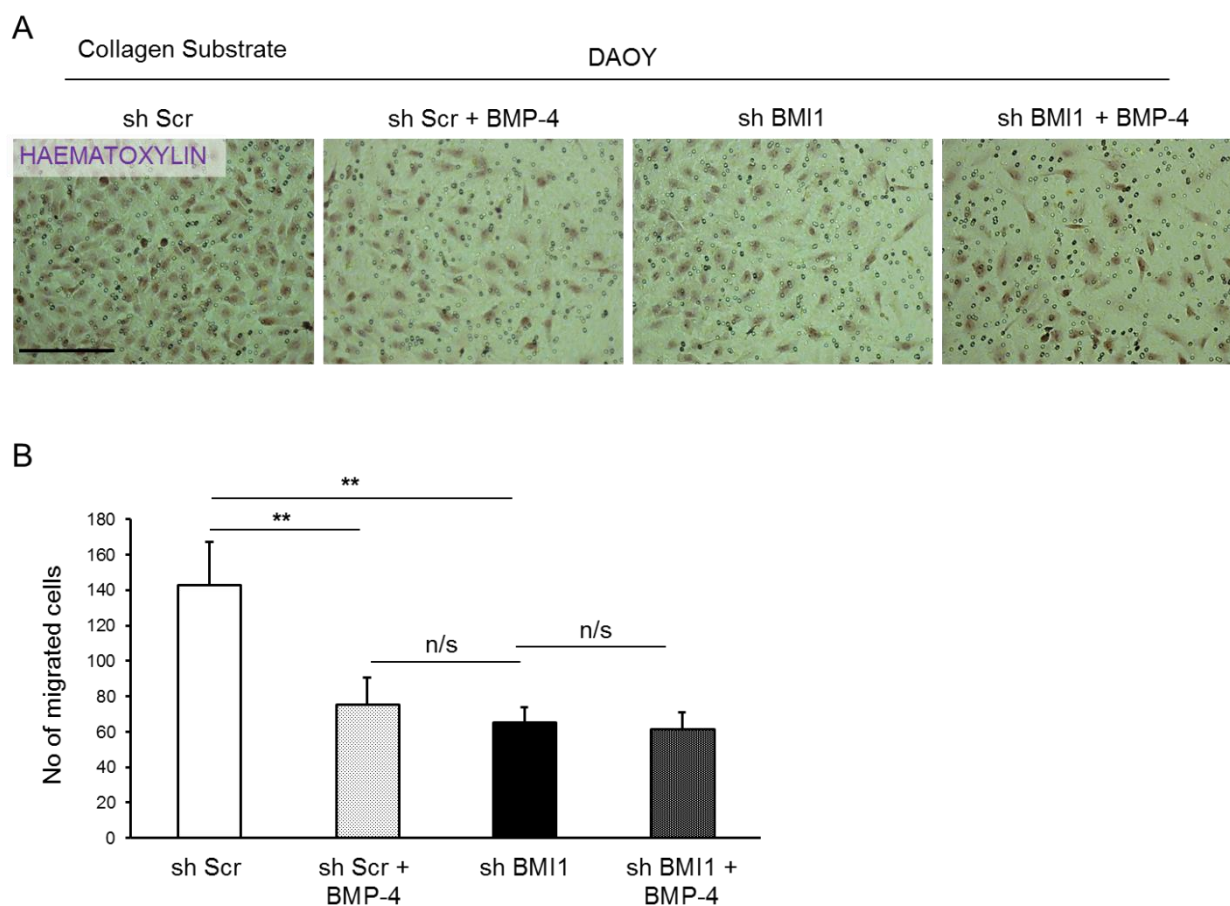
Fig. 4.9 BMP treatment reduces *in vitro* invasion in DAOY.

(A) Pictures (20x magnification) of the bottom surface of the Transwell® inserts coated with collagen substrate, after scraping the cells from top surface, representing only the migrated (invaded) cells at end of 12 hr. From left to right - shRNA Scr, shRNA Scr + BMP-4, shRNA BMI1 and shRNA BMI1 + BMP-4 treated cells. There is a significant decrease in number of cell invasion/migration through collagen seen in shRNA Scr + BMP-4 treated cells compared to shRNA Scr only treated cells. This decrease is comparable to and similar to that seen upon shRNA BMI1 treated cells. There is no further change in invasion with concomitant shRNA BMI1 + BMP-4 treatment. **(B)** Quantitation of average number of migrated/invaded cells (from four replicas) through collagen substrate. Scale bar in **(A)** = 20 µm. Error bars in **(B)** represent SD (n=4). **, $p < 0.01$. Abbreviation: BMP, Bone Morphogenetic Protein.

These results show that the effects of exogenous BMP-4 treatment on *in vitro* cell migration/invasion in MB cell lines are similar to those obtained upon BMI1 knock down and the lack of additional changes seen upon concomitant BMP-4 treatment in BMI1 silenced cells raise the possibility that BMI1 expression is essential for BMP mediated effect on the cells

4.4 Discussion

The events leading to metastasis such as detachment of the cells, dissemination, attachment and growth at the secondary site occur as result of epithelial cells temporarily acquiring mesenchymal features (Meng and Wu 2012). Collectively these changes are termed as epithelial-mesenchymal transition (EMT, originally described in embryogenesis) which include changes in cell-cell/ cell-extracellular matrix adhesion, cell motility and cell cytoskeleton, which are orchestrated by complex molecular changes (Yilmaz and Christofori 2009). As discussed above, BMPs are implicated in induction of EMT and metastasis of several cancers (Bailey, Singh et al. 2007). They are known to have contradictory roles depending on the cancer tissue type and their effects must be interpreted individually. Here we observe changes in cell adhesion, cell motility and invasion phenotypes in MB cells in response to BMI1 silencing. Interestingly all of these changes were reversible upon concomitant inhibition of BMP signalling by Noggin, suggesting that the above cellular effects of BMI1 are mediated by BMP pathway.

Differential expression of selected cell adhesion/ECM molecules observed among BMI1 silenced MB cells supports the notion that BMI1 regulates MB dissemination or metastasis. To briefly discuss the relevance of cell adhesion/ECM molecules that we studied – (1) Thrombospondins are adhesive glycoprotein that mediates cell-to-cell and cell-to-matrix interactions, and they bind to fibrinogen, fibronectin and collagens. Thrombospondin 1&2 (THBS 1/2) are overexpressed in medulloblastoma (MacDonald, Brown et al. 2001; Wiederschain, Chen et al. 2007). (2) CD44 is a cell-surface glycoprotein receptor for hyaluronic acid and is known to be expressed in primitive neuroectodermal tumours (Parker and Pilkington 2005). (3) Matrix

metalloproteinase (MMP) are zinc dependent enzyme family involved in breakdown of extracellular matrix, mainly degrading type I, II and III collagens. They are known to be expressed in medulloblastoma albeit with variability in different subtypes (Vince, Herbold et al. 2001; Ozen, Krebs et al. 2004). All of these molecules are shown to be modulated by TGF-β/BMP – SMAD signalling pathway in EMT and metastasis of various malignancies (reviewed in (Ikushima and Miyazono 2010)). It is therefore possible that the differential expression of THSB and CD44 seen in BMI1 silenced D-458 cells could be secondary to BMP pathway activation.

Bmi1 has been shown to control cell proliferation and senescence in physiological conditions and in the cancer related context by regulating the ink4a/arf locus (Jacobs, Kieboom et al. 1999). Bmi1 is shown to be overexpressed in proliferating precursor cells during cerebellar development (Leung, Lingbeek et al. 2004). In our study we observed a decrease in proliferation of DAOY cells upon BMI1 knock down. This is in keeping with the published literature (Wiederschain, Chen et al. 2007; Wang, Venugopal et al. 2012). Interestingly we did not observe a difference when BMP pathway was concomitantly suppressed, supporting the view that the effects of proliferation is independent of BMP pathway.

In our study we did not detect any significant changes in apoptosis (using Annexin V assay) in DAOY cell lines in response to BMI1 downregulation. This is in contrast to published literature (Wiederschain, Chen et al. 2007) where BMI1 knock down was shown to increase apoptosis (cells in subG1 phase, using Propidium idodide assay) in DAOY cells. Although the reason of this discrepancy is at present unknown, it is possible that the effect on apoptosis could depend on level of BMI1 knock down achieved.

Although different BMPs are known to have contradictory roles in different cancers (reviewed in (Thawani, Wang et al. 2010)), in the MB context, BMP-2 and BMP-4 have been shown to prevent cerebellar granule cell precursor cell proliferation (Rios, Alvarez-Rodriguez et al. 2004). BMP-4 is reported to have inhibitory role in glioma tumour growth (Piccirillo, Reynolds et al. 2006; Liu, Tian et al. 2010). Furthermore, there is evidence to suggest that BMP-2 and BMP-4 inhibit tumour growth *in vitro* and *in vivo* (Hallahan, Pritchard et al. 2003; Zhao, Ayrault et al. 2008). Therefore BMPs are potential therapeutic targets for MB treatment. In fact, BMP-2 inducing agent 13-cis retinoic acid, either alone or in combination with other chemotherapeutic agents has been shown to effectively reduce *in vivo* MB tumour growth in a pre-clinical study (Spiller, Ditzler et al. 2008). Vrijens et al., have described small molecule BMP activators which could potentially be developed as a medulloblastoma treatment (Vrijens, Lin et al. 2013).

Here we observe reduced invasion upon BMP-4 treatment in DAOY cell lines, in a similar fashion as observed upon BMI1 downregulation. Interestingly, exogenous BMP-4 treatment did not exert an additional effect when applied after BMI1 knock down. These findings raise the possibility that expression of BMI1 could represent a biomarker for MB which could benefit from treatment with small molecules acting as BMP agonists. However further validation studies using primary human medulloblastoma tissue samples and pre-clinical studies using genetically engineered mouse models are necessary to confirm these preliminary data.

Having established that BMI1 regulates cell adhesion, migration and invasion properties of MB cell lines *in vitro* via suppression of BMP signalling, we further studied their effects on primary cell growth and invasion using *ex vivo* and *in vivo* models.

CHAPTER 5 Ex vivo organotypic co-culture assay reveals effects of BMI1 on cell migration properties in MB cells.

5.1 Introduction

Our results so far have shown that i) BMI1 silencing causes aberrant activation of BMP signalling in primary human MB cells and in MB cell lines, and ii) BMI1 regulates cell adhesion, migration and invasion properties of MB cell lines *in vitro* via suppression of BMP signalling in MB cell lines. Here, we set out to further characterise the effects of BMI1 knock down on growth and migration of primary human MB cells using an *ex vivo* model – the organotypic cerebellar slice (OCS) co-culture. We decided to use this model because *in vitro* models such as the Transwell migration assay (or Boyden chamber assay) and the wound healing assay would not be suitable for the primary cells which grow as tumour spheres in culture. In parallel, the experiments were conducted also on DAOY cells to compare the results of the *ex vivo* assay with those obtained in cell culture.

The OCS assay was originally developed to study neuron-specific interactions and neuronal development of the cerebellum because it retains some aspects of the anatomical complexity of the developing cerebellum (Tanaka, Tomita et al. 1994). Organotypic brain slice cultures have been successfully used to study glioma cell invasion (de Bouard, Christov et al. 2002; Jung, Kim et al. 2002; Palfi, Swanson et al. 2004) and to quantify proliferation and angiogenesis of glioma cell lines (De Bouard, Guillamo et al. 2003; Guillamo, de Bouard et al. 2009). In brief, the brain explants are placed on a porous membrane to form an interface between medium and air, and co-cultured with fluorescence tagged tumour cell spheres for relevant assessments. The main advantage of this method is that the cytoarchitectural and

morphological characteristics of the tissue are maintained for a few days to a couple of weeks (Stoppini, Buchs et al. 1991). Moreover, this method recapitulates the cellular and extracellular matrix conditions *in vivo, thus* allowing us to assess their invasion and motility in an environment closely mimicking *in vivo* conditions.

5.2 Experimental design and methodology:

5.2.1 Organotypic cerebellar slice (OCS) preparation:

The OCS was prepared in accordance to previously published literature (Guillamo, de Bouard et al. 2009; Farioli-Vecchioli, Cina et al. 2012). The brains were isolated from P4-P6 C57BL/6 pups after decapitation by carefully separating and peeling the skull, and then collected in ice cold dissection buffer. The dissection buffer was prepared by supplementing 200 ml of Hank's Balanced Solution (HBSS) with 2 ml of 45% glucose (Sigma) and 3 ml of Amphotericin B (Sigma). The cerebellum was dissected from the brain and the attached meninges were removed. The cerebellum was sectioned sagittally at 420 μm thickness using McIlwain tissue chopper (The Mickle Lab. Engineering Co. Ltd.). The chopped slices were then transferred on to a Teflon disk (Fischer), containing dissection buffer, and individual slices were gently separated. The slices were kept cold for 1 hour to prevent overt gliosis.

Millicell-CM insert (Millipore), a porous membrane, was placed in each well of a 6-well plate, and 1.3 ml of culture media was added to the bottom of each well. The plate was incubated at 37^0C for at least 1 hour. The culture media is prepared by supplementing 50 ml of MEM (Sigma) with 25 ml of HBSS, 25 ml of horse serum (GIBCO), 0.5 ml of 200 mM glutamine (GIBCO), 1 ml of 45% glucose and 1.5 ml of Amphotericin B. Then, under stereomicroscopy (Zeiss, KL1500 LCD) 3 - 5 viable cerebellar slices were selected and plated on each Millicell-CM insert. The slices

were incubated at 37^0C for 24 hr before co-culturing with the tumour spheres and the co-culture was continued for 8 days. The culture media was replaced every 3 days.

5.2.2 Generation of tumour cell spheres:

In order to perform co-culture assay, it was necessary to culture MB cells as tumor spheres. For DAOY cells, the spheres were generated as per previously published protocol (Meng, Kallinteri et al. 2007). 0.5-1 x 10^6 DAOY cells which were previously labelled with GFP as described in M&M (chapter 2, section 2.2.3.1) and in chapter 3, were harvested from monolayer culture and cultured in a 25 cm^2 screw-top culture flasks (Falcon) with 10 ml complete media. These flasks were maintained at 37^oC on an orbital incubator (Stuart Scientific) at a constant rotation of 70 rev/min. Following 24 hr incubation, tumour spheres were obtained (Fig. 5.1A).

ICb-1299 cells were cultured at 37^0C in ultra-low attachment 6-well plate (Costar) to ensure tumour sphere of adequate size were obtained (Wang, Wang et al. 2008). The cells were cultured in Dulbecco's MEM medium containing F12 (Invitrogen) supplemented with EGF 20 ng/ml (Peprotech), FGF 20 ng/ml (Peprotech), 1% B27 (Invitrogen) and 1% penicillin-streptomycin (Sigma). After 3 days incubation, satisfactory tumour spheres were obtained (Fig 5.1 B), which were used to co-culture with organotypic cerebellar slice culture to assess cell migration.

.
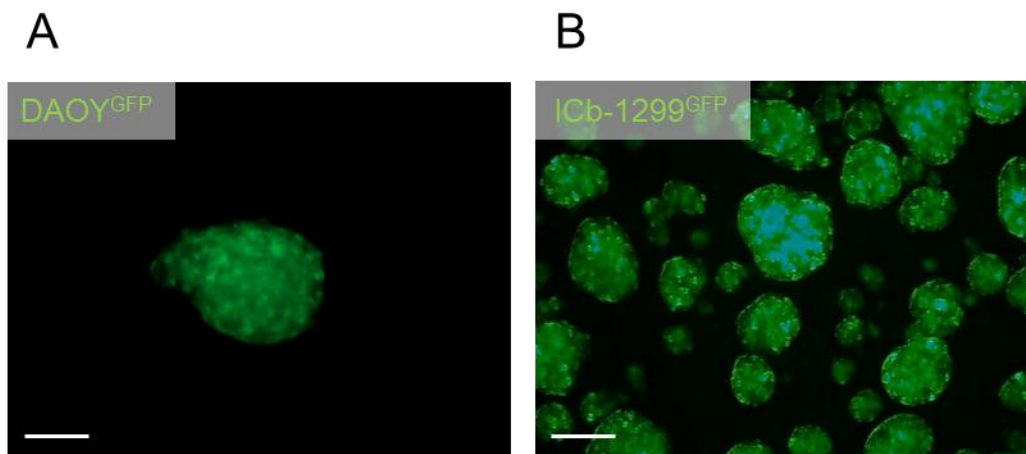
Fig. 5.1 Generation of tumour spheres for the co-culture assay.

(A) Tumour sphere from DAOY cells generated as a result of culturing them in a flask and incubating on an orbital rotator for 24 hr. **(B)** Tumour spheres from ICb-1299 cells generated as a result of culturing them in ultra-low attachment plates with culture media supplemented with growth factors. Generation of tumour spheres enabled co-culturing with the *ex vivo* OCS. Scale bars in A and B = 200 µm.

5.2.3 Organotypic cerebellar slice (OCS) and tumour cell sphere co-culture:

The tumour spheres were then seeded on the cerebellar slice cultures under a dissecting microscope (Leica M165C) and incubated for 8 days. The co-cultures were then fixed with cold 4% PFA for 15-20 min and the membrane of the insert was carefully cut to include the co-culture slices, which were transferred on to glass slides with the co-culture side facing up. The co-cultures were stained with DAPI nuclear stain and mounted with a glass coverslip. The tumour cells could be identified by their GFP positivity induced by the lentiviral infection. The schematic of the method of the OCS co-culture is shown in Fig 5.2.
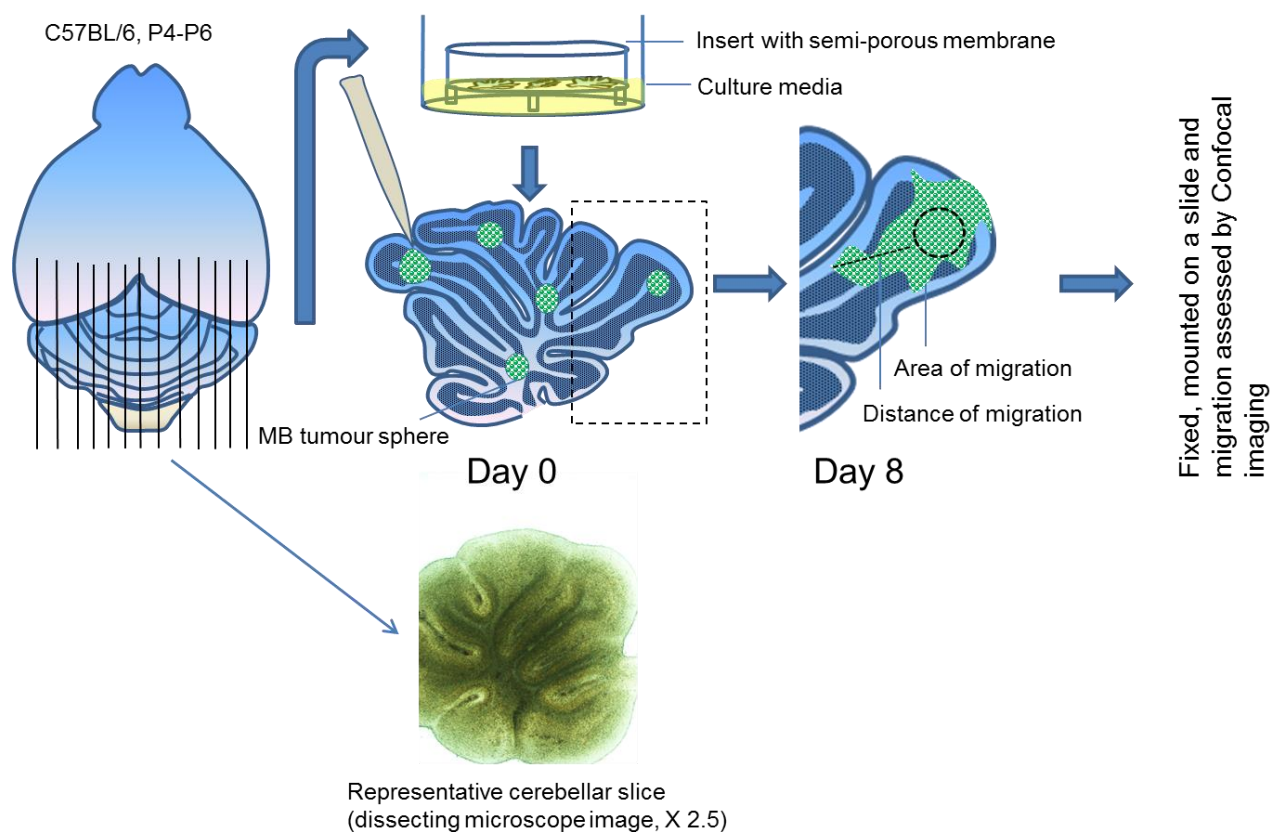
Fig. 5.2 Schematic of Organotypic Cerebellar Slice (OCS) – tumour sphere co-culture assay.

The cerebellum harvested from C57/BL6 pups was sliced at 420 µm thickness, and the slices were cultured on semi-porous membrane placed in a plate containing culture media. GFP lentivirus infected MB tumour spheres from DAOY or ICb-1299 cells were seeded on the slices, co-cultured for 8 days and fixed. The area of migration and distance of migration after 8 days was analysed using confocal microscopy.

5.2.4 Imaging and analysis:

Tumour cells could be identified because of their GFP positivity against the other

DAPI positive cerebellar cells. The images were captured with Confocal 710

microscope (Zeiss) at a magnification of 10X (for DAOY), 20X (for ICb1299) and 20X

(for DAOY), 40X oil (for ICb1299) for area and distance assessment respectively.

Lower magnification was suitable to capture the entire area of migration whereas

more precise individual distance of migration could be assessed more accurately by

using higher magnification images. The difference in magnification used for the

measurements of DAOY and ICb1299 is because DAOY are considerably larger in

size as compared to ICb1299. Cell migration was assessed using three parameters – i) percentage of invasion area (total area – tumour area/ total area x 100) and ii) maximum distance of migration (distance in µm from the periphery of the initial tumour sphere to the most distally migrated tumour cell), and iii) The depth of invasion in µm using Zen 2011 software (Zeiss). Three areas were assessed on each slice and a total of three slices were analysed for each experimental group. The experiments were conducted in technical and biological triplicates. The depth of invasion from the surface was measured by using Z-stack analysis (Froeling, Mirza et al. 2009).

5.3 Results

5.3.1 *BMI1* silencing causes a reduction in the migration area of primary MB cells ICb-1299 and of the MB cell line DAOY.

We prepared organotypic cerebellar slices of 420 µm nominal thickness from the cerebellum of C57BL/6 P4-6 pups and cultured them on porous membranes in a chamber containing medium for a minimum of 24 hours. Primary cells ICb-1299 transfected with shRNA were maintained as tumour spheres as short term cultures. For better comparison, shRNA transfected DAOY were also cultured as tumour spheres for this specific experiment. Tumour spheres (at least 3-5 spheres/slice) were then transferred onto the surface of viable OCS slices and co-cultured for 8 days.

After 8 days of co-culture, we observed a reduced migration area in both DAOY[BMI1kd] and ICb1299[BMI1kd] as compared to DAOY[Scr] and ICb-1299[Scr] respectively – 43.63% (± 6.06) vs 64.23% (± 7.83) in DAOY (p=0.021) [Fig 5.3 A,C,E] and 35.34% (± 2.64) vs 48.19% (± 3.74) in ICb1299 (p=0.008) [Fig 5.3 B,D,E].
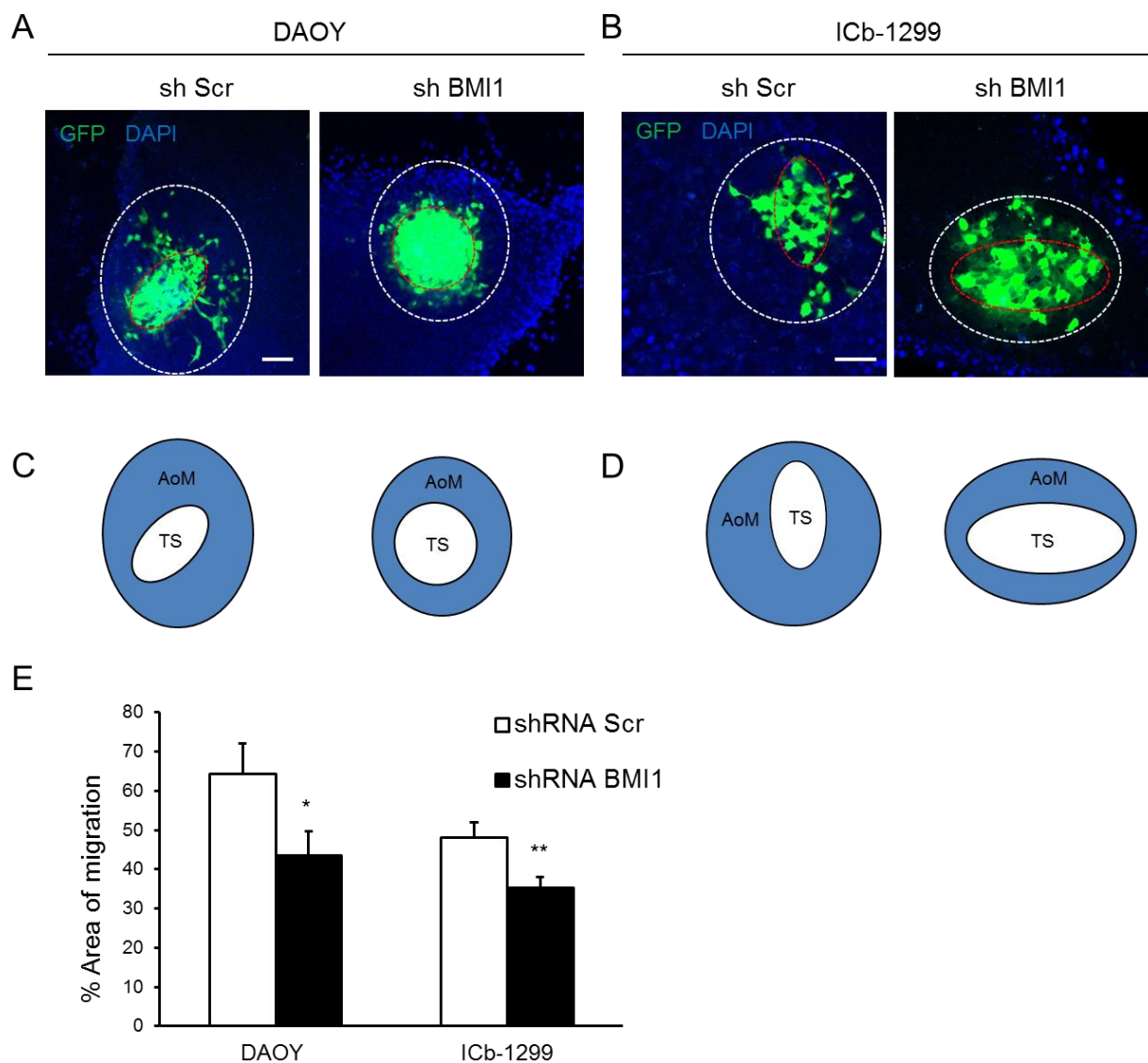
Fig. 5.3 BMI1 silenced tumour spheres show reduced migration area in an *ex vivo* OCS co-culture.

(A) A reduction in the migration area is noted in DAOY[BMI1kd] tumour sphere (right), compared to DAOY[Scr] (left). The white dotted line is drawn to represent total the area of migration at the end of 8 days, and the red dotted line represents the area of initial tumour sphere. **(B)** A reduction of migration area is noted also for ICb-1299[BMI1kd], tumour spheres (right) as compared to ICb-1299[Scr] (left). **(C and D)** Schematic representation of the area of migration for DAOY **(C)** and ICb-1299 **(D)**. The inner white spheres, TS, represent the initially seeded tumour spheres, corresponding to the red dotted lines from **(A and B)**. The outer circle represents the area of migration at the end of 8 days of co-culture; The blue area, AoM, is the representation of the area of migration, corresponding to white dotted lines in **(A and B)**. AoM is calculated by subtracting TS from the total area. **(E)** Quantification of average area of migration (%) from three independent experiments for both DAOY and ICb-1299 co-cultures. Three areas were assessed on each slice and a total of three slices were analysed in each group. Error bars represent SD (n=3). *, $p<0.05$; **, $p<0.01$. Scale bar in **(A)** = 100 µm, and in **(B)** = 20 µm. Abbreviation: AoM, Area of Migration; TS, Tumour Sphere (initially seeded).

These results raised the possibility that cell migration was affected also in primary MB cells in an ex vivo co-culture assay. However, as we had established that BMI1 knock down reduced the proliferative capacity of MB cells, it was essential to exclude that the reduction in migration area was not due to passive distribution secondary to the reduced proliferation caused by BMI1 knock down. To address this point, the maximum distance of migration of individual cells was also analysed.

5.3.2 MB cells show a reduced distance of migration upon BMI1 knock down

Three fluorescent high magnification images were acquired per slice from the periphery of the original tumour sphere where individual tumour cell were seen to migrate away. The distance between the farthest migrated cell and the edge of the original tumour sphere was measured in µm using Zen software. The experiment was conducted in triplicates. The average distance of migration was determined between BMI1 knock down and control groups.

After 8 days of co-culture, we observed a significantly reduced average distance of migration in both DAOY^{BMI1kd} and ICb1299^{BMI1kd} as compared to DAOY^{Scr} and ICb-1299^{Scr} respectively – 157.40 µm (± 23.38) vs 250.03 µm (± 34.71) in DAOY (p=0.017) [Fig 5.4 A,C], and 80.50 µ (± 23.37) vs 115.28 µm (± 34.71) in ICb1299 (p=0.041) [Fig 5.4 B, C].
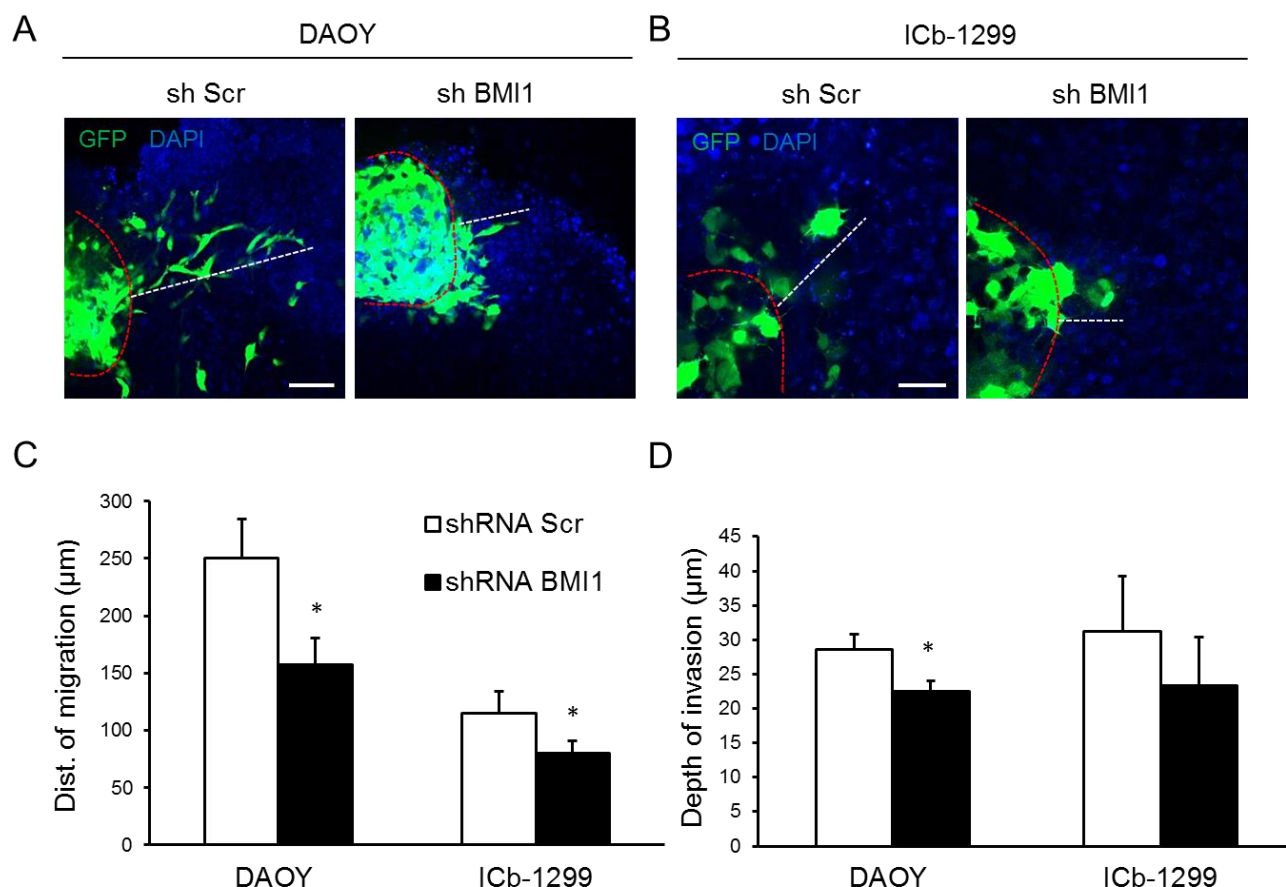
Fig. 5.4 BMI1 silenced tumour spheres show reduced distance of migration in an *ex vivo* OCS co-culture.

(A) A reduction in the maximum distance of migration is noted in shRNA BMI1 treated DAOY tumour sphere (right), compared to shRNA Scr treated sphere (left). The white dotted drawn represents the distance of the farthest cell to the edge of the initial tumour sphere (marked with red dotted line). **(B)** A reduction in the maximum distance of migration is noted also in ICb-1299, shRNA BMI1 treated tumour sphere (right) as compared to shRNA Scr treated sphere (left). **(C)** Quantification of average distance of migration (μm) from three independent experiments for both DAOY and ICb-1299. **(D)** Quantification of average depth of invasion (μm) using Z stack analysis from three independent experiments for both DAOY and ICb-1299. Three areas were assessed on each slice and a total of three slices were analysed in each group. Error bars represent SD (n=3). *, p<0.05. Scale bar in **(A)** = 40 μm, and in **(B)** = 20 μm.

In keeping with the results of the *in vitro* experiments, the *ex vivo* experiment show reduction in cell motility and migration of DAOY cells upon BMI1 knock down. Moreover, reduction in migration was observed also in short term cultures of the primary MB cells ICb1299 upon BMI1 knock down. This validates the notion that BMI1 plays a role in regulating the migratory properties of MB cells.

The depth of tumour cell invasion from the surface of the slice to the deepest invasive cell within the slice parenchyma was assessed from the areas adjacent to the original tumour sphere. This was done using Z stack series imaging by confocal microscopy and the distance (in μm) of depth of invasion was assessed using Zen software. There was a significantly reduced average depth of invasion observed in DAOY^{BMI1kd} as compared to DAOY^{Scr} 22.48 μm (± 1.57) vs 28.52 μm (± 2.30), p=0.018 [Fig 5.4 D]. Although there was a trend towards decreased depth of invasion observed in ICb-1299^{BMI1kd} as compared to ICb-1299^{Scr}, the results were not statistically significant – 23.39 μm (± 7.02) vs 31.22 μm (± 8.03) p=0.178 [Fig 5.4 D].

5.4 Discussion

In this part of the study we have taken advantage of organotypic cerebellar slices isolated from neonatal mice and co-cultured them with human MB tumour cell sphere as an *ex vivo* model to investigate MB tumour cell migration. With this model, we have 1) validated the *in vitro* findings in a model closer to physiological *in vivo* conditions, and 2) confirmed the *in vitro* findings of the DAOY cell lines using the primary MB cells ICb-1299.

Studying the invasive and metastatic characteristics of the tumour cells would be provide more precise assessment of the tumour cell behaviour and would have better translational value. Meng et al., describe the suitability of cerebellar slice and MB cell tumour sphere co-culture model to study invasion (Meng, Kallinteri et al. 2007). They demonstrate that the DAOY tumour aggregate first attached to the organotypic cerebellar slice and then invaded into the slice parenchyma replacing the normal tissue. By studying the invasion pattern by confocal and electron

microscopy, they also suggest that cerebellar slices are more conducive to study MB invasion as compared to cerebral slices. Here we observe a trend of reduced slice invasion in ICb-1299[BMI1kd] cell and a significantly reduced invasion of DAOY[BMI1kd] into the cerebellar slice parenchyma. This is in keeping with the reduced in vitro invasion observed in Transwell assay and is supportive of our notion that Bmi1 plays a role in modulating the invasive properties of the MB tumour cells.

In order to examine whether BMI1-mediated repression of the BMP pathway remains intact in MB, in collaboration with Michael Taylor group from The Hospital for Sick Children, University of Toronto, we re-examined a publicly available transcriptome-wide analysis of DAOY MB cell line (Wiederschain, Chen et al. 2007). We identified 1483 genes differentially expressed between DAOY[BMI1kd] and control DAOY cells. A Gene Set Enrichment Analysis (GSEA) identified over-represented canonical pathways that included genes related to ECM-receptor interactions as well as the TGF-β pathway. Importantly among the deregulated cell adhesion molecules (ITGA3, LAMB3, LAMC1, COL7A1, Thrombospondin 1 and CD44), several genes either represented the human homologue of the genes identified in BMI1-/- granule cell progenitors (Chapter 4, Table 4.1) or belong to the same protein family.

To further strengthen the connection between *BMI1* and TGF-β-regulated cell adhesion molecules identified in murine cells and MB cell lines with human primary MB samples, we examined 282 non-WNT primary MBs, previously profiled using Affymetrix Human Gene 1.1ST arrays. Using unsupervised hierarchical clustering (HCL) we demonstrate that two Group 4 molecular variants existed - *BMI1*-high, TP53-low and *BMI1*-low, TP53-low, which largely cluster apart suggesting that a distinct transcriptome-wide gene signature associate with the expression of *BMI1*. To elucidate the specific pathways associated with these two sets of Group 4 tumours, a

transcriptome-wide supervised Significance Analysis of Microarrays (SAM) was performed. Interestingly, only 190 unique genes demonstrate statistically differential gene expression changes in BMI1 high subset as compared to BMI1 low subset of Group 4 MBs. Overrepresented Gene Ontologies (GO) include: regulation of secretion, oxidoreductase activity and, extracellular matrix structural constituents. In the latter category, statistically significant downregulation of Laminin B1 (LAMB1, -1.93) and upregulation of EFEMP2 (+1.71), FBN2 (+2.21), SMC3 (1.53), Thrombospondin 4 (THBS4, +2.12) were detected. The above bioinformatics analysis was performed with the help of Adrian Dubuc and Marc Remke from Michael Taylor group (unpublished data). These data suggest that BMI1 exerts its role in human MB pathogenesis at least in part through modulation of the expression of cell adhesion genes, potentially via BMP pathway repression.

Invasion is a complex process by itself which in addition to cell-cell and cell-ECM interaction, would also depend on other host tissue factors such as angiogenesis (Pilkington 1994). The rate of tumour cell proliferation may also influence the assessment of the depth of the tumour. Furthermore, certain factors such as necrosis of the core of the slices over time (Lossi, Alasia et al. 2009), limits accurate assessment of depth of migration and hence the true invasion. While OCS co-cultured was a good model to validate our *in vitro* observations related to cell migration, we next set out to validate the growth and invasion of MB cells using an *in vivo* mouse model.

CHAPTER 6 Tumour volume and parenchymal invasion but not leptomeningeal spreading is controlled by BMI1 in an orthotopic MB xenograft model.

6.1 Introduction

Medulloblastoma are aggressive tumours with approximately one-third of cases presenting with metastatic disease at diagnosis and up to two-third of cases relapsing to treatment presenting with leptomeningeal disease (Reviewed in (Packer 1999)). Medulloblastoma is defined by its proclivity to disseminate via CSF route to brain and spinal cord (Mumert, Dubuc et al. 2012), and presence of metastasis at the time of diagnosis is considered a powerful independent prognostic factor (Zeltzer, Boyett et al. 1999). The mechanism for leptomeningeal spread vary to that of local tumour invasion (Laerum 1997), albeit, local invasion is also an important factor determining the treatment response and survival outcome (Riffaud, Saikali et al. 2009; Sikkema, den Dunnen et al. 2012). Chang et al. classified MBs with presence of local invasion and brain stem invasion into a higher tumour stage – T3 from T1 or T2, reflective of poorer outcome (Chang, Housepian et al. 1969). It was therefore relevant to study the invasive characteristics of our MB cells using a suitable *in vivo* model. Genetically engineered mouse (GEM) model would be an ideal tool for this. But prior to embarking on sophisticated GEM model, which is relatively expensive and has longer latency, we chose to perform our validation experiments on an alternative suitable, *in vivo* xenograft (transplant from a different species) model. This model provides the advantage of being able to study the characteristics of cells from human origin as opposed to those from murine origin in GEM model. Orthotopic (normal or usual position) xenograft transplants in immune-deficient mouse is a well-established model to study tumour invasion and metastasis in several cancers (Tan

and Chu 1985) including brain cancers (Giannini, Sarkaria et al. 2005).Furthermore, the use of GFP labelling to study tumour invasion and metastasis of individual cell by fluorescent imaging monitoring is also well established (MacDonald, Tabrizi et al. 1998; Zhang, Li et al. 2002).

So far, our *in vitro* experiments have shown that BMI1 controls MB cell adhesion, cell migration and invasion in a BMP dependent manner. We have also observed effects of BMI1 on MB cell migration in an organotypic *ex vivo* experiment. Here we set out to determine the contribution of BMI1 to *in vivo* tumour growth and invasive characteristics. Short term cultures of lentiviral shRNA BMI1 infected primary MB cells ICb-1299, and their control counterpart were orthotopically transplanted in NOD-SCID mice. To be able to compare the results obtained *in vivo* with the experiments carried out *in vitro*, DAOY cells were also xenografted Following transplantation, we first assessed if an effective BMI1 knock down was maintained in the xenograft tumours at the end of the termination of the experiment. Then we performed immunohistochemistry to assess whether BMP pathway activation observed *in vitro* upon BMI1 knock down would be occurring also *in vivo*. Four independent functional parameters were compared between BMI1 silenced xenografts and controls – i) tumour volume, ii) intraparenchymal invasion, iii) spread along the Virchow-Robin spaces, and iv) tumour burden within the spinal cord.

6.2 Experimental design and methodology

6.2.1 Intra-cerebellar transplantation in NOD-SCID mice

The animal procedures were carried out as per the Animals Scientific Procedures Act 1986 as described in M&M (Chapter 2, section 2.9). Briefly, the neonatal (P4 – P6) NOD-SCID mice were first anaesthetised and a constant quantity of 1×10^5 cells shRNA lentivirus transfected MB tumour cells in 3-5 µl sterile PBS were transplanted in to right cerebellar hemisphere. The cells were injected using a stereotaxic frame (coordinates: 1-2 mm lateral and 1-2 mm posterior to lambda suture, and 2-3 mm deep) with a 25 µl Hamilton syringe/26 gauge needle. A total of 19 mice were injected with ICb-1299 cells (10 scrambled, 9 BMI1 knock down) and 18 mice with DAOY cells (9 scrambled, 9 BMI1 knock down). The mice were culled if they developed neurological signs or at the end of the experiment which was 12 weeks after transplantation. The brain was harvested from these animals, the cerebellum and the brain stem were dissected from the rest of the forebrain and they were fixed in 4% PFA, followed by treatment with 30% sucrose and cryopreservation in OCT compound. The spinal cord was also isolated from these animals as described below in section 6.2.6.

6.2.2 Cryostat tissue sectioning

The OCT embedded cerebellum and brain stem samples were sectioned in their entirety at 20 µm thickness interval. The sections from each sample were transferred to twelve glass slides serially (ie. 1-12 sections to slides 1-12 and 13 – 24 sections to slide 1 – 12 again etc.) to ensure that each slide would represent the entire sample.

The slides were labelled and left to dry overnight. The dried sections were stored at -80^0C until stereology and confocal microscopy analysis was performed.

6.2.3 Immunohistochemistry

Immunohistochemistry was used to i) test the efficiency of BMI1 knock down and ii) to test pSMAD1,5,8 expression in MB tumour cells following xenograft transplantation. The procedure was performed as described in M&M (chapter 2, section 2.10.3). Briefly, the sections were first incubated with blocking solution (NDS or NGS) for 1 hr and treated with either BMI1 or pSMAD1,5,8 primary antibody overnight. Appropriate fluorescent secondary antibody (red, either 568 or 546 nm) was then added for 2 hr. The primary and secondary antibodies used along with their concentrations are listed in Table 6.1. The sections were mounted with DAPI containing mounting medium and coverslipped. The GFP positive tumour regions were identified under confocal microscope and five random high power images (63X oil for BMI1 and 100X oil for pSMAD1,5,8 assessment) were acquired per each case. The experiment was done in triplicates (three different cases were used for each group). The number of pSMAD1,5,8 positive (red) cells were counted and average counts were compared between shRNA BMI1 knock down and control groups in both DAOY and ICb-1299 xenografts. The statistical significance was calculated using student's *t test*.

Table 6.1 Details of primary antibodies used for immunofluorescence.

For antigen to be detected	Primary antibody used	Company	Concentration	Alexa Fluor® secondary antibody (Invitrogen)
BMI1	Goat polyclonal anti-Bmi1	Santa Cruz Biotechnology (sc-8906)	1:200	donkey anti-goat IgG 568 (red) A11057
pSMAD1,5,8	Rabbit polyclonal anti-phosphoSmad1/5/8	Cell signalling (9511)	1:100	Goat anti-rabbit 546 (red) IgG A11035

6.2.4 Tumour volume estimation by stereomicroscopy using Cavalieri probe

As each of the 12 slides prepared above are a true representation of the entire xenograft, one slides for each sample was chosen for this assessment. The slide was mounted using DAPI containing medium and covered with a glass coverslip. Every section on the slide was screened for tumour GFP positivity under fluorescence stereomicroscope (Nikon Eclipse 80*i*) using 10X (aperture 0.45) objective. The tumour volume was estimated by Cavalieri probe using Stereo Investigator 10 software (MicroBrightField, Inc.) in accordance with previously published literature (Villeneuve, Tremblay et al. 2005; Ghulam Muhammad, Candolfi et al. 2009). The GFP positive tumour regions recognised under stereomicroscope were marked using grid points, set at 20 µm grid spacing. The tumour regions were marked on multiple sections by driving the LEP motorised stage along X and Y axes. The grids overlapping the tumour areas were counted by the software and were converted into volume estimates after accounting for the non-consecutive section interval (which was constant at 12) and section thickness (which was constant at 20 µm). The results generated were collated in excel spread sheet and averaged for all samples. The average tumour volume estimates were compared between shRNA BMI1 silenced xenografts with scrambled controls for both ICb-1299 and DAOY groups. The statistical significance was calculated by student's *t test*.

6.2.5 Depth of tumour invasion measurement by confocal microscopy

One of the twelve slides prepared (section 6.2.2) which is representative of the entire xenograft was mounted using DAPI containing medium and covered with a glass coverslip. As for stereomicroscopy, all sections on the slide were screened for GFP

positive tumour. On each slide three tumour regions with intraparenchymal (cerebellum or brain stem) invasion or spread along Virchow Robin space were imaged at 20X magnification using Confocal microscope. The maximum depth of invasion - distance in µm from the pial surface to the farthest invading/spreading tumour cell was measured in each region using ImageJ 1.43u software (National Institutes of Health, USA). The distances were averaged for each case and compared between shRNA BMI1 silenced and scrambled groups for both ICb-1299 and DAOY xenografts. The statistical significance was calculated by student's *t test*.

6.2.6 Spinal cord dissection and tumour burden analysis

The spinal cords of the engrafted animals were harvested to assess tumour burden as an evidence of metastatic spread, as described in M&M (chapter 2, section 2.9.4.3). The harvested cords were fixed in 10% formalin and longitudinally divided in to 5-7 segments approximately corresponding to their anatomic levels and embedded in paraffin blocks. The blocks were sectioned at 4-5 µm thickness and were stained with H&E for morphological analysis of tumour burden. The sections from all the samples were screened for presence of tumour deposits in the spinal cord, identified by histological characteristics of medulloblastoma. The rate of tumour positivity in shRNA BMI1 silenced xenografts were compared with controls.

The schematic of in vivo xenograft generation and analysis is represented in Fig 6.1.
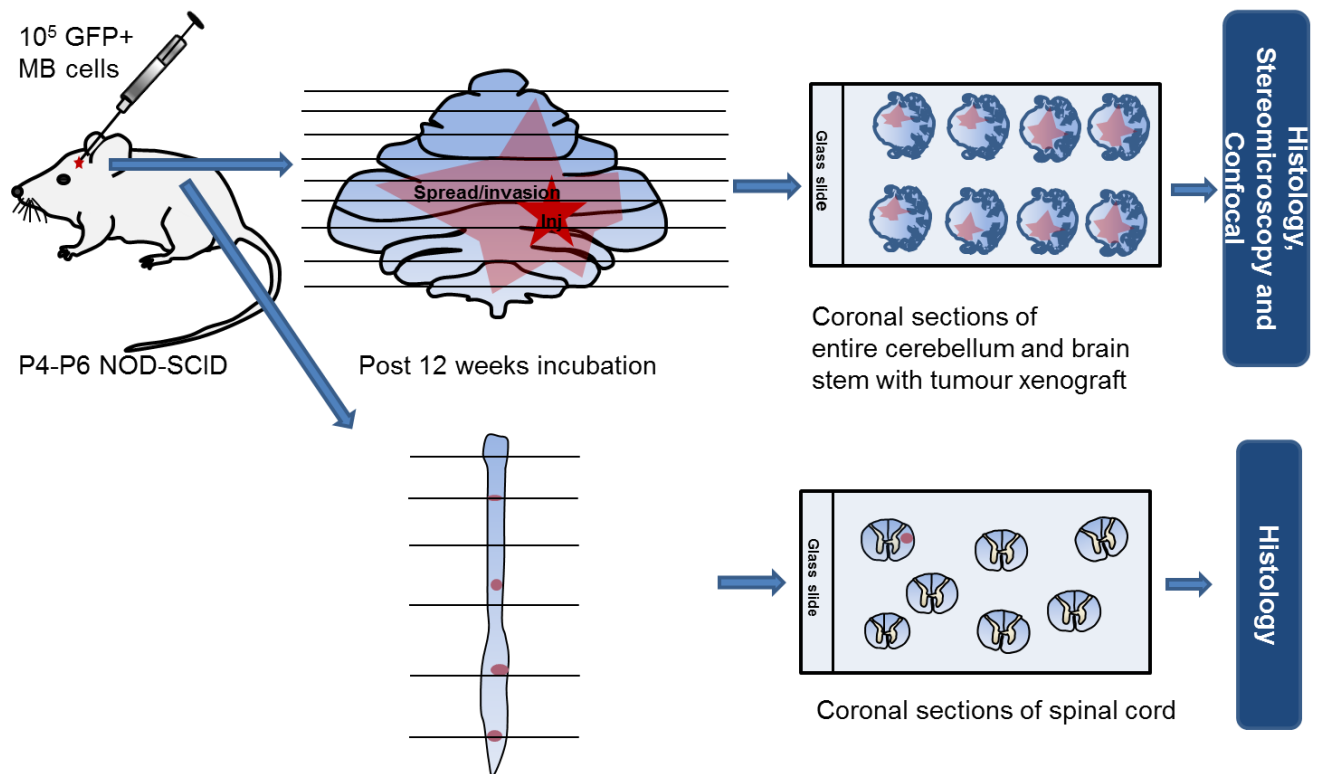
Fig. 6.1 Schematic of orthotopic xenograft generation and analysis.

Lentivirus infected, GFP labelled, DAOY or ICb-1299 cells were injected into right cerebellar hemisphere of NOD-SCID pups. The cerebellum and brain stem were isolated 12 weeks later at the latest, fixed and cryopreserved. The entire cerebellum and brain stem were serially sectioned and screened for the presence of tumour by histology and immunohistochemistry. The volume estimates of xenografts were compared between shRNA BMI1 and shRNA Scr treated cells by stereomicroscopy using Cavalieri method. The depth of tumour cell invasion was analysed and compared using confocal microscopy. In addition, spinal cords of all primary tumour positive cases were collected, sectioned and screened for the presence of tumour deposits.

6.3 Results:

6.3.1 Intracerebellar injection of MB cells yields tumour xenografts

A constant number (1×10^5 in 3-5 µl) of shRNA transfected ICb-1299 or DAOY cells were injected in to right cerebellar hemisphere of each NOD-SCID mouse. A total of 19 mice (9 males, 10 females) were injected with ICb-1299 cells (10 scrambled, 9 BMI1 knock down) and 18 mice (7 males, 11 females) with DAOY cells (9 scrambled, 9 BMI1 knock down) [Fig 6.2A]. Unless they developed symptoms, they were sacrificed at twelve weeks after transplantation.

Among DAOY engrafted mice, two of nine mice (22.2%) with DAOY^{Scr} and one of ten mice (10%) with ICb-1299^{Scr} developed neurological symptoms related to tumour growth at 8 weeks and 10 weeks respectively and hence had to be terminated at those time points. The rest of the DAOY^{Scr} / ICb-1299^{Scr} and all of DAOY^{BMI1kd} / ICb-1299^{BMI1kd} xenografted mice were asymptomatic and were terminated at 12 weeks (Fig 6.2 B). Kaplan-Meier survival plot comparing the BMI1 knock down xenografts with controls did not show statistically significant difference in the survival estimation (using Log Rank test) between the groups Fig 6.2 C and D).

All DAOY engrafted mice (18/18, 100%) developed a tumour and no significant difference in tumour take was found also between ICb-1299^{Scr} (6 of 10, 60%) and ICb-1299^{BMI1kd} (6 of 9, 66%) engrafted mice (Fig 6.2 E).

A

		Male	Female	**Total (N)**
DAOY	Sh Scr	3	6	9
	Sh BMI1	4	5	9
	Total (N)	7	11	18
ICb1299	Sh Scr	4	6	10
	Sh BMI1	5	4	9
	Total (N)	9	10	19

B

C

D

E
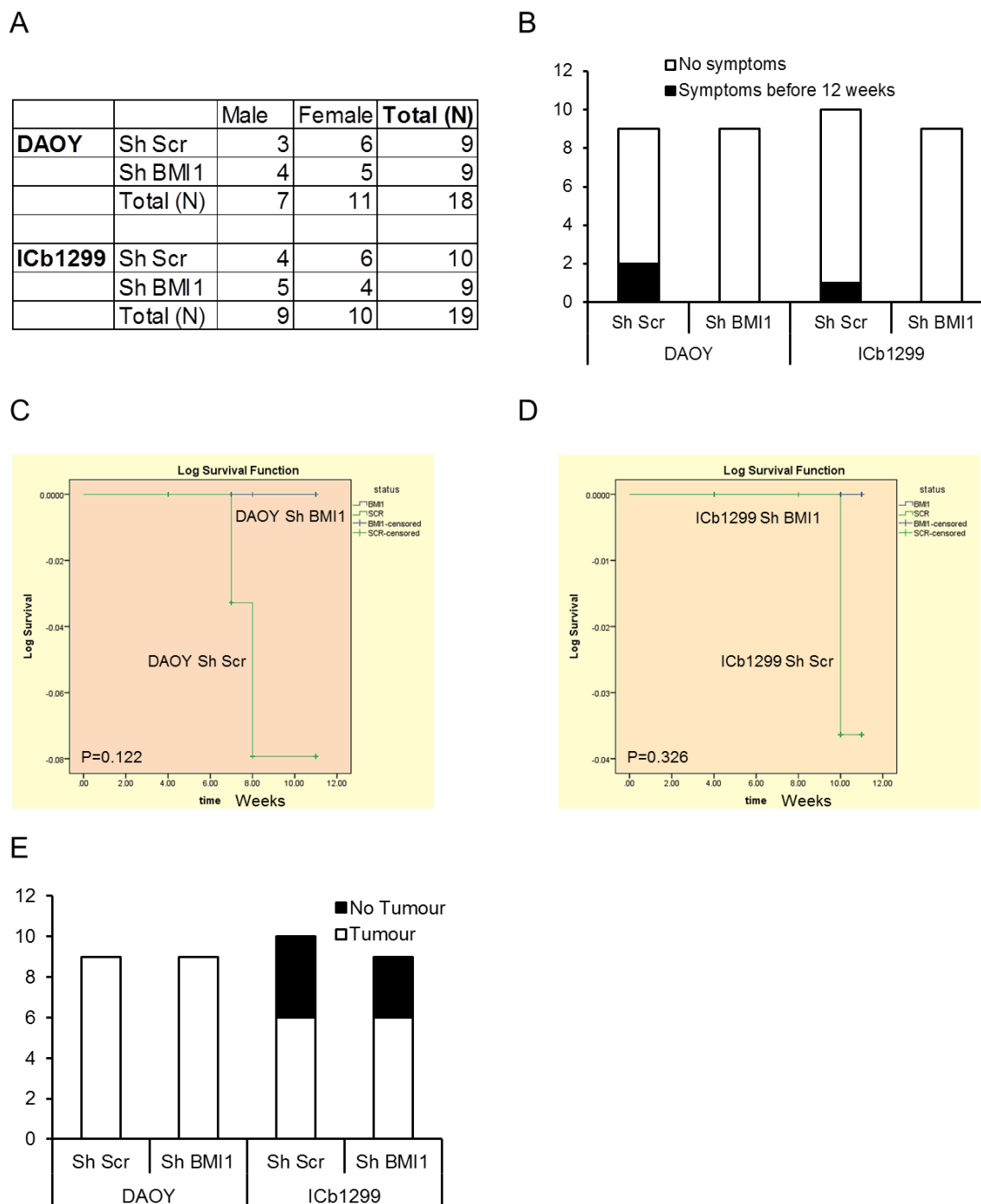
Fig. 6.2 Statistics of MB xenografts generated.

(A) Tabulation of number and gender of mice injected with DAOY or ICb-1299 cells. **(B)** Graph representing number of mice that were symptomatic (terminated) before 12 weeks in each group. No mice with shRNA BMI1 transplants were symptomatic while a minor fraction of shRNA Scr transplanted mice developed symptoms prior to 12 weeks. **(C and D)** Kaplan-Meier curve comparing survival estimates of shRNA BMI1 transplants against shRNA Scr transplants in DAOY **(C)** and ICb-1299 **(D)**. There was no significant difference in survival estimates in either group on Log-Rank analysis. **(E)** Graph depicting fraction of tumour-take in DAOY and ICb-1299 transplants. All of DAOY transplanted mice developed tumour, while the tumour uptake among ICb-1299 transplants was 60-66%.

Histological and immunohistochemical analysis was carried out to confirm the

diagnosis. Histologically the DAOY xenografts consist of multifocal tumour growth in

the cerebellum and the brain stem composed of poorly differentiated densely packed

round to oval neoplastic cells with hyperchromatic nuclei surrounded by scanty

cytoplasm. Occasional tumour cell rosettes and nodules were present, reminiscent of

both classic and desmoplastic medulloblastoma morphology (Giangaspero, Binger et

al. 2000) [Fig 6.3 A and B]. ICb-1299 xenografts also showed similar features to that

of DAOY xenografts. However, the tumour cells showed more abundant cytoplasm,

prominent nuclear moulding and there were areas of necrosis. The features were

reminiscent of anaplastic medulloblastoma (Shu, Wong et al. 2008) [Fig 6.3 C and

D]. Immunohistochemistry revealed ICb-1299 generated tumours to be diffusely

positive for synaptophysin (Fig 6.3 E), and negative for GFAP (Fig 6.3 F), in keeping

with that seen in medulloblastoma (Giangaspero, Binger et al. 2000).
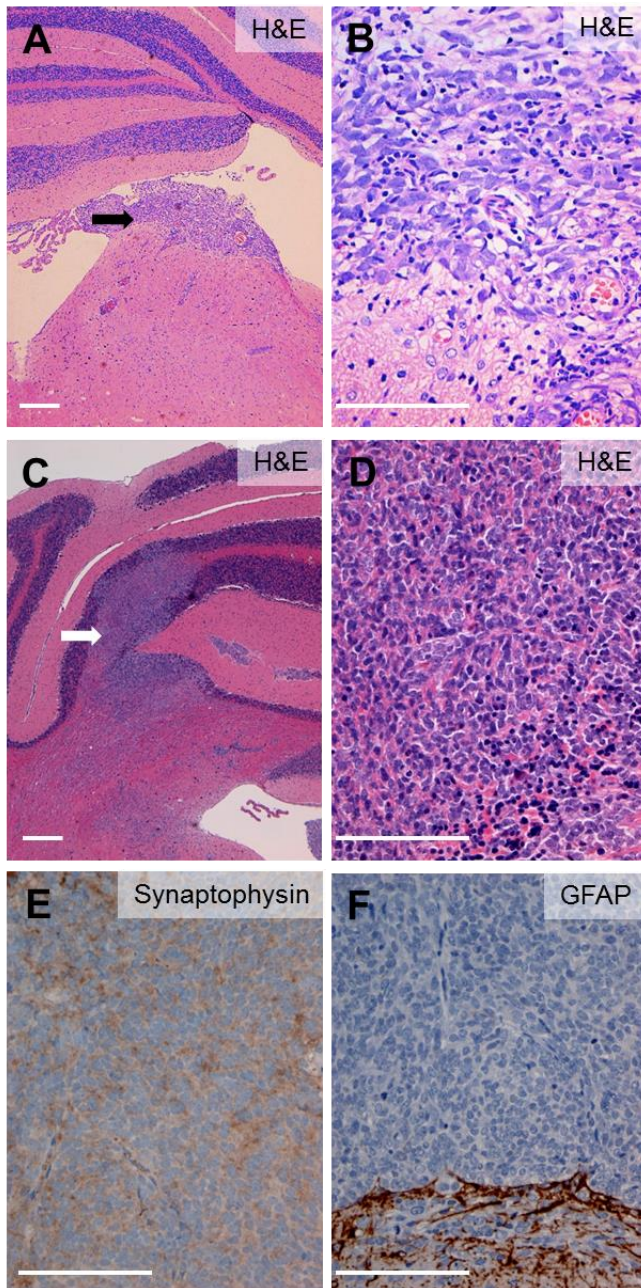
Fig. 6.3 Histology and immunohistochemisty of xenograft tumours confirming features of MB.

(A) H&E section showing medulloblastoma (black arrow), upon DAOY (shRNA Scr treated) cells xenograft. In this case, the tumour is present in the brain stem, abutting cerebellum, and tumour infiltration to parenchyma is seen. **(B)** High power view of area corresponding to arrow head in **(A)**, showing poorly differentiated densely packed round to oval neoplastic cells with hyperchromatic nuclei surrounded by scanty cytoplasm. **(C)** H&E section showing medulloblastoma (white arrow), upon ICb-1299 (shRNA Scr treated) primary cells xenograft . In this case, the tumour is present in the cerebellum and extends into the brain stem. **(D)** High power view of area corresponding to arrow head in **(C)**, showing histological features resembling DAOY xenograft, but in addition the tumour cells showed more abundant cytoplasm and prominent nuclear moulding. Furthermore, immunohistochemistry reveals ICb-1299 xenograft to be Synaptophysin (membrane) positive **(E)**, and GFAP negative **(F)**, in keeping with the expression pattern that is seen in human medulloblastoma. The lower part of **(F)** shows GFAP positivity in reactive astrocytes of the surrounding brain tissue. Scale bar in (A) and (C) = 50 µm, and in (B), (D), (E) and (F) = 20 µm.

Having confirmed the histological identity of the xenografts, we set out to investigate if protracted BMI1 knock down was maintained in the xenografted tumour cells.

6.3.2 BMI1 knock down is confirmed in the xenografts.

Prior to functional analysis of the xenografts, it was important to confirm stable BMI1 knock down induced by lentiviral shRNA transfection of MB cells pre-injection in the xenografts 12 weeks after engraftment. Previous studies in which tumour xenografts were generated following shRNA lentivirus based BMI1 knock down in hepatocellular carcinoma cells (Chiba, Miyagi et al. 2008) and in medulloblastoma cells (Wang, Venugopal et al. 2012) have shown stable knock down 14 weeks and 8 weeks after engraftment respectively. Here we performed immunohistochemical analysis on three xenografts from each cell type to assess BMI1 expression. The cryosections were treated with anti-Bmi1 antibody and stained with fluorescent secondary antibody (Alexa Fluor 568, red), counterstained with DAPI nuclear stain and examined by confocal microscopy. Five regions from each tumour sample, three samples from each group, were examined.

There was prominent reduction of BMI1 expression noted in xenograft tumours arising from DAOY[BMI1kd] and ICb-1299[BMI1kd] transplants as compared to those arising from the respective scrambled treated control cells (Fig 6.4). This confirmed an efficient protracted BMI1 knock down which was maintained 12 weeks after injection. .
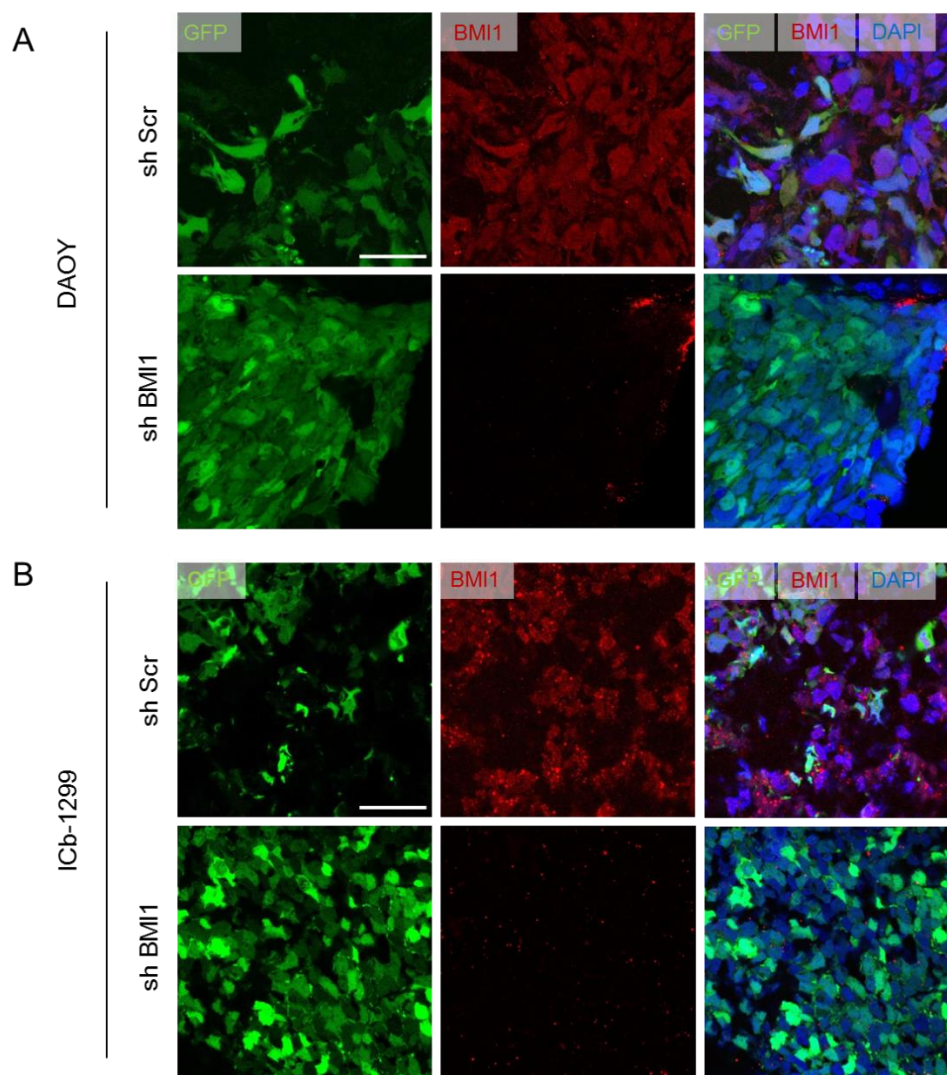
Fig. 6.4 GFP positivity and efficient BMI1 knock down is maintained in the xenografts.

(A and B) BMI1 immunohistochemistry on xenografts reveals an effective knock down in shRNA BMI1 treated cells (lower panel) as compared to shRNA Scr treated cells (upper panel) in both DAOY **(A)** and ICb-1299 **(B)**. Five fields in each sample and three samples from each group were screened, in which similar difference in BMI1 expression was noted. Left – GFP (green) channel, middle – BMI1 (red) channel, right – merge. A strong GFP signal is retained in the xenograft cells, which makes it suitable for further fluorescent microscopy tracing of the cells. Scale bar in **(A)** and **(B)** = 20 µm.

6.3.3 An increased phosphorylation of SMAD 1,5,8 is seen in BMI1 silenced xenografts

Our *in vitro* results have shown that BMI1 silencing causes de-repression of BMP

signalling in primary human MB cells ICb-1299 and in MB cell lines DAOY (chapter

3, Figs 3.6 and Fig 3.5). Having established that an efficient protracted BMI1 knock

down was maintained in the medulloblastoma xenografts, we set out to determine the BMP pathway status in these tumours.

We performed pSMAD1,5,8 immunohistochemical labelling on DAOY[BMI1kd], DAOY[Scr], ICb-1299[BMI1kd] and ICb-1299[Scr] tumours, as previously described. Briefly, the cryosections were treated with anti-pSmad1,5,8 antibody and stained with fluorescent secondary antibody (Alexa Fluor 546, red), counterstained with DAPI nuclear stain and examined by confocal microscopy. Five regions from each tumour sample were imaged at high power (100X oil) and the percentage of pSMAD1,5,8 positive (red) cells per field (pSMAD1,5,8 positive/total DAPI positive cells x 100) were counted. Average counts were compared between shRNA BMI1 knock down and control groups in both DAOY and ICb-1299 xenografts. The statistical significance was calculated using student's *t test*

The average number of xenograft tumour cells expressing pSMAD1,5,8 was increased in BMI1 silenced group as compared to scrambled group – 38.27% (±6.16) vs 16.02% (± 3.51) in DAOY (p=0.005) [Fig 6.5 A and C], and 32.77% (±6.0) vs 12.33% (±1.50) in ICb-1299 (p<0.01) [Fig. 6.5 B and C], in keeping with the notion that BMP pathway de-repression is induced by BMI1 silencing also *in vivo*.
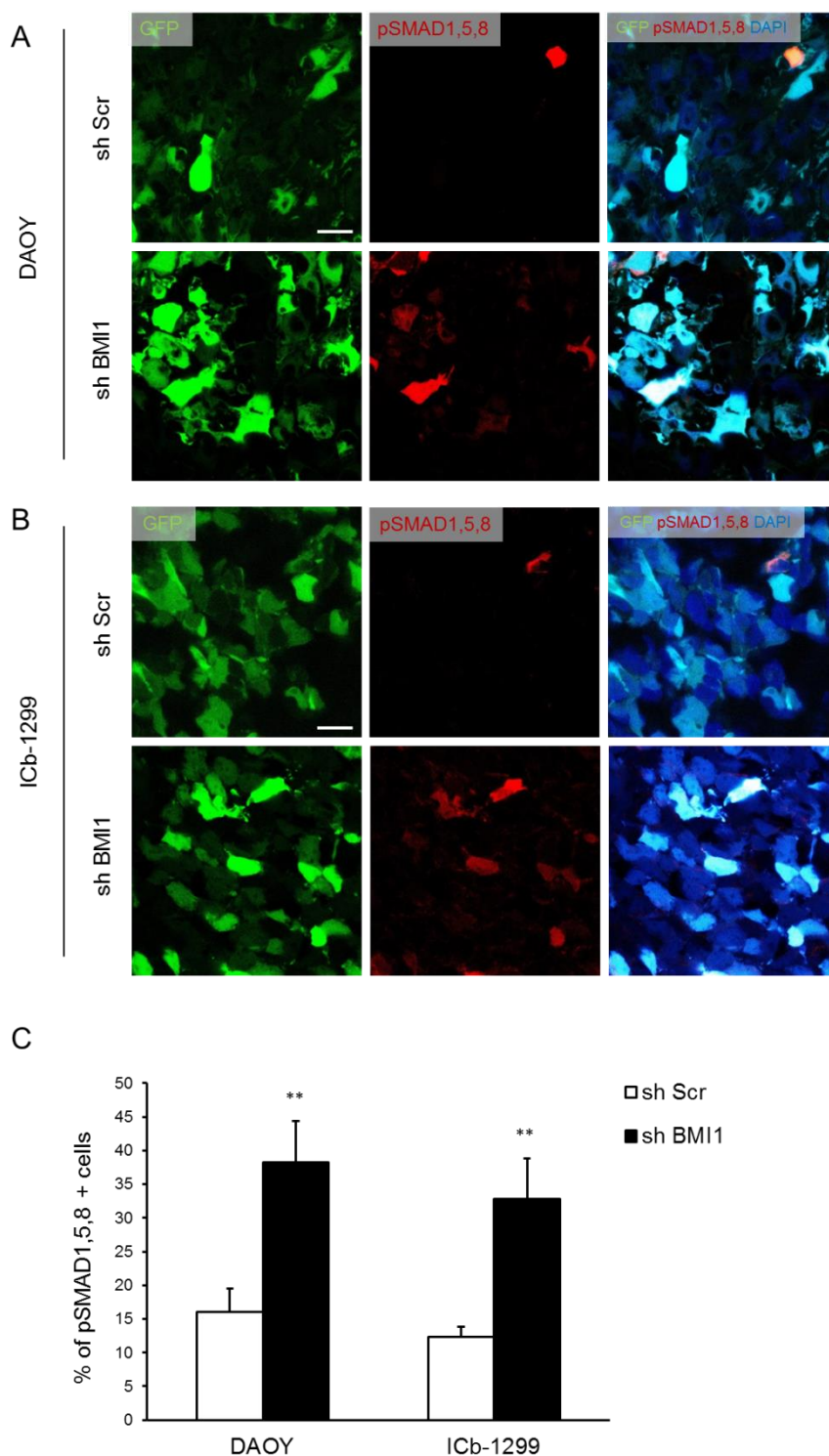
Fig. 6.5 pSMAD1,5,8 expression is increased in BMI1 silenced xenografts.
(A and B) pSMAD1,5,8 immunohistochemistry on xenografts reveals an increased expression in
shRNA BMI1 treated cells (lower panel) as compared to shRNA Scr treated cells (upper panel) in both
DAOY **(A)** and ICb-1299 **(B)**. Left – GFP (green) channel, middle – pSMAD1,5,8 (red) channel, right –
merge. **(C)** Quantitation of the number of pSMAD1,5,8 positive cells per field shows a significant
increase in the average percentage, in both DAOY and ICb-1299. Five fields in each sample and
three samples from each group were analysed. Scale bar in **(A)** and **(B)** = 10 μm. Error bars in **(C)**
represent SD (n=3). **, $p < 0.01$.

6.3.4 BMI1 silenced xenografts show reduced tumour volume estimates.

In line with other studies, we previously observed reduced proliferation in DAOY[BMI1kd] in comparison to DAOY[Scr] (Chapter 4, Fig 4.7). We also noted a reduced area of migration in DAOY[BMI1kd] and ICb-1299[BMI1kd] cells in organotypic cerebellar slice co-culture assay in comparison to their scrambled counterparts (Chapter 5, Fig 5.3). Here, we tested the effects of BMI1 knock down in these cells on the *in vivo* tumour growth by means of analysis of the tumour volume estimates of the xenografts. Briefly, representative sections of each xenograft were stained with DAPI and analysed using stereomicroscope (under fluorescence filter). The overlapping GFP positive tumour regions were grid-marked using Stereo Investigator software and the tumour volume was estimated using Cavalieri probe (Villeneuve, Tremblay et al. 2005; Ghulam Muhammad, Candolfi et al. 2009) after accounting for non-consecutive section interval and section thickness. The average tumour volume estimates (in mm^3) were compared between shRNA BMI1 silenced xenografts with scrambled controls for both ICb-1299 and DAOY groups. The statistical significance was calculated by student's *t test*.

The average total tumour volume estimates for DAOY[BMI1kd] (n=9) and ICb-1299[BMI1kd] (n=6) were reduced as compared to that of DAOY[Scr] (n=9) and ICb-1299[Scr] (n=6) xenografts respectively - 2.39 mm^3 (± 1.63) vs 5.18 mm^3 (± 2.57) for DAOY (p=0.009) [Fig. 6.6 C] and 3.35 mm^3 (± 1.05) vs 9.24 mm^3 (± 3.09) for ICb-1299 (p=0.001) [Fig 6.6 A-C].
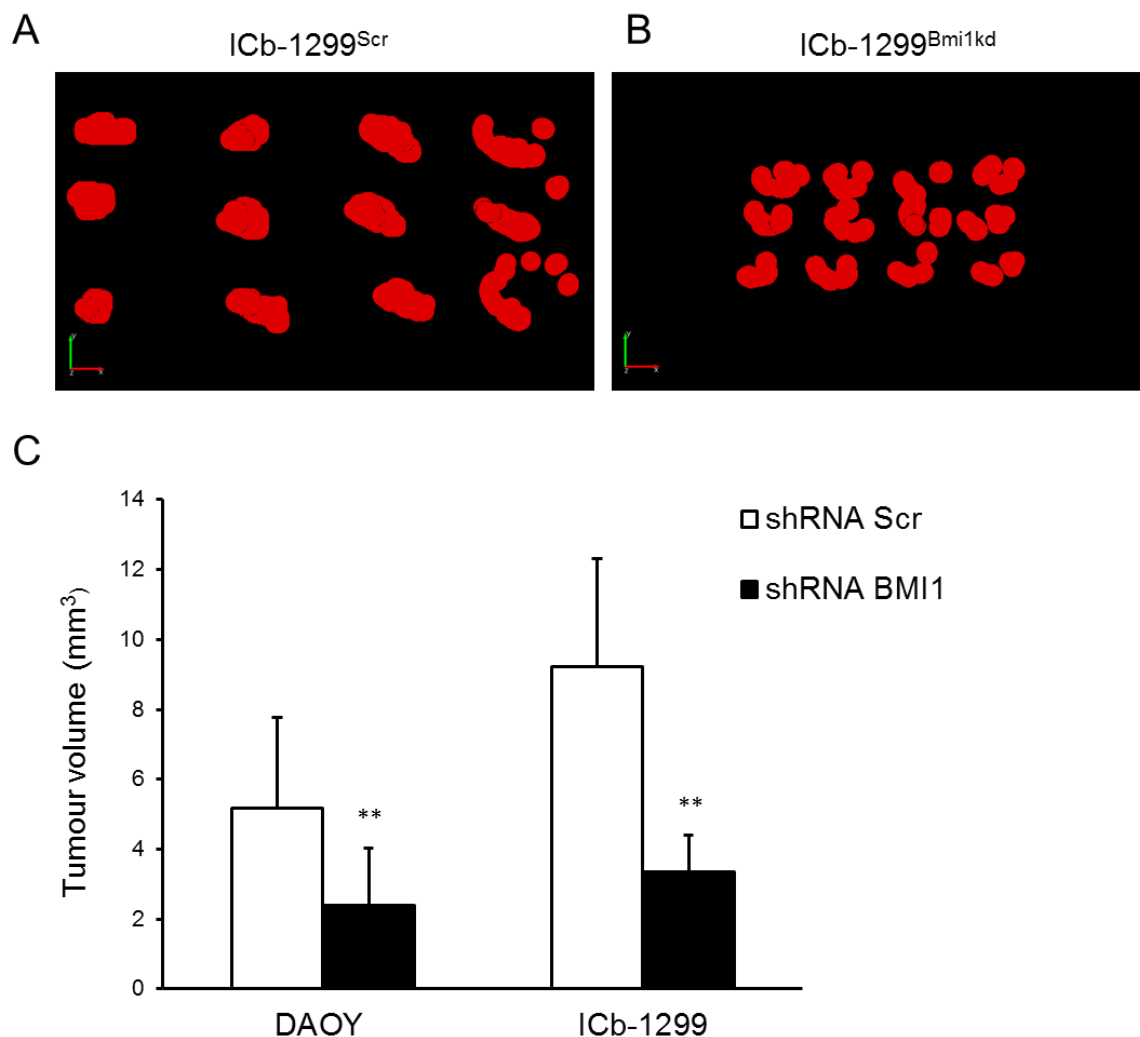
Fig. 6.6 Xenograft tumour volume estimates.

(A and B) A 2-D representation of tumour volume estimates using Cavalieri probe by Stereo Investigator software. The overlapping tumour areas marked during Stereomicroscopic evaluation are represented in red (20 μ grid spacing used).The total tumour volume was estimated after accounting for the non-consecutive section interval (which was constant at 12) and section thickness (which was constant at 20 μm). The total tumour volume estimate in xenograft arising from shRNA BMI1 treated cells **(B)** was lower than that of shRNA Scr treated cells **(A)**. **(C)** The average tumour volume estimate from all the xenografts analysed show a reduction in BMI1 knock down tumours as compared to controls, in both DAOY and ICb-1299. Error bars in **(C)** represent SD (n≥6). **, $p < 0.01$.

Although we cannot exclude that an effect of BMI1 knock down on BMP mediated

cell adhesion/migration/invasion could have contributed to the phenotype, the most

likely scenario is that it is mainly attributable to the BMI1 mediated impact on

proliferation. To further decipher the role of BMI1 in MB tumour cell invasion *in vivo*, we investigated the parenchymal invasion of the xenografts.

6.3.5 BMI1 silenced xenografts show reduced intraparenchymal tumour invasion

The extent of local (cerebellar) and brain stem invasion is prognostically highly significant (Chang, Housepian et al. 1969; Riffaud, Saikali et al. 2009; Sikkema, den Dunnen et al. 2012). In our study, we have previously observed reduced *in vitro* invasion of DAOY[BMI1kd] cells in a BMP dependent fashion (Chapter 4, Fig 4.5). We have also observed reduced distance of migration in DAOY[BMI1kd] and ICb-1299[BMI1kd] in an *ex vivo* experiment (Chapter 5, Fig 5.4). Wang et al. have demonstrated reduced *in vivo* tumour infiltration upon BMI1 knock down in DAOY cells grown as tumour spheres (Wang, Venugopal et al. 2012). Here we analysed our xenografts for cerebellar and brain stem invasion, at single cell level, taking advantage of the GFP labelling induced by lentiviral infection. Briefly, representative sections were stained with DAPI and examined by confocal microscopy. Three regions with intraparencymal (cerebellum or brain stem) invasion were imaged at 20X magnification. The images were analysed with ImageJ software and the maximum depth of invasion, which was the distance in μm from the pial surface to the farthest invading tumour cell was assessed. The measurements were averaged for each case and compared between shRNA BMI1 silenced and scrambled groups for both ICb-1299 and DAOY xenografts. The statistical significance was calculated by student's *t test*.

Interestingly, the average depth of invasion into the cerebellar parenchyma from the pial surface revealed a significant reduction for both DAOY[BMI1kd] and ICb-1299[BMI1kd] xenografts as compared to DAOY[Scr] and ICb-1299[Scr] respectively - 141.35 µm (± 51.51) vs 216.61 µm (± 61.24) for DAOY (p0.008) [Fig 6.7 B], and 159.74 µm (± 34.96) vs 239.49 µm (± 25.75) for ICb-1299 (p=0.001) [Fig. 6.7 A and B].
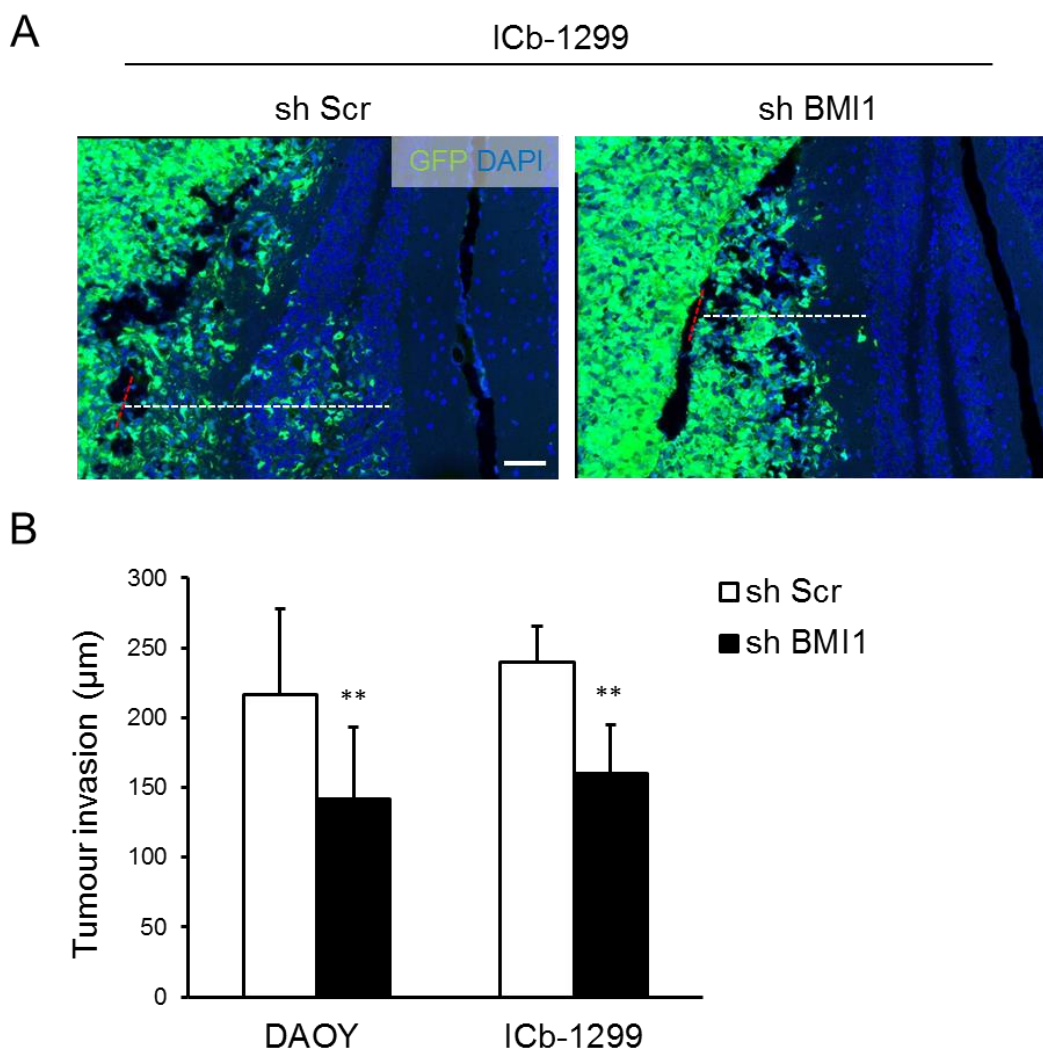
Fig. 6.7 Reduced cerebellar intraparenchymal infiltration in BMI1 silenced MB xenografts.

The depth of invasion (marked with white dotted line) was measured as the distance in µm from the pial surface of the cerebellum (marked with red dotted line) to the deepest GFP positive cell within the cerebellar parenchyma. **(A)** The maximum depth of tumour cell infiltration in xenograft arising from shRNA BMI1 treated cells (right) was lower than that of shRNA Scr treated cells (left). **(B)** The average distance of tumour cell infiltration from all the xenografts analysed show a reduction in BMI1

knock down tumours as compared to controls, in both DAOY and ICb-1299. Three different regions from each sample group were analysed. Scale bar in **(A)** = 50 µm. Error bars in **(B)** represent SD (n≥6). **, p<0.01.

Similar findings were also recorded when measuring the depth of tumour cell invasion into the brain stem – 401.78 µm (± 126.41) in DAOY[BMI1kd] vs 575.83 µm (± 175.91) in DAOY[Scr] (p=0.018) [Fig 6.8 B], and 332.78 µm (± 39.23) in ICb-1299[BMI1kd] vs 459.09 µm (± 62.06) in ICb-1299[Scr] (p=0.001) [Fig.6.8 A and B]. Additionally, there were more prominent necrotic areas noted in the brain stem as compared to the cerebellum in ICb-1299 xenografts, although this finding was not quantified. The infiltration of the tumour cells into the brain stem was deeper as compared to the cerebellum.
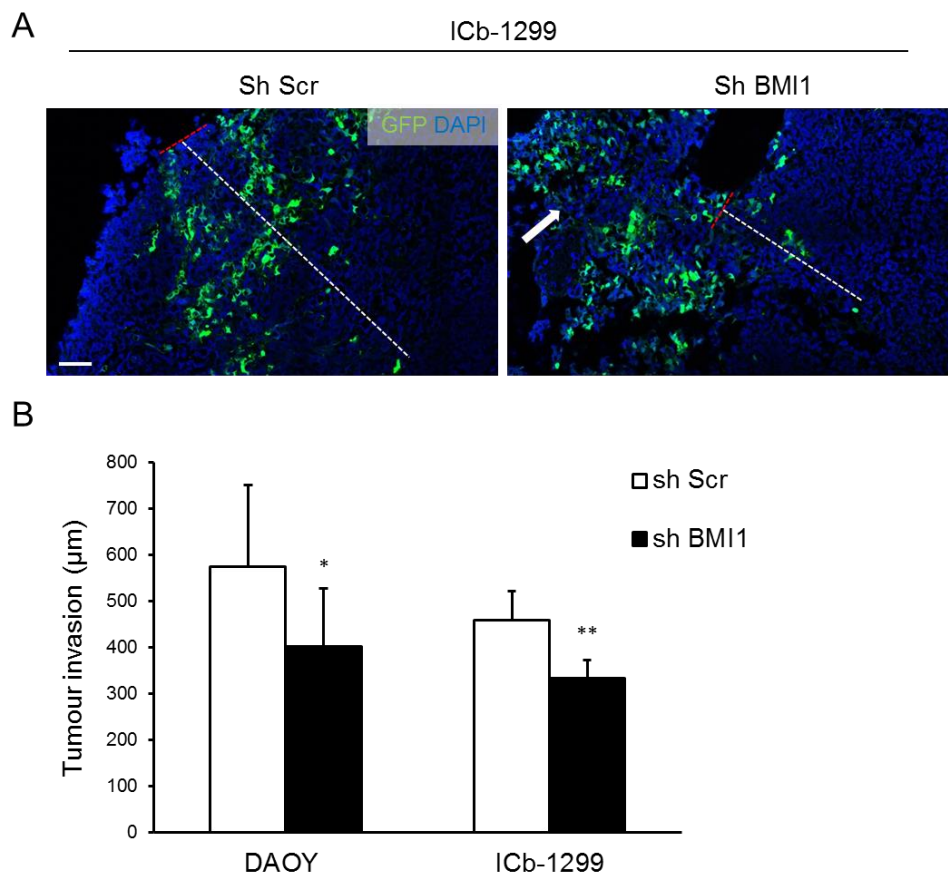
Fig. 6.8 Reduced brain stem intraparenchymal infiltration in BMI1 silenced MB xenografts.

The depth of invasion (marked with white dotted line) was measured as the distance in µm from the pial surface of the brain stem (marked with red dotted line) to the deepest GFP positive cell within the brain stem parenchyma. **(A)** The maximum depth of tumour cell infiltration in xenograft arising from shRNA BMI1 treated cells (right) was lower than that of shRNA Scr treated cells (left). The white arrow indicates tumour mass superficial to the brain stem pial surface. **(B)** The average distance of tumour cell infiltration from all the xenografts analysed show a reduction in BMI1 knock down tumours as compared to controls, in both DAOY and ICb-1299. Three different regions from each sample group were analysed. Scale bar in **(A)** = 50 µm. Error bars in **(B)** represent SD (n≥6). *, p<0.05; **, p<0.01.

In summary, reduced intraparenchymal invasion was observed in both DAOY[BMI1kd] and ICb-1299[BMI1kd] xenografts as compared to their control counterparts. These observations are in agreement with our *in vitro* results where reduced invasion was noted in a Transwell® assay in DAOY[BMI1kd] in comparison to DAOY[Scr].

6.3.6 BMI1 silenced xenografts show no change in the spreading along the Virchow Robin spaces or in the tumour burden in the spinal cord.

Primary CNS malignancies may also disseminate via certain minor routes such as subpial, perineuronal (satellitosis), intravascular and Virchow Robin spaces. Virchow Robin spaces are microscopic channels that follow along the arterioles which penetrate into the brain substance from the subarachnoid space (Patankar, Mitra et al. 2005). In addition to CSF and leptomeningel routes, medulloblastoma disseminate locally in the brain via Virchow Robin spaces (Roger E McLendon 2006). Therefore we chose to investigate spread along Virchow Robin space in our *in vivo* study. Similar to depth of invasion analysis described above, representative sections of each xenograft was stained with DAPI and examined by confocal microscopy. Three regions of tumour spread along the Virchow Robin spaces were imaged for each case. The maximum depth of spread in µm from the surface was measured in each region, averaged and compared between shRNA BMI1 silenced

and scrambled groups for both ICb-1299 and DAOY xenografts. The statistical

significance was calculated by student's *t test*.

There was no statistically significant differences noted in the average distance of

spreading along the Virchow Robin spaces between BMI1 knock down and

scrambled groups of xenografts - 448.80 μm (± 98.03) in DAOY^{BMI1kd} vs 553.95 μm

(± 231.05) in DAOY^{Scr} (p=0.126) [Fig 6.9 B], and 482.33 μm (± 56.46) in ICb-

1299^{BMI1kd} vs 481.04 μm (± 94.64) in ICb-1299^{Scr} (p=0.489) [Fig.6.9 A and B].
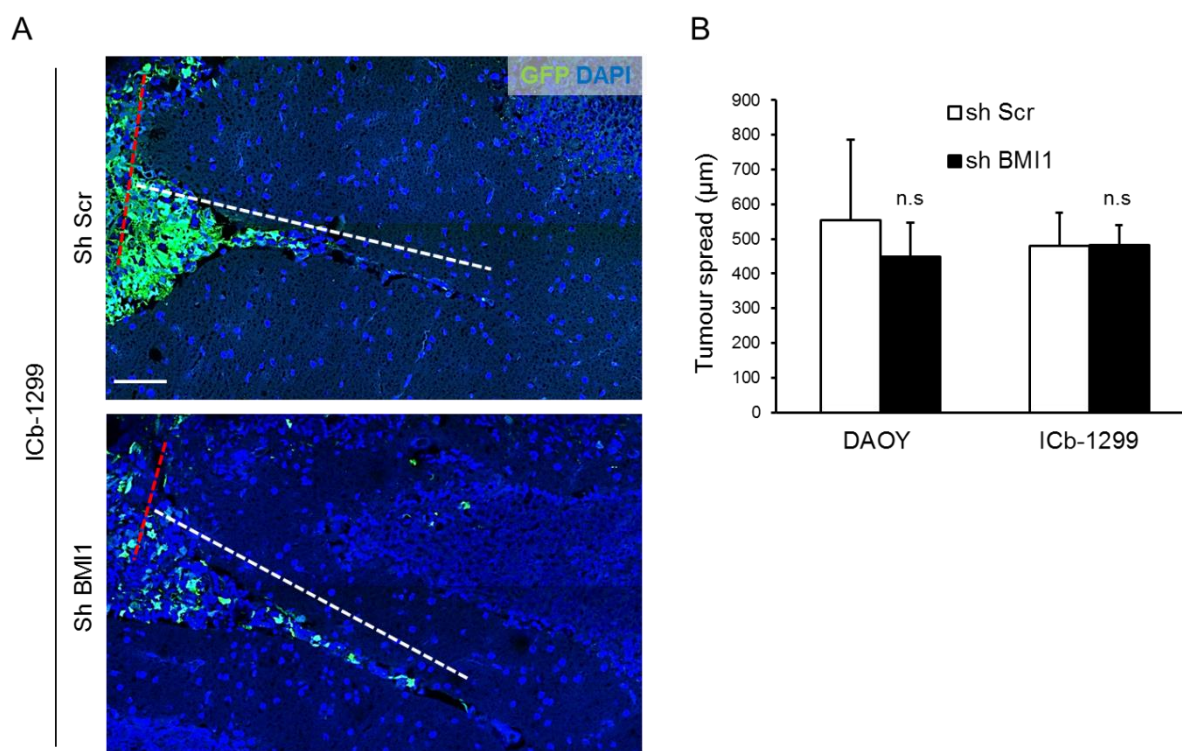
Fig. 6.9 There is no change in the spreading along Virchow-Robin space in BMI1 silenced MB xenografts.

The spread/migration (marked with white dotted line) of MB cell along the Virchow-Robin (VR) spaces (which are the channels along the arterioles) was measured as the distance in μm from the pial surface of the cerebellum/brain stem (marked with red dotted line) to the deepest GFP positive cell along the VR space. **(A)** There is no notable difference in maximum depth of tumour cell spread/migration along the VR space in xenograft arising from shRNA BMI1 treated cells (lower), compared to that of shRNA Scr treated cells (top). **(B)** The average distance of tumour cell spread/migration from all the xenografts analysed show no difference in BMI1 knock down tumours as compared to controls, in either DAOY or ICb-1299. Three different regions from each sample group were analysed. Scale bar in **(A)** = 50 μm. Error bars in **(B)** represent SD (n≥6).

Dissemination of medulloblastoma to the spinal cord via CSF and leptomeningeal remains paramount in determining tumour prognosis (Zeltzer, Boyett et al. 1999; Mumert, Dubuc et al. 2012). Even the presence of microscopic local leptomeningeal tumour spread has been suggested to bear prognostic significance in medulloblastoma (Ayan, Kebudi et al. 1997). Therefore, we determined the tumour burden in the spinal cord in the MB engrafted animals. The spinal cords were fixed in formalin, sectioned into multiple segments and examined histologically for any presence of tumour deposits. The rate of tumour positivity in shRNA BMI1 silenced transplants were compared with control transplants.

None of the twelve ICb-1299 xenografts had associated spinal deposits. However, microscopic MB tumour deposits (Fig 6.10 A), with features similar to those seen at the primary implantation site, were seen in approximately two third of DAOY transplanted cases. Importantly, there was no difference in the incidence or rate of tumour burden between DAOY[Scr] (6 of 9, 66%) and DAOY[BMI1kd] (6 of 9, 66%) transplants (Fig 6.10 B).

In conclusion, contrary to the intraparenchymal invasion results, BMI1 knock down did not seem to influence the spreading along the Virchow Robin spaces or the rate of spinal cord seeding in our xenograft model.
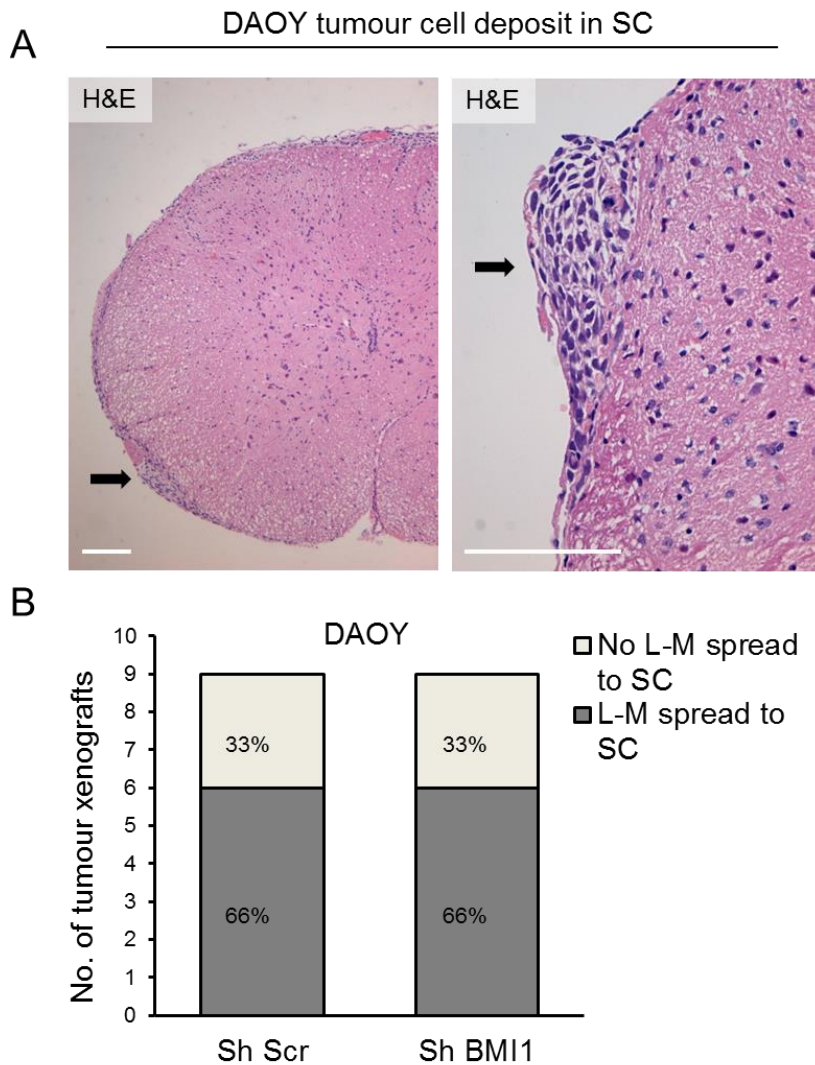
Fig. 6.10 Spinal cord tumour burden in DAOY xenografts.

(A) H&E section of spinal cord from DAOY engrafted animals showing leptomeningeal tumour deposit (black arrow) with histological features similar to that of the primary implant. Left – low power, right – high power image. **(B)** Quantitation of incidence of tumour burden between sh Scr and sh BMI1 treated DAOY transplants shows no difference. Abbreviation: L-M, leptomeningeal. Scale bar in (A) = 20 µm.

6.4 Discussion

In this part of the study we demonstrate that xenografts originating from BMI1 knock down MB cells are smaller and show reduced intraparenchymal invasion as compared to their scrambled counterpart. Increased pSMAD1,5,8 expression was

found also within BMI1 silenced xenografts. These observations suggest that i) BMI1 controls both tumour growth and parenchymal invasion in MB xenografts, although this may be achieved through different mechanisms and ii) confirms that BMI1 knock down in MB cells reactivates BMP signalling pathway also *in vivo,* consistent with our *in vitro* results.

Several genes and pathways are known which confer aggressiveness in medulloblastoma. Genetic profiling of metastatic medulloblastoma by Mumert et al. demonstrate that Shh-induced MBs tend to be localised, while ERAS, LHX1, and CCRK are metastasis-inducing which are overexpressed in aggressive subgroups of human MBs (Mumert, Dubuc et al. 2012). Expression profiling of metastatic and non-metastatic primary human MB by MacDonald et al. show several dysregulated genes associated with PDGFRA and RAS/MAPK signaling pathway (MacDonald, Brown et al. 2001). Furthermore, MB with molecular profiling of group 3 (mainly *MYC* amplification associated) and group 4 (mainly isochromosome 17q associated) are known to be more aggressive (higher metastasis and poorer prognosis) compared to Shh or Wnt groups (Kool, Korshunov et al. 2012; Taylor, Northcott et al. 2012).

In chapter 4, we discussed the differential expression of certain cell adhesion/ECM molecules that was observed in relation to BMI1 expression in developing granule neurones in mouse cerebella (Xinyu Zhang, unpublished data), and our current observation of dysregulated expression of CD44 and THSB in BMI1 knock down MB cells. In chapter 5, we identified deregulated cell adhesion/ECM genes namely LAMB1, EFEMP2, FBN2, SMC3, and THBS4 in relation to BMI1 expression in primary MB (Adrian Dubuc, Mark Remke; unpublished data). Impairment of the Cadherin family of transmembrane glycoproteins, in particular downregulation of E-cadherin, and switch from E-cadherin to N-cadherin, has a strong affiliation to EMT

and cancer invasiveness (Shiozaki, Oka et al. 1996). BMI1 overexpression has been shown to repress E-cadherin, and induce EMT (Yang, Hsu et al. 2010). Integrins are transmembrane glycoproteins, which are physiologically expressed. However certain cancers can be associated with high integrin expression, which could be a marker of aggressive phenotypes (Shirakihara, Kawasaki et al. 2013; Tome, Kimura et al. 2013). There is evidence that Bmi1 modulates integrin-mediated cell adhesion in murine neural stem cells in a novel Ink4a/Arf-independent manner (Bruggeman, Hulsman et al. 2009). TGF-β/BMP - SMAD pathways cross talk with other pathways which regulate cadherin and integrins and trigger EMT (reviewed in (Huber, Kraut et al. 2005; Thiery and Sleeman 2006)). Therefore it is plausible that changes in cell adhesion, cell motility and invasion phenotypes observed in response to BMI1 silencing of MB cells in our study can also be due to deregulation of cadherin or integrin family of proteins, probably mediated by BMP signalling. However this is speculative at this stage and would need validation. We plan to undertake a genome-wide analysis of Group 4 primary MB cells to understand the BMI1 associated molecular mechanisms more comprehensively (discussed in chapter 8).

In Wang et al. study, mice implanted with DAOY spheres with BMI1 knock down showed better survival, with corresponding tumours showing reduced local tumour infiltration as compared to controls, but they did not observe difference in tumour volumes between the two groups (Wang, Venugopal et al. 2012). Although, there was no difference in survival projection or tumour take between BMI1 knock down and control groups in our study, the difference in parenchymal invasion that we observed correlates to Wang et al. study. In line with our results, there is evidence

that xenografts generated from BMI1 knock down cells resulted in reduced tumour volume in various cancer including breast cancer (Hoenerhoff, Chu et al. 2009), pancreatic cancer (Yin, Wei et al. 2011) and laryngeal cancer (Yao, Wang et al. 2013). Interestingly we did not see increased spreading of MB cells along VR spaces in our xenograft model and tumours expressing high levels of BMI1 were not associated with higher incidence of spinal metastasis, therefore implying that the molecular mechanisms regulating intraparenchymal invasion and leptomeningeal spread may be different. In support of this, Wu et al. have shown that in both mouse and human medulloblastoma, metastatic tumour was genetically divergent from the matched primary tumour, suggesting that only certain cells from the primary tumour have the ability to metastasise (Wu, Northcott et al. 2012).

In order to validate the phenotypes observed upon BMI1 knock down in our study, we set out to investigate if an inverse relationship between BMI1 expression and BMP pathway activation exists in the primary human MB tissue. To do this, we studied the expression pattern of BMI1 and pSMAD1,5,8 in primary human MB tissue micro array.

CHAPTER 7 Preliminary pSMAD expression analysis in primary MB tissue demonstrate weak correlations warranting further evaluation

7.1 Introduction

Medulloblastoma develops as a result of deregulated developmental mechanisms, and in the context of cerebellar development, BMI1 is thought to be a downstream target of SHH pathway (reviewed in (Marino 2005)). Shh and BMP pathways antagonise each other to regulate granule cell progenitor proliferation during cerebellar development (reviewed in (Rodini, Suzuki et al. 2010; Roussel and Hatten 2011). Our group have recently demonstrated that during cerebellar development Bmi1 critically influences cell-cell interactions via specific inhibition of BMP signalling (Zhang, Santuccione et al. 2011). However, to our knowledge there is no previous literature linking BMI1 and BMP signalling to medulloblastoma pathogenesis. BMPs (BMP-2 and/or BMP-4) have been shown to prevent cerebellar granule cell precursor cell (putative cell of origin for MB) proliferation (Rios, Alvarez-Rodriguez et al. 2004) and shown to have inhibitory role in medulloblastoma growth (Hallahan, Pritchard et al. 2003; Zhao, Ayrault et al. 2008). Therefore BMPs may be potential therapeutic targets for MB treatment, and furthermore, BMI1 expression could be potential biomarker for those MB which may benefit from small molecule BMP agonist treatment. With this in view we attempted to validate the notion that BMI1 represses BMP pathway, i.e., an inverse relationship existed between BMI1 and BMP pathway status, using primary human MB tissue samples

Tissue Micro Arrays (TMAs) are arrays of several different tissue samples represented as cylindrical cores on a single slide which enable rapid and simultaneous immunohistochemical analysis of multiple samples. They were first

described in 1987 (Wan, Fortuna et al. 1987) and popularised as high throughput method for molecular analysis in 1998 (Kononen, Bubendorf et al. 1998). We have taken advantage of two TMAs containing a total of 362 MB samples to conduct preliminary expression correlation analysis following immunohistochemistry for BMI1 and pSMAD1,5,8 to test the feasibility of their use to validate our findings in MB cells.

7.2 Experimental Design and methodology

7.2.1 Primary human medulloblastoma TMA

For validation on human primary MB tissue, we used two different TMA sets. The first TMA set (referred to as TMA I) comprised one slide containing 64 MB tumour cores which was prepared at Institute of Clinical Pathology, Department of Pathology, University of Zürich, Switzerland. The second set (referred to as TMA II) comprised two slides containing a total of 298 MB tumour cores which was prepared by our collaborator Dr Stefan Pfister from German Cancer Research Centre DKFZ, Heidelberg, Germany. Supplementary information available with TMAs included histological types for the former set and molecular subgroups for the latter set. Immunohistochemistry using pSMAD1,5,8 and/or BMI1 antibody was performed on the paraffin sections of the TMAs as described in M&M (chapter 2, section 2.10). The primary and secondary antibodies used along with the staining conditions are listed in Table 7.1.

Table 7.1 Antibodies and the conditions used for TMA immunohistochemistry by ABC method

For antigen to be detected	Primary antibody used	Secondary antibody used	Blocking agent used
BMI1	Rabbit polyclonal anti-Bmi1 (Abcam ab38295), 1:100, overnight incubation at RT.	Universal biotinylated anti-mouse/anti-rabbit IgG (Vector) raised from horse, 1 hr at RT.	2.5% Normal horse serum (Vector), 1 hr RT
pSMAD1,5,8	Rabbit polyclonal anti-phosphoSmad1/5/8 (Millipore AB3848), 1:100, overnight incubation at RT.		

7.2.2 Assessment and analysis of expression

The protein expression was assessed by myself and Prof. Marino with >90% concordance. The expression pattern was scored as 0 = negative, 1 = mildly positive, 2 = strongly positive for both markers (Fig 7.1). In addition, for BMI1 staining the positive scores were suffixed with 'f' of 'd' corresponding to focal or diffuse staining pattern respectively (Fig 7.1 B,C). There was no focal/diffuse criteria for pSMAD1,5,8 as the tumour either stained diffusely for this marker or not at all (Fig 7.1 D,E,F).

Non-parametric correlation analysis was carried out on the immunohistochemical assessment data using SPSS® statistical package version 20 (IBM®). Spearman correlation (Spearman rank correlation) coefficient (de Siqueira Santos, Takahashi et al. 2013) was computed to identify significant association between the two biomarkers or between the biomarker and the molecular subgroup. A coefficient value of 0.2 or more was considered as an indicator of strong correlation (McDonnell, Chari et al. 2008), and $p<0.05$ was considered as statistically significant. Coefficient value with a minus sign is indicative of an inverse or negative correlation, and that with at plus sign is indicative of a positive or direct correlation.

7.3 Results

7.3.1 There is a weak inverse correlation between BMI1 and pSMAD1,5,8 expression in MBs.

First we examined the TMA I set, containing 64 MBs. TMA I was treated with both

pSMAD1,5,8 and BMI1 antibodies. An expression score was assigned to each

tumour contained within the TMAs as described above (section 7.2.2) [Fig 7.1]. .
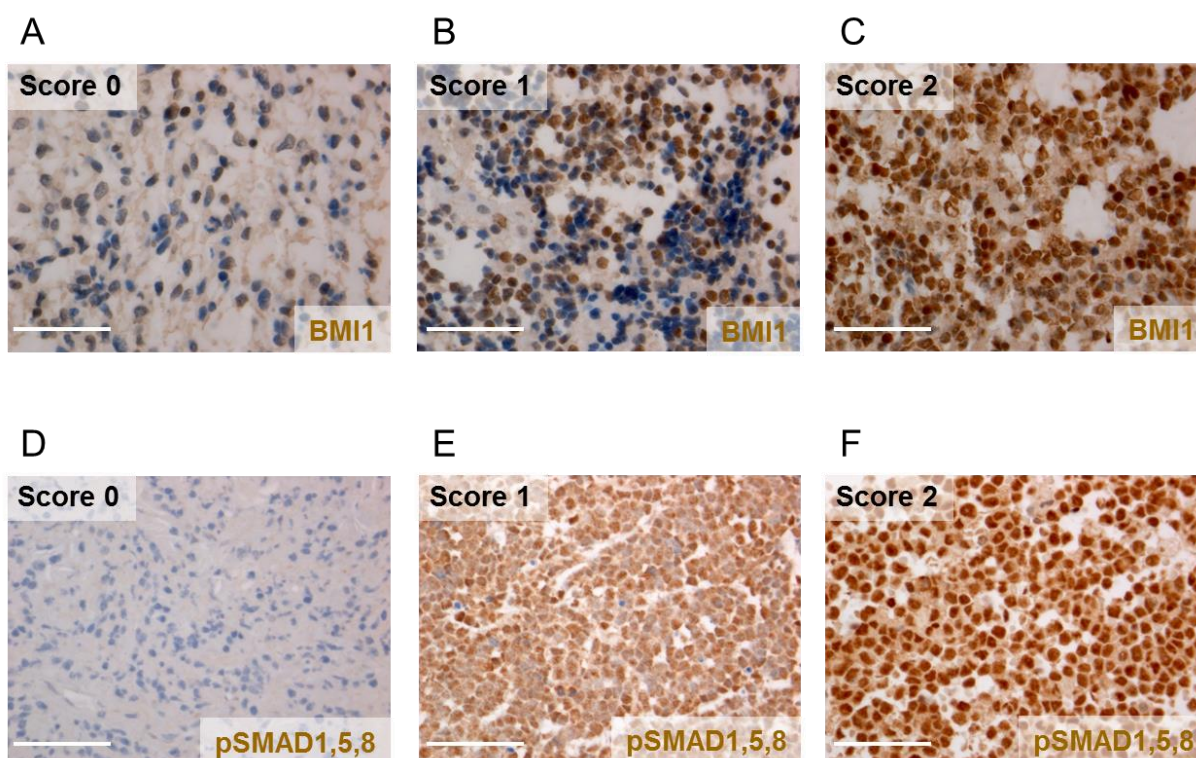
Fig. 7.1 Immunohistochemistry scoring of Tissue Micro Array.

(A-C) Representative sections of primary human medulloblastoma tumour samples showing variable intensity of BMI1 (nuclear) staining, where score 0 = negative, 1 = mild and 2 = strong expression. BMI1 expression was in addition further classified as focal 'f' **(B)** or diffuse'd' **(C)** depending on the extent of staining observed. **(D-F)** Representative sections of primary human medulloblastoma tumour samples showing variable intensity of pSMAD1,5,8 staining (predominantly nuclear). All pSMAD1,5,8 positive cases showed diffuse staining pattern. Scale bar in all = 10μm.

Expression correlation analysis was performed using SPSS statistical package. The expression analysis data were cross tabulated and Spearman correlation co-efficient value was generated.

Analysis of correlation between BMI1 and pSMAD1,5,8 expression among tumours of TMA I subset showed a weak negative (indirect) correlation score of -0.038 with no statistical significance (p=0.764, n=64) [Fig 7.2].

A

Spearman Correlation value **-0.038, P=0.764**
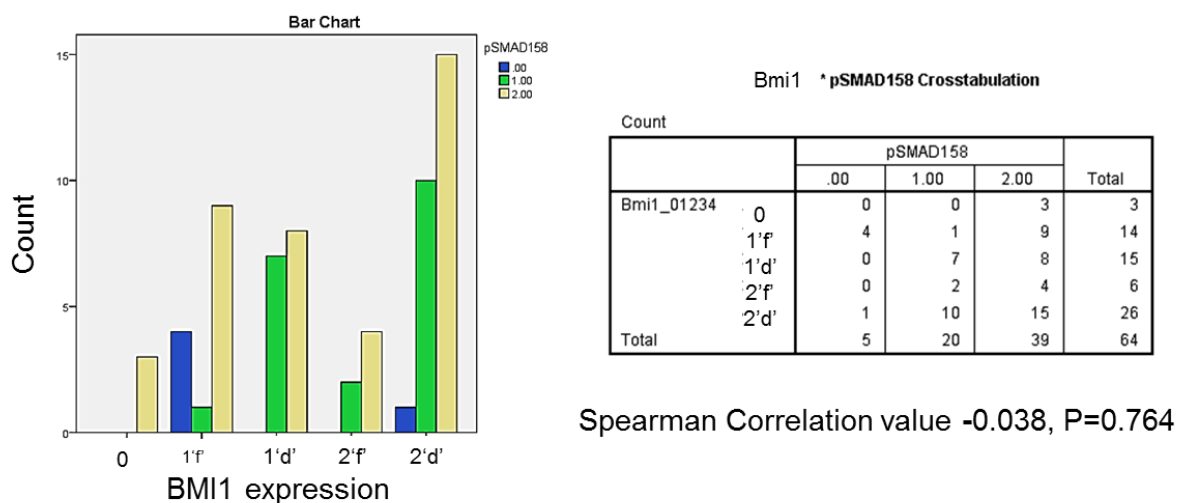
Fig. 7.2 Correlation analysis of BMI1 and pSMAD1,5,8 expression in TMA I.

(A) There is a trend of negative expression correlation between BMI1 and pSMAD1,5,8 expression. But the correlation in this small cohort is weak and has no statistical significance. Bar graph on the left showing case distribution according to their expression scores, with breakdown of the cases in the table on the right.

The trend of negative or indirect correlation observed in this small cohort analysed could be in keeping with our findings on the cell lines where we observe an inverse relationship between BMI1 expression and pSMAD1,5,8 expression in two MB cell lines and primary MB cells of Group 4. However it is necessary that the power of the study is strengthened by increasing the number of tumour cases. We plan to achieve this by analyzing BMI1 expression from TMA II subset, further adding 298 cases. We

will obtain BMI1 expression data for TMA II set from our collaborators and further validate them with immunohistochemistry.

While we are in the process of obtaining BMI1 expression data on TMA II, we performed an interim correlation analysis on TMA II dataset, comparing pSMAD1,5,8 expression with MB Groups.

7.3.2 There is a significant correlation of pSMAD1,5,8 expression in certain subgroups of MB.

Here TMA II set, with 298 MB tumours were used for immunohistochemical analysis using pSMAD1,5,8 only. The pSMAD1,5,8 expression (indicating an activated BMP signalling pathway) analysis between Group 4 and non-Group 4, had a significant positive or direct correlation between Group 4 and non-Group 4 MBs (correlation coefficient of + 0.169, p=0.037, n=152) [Fig 7.3 A]. This means that among the 152 inclusion cases (tissue cores with measurable immunohistochemical staining) analysed, Group 4 MBs were likely to have higher expression of pSMAD1,5,8 as compared to non-Group 4 MBs. This relationship is contrary to observation from our current in vitro/in vivo study, where we see a low pSMAD1,5,8 expression in Group 4 primary cells, which was increased upon BMI1 knock down. However correlation of these results with data on the expression of BMI1 is essential to draw any firm conclusion.

There was a significant negative (indirect) pSMAD1,5,8 expression correlation among Group WNT as compared to non-Group WNT cases (correlation coefficient - 0.185, p=0.023, n=152) [Fig 7.3 B]. This means that among the 152 inclusion cases analysed, WNT Group cases were likely to have lower or no pSMAD1,5,8 expression as compared to non-WNT Group cases. However, there was no significant

pSMAD1,5,8 expression correlation among Group SHH vs non-Group SHH and Group C vs non-Group C cases.

A

Group_D * pSMAD158 Crosstabulation

Count

		pSMAD158			Total
		.00	1.00	2.00	
Group_D	.00	16	33	36	85
	1.00	11	14	42	67
Total		27	47	78	152

Spearman Correlation value +0.169, **P=0.037**

B

Group_WNT * pSMAD158 Crosstabulation

Count

		pSMAD158			Total
		.00	1.00	2.00	
Group_WNT	.00	23	43	76	142
	1.00	4	4	2	10
Total		27	47	78	152

Spearman Correlation value -0.185, **P=0.023**
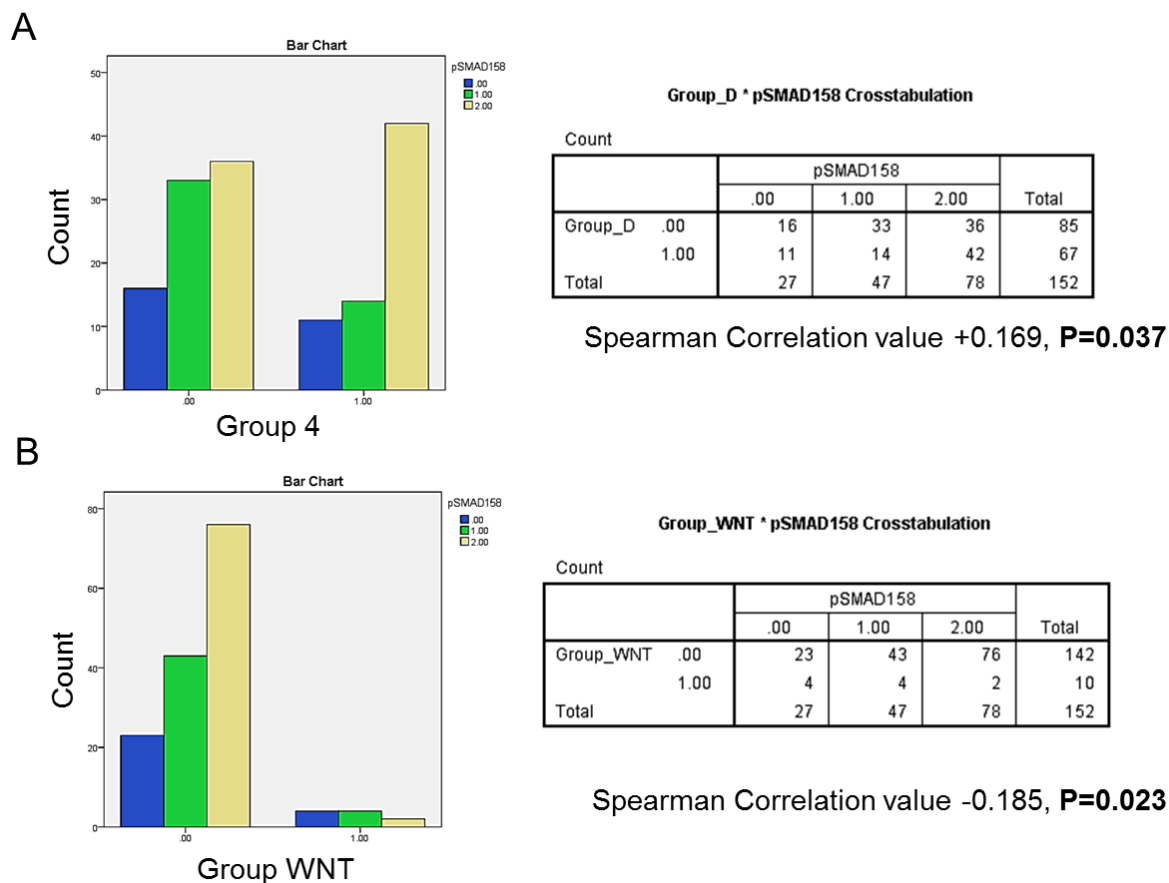
Fig. 7.3 Correlation analysis of pSMAD1,5,8 expression and MB subgroups in TMA II.

(A) pSMAD1,5,8 expression correlation between Group 4 vs non-Group 4 cases, showing a positive correlation. **(B)** pSMAD1,5,8 expression correlation between Group WNT vs non-Group WNT cases, showing a significant negative correlation. The bar graphs on the left show case distribution according to their expression scores or Group distribution. Group distribution is on X-axis, where, 1 = cases belonging to that Group, 0 = cases from other Groups. The tables on the right contain the breakdown of number of cases. For pSMAD1, 5,8, 0 = negative, 1 = mild positive, 2 = strong positive staining. p<0.05 was considered as statistically significant.

7.3.2 There is a significant direct correlation of pSMAD2 expression in MB Group SHH.

The SMAD2 and SMAD3 proteins are activated by a closely related, but different leg of the TGF-β pathway, induced by TGF-β1, and phosphorylation of SMAD2 and

SMAD3 are a reliable indicator of activation of TGF-β signalling pathway (Nakao, Imamura et al. 1997). SMAD2 and SMAD3 are phosphorylated via TGF-β (TβRI) and activin (ActRIB) receptors, whereas SMAD1, SMAD5 and SMAD8 are activated by BMP (ALK-1, ALK-2, BMP-RIA/ALK-3 and BMP-RIB/ALK-6) receptors in response to BMP ligands (Derynck and Zhang 2003). Nevertheless, both phosphorylated pSMAD2,3 and pSMAD1,5,8 have a common downstream target, SMAD4, where phosphorylated pSMAD4 translocate into the nucleus and regulates transcription (chapter 1, Fig 1.7). This convergence of pathways on SMAD4 caught our interest, and therefore we analysed the expression pattern of already known pSMAD2 in TMA II set.

First, comparison of pSMAD2 staining scores with pSMAD1,5,8 scores was done, which showed a significant positive (direct) correlation (correlation coefficient of +0.187, p=0.026, n=142) [Fig 7.4 A]. This means that activation of TGF-β pathway and closely related BMP pathway are directly related in the MB cases analysed across all the subgroups.

The expression pattern of pSMAD2 was further analysed in different MB subgroups. There was a significant positive (direct) pSMAD2 expression correlation among Group SHH vs non-Group SHH cases (correlation value of +0.292, p<0.001, n = 272) [Fig 7.4 B]. This means that the Group SHH MBs are more likely to have TGF-β pathway activation in comparison to non-SHH MBs. There was no significant pSMAD2 expression correlation among Group WNT vs non-Group WNT, Group C vs non-Group C or Group D vs non-Group D cases.

A
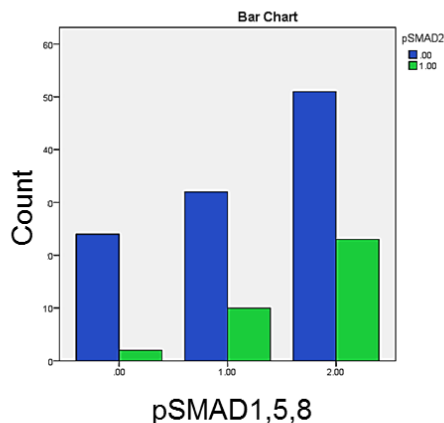
pSMAD158 * pSMAD2 Crosstabulation

Count

		pSMAD2		
		.00	1.00	Total
pSMAD158	.00	24	2	26
	1.00	32	10	42
	2.00	51	23	74
Total		107	35	142

Spearman Correlation value +0.187, **P=0.026**

B
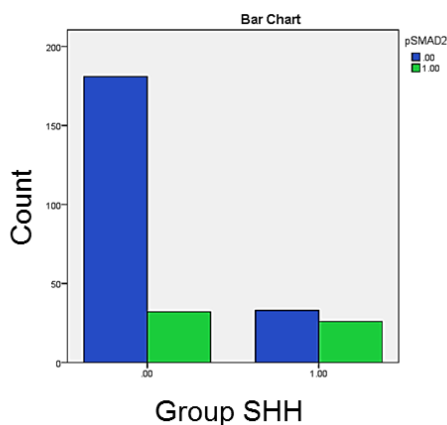
Group_SHH * pSMAD2 Crosstabulation

Count

		pSMAD2		
		.00	1.00	Total
Group_SHH	.00	181	32	213
	1.00	33	26	59
Total		214	58	272

Spearman Correlation value +0.292, **P<0.001**

Fig. 7.4 Correlation analysis of pSMAD2 expression and MB subgroups in TMA II

(A) Expression correlation between pSMAD1,5,8 vs pSMAD2, showing a significant positive correlation among the 142 cases included. **(B)** pSMAD2 expression correlation between Group SHH vs non-Group SHH cases, showing a significant positive correlation. The bar graphs on the left show case distribution according to their expression scores or Group distribution. Expression score distribution is on X-axis in **(A)**. In **(B)**, the X-axis has the Group distribution, where 1 = cases belonging to that Group, 0 = cases from other Groups. The tables on the right contain the breakdown of number of cases. For pSMAD2, 0 = negative, 1 = positive staining. For pSMAD1, 5,8, 0 = negative, 1 = mild positive, 2 = strong positive staining. p<0.05 was considered as statistically significant.

7.4 Discussion

Here we observed a trend of inverse correlation between BMI1 and pSMAD1,5,8 expression in TMA I (n=64), but the correlation was not statistically significant. However we are keen to further analyse this expression pattern also in TMA II (n = 298) thereby increasing the power of the study.

BMI1 expression is reported to be expressed across all molecular subgroups of MB, but its expression is shown to be enriched in non-SHH/non-WNT groups, particularly in Group 4 MBs (Behesti, Bhagat et al. 2013). In this current study we detected an increased BMI1 in the primary cells of Group 4, with a low pSMAD1,5,8 expression. Upon BMI1 knock down these cells showed an increased pSMAD1,5,8 expression indicative of derepression of BMP pathway (chapter 3, section 3.3.3, Fig 3.6). These findings made us curious to study the pSMAD1,5,8 expression pattern in different subgroups (subgroups specification was already known) of primary human MBs. We observed a positive (direct) pSMAD1,5,8 expression correlation in Group 4 as compared to non-Group 4 MBs. But we felt that the correlation value is too weak (correlation coefficient of +0.169, p=0.037) to confidently interpret these results. A strong correlation is indicated with correlation coefficient is ≥0.2. Similar analysis with other subgroups showed no significant correlation for Group SHH vs non-Group SHH or Group 3 vs non-Group 3, but a negative correlation in Group WNT vs non-Group WNT MBs (correlation coefficient -0.185, p=0.023). Again this correlation was rather weak. Therefore we felt that there is a need to analyse more primary cases to establish a better pSMAD1,5,8 expression correlation in different subgroups, in particular that of Group 4, which would be of relevance to our current study. To this end, we are currently optimising conditions to stain TMA I with KCNA1 antibody,

which has been suggested as a marker of Group 4 (Northcott, Korshunov et al. 2011).

Similar to BMPs, members of the TGF-β signalling pathway, including SMAD2/3 have been shown regulate EMT differently in different physiological conditions and in different cancers (reviewed in (Zavadil and Bottinger 2005; Leivonen and Kahari 2007)). This complex role of TGF-β signalling in cancer invasion and metastasis is exemplified by its dual role reported in pathogenesis of certain cancers such as breast carcinoma (Kang, Siegel et al. 2003; Deckers, van Dinther et al. 2006). Here we observed a weak but positive or direct correlation between pSMAD2 (TGF-β1 induced) and pSMAD1,5,8 expression (BMP induced) [correlation coefficient of +0.187, p=0.026, n=142]. This is in keeping with a study where both pSMAD2 and pSMAD1,5,8 are shown to be expressed or repressed in the same direction in primary breast cancer tissue (Katsuno, Hanyu et al. 2008), but analysis of higher number of cases is indicated to confirm this. However, interestingly, a strong positive correlation (correlation coefficient of +0.292) with high statistical significance (p<0.001) was noted for pSMAD2 expression in Group SHH as compared to non-Group SHH. Evidently larger number of inclusion cases (n=272) makes this association stronger. This reiterates the need to include further cases and to re-analyse expression correlation between BMI1 and pSMAD1,5,8 in order to validate our current findings in primary MB tumour samples. It would be certainly interesting to further investigate pSMAD2-Group SHH and pSMAD2-pSMAD1,5,8 connection we have observed. But prior to embarking on SMAD2/TGF-β pathway, we would like to focus on BMP pathway, which is more relevant to our current project

The future plan for TMA analysis is to obtain BMI1 expression data for TMA II which would enable us to add them to the data obtained with TMA I to increase the power of the study. Depending on the initial results, we will then extend the study to investigate the expression of other relevant cell adhesion/ECM markers such as CD44, THSB and MMP 10 which would help us validate the differential expression of these genes/molecules noted in murine GCPs of developing cerebella and in the human MB cell line, in relation to Bmi1 expression, as described in chapter 4.

CHAPTER 8 Discussion

8.1 Summary of principal findings

In this study we have demonstrated a novel connection between the Polycomb gene *BMI1* and the BMP pathway in the pathogenesis of human MB. BMI1 represses BMP signalling pathway, as assessed by increased phosphorylation of SMAD1,5,8 proteins, indicative of derepression of the BMP pathway, upon BMI1 knock down in MB cell lines and in primary MB cells of Group 4. We have shown that BMI1 controls MB cell adhesion, cell migration and invasion in a BMP dependent manner *in vitro*. The effects of BMI1 on MB cell migration and invasion was observed also in an *ex vivo* assay. Using an *in vivo* xenograft model of primary Group 4 MB cells we have demonstrated that BMI1 controls parenchymal invasion. Furthermore, we observed that BMP-4 treatment reduced *in vitro* invasion in a MB cell line, in a similar fashion as seen upon BMI1 downregulation.

Our preliminary findings on primary human MB tumours shows a trend toward an inverse correlation between BMI1 expression and pSMAD1,5,8 in keeping with our findings on the cell lines and the primary MB cells, although further validation with more cases will be required to enhance statistical power and validate these results.

In summary, the data so far raise the possibility that expression of BMI1 could represent a biomarker for MB which could benefit from treatment with small molecules acting as BMP agonists.

8.2 Discussion and outlook

MB is the commonest intracranial paediatric malignancy and despite advances in treatment, it is still associated with high mortality and serious treatment related morbidities (Polkinghorn and Tarbell 2007). With the advent of integrated genomics platforms to classify MBs into molecular subgroups, our understanding of the pathogenesis and basic biology of these tumours has advanced in recent years (Kool, Koster et al. 2008; Cho, Tsherniak et al. 2011; Northcott, Korshunov et al. 2011). Patient risk stratification is evolving to include a combination of clinico-pathological and molecular factors that reflect the clinical relevance (Ellison 2010). However further understanding of the molecular pathogenesis involved in this heterogeneous disease is needed to be able to effectively risk-stratify the patients and to develop targeted individualised therapy, thereby avoiding undesirable side effects. In this study we explore the role of the Polycomb gene BMI1 in MB cell invasion and its connection to the BMP signalling pathway.

The best characterised role of BMI1 in human cancers is related to the regulation of cell proliferation and senescence via suppression of p16Ink4a/p19Arf cell cycle inhibition pathways (Jacobs, Kieboom et al. 1999; Jacobs, Scheijen et al. 1999; Meng, Luo et al. 2010) which in turn regulates the activity of cyclin D, Cdk4/Cdk6 and p53 (reviewed in (Kim and Sharpless 2006)). BMI1 is overexpressed in a significant proportion of human MB and its best characterised role is a pro-proliferative one in the context of SHH driven tumorigenesis (Leung, Lingbeek et al. 2004; Michael, Westerman et al. 2008). However, recently our team have reported that Bmi1 regulates cell adhesion and migration of cerebellar progenitors through repression of the BMP pathway (Zhang, Santuccione et al. 2011). In this study we

demonstrate that BMI1 represses BMP pathway in human MB cells, and in fact BMI1 knock down caused an aberrant activation of BMP pathway. These findings are in keeping with the study of Bracken and co-authors in which they show by gene expression profiling of human embryonic fibroblasts in combination with ChIP-on-chip experiments, that BMPs are direct targets of BMI1 (Bracken, Dietrich et al. 2006). Similarly, by combining ChIP-seq with *in vivo* RNAi screening, Gargiulo et al. have demonstrated a role for Bmi1 in adult neural progenitor and glioma cells via transcriptional repression of genes responsive to TGF-β/BMP signalling pathway, such as Atf3 (activating transcription factor 3), highlighting p16INK4a/p19ARF-independent functions for BMI1 in development and cancer (Gargiulo, Cesaroni et al. 2013).

BMPs are members of the TGF-β family of proteins, and their role during cerebellar development and in MB pathogenesis is well characterized [reviewed in (Behesti and Marino 2009)]. BMPs are known to antagonize Shh-dependent proliferation and induce differentiation of GNPs (Zhao, Ayrault et al. 2008). BMP-mediated regulation of cell adhesion and of the cellular interactions with the extracellular matrix have been demonstrated also in soft tissues (Wang, Kim et al. 2012). Here, we show that BMI1 controls tumour volume and intraparenchymal invasion in an orthotopic xenograft model of MB, and that BMI1 silencing causes a reduced *in vivo* pSMAD1,5,8 expression indicative of BMP pathway activation. While the reduced tumour volume observed in BMI1-silenced cells is in keeping with previous reports where reduced tumour growth was seen in subcutaneous DAOY xenografts upon shRNA BMI1 knock down (Wiederschain, Chen et al. 2007), the effect on brain invasion is novel. Our data together with the results of the *in vitro* migration assays which show that cell adhesion and motility are controlled by BMI1 through BMP

pathway inhibition raise the possibility that this mechanism also underpins the *in vivo* phenotype. We observed reduced individual cell motility among DAOY[BMI1kd], hence supporting the notion that BMI1 influences cell invasion phenotype (those observed *in vitro* and *in vivo*), independent to its effects on cell proliferation.

Reanalysis of a previously published dataset of DAOY[BMI1kd] (Wiederschain, Chen et al. 2007), revealed deregulation of TGF-β pathway and differential expression of several cell adhesion molecules such as Integrins, Laminins, Collagens, Thrombospondin and CD44 (analysis done by Adrian Dubuc and Mark Remke from Michael Taylor group, unpublished data). Several of these genes either represented the human homologue of the genes identified in Bmi1-/- granule cell progenitors in a BMP dependent fashion (experiments performed by Xinyu Zhang, Marino Lab) or belong to the same protein family. Furthermore, differential expression of Thrombosponin1/2 and CD44 was seen in this study in BMI1 silenced MB cell lines D-458.

Expression of BMI1 is enriched preferentially in Group 4 human MB and overexpression of Bmi1 in the granule cell lineage in the mouse induces MB, albeit, only in the context of p53 deletion (Behesti, Bhagat et al. 2013). A biostatistical analysis of human Group 4 MB overexpressing BMI1 while concomitantly expressing low levels of p53 revealed a set of differentially expressed genes, which affected extracellular matrix structural constituents (Adrian Dubuc and Mark Remke, unpublished data). Among these genes, again members of the Thrombospondin and Laminin families were detected. Thrombospondins are strongly expressed in postmitotic premigratory GNPs (O'Shea, Liu et al. 1990) where they bind to Integrins, which are involved in the control of GNPs proliferation in cooperation with SHH, as shown in mice lacking Integrin β1 (Blaess, Graus-Porta et al. 2004). Interestingly

type IV collagens induce expression of Thrombospondins and the role of these matrix proteins in regulation of differentiation of CNS progenitors has been demonstrated (Lu and Kipnis 2010). Members of both the Thrombospondin and (Zhou, Picard et al. 2010) and collagen families (Pomeroy, Tamayo et al. 2002) are deregulated in human MB with an aggressive phenotype. Together these data raise the possibility that invasion of MB cells is regulated by BMI1 through BMP-mediated control of cell adhesion. Interestingly we did not see increased spreading of MB cells along VR spaces in our xenograft model and tumours expressing high levels of BMI1 were not associated with higher incidence of spinal deposits, therefore implying that the molecular mechanisms regulating intraparenchymal invasion and leptomeningeal spread may be different

In keeping with the published literature (Wiederschain, Chen et al. 2007; Wang, Venugopal et al. 2012), we observed a decreased proliferation of DAOY cells in a BMP pathway-independent fashion *in vitro*, which is likely to contribute to the reduced tumour volume observed in our xenografts of DAOY[BMI1kd] cells. Insulin like growth factor I receptor (IGF-IR) and members of TAM (Tyro3, Axl and Mer) receptor tyrosine kinases are shown to be overexpressed in primary human schwannomas and promote tumour cell proliferation, cell to matrix adhesion and tumour cell survival (Ammoun, Schmid et al. 2012; Ammoun, Provenzano et al. 2013). BMI1 is shown to mediate repression of IGF-IR transcription in prostate cancer (Goel, Chang et al. 2012), and another PcG gene EZH2 is shown to control transcription of AXL receptor kinase in human glioblastoma (Ott, Litzenburger et al. 2012). Therefore it would be interesting to study the relationship between BMI1 and IGF-IR and the members of TAM receptor kinases in context of MB cell proliferation.

Contrary to a previous study (Wiederschain, Chen et al. 2007), we did not observe an impact of BMI1 silencing on apoptosis in DAOY MB cells. Although the reason of this discrepancy is at present unknown, it is possible that the effect on apoptosis could depend on the level of BMI1 knock down achieved. Watson and Eilers et al. have shown the role of certain proto-oncogenes such as c-Jun in regulation of apoptosis of developing neurons including that of cerebellar granule neurons (Watson, Eilers et al. 1998; Eilers, Whitfield et al. 1999). It would be of interest to study if there is any association of c-Jun with BMI1 in apoptotic mechanisms of human MB.

Due to the essential role of BMI1 in maintenance of haematopoietic and neural stem cells (Valk-Lingbeek, Bruggeman et al. 2004), targeted inhibition of BMI1 could potentially cause serious side effects. For similar reasons small molecule drugs that reduce BMI1 protein levels may not be safe in cancer treatment (Cao, Bombard et al. 2011). Glioblastoma tumour stem cells treated with BMPs, in particular BMP-4, showed a reduced tumorigenicity due to reduced proliferation and induction of differentiation (Piccirillo, Reynolds et al. 2006). Proliferation arrest and induction of differentiation following BMP treatment (BMP-2/BMP-4) has been shown also in MBs (Zhao, Ayrault et al. 2008), raising the possibility that small molecules acting as BMP agonists could be implemented in the treatment of patients with MB. Importantly, we show that the impact of BMP treatment on the invasive and proliferative properties of MB cells is most effective when BMI1 is expressed at high levels; raising the possibility that BMI1 could be used as a biomarker to identify groups of patients who can benefit from a treatment with BMP agonists.

MB, in particular those of SHH Group are thought to arise from GNPs and cerebellar neural stem cells (Goodrich, Milenkovic et al. 1997; Sutter, Shakhova et al. 2010).

The cell of origin of Group 4 MB is not well understood. Our data raise the possibility that these MB may also originate from GNPs but may have lost SHH dependency during their oncogenic transformation pathway. Alternatively, BMI1-mediated repression of BMP could be a molecular feature of MB overexpressing BMI1 independently of the molecular group they belong to.

Genetically engineered mouse (GEM) models are a valuable tool for deciphering the molecular and cellular mechanisms of human diseases including cancer, and they can be useful preclinical models for testing targeted drug treatments (Wu, Northcott et al. 2011). GEM model with Shh pathway aberrations have been extensively developed (Lau, Schmidt et al. 2012) while models of non-SHH tumours are rare. It would be important to validate the potential use of BMP agonists in GEM models of MBs overexpressing BMI1. An example of such a GEM model with BMI1 overexpression is NeuroD2:SmoA1 model, which expresses the constitutively active mutant of *Smoothened*, SmoA1 in cerebellar GNPs, and it is known to yield MB at 94% penetrance at an average age of 2 months (Hatton, Villavicencio et al. 2008). A further development of this model, the Math1-Cre:SmoM2, have been shown to develop MB an earlier age and at full penetrance with 100% tumour rate (Schuller, Heine et al. 2008). Importantly, the incidence of tumours arising from GNPs expressing oncogenic Smo is known to drop dramatically in Bmi1-/- background (Michael, Westerman et al. 2008). It would therefore be interesting to study BMP pathway activation in these mice to further validate our findings in a genetically engineered model. Furthermore, the response to BMP treatment could be studied in cells isolated from these tumours to test their effects in a pre-clinical model. However, recent evidences suggest that BMI1 expression is enriched in non-SHH (and non-WNT) human MBs, especially in Group 4 tumours, hence a SHH MB model

may not represent the best choice. As the molecular classification and sub-classification of MBs is advancing rapidly, we feel that validation of our current findings in a subgroup specific manner would enhance the translational value of our study.

Furthermore it would be interesting to carry out a genome wide screening to elucidate more comprehensively the molecular mechanisms underpinning the phenotype observed upon BMI1 downregulation in primary MB cells of Group 4.

In the context of the current project, we have established conditions to stably knock down BMI1 with lentiviral mediated shRNA technique in primary MB cells, including those of Group 4. To assess direct and indirect effects on transcription of targets and to obtain an in-depth view of the transcriptome, including potentially novel transcripts, effects on splicing and very sensitive assessment of transcriptional levels, we plan to take advantage of the RNA-Seq techniques. Whole genome analysis of small RNA, including miRNA will also be carried out, as their crosstalk with PcG genes is well established in both normal and neoplastic cells (Cao, Mani et al. 2011). It would be interesting to focus in particular on genes and pathways that can extend our understanding of the phenotype observed such as for example, ECM interaction/cell adhesion/BMP pathway.

Understanding the diverse molecular mechanisms underpinning the heterogeneity of MB is the essential first step toward the design of novel more tailored therapies for this disease. BMI1 plays an essential role in the pathogenesis of MB, particularly those of Group 4. A comprehensive analysis of the direct and indirect effects on transcription of target genes downstream of BMI1 is essential to better understand the molecular basis of this highly aggressive subgroup of MB. The results obtained

from this study have the potential not only to benefit the scientific community but also to significantly contribute to improve the diagnosis, disease stratification and treatment of patients with MB.

REFERENCES

Abacioglu, U., O. Uzel, et al. (2002). "Medulloblastoma in adults: treatment results and prognostic factors." Int J Radiat Oncol Biol Phys **54**(3): 855-860.

Adamson, D. C., Q. Shi, et al. (2010). "OTX2 is critical for the maintenance and progression of Shh-independent medulloblastomas." Cancer Res **70**(1): 181-191.

Adesina, A. M., J. Nalbantoglu, et al. (1994). "p53 gene mutation and mdm2 gene amplification are uncommon in medulloblastoma." Cancer Res **54**(21): 5649-5651.

Akasaka, T., M. Kanno, et al. (1996). "A role for mel-18, a Polycomb group-related vertebrate gene, during theanteroposterior specification of the axial skeleton." Development **122**(5): 1513-1522.

Al-Halabi, H., A. Nantel, et al. (2011). "Preponderance of sonic hedgehog pathway activation characterizes adult medulloblastoma." Acta Neuropathol **121**(2): 229-239.

Albright, A. L., J. H. Wisoff, et al. (1996). "Effects of medulloblastoma resections on outcome in children: a report from the Children's Cancer Group." Neurosurgery **38**(2): 265-271.

Alder, J., K. J. Lee, et al. (1999). "Generation of cerebellar granule neurons in vivo by transplantation of BMP-treated neural progenitor cells." Nat Neurosci **2**(6): 535-540.

Aldosari, N., S. H. Bigner, et al. (2002). "MYCC and MYCN oncogene amplification in medulloblastoma. A fluorescence in situ hybridization study on paraffin sections from the Children's Oncology Group." Arch Pathol Lab Med **126**(5): 540-544.

Alkema, M. J., N. M. van der Lugt, et al. (1995). "Transformation of axial skeleton due to overexpression of bmi-1 in transgenic mice." Nature **374**(6524): 724-727.

Altman J, B. S. (1997). Development of the cerebellar system: in relation to its evolution, structure, and function., CRC press, Inc.

Alvarez-Rodriguez, R., M. Barzi, et al. (2007). "Bone morphogenetic protein 2 opposes Shh-mediated proliferation in cerebellar granule cells through a TIEG-1-based regulation of Nmyc." J Biol Chem **282**(51): 37170-37180.

Ammoun, S., L. Provenzano, et al. (2013). "Axl/Gas6/NFkappaB signalling in schwannoma pathological proliferation, adhesion and survival." Oncogene.

Ammoun, S., M. C. Schmid, et al. (2012). "The role of insulin-like growth factors signaling in merlin-deficient human schwannomas." Glia **60**(11): 1721-1733.

Angley, C., M. Kumar, et al. (2003). "Signaling by bone morphogenetic proteins and Smad1 modulates the postnatal differentiation of cerebellar cells." J Neurosci **23**(1): 260-268.

Arihiro, K. and K. Inai (2001). "Expression of CD31, Met/hepatocyte growth factor receptor and bone morphogenetic protein in bone metastasis of osteosarcoma." Pathol Int **51**(2): 100-106.

Arras, M., P. Autenried, et al. (2001). "Optimization of intraperitoneal injection anesthesia in mice: drugs, dosages, adverse effects, and anesthesia depth." Comp Med **51**(5): 443-456.

Avet-Loiseau, H., A. M. Venuat, et al. (1999). "Comparative genomic hybridization detects many recurrent imbalances in central nervous system primitive neuroectodermal tumours in children." Br J Cancer **79**(11-12): 1843-1847.

Ayan, I., R. Kebudi, et al. (1997). "Microscopic local leptomeningeal invasion at diagnosis of medulloblastoma." International Journal of Radiation Oncology Biology Physics **39**(2): 461-466.

Ayrault, O., H. Zhao, et al. (2010). "Atoh1 inhibits neuronal differentiation and collaborates with Gli1 to generate medulloblastoma-initiating cells." Cancer Res **70**(13): 5618-5627.

Badiali, M., A. Pession, et al. (1991). "N-myc and c-myc oncogenes amplification in medulloblastomas. Evidence of particularly aggressive behavior of a tumor with c-myc amplification." Tumori **77**(2): 118-121.

Bailey, C. C., A. Gnekow, et al. (1995). "Prospective randomised trial of chemotherapy given before radiotherapy in childhood medulloblastoma. International Society of Paediatric Oncology (SIOP) and the (German) Society of Paediatric Oncology (GPO): SIOP II." Med Pediatr Oncol **25**(3): 166-178.

Bailey, J. M., P. K. Singh, et al. (2007). "Cancer metastasis facilitated by developmental pathways: Sonic hedgehog, Notch, and bone morphogenic proteins." J Cell Biochem **102**(4): 829-839.

Bailey, P. and H. Cushing (1925). "Medulloblastoma Cerebelli: A common type of midcerebellar glioma of childhood." Arch Neurol Psychiatry(14): 192-224.

Bale, S. J., R. T. Falk, et al. (1998). "Patching together the genetics of Gorlin syndrome." J Cutan Med Surg **3**(1): 31-34.

Batra, S. K., R. E. McLendon, et al. (1995). "Prognostic implications of chromosome 17p deletions in human medulloblastomas." J Neurooncol **24**(1): 39-45.

Behesti, H., H. Bhagat, et al. (2013). "Bmi1 overexpression in the cerebellar granule cell lineage of mice affects cell proliferation and survival without initiating medulloblastoma formation." Dis Model Mech **6**(1): 49-63.

Behesti, H. and S. Marino (2009). "Cerebellar granule cells: insights into proliferation, differentiation, and role in medulloblastoma pathogenesis." Int J Biochem Cell Biol **41**(3): 435-445.

Ben-Arie, N., H. J. Bellen, et al. (1997). "Math1 is essential for genesis of cerebellar granule neurons." Nature **390**(6656): 169-172.

Biegel, J. A., C. D. Burk, et al. (1992). "Evidence for a 17p tumor related locus distinct from p53 in pediatric primitive neuroectodermal tumors." Cancer Res **52**(12): 3391-3395.

Bigner, S. H., J. Mark, et al. (1988). "Structural chromosomal abnormalities in human medulloblastoma." Cancer Genet Cytogenet **30**(1): 91-101.

Blaess, S., D. Graus-Porta, et al. (2004). "Beta1-integrins are critical for cerebellar granule cell precursor proliferation." J Neurosci **24**(13): 3402-3412.

Bouffet, E., J. L. Bernard, et al. (1992). "M4 protocol for cerebellar medulloblastoma: supratentorial radiotherapy may not be avoided." Int J Radiat Oncol Biol Phys **24**(1): 79-85.

Bourdeaut, F., C. Miquel, et al. (2013). "Rubinstein-Taybi syndrome predisposing to non-WNT, non-SHH, group 3 medulloblastoma." Pediatr Blood Cancer.

Bourgouin, P. M., D. Tampieri, et al. (1992). "CT and MR imaging findings in adults with cerebellar medulloblastoma: comparison with findings in children." AJR Am J Roentgenol **159**(3): 609-612.

Boyer, L. A., K. Plath, et al. (2006). "Polycomb complexes repress developmental regulators in murine embryonic stem cells." Nature **441**(7091): 349-353.

Bracken, A. P., N. Dietrich, et al. (2006). "Genome-wide mapping of Polycomb target genes unravels their roles in cell fate transitions." Genes Dev **20**(9): 1123-1136.

Brown, H. G., J. L. Kepner, et al. (2000). ""Large cell/anaplastic" medulloblastomas: a Pediatric Oncology Group Study." J Neuropathol Exp Neurol **59**(10): 857-865.

Brown, W. D., C. J. Tavare, et al. (1995). "The applicability of Collins' Law to childhood brain tumors and its usefulness as a predictor of survival." Neurosurgery **36**(6): 1093-1096.

Bruggeman, S. W., D. Hulsman, et al. (2007). "Bmi1 controls tumor development in an Ink4a/Arf-independent manner in a mouse model for glioma." Cancer Cell **12**(4): 328-341.

Bruggeman, S. W., M. E. Valk-Lingbeek, et al. (2005). "Ink4a and Arf differentially affect cell proliferation and neural stem cell self-renewal in Bmi1-deficient mice." Genes Dev **19**(12): 1438-1443.

Brugieres, L., G. Pierron, et al. (2010). "Incomplete penetrance of the predisposition to medulloblastoma associated with germ-line SUFU mutations." J Med Genet **47**(2): 142-144.

Brummelkamp, T. R., R. Bernards, et al. (2002). "A system for stable expression of short interfering RNAs in mammalian cells." Science **296**(5567): 550-553.

Bunin, G. R., R. R. Kuijten, et al. (1993). "Relation between maternal diet and subsequent primitive neuroectodermal brain tumors in young children." N Engl J Med **329**(8): 536-541.

Burger, P. C., F. C. Grahmann, et al. (1987). "Differentiation in the medulloblastoma. A histological and immunohistochemical study." Acta Neuropathol **73**(2): 115-123.

Burger, P. C. and B. Scheithauer (1994). Tumours of the Central Nervuos System. Washington.

Cao, L., J. Bombard, et al. (2011). "BMI1 as a novel target for drug discovery in cancer." J Cell Biochem **112**(10): 2729-2741.

Cao, Q., R. S. Mani, et al. (2011). "Coordinated regulation of polycomb group complexes through microRNAs in cancer." Cancer Cell **20**(2): 187-199.

Carrie, C., J. Grill, et al. (2009). "Online quality control, hyperfractionated radiotherapy alone and reduced boost volume for standard risk medulloblastoma: long-term results of MSFOP 98." J Clin Oncol **27**(11): 1879-1883.

Carrie, C., C. Lasset, et al. (1994). "Multivariate analysis of prognostic factors in adult patients with medulloblastoma. Retrospective study of 156 patients." Cancer **74**(8): 2352-2360.

Castellino, R. C., B. G. Barwick, et al. (2010). "Heterozygosity for Pten promotes tumorigenesis in a mouse model of medulloblastoma." PLoS One **5**(5): e10849.

CCRG. (2010, 2010). "National Registry of Childhood Tumours " Retrieved 21 October, 2013, from http://www.ccrg.ox.ac.uk/.

Chan, A. W., N. J. Tarbell, et al. (2000). "Adult medulloblastoma: prognostic factors and patterns of relapse." Neurosurgery **47**(3): 623-631; discussion 631-622.

Chang, C. H., E. M. Housepian, et al. (1969). "An operative staging system and a megavoltage radiotherapeutic technic for cerebellar medulloblastomas." Radiology **93**(6): 1351-1359.

Chang, K., K. Marran, et al. (2013). "Packaging shRNA Retroviruses." Cold Spring Harb Protoc **2013**(8).

Chen, D., M. Zhao, et al. (2004). "Bone morphogenetic proteins." Growth Factors **22**(4): 233-241.

Chen, Y., A. Bhushan, et al. (1997). "Smad8 mediates the signaling of the ALK-2 [corrected] receptor serine kinase." Proc Natl Acad Sci U S A **94**(24): 12938-12943.

Chi, S. N., S. L. Gardner, et al. (2004). "Feasibility and response to induction chemotherapy intensified with high-dose methotrexate for young children with newly diagnosed high-risk disseminated medulloblastoma." J Clin Oncol **22**(24): 4881-4887.

Chiba, T., S. Miyagi, et al. (2008). "The polycomb gene product BMI1 contributes to the maintenance of tumor-initiating side population cells in hepatocellular carcinoma." Cancer Research **68**(19): 7742-7749.

Chizhikov, V. and K. J. Millen (2003). "Development and malformations of the cerebellum in mice." Mol Genet Metab **80**(1-2): 54-65.

Cho, Y. J., A. Tsherniak, et al. (2011). "Integrative genomic analysis of medulloblastoma identifies a molecular subgroup that drives poor clinical outcome." J Clin Oncol **29**(11): 1424-1430.

Ciemerych, M. A., A. M. Kenney, et al. (2002). "Development of mice expressing a single D-type cyclin." Genes Dev **16**(24): 3277-3289.

Clifford, S. C., M. E. Lusher, et al. (2006). "Wnt/Wingless pathway activation and chromosome 6 loss characterize a distinct molecular sub-group of medulloblastomas associated with a favorable prognosis." Cell Cycle **5**(22): 2666-2670.

Cogen, P. H. and J. D. Donahue (1999). Approaches to the posterior fossa in children. Cranial Microsurgery: Approaches and Techniques. L. N. Sekhar and E. de Oliveira. New York, Thieme**:** 399-404.

Colt, J. S. and A. Blair (1998). "Parental occupational exposures and risk of childhood cancer." Environ Health Perspect **106 Suppl 3**: 909-925.

CRUK. (2008-2010). "Childhood cancer incidence statistics." Retrieved 21 October 2013, from http://www.cancerresearchuk.org/cancer-info/cancerstats/childhoodcancer/incidence/#source8.

Dahmane, N. and A. Ruiz i Altaba (1999). "Sonic hedgehog regulates the growth and patterning of the cerebellum." Development **126**(14): 3089-3100.

Davis, F. G., S. Freels, et al. (1998). "Survival rates in patients with primary malignant brain tumors stratified by patient age and tumor histological type: an analysis based on Surveillance, Epidemiology, and End Results (SEER) data, 1973-1991." J Neurosurg **88**(1): 1-10.

de Bont, J. M., R. J. Packer, et al. (2008). "Biological background of pediatric medulloblastoma and ependymoma: a review from a translational research perspective." Neuro Oncol **10**(6): 1040-1060.

de Bouard, S., C. Christov, et al. (2002). "Invasion of human glioma biopsy specimens in cultures of rodent brain slices: a quantitative analysis." J Neurosurg **97**(1): 169-176.

De Bouard, S., J. S. Guillamo, et al. (2003). "Antiangiogenic therapy against experimental glioblastoma using genetically engineered cells producing interferon-alpha, angiostatin, or endostatin." Human Gene Therapy **14**(9): 883-895.

de Haas, T., E. Oussoren, et al. (2006). "OTX1 and OTX2 expression correlates with the clinicopathologic classification of medulloblastomas." J Neuropathol Exp Neurol **65**(2): 176-186.

de Siqueira Santos, S., D. Y. Takahashi, et al. (2013). "A comparative study of statistical methods used to identify dependencies between gene expression signals." Brief Bioinform.

Deckers, M., M. van Dinther, et al. (2006). "The tumor suppressor Smad4 is required for transforming growth factor beta-induced epithelial to mesenchymal transition and bone metastasis of breast cancer cells." Cancer Res **66**(4): 2202-2209.

Derynck, R. and Y. E. Zhang (2003). "Smad-dependent and Smad-independent pathways in TGF-beta family signalling." Nature **425**(6958): 577-584.

Deutsch, M., P. R. Thomas, et al. (1996). "Results of a prospective randomized trial comparing standard dose neuraxis irradiation (3,600 cGy/20) with reduced neuraxis irradiation (2,340 cGy/13) in patients with low-stage medulloblastoma. A Combined Children's Cancer Group-Pediatric Oncology Group Study." Pediatr Neurosurg **24**(4): 167-176; discussion 176-167.

Dhall, G., H. Grodman, et al. (2008). "Outcome of children less than three years old at diagnosis with non-metastatic medulloblastoma treated with chemotherapy on the "Head Start" I and II protocols." Pediatr Blood Cancer **50**(6): 1169-1175.

Dolman, C. L. (1988). "Melanotic medulloblastoma. A case report with immunohistochemical and ultrastructural examination." Acta Neuropathol **76**(5): 528-531.

Dufour, C., A. Beaugrand, et al. (2012). "Metastatic Medulloblastoma in Childhood: Chang's Classification Revisited." Int J Surg Oncol **2012**: 245385.

Duncan, M. K., L. Bordas, et al. (1997). "Expression of the helix-loop-helix genes Id-1 and NSCL-1 during cerebellar development." Dev Dyn **208**(1): 107-114.

Eberhart, C. G. (2012). "Three down and one to go: modeling medulloblastoma subgroups." Cancer Cell **21**(2): 137-138.

Ehebauer, M., P. Hayward, et al. (2006). "Notch signaling pathway." Sci STKE **2006**(364): cm7.

Eilers, A., J. Whitfield, et al. (1999). "c-Jun and Bax: regulators of programmed cell death in developing neurons." Biochem Soc Trans **27**(6): 790-797.

Ellison, D. (2002). "Classifying the medulloblastoma: insights from morphology and molecular genetics." Neuropathol Appl Neurobiol **28**(4): 257-282.

Ellison, D., S. Love, et al. (2004). Neuropathology, Elsevier.

Ellison, D. W. (2010). "Childhood medulloblastoma: novel approaches to the classification of a heterogeneous disease." Acta Neuropathol **120**(3): 305-316.

Ellison, D. W., J. Dalton, et al. (2011). "Medulloblastoma: clinicopathological correlates of SHH, WNT, and non-SHH/WNT molecular subgroups." Acta Neuropathol **121**(3): 381-396.

Ellison, D. W., M. Kocak, et al. (2011). "Definition of disease-risk stratification groups in childhood medulloblastoma using combined clinical, pathologic, and molecular variables." J Clin Oncol **29**(11): 1400-1407.

Ellison, D. W., O. E. Onilude, et al. (2005). "beta-Catenin status predicts a favorable outcome in childhood medulloblastoma: the United Kingdom Children's Cancer Study Group Brain Tumour Committee." J Clin Oncol **23**(31): 7951-7957.

Fan, X., I. Mikolaenko, et al. (2004). "Notch1 and notch2 have opposite effects on embryonal brain tumor growth." Cancer Res **64**(21): 7787-7793.

Farioli-Vecchioli, S., I. Cina, et al. (2012). "Tis21 Knock-Out Enhances the Frequency of Medulloblastoma in Patched1 Heterozygous Mice by Inhibiting the Cxcl3-Dependent Migration of Cerebellar Neurons." Journal of Neuroscience **32**(44): 15547-15564.

Fattet, S., C. Haberler, et al. (2009). "Beta-catenin status in paediatric medulloblastomas: correlation of immunohistochemical expression with mutational status, genetic profiles, and clinical characteristics." J Pathol **218**(1): 86-94.

Ferretti, E., L. Di Marcotullio, et al. (2006). "Alternative splicing of the ErbB-4 cytoplasmic domain and its regulation by hedgehog signaling identify distinct medulloblastoma subsets." Oncogene **25**(55): 7267-7273.

Fiaschetti, G., D. Castelletti, et al. (2011). "Bone morphogenetic protein-7 is a MYC target with prosurvival functions in childhood medulloblastoma." Oncogene.

Flora, A., T. J. Klisch, et al. (2009). "Deletion of Atoh1 disrupts Sonic Hedgehog signaling in the developing cerebellum and prevents medulloblastoma." Science **326**(5958): 1424-1427.

Frank, A. J., R. Hernan, et al. (2004). "The TP53-ARF tumor suppressor pathway is frequently disrupted in large/cell anaplastic medulloblastoma." Brain Res Mol Brain Res **121**(1-2): 137-140.

Froeling, F. E., T. A. Mirza, et al. (2009). "Organotypic culture model of pancreatic cancer demonstrates that stromal cells modulate E-cadherin, beta-catenin, and Ezrin expression in tumor cells." Am J Pathol **175**(2): 636-648.

Gajjar, A., M. Chintagumpala, et al. (2006). "Risk-adapted craniospinal radiotherapy followed by high-dose chemotherapy and stem-cell rescue in children with newly diagnosed medulloblastoma (St Jude Medulloblastoma-96): long-term results from a prospective, multicentre trial." Lancet Oncol **7**(10): 813-820.

Garel, C., C. Fallet-Bianco, et al. (2011). "The fetal cerebellum: development and common malformations." J Child Neurol **26**(12): 1483-1492.

Gargiulo, G., M. Cesaroni, et al. (2013). "In vivo RNAi screen for BMI1 targets identifies TGF-beta/BMP-ER stress pathways as key regulators of neural- and malignant glioma-stem cell homeostasis." Cancer Cell **23**(5): 660-676.

Geyer, J. R., R. Sposto, et al. (2005). "Multiagent chemotherapy and deferred radiotherapy in infants with malignant brain tumors: a report from the Children's Cancer Group." J Clin Oncol **23**(30): 7621-7631.

Ghulam Muhammad, A. K., M. Candolfi, et al. (2009). "Antiglioma immunological memory in response to conditional cytotoxic/immune-stimulatory gene therapy: humoral and cellular immunity lead to tumor regression." Clin Cancer Res **15**(19): 6113-6127.

Giangaspero, F., S. H. Binger, et al. (2000). Medulloblastoma. Tumours of the Nervous System. C. W. Kleihues P. Lyon, France, IARC 129-137.

Giangaspero, F., G. Perilongo, et al. (1999). "Medulloblastoma with extensive nodularity: a variant with favorable prognosis." J Neurosurg **91**(6): 971-977.

Giangaspero, F., L. Rigobello, et al. (1992). "Large-cell medulloblastomas. A distinct variant with highly aggressive behavior." Am J Surg Pathol **16**(7): 687-693.

Giannini, C., J. N. Sarkaria, et al. (2005). "Patient tumor EGFR and PDGFRA gene amplifications retained in an invasive intracranial xenograft model of glioblastoma multiforme." Neuro-Oncology **7**(2): 164-176.

Gibson, P., Y. Tong, et al. (2010). "Subtypes of medulloblastoma have distinct developmental origins." Nature **468**(7327): 1095-1099.

Gilbertson, R. J. and D. W. Ellison (2008). "The origins of medulloblastoma subtypes." Annu Rev Pathol **3**: 341-365.

Giordana, M. T., P. Schiffer, et al. (1999). "Epidemiology of adult medulloblastoma." Int J Cancer **80**(5): 689-692.

Glinsky, G. V., O. Berezovska, et al. (2005). "Microarray analysis identifies a death-from-cancer signature predicting therapy failure in patients with multiple types of cancer." J Clin Invest **115**(6): 1503-1521.

Godlewski, J., M. O. Nowicki, et al. (2008). "Targeting of the Bmi-1 Oncogene/Stem Cell Renewal Factor by MicroRNA-128 Inhibits Glioma Proliferation and Self-Renewal." Cancer Research **68**(22): 9125-9130.

Goel, H. L., C. Chang, et al. (2012). "VEGF/neuropilin-2 regulation of Bmi-1 and consequent repression of IGF-IR define a novel mechanism of aggressive prostate cancer." Cancer Discov **2**(10): 906-921.

Goldowitz, D. and K. Hamre (1998). "The cells and molecules that make a cerebellum." Trends Neurosci **21**(9): 375-382.

Goodrich, L. V., L. Milenkovic, et al. (1997). "Altered neural cell fates and medulloblastoma in mouse patched mutants." Science **277**(5329): 1109-1113.

Griffin, C. A., A. L. Hawkins, et al. (1988). "Chromosome abnormalities in pediatric brain tumors." Cancer Res **48**(1): 175-180.

Grill, J., C. Sainte-Rose, et al. (2005). "Treatment of medulloblastoma with postoperative chemotherapy alone: an SFOP prospective trial in young children." Lancet Oncol **6**(8): 573-580.

Grimmer, M. R. and W. A. Weiss (2008). "BMPs oppose Math1 in cerebellar development and in medulloblastoma." Genes Dev **22**(6): 693-699.

Guillamo, J. S., S. de Bouard, et al. (2009). "Molecular mechanisms underlying effects of epidermal growth factor receptor inhibition on invasion, proliferation, and angiogenesis in experimental glioma." Clin Cancer Res **15**(11): 3697-3704.

Guo, B. H., Y. Feng, et al. (2011). "Bmi-1 promotes invasion and metastasis, and its elevated expression is correlated with an advanced stage of breast cancer." Mol Cancer **10**(1): 10.

Guo, X. and X. F. Wang (2009). "Signaling cross-talk between TGF-beta/BMP and other pathways." Cell Res **19**(1): 71-88.

Hall, A. C., F. R. Lucas, et al. (2000). "Axonal remodeling and synaptic differentiation in the cerebellum is regulated by WNT-7a signaling." Cell **100**(5): 525-535.

Hallahan, A. R., J. I. Pritchard, et al. (2003). "BMP-2 mediates retinoid-induced apoptosis in medulloblastoma cells through a paracrine effect." Nat Med **9**(8): 1033-1038.

Hallonet, M. E. and N. M. Le Douarin (1993). "Tracing neuroepithelial cells of the mesencephalic and metencephalic alar plates during cerebellar ontogeny in quail-chick chimaeras." Eur J Neurosci **5**(9): 1145-1155.

Hamilton, S. R., B. Liu, et al. (1995). "The molecular basis of Turcot's syndrome." N Engl J Med **332**(13): 839-847.

Hatten, M. E. (1999). "Central nervous system neuronal migration." Annu Rev Neurosci **22**: 511-539.

Hatten, M. E. and N. Heintz (1995). "Mechanisms of neural patterning and specification in the developing cerebellum." Annu Rev Neurosci **18**: 385-408.

Hatten, M. E. and M. F. Roussel (2011). "Development and cancer of the cerebellum." Trends Neurosci **34**(3): 134-142.

Hatton, B. A., E. H. Villavicencio, et al. (2008). "The Smo/Smo model: hedgehog-induced medulloblastoma with 90% incidence and leptomeningeal spread." Cancer Res **68**(6): 1768-1776.

Haupt, Y., W. S. Alexander, et al. (1991). "Novel zinc finger gene implicated as myc collaborator by retrovirally accelerated lymphomagenesis in E mu-myc transgenic mice." Cell **65**(5): 753-763.

He, X. M., C. J. Wikstrand, et al. (1991). "Differentiation characteristics of newly established medulloblastoma cell lines (D384 Med, D425 Med, and D458 Med) and their transplantable xenografts." Lab Invest **64**(6): 833-843.

Herrup, K. and B. Kuemerle (1997). "The compartmentalization of the cerebellum." Annu Rev Neurosci **20**: 61-90.

Hershatter, B. W., E. C. Halperin, et al. (1986). "Medulloblastoma: the Duke University Medical Center experience." Int J Radiat Oncol Biol Phys **12**(10): 1771-1777.

Hoenerhoff, M. J., I. Chu, et al. (2009). "BMI1 cooperates with H-RAS to induce an aggressive breast cancer phenotype with brain metastases." Oncogene **28**(34): 3022-3032.

Hogan, B. L. (1996). "Bone morphogenetic proteins: multifunctional regulators of vertebrate development." Genes Dev **10**(13): 1580-1594.

Hong, X., F. Jiang, et al. (2007). "Decrease of endogenous vascular endothelial growth factor may not affect glioma cell proliferation and invasion." J Exp Ther Oncol **6**(3): 219-229.

Hoodless, P. A., T. Haerry, et al. (1996). "MADR1, a MAD-related protein that functions in BMP2 signaling pathways." Cell **85**(4): 489-500.

Horiuchi, D., N. E. Huskey, et al. (2012). "Chemical-genetic analysis of cyclin dependent kinase 2 function reveals an important role in cellular transformation by multiple oncogenic pathways." Proc Natl Acad Sci U S A **109**(17): E1019-1027.

Hsieh, P. C., C. T. Wu, et al. (2008). "The clinical experience of medulloblastoma treatment and the significance of time sequence for development of leptomeningeal metastasis." Childs Nerv Syst **24**(12): 1463-1467.

Hu, J. and A. S. Verkman (2006). "Increased migration and metastatic potential of tumor cells expressing aquaporin water channels." FASEB J **20**(11): 1892-1894.

Huang, H., B. M. Mahler-Araujo, et al. (2000). "APC mutations in sporadic medulloblastomas." Am J Pathol **156**(2): 433-437.

Huang, H., R. Reis, et al. (1999). "Identification in human brain tumors of DNA sequences specific for SV40 large T antigen." Brain Pathol **9**(1): 33-42.

Hubert, T., S. Grimal, et al. (2009). "Collagens in the developing and diseased nervous system." Cell Mol Life Sci **66**(7): 1223-1238.

Huelsken, J. and J. Behrens (2002). "The Wnt signalling pathway." J Cell Sci **115**(Pt 21): 3977-3978.

Hugo, H., M. L. Ackland, et al. (2007). "Epithelial--mesenchymal and mesenchymal--epithelial transitions in carcinoma progression." J Cell Physiol **213**(2): 374-383.

Iantosca, M. R., C. E. McPherson, et al. (1999). "Bone morphogenetic proteins-2 and -4 attenuate apoptosis in a cerebellar primitive neuroectodermal tumor cell line." J Neurosci Res **56**(3): 248-258.

Ikushima, H. and K. Miyazono (2010). "TGFbeta signalling: a complex web in cancer progression." Nat Rev Cancer **10**(6): 415-424.

Ille, F. and L. Sommer (2005). "Wnt signaling: multiple functions in neural development." Cell Mol Life Sci **62**(10): 1100-1108.

Inda, M. M., J. Mercapide, et al. (2004). "PTEN and DMBT1 homozygous deletion and expression in medulloblastomas and supratentorial primitive neuroectodermal tumors." Oncol Rep **12**(6): 1341-1347.

Jacobs, J. J., K. Kieboom, et al. (1999). "The oncogene and Polycomb-group gene bmi-1 regulates cell proliferation and senescence through the ink4a locus." Nature **397**(6715): 164-168.

Jacobs, J. J., B. Scheijen, et al. (1999). "Bmi-1 collaborates with c-Myc in tumorigenesis by inhibiting c-Myc-induced apoptosis via INK4a/ARF." Genes Dev **13**(20): 2678-2690.

Jacobsen, P. F., D. J. Jenkyn, et al. (1985). "Establishment of a human medulloblastoma cell line and its heterotransplantation into nude mice." J Neuropathol Exp Neurol **44**(5): 472-485.

Jakacki, R. I., P. C. Burger, et al. (2012). "Outcome of children with metastatic medulloblastoma treated with carboplatin during craniospinal radiotherapy: a Children's Oncology Group Phase I/II study." J Clin Oncol **30**(21): 2648-2653.

Jallo, G. I. and M. A. (2012, March 2012). "Medulloblastoma Clinical Presentation." Retrieved 22 October, 2013, from http://emedicine.medscape.com/article/1181219-clinical.

Jiang, L., J. Li, et al. (2009). "Bmi-1, stem cells and cancer." Acta Biochim Biophys Sin (Shanghai) **41**(7): 527-534.

Jiang, L., J. Wu, et al. (2012). "Bmi-1 promotes the aggressiveness of glioma via activating the NF-kappaB/MMP-9 signaling pathway." BMC Cancer **12**: 406.

Jones, D. T., N. Jager, et al. (2012). "Dissecting the genomic complexity underlying medulloblastoma." Nature **488**(7409): 100-105.

Jones, T. A., B. W. Ogunkolade, et al. (2011). "Widespread expression of BORIS/CTCFL in normal and cancer cells." PLoS One **6**(7): e22399.

Jung, S., H. W. Kim, et al. (2002). "Brain tumor invasion model system using organotypic brain-slice culture as an alternative to in vivo model." J Cancer Res Clin Oncol **128**(9): 469-476.

Kadin, M. E., L. J. Rubinstein, et al. (1970). "Neonatal cerebellar medulloblastoma originating from the fetal external granular layer." J Neuropathol Exp Neurol **29**(4): 583-600.

Kang, M. H., J. S. Kim, et al. (2010). "BMP2 accelerates the motility and invasiveness of gastric cancer cells via activation of the phosphatidylinositol 3-kinase (PI3K)/Akt pathway." Exp Cell Res **316**(1): 24-37.

Kang, M. K., R. H. Kim, et al. (2007). "Elevated Bmi-1 expression is associated with dysplastic cell transformation during oral carcinogenesis and is required for cancer cell replication and survival." Br J Cancer **96**(1): 126-133.

Kang, Y., P. M. Siegel, et al. (2003). "A multigenic program mediating breast cancer metastasis to bone." Cancer Cell **3**(6): 537-549.

Katagiri, T., M. Imada, et al. (2002). "Identification of a BMP-responsive element in Id1, the gene for inhibition of myogenesis." Genes Cells **7**(9): 949-960.

Katsuno, Y., A. Hanyu, et al. (2008). "Bone morphogenetic protein signaling enhances invasion and bone metastasis of breast cancer cells through Smad pathway." Oncogene **27**(49): 6322-6333.

Kawamura, C., M. Kizaki, et al. (2000). "Bone morphogenetic protein-2 induces apoptosis in human myeloma cells with modulation of STAT3." Blood **96**(6): 2005-2011.

Kenney, A. M., M. D. Cole, et al. (2003). "Nmyc upregulation by sonic hedgehog signaling promotes proliferation in developing cerebellar granule neuron precursors." Development **130**(1): 15-28.

Kho, A. T., Q. Zhao, et al. (2004). "Conserved mechanisms across development and tumorigenesis revealed by a mouse development perspective of human cancers." Genes Dev **18**(6): 629-640.

Kim, W. Y. and N. E. Sharpless (2006). "The regulation of INK4/ARF in cancer and aging." Cell **127**(2): 265-275.

Kirmizis, A., S. M. Bartley, et al. (2003). "Identification of the polycomb group protein SU(Z)12 as a potential molecular target for human cancer therapy." Mol Cancer Ther **2**(1): 113-121.

Kleer, C. G., Q. Cao, et al. (2003). "EZH2 is a marker of aggressive breast cancer and promotes neoplastic transformation of breast epithelial cells." Proc Natl Acad Sci U S A **100**(20): 11606-11611.

Kleinman, H. K., M. L. McGarvey, et al. (1982). "Isolation and characterization of type IV procollagen, laminin, and heparan sulfate proteoglycan from the EHS sarcoma." Biochemistry **21**(24): 6188-6193.

Knoepfler, P. S., P. F. Cheng, et al. (2002). "N-myc is essential during neurogenesis for the rapid expansion of progenitor cell populations and the inhibition of neuronal differentiation." Genes Dev **16**(20): 2699-2712.

Kononen, J., L. Bubendorf, et al. (1998). "Tissue microarrays for high-throughput molecular profiling of tumor specimens." Nat Med **4**(7): 844-847.

Kool, M., A. Korshunov, et al. (2012). "Molecular subgroups of medulloblastoma: an international meta-analysis of transcriptome, genetic aberrations, and clinical data of WNT, SHH, Group 3, and Group 4 medulloblastomas." Acta Neuropathol **123**(4): 473-484.

Kool, M., J. Koster, et al. (2008). "Integrated genomics identifies five medulloblastoma subtypes with distinct genetic profiles, pathway signatures and clinicopathological features." PLoS One **3**(8): e3088.

Korchynskyi, O. and P. ten Dijke (2002). "Identification and functional characterization of distinct critically important bone morphogenetic protein-specific response elements in the Id1 promoter." J Biol Chem **277**(7): 4883-4891.

Korshunov, A., M. Remke, et al. (2010). "Adult and pediatric medulloblastomas are genetically distinct and require different algorithms for molecular risk stratification." J Clin Oncol **28**(18): 3054-3060.

Kortmann, R. D., J. Kuhl, et al. (2000). "Postoperative neoadjuvant chemotherapy before radiotherapy as compared to immediate radiotherapy followed by maintenance chemotherapy in the treatment of medulloblastoma in childhood: results of the German prospective randomized trial HIT '91." Int J Radiat Oncol Biol Phys **46**(2): 269-279.

Koscielny, G., V. Le Texier, et al. (2009). "ASTD: The Alternative Splicing and Transcript Diversity database." Genomics **93**(3): 213-220.

Koziol, L. F., D. Budding, et al. (2013). "Consensus Paper: The Cerebellum's Role in Movement and Cognition." Cerebellum.

Krynska, B., L. Del Valle, et al. (1999). "Detection of human neurotropic JC virus DNA sequence and expression of the viral oncogenic protein in pediatric medulloblastomas." Proc Natl Acad Sci U S A **96**(20): 11519-11524.

Kuhl, J., H. L. Muller, et al. (1998). "Preradiation chemotherapy of children and young adults with malignant brain tumors: results of the German pilot trial HIT'88/'89." Klinische Padiatrie **210**(4): 227-233.

Kurayoshi, M., N. Oue, et al. (2006). "Expression of Wnt-5a is correlated with aggressiveness of gastric cancer by stimulating cell migration and invasion." Cancer Res **66**(21): 10439-10448.

Laerum, O. D. (1997). "Local spread of malignant neuroepithelial tumors." Acta Neurochirurgica **139**(6): 515-522.

Landberg, T. G., M. L. Lindgren, et al. (1980). "Improvements in the radiotherapy of medulloblastoma, 1946-1975." Cancer **45**(4): 670-678.

Langenfeld, E. M., S. E. Calvano, et al. (2003). "The mature bone morphogenetic protein-2 is aberrantly expressed in non-small cell lung carcinomas and stimulates tumor growth of A549 cells." Carcinogenesis **24**(9): 1445-1454.

Lasorella, A., T. Uo, et al. (2001). "Id proteins at the cross-road of development and cancer." Oncogene **20**(58): 8326-8333.

Lau, J., C. Schmidt, et al. (2012). "Matching mice to malignancy: molecular subgroups and models of medulloblastoma." Childs Nerv Syst **28**(4): 521-532.

Lee, A., J. D. Kessler, et al. (2005). "Isolation of neural stem cells from the postnatal cerebellum." Nat Neurosci **8**(6): 723-729.

Lee, M., J. H. Wisoff, et al. (1994). "Management of hydrocephalus in children with medulloblastoma: prognostic factors for shunting." Pediatr Neurosurg **20**(4): 240-247.

Lee, T. I., R. G. Jenner, et al. (2006). "Control of developmental regulators by Polycomb in human embryonic stem cells." Cell **125**(2): 301-313.

Leivonen, S. K. and V. M. Kahari (2007). "Transforming growth factor-beta signaling in cancer invasion and metastasis." Int J Cancer **121**(10): 2119-2124.

Lemire RJ, L. J., Leech RW, Alvord Economides, A. N., Ed. (1975). Normal and abnormal development of the human nervous system., Harper & Row.

Leung, C., M. Lingbeek, et al. (2004). "Bmi1 is essential for cerebellar development and is overexpressed in human medulloblastomas." Nature **428**(6980): 337-341.

Li, X. N., Q. Shu, et al. (2007). "Differential expression of survivin splice isoforms in medulloblastomas." Neuropathol Appl Neurobiol 33(1): 67-76.

Liang, Y., M. Diehn, et al. (2008). "Type I collagen is overexpressed in medulloblastoma as a component of tumor microenvironment." J Neurooncol 86(2): 133-141.

Liu, B., D. Tian, et al. (2010). "Effect of bone morphogenetic protein 4 in the human brain glioma cell line U251." Cell Biochem Biophys 58(2): 91-96.

Lo Muzio, L. (2008). "Nevoid basal cell carcinoma syndrome (Gorlin syndrome)." Orphanet J Rare Dis 3: 32.

Locklin, R. M., B. L. Riggs, et al. (2001). "Assessment of gene regulation by bone morphogenetic protein 2 in human marrow stromal cells using gene array technology." J Bone Miner Res 16(12): 2192-2204.

Lopez-Rovira, T., E. Chalaux, et al. (2002). "Direct binding of Smad1 and Smad4 to two distinct motifs mediates bone morphogenetic protein-specific transcriptional activation of Id1 gene." J Biol Chem 277(5): 3176-3185.

Lossi, L., S. Alasia, et al. (2009). "Cell death and proliferation in acute slices and organotypic cultures of mammalian CNS." Progress in Neurobiology 88(4): 221-245.

Louis, D. N., H. Ohgaki, et al. (2007). "The 2007 WHO classification of tumours of the central nervous system." Acta Neuropathol 114(2): 97-109.

Louvi, A. and S. Artavanis-Tsakonas (2006). "Notch signalling in vertebrate neural development." Nat Rev Neurosci 7(2): 93-102.

Lowe, S. W. and C. J. Sherr (2003). "Tumor suppression by Ink4a-Arf: progress and puzzles." Curr Opin Genet Dev 13(1): 77-83.

Lu, Z. and J. Kipnis (2010). "Thrombospondin 1--a key astrocyte-derived neurogenic factor." Faseb J.

Luyten, F. P., N. S. Cunningham, et al. (1989). "Purification and partial amino acid sequence of osteogenin, a protein initiating bone differentiation." J Biol Chem 264(23): 13377-13380.

MacDonald, T. J., K. M. Brown, et al. (2001). "Expression profiling of medulloblastoma: PDGFRA and the RAS/MAPK pathway as therapeutic targets for metastatic disease." Nat Genet 29(2): 143-152.

MacDonald, T. J., B. R. Rood, et al. (2003). "Advances in the diagnosis, molecular genetics, and treatment of pediatric embryonal CNS tumors." Oncologist 8(2): 174-186.

MacDonald, T. J., P. Tabrizi, et al. (1998). "Detection of brain tumor invasion and micrometastasis in vivo by expression of enhanced green fluorescent protein." Neurosurgery 43(6): 1437-1442.

Machold, R. P., D. J. Kittell, et al. (2007). "Antagonism between Notch and bone morphogenetic protein receptor signaling regulates neurogenesis in the cerebellar rhombic lip." Neural Dev 2: 5.

Maeda, H., C. Fujimoto, et al. (2003). "Quantitative real-time PCR using TaqMan and SYBR Green for Actinobacillus actinomycetemcomitans, Porphyromonas gingivalis, Prevotella intermedia, tetQ gene and total bacteria." FEMS Immunol Med Microbiol 39(1): 81-86.

Manoranjan, B., X. Wang, et al. (2013). "FoxG1 interacts with Bmi1 to regulate self-renewal and tumorigenicity of medulloblastoma stem cells." Stem Cells 31(7): 1266-1277.

Marino, S. (2005). "Medulloblastoma: developmental mechanisms out of control." Trends Mol Med 11(1): 17-22.

Marino, S., M. Vooijs, et al. (2000). "Induction of medulloblastomas in p53-null mutant mice by somatic inactivation of Rb in the external granular layer cells of the cerebellum." Genes Dev 14(8): 994-1004.

Massague, J. and Y. G. Chen (2000). "Controlling TGF-beta signaling." Genes Dev 14(6): 627-644.

McDonnell, T. J., N. S. Chari, et al. (2008). "Biomarker expression patterns that correlate with high grade features in treatment naive, organ-confined prostate cancer." BMC Med Genomics 1: 1.

McKean-Cowdin, R., P. Razavi, et al. (2013). "Trends in childhood brain tumor incidence, 1973-2009." J Neurooncol.

McLendon, R. E., H. S. Friedman, et al. (1999). "Diagnostic markers in paediatric medulloblastoma: a Paediatric Oncology Group Study." Histopathology **34**(2): 154-162.

McManamy, C. S., J. M. Lamont, et al. (2003). "Morphophenotypic variation predicts clinical behavior in childhood non-desmoplastic medulloblastomas." J Neuropathol Exp Neurol **62**(6): 627-632.

McManamy, C. S., J. Pears, et al. (2007). "Nodule formation and desmoplasia in medulloblastomas-defining the nodular/desmoplastic variant and its biological behavior." Brain Pathol **17**(2): 151-164.

McManus, M. T. and P. A. Sharp (2002). "Gene silencing in mammals by small interfering RNAs." Nat Rev Genet **3**(10): 737-747.

McNeil, D. E., T. R. Cote, et al. (2002). "Incidence and trends in pediatric malignancies medulloblastoma/primitive neuroectodermal tumor: a SEER update. Surveillance Epidemiology and End Results." Med Pediatr Oncol **39**(3): 190-194.

Meng, F. and G. Wu (2012). "The rejuvenated scenario of epithelial-mesenchymal transition (EMT) and cancer metastasis." Cancer Metastasis Rev **31**(3-4): 455-467.

Meng, S., M. Luo, et al. (2010). "Identification and characterization of Bmi-1-responding element within the human p16 promoter." J Biol Chem **285**(43): 33219-33229.

Meng, W., P. Kallinteri, et al. (2007). "Evaluation of poly (glycerol-adipate) nanoparticle uptake in an in vitro 3-D brain tumor co-culture model." Exp Biol Med (Maywood) **232**(8): 1100-1108.

Menghi, F., T. S. Jacques, et al. (2011). "Genome-wide analysis of alternative splicing in medulloblastoma identifies splicing patterns characteristic of normal cerebellar development." Cancer Res **71**(6): 2045-2055.

Metcalfe, C. and M. Bienz (2011). "Inhibition of GSK3 by Wnt signalling--two contrasting models." J Cell Sci **124**(Pt 21): 3537-3544.

Michael, L. E., B. A. Westerman, et al. (2008). "Bmi1 is required for Hedgehog pathway-driven medulloblastoma expansion." Neoplasia **10**(12): 1343-1349, 1345p following 1349.

Millen, K. J., W. Wurst, et al. (1994). "Abnormal embryonic cerebellar development and patterning of postnatal foliation in two mouse Engrailed-2 mutants." Development **120**(3): 695-706.

Miller, W. H., Jr. (1998). "The emerging role of retinoids and retinoic acid metabolism blocking agents in the treatment of cancer." Cancer **83**(8): 1471-1482.

Miyata, T., T. Maeda, et al. (1999). "NeuroD is required for differentiation of the granule cells in the cerebellum and hippocampus." Genes Dev **13**(13): 1647-1652.

Miyazawa, K., T. Himi, et al. (2000). "A role for p27/Kip1 in the control of cerebellar granule cell precursor proliferation." J Neurosci **20**(15): 5756-5763.

Miyazono, K., S. Maeda, et al. (2005). "BMP receptor signaling: transcriptional targets, regulation of signals, and signaling cross-talk." Cytokine Growth Factor Rev **16**(3): 251-263.

Miyazono, K., P. ten Dijke, et al. (2000). "TGF-beta signaling by Smad proteins." Adv Immunol **75**: 115-157.

Mizugishi, K., J. Aruga, et al. (2001). "Molecular properties of Zic proteins as transcriptional regulators and their relationship to GLI proteins." J Biol Chem **276**(3): 2180-2188.

Mollenhauer, J., S. Wiemann, et al. (1997). "DMBT1, a new member of the SRCR superfamily, on chromosome 10q25.3-26.1 is deleted in malignant brain tumours." Nat Genet **17**(1): 32-39.

Molofsky, A. V., R. Pardal, et al. (2003). "Bmi-1 dependence distinguishes neural stem cell self-renewal from progenitor proliferation." Nature **425**(6961): 962-967.

Montagnani, S., C. Castaldo, et al. (2000). "Extra cellular matrix features in human meninges." Ital J Anat Embryol **105**(3): 167-177.

Moskovits, N., A. Kalinkovich, et al. (2006). "p53 Attenuates cancer cell migration and invasion through repression of SDF-1/CXCL12 expression in stromal fibroblasts." Cancer Res **66**(22): 10671-10676.

Moustakas, A., K. Pardali, et al. (2002). "Mechanisms of TGF-beta signaling in regulation of cell growth and differentiation." Immunol Lett **82**(1-2): 85-91.

Mumert, M., A. Dubuc, et al. (2012). "Functional Genomics Identifies Drivers of Medulloblastoma Dissemination." Cancer Research **72**(19): 4944-4953.

Nakao, A., T. Imamura, et al. (1997). "TGF-beta receptor-mediated signalling through Smad2, Smad3 and Smad4." EMBO J **16**(17): 5353-5362.

NCI. (2013, 01 August 2013). "Treatment of Newly Diagnosed Childhood Medulloblastoma." Childhood Central Nervous System Embryonal Tumors Treatment (PDQ®) Retrieved 23 October, 2013, from http://www.cancer.gov/cancertopics/pdq/treatment/childCNSembryonal/healthprofessional/page5#Reference5.36.

Nishimura, R., Y. Kato, et al. (1998). "Smad5 and DPC4 are key molecules in mediating BMP-2-induced osteoblastic differentiation of the pluripotent mesenchymal precursor cell line C2C12." J Biol Chem **273**(4): 1872-1879.

Northcott, P. A., L. A. Fernandez, et al. (2009). "The miR-17/92 polycistron is up-regulated in sonic hedgehog-driven medulloblastomas and induced by N-myc in sonic hedgehog-treated cerebellar neural precursors." Cancer Res **69**(8): 3249-3255.

Northcott, P. A., T. Hielscher, et al. (2011). "Pediatric and adult sonic hedgehog medulloblastomas are clinically and molecularly distinct." Acta Neuropathol **122**(2): 231-240.

Northcott, P. A., A. Korshunov, et al. (2011). "Medulloblastoma comprises four distinct molecular variants." J Clin Oncol **29**(11): 1408-1414.

Northcott, P. A., Y. Nakahara, et al. (2009). "Multiple recurrent genetic events converge on control of histone lysine methylation in medulloblastoma." Nat Genet **41**(4): 465-472.

O'Carroll, D., S. Erhardt, et al. (2001). "The polycomb-group gene Ezh2 is required for early mouse development." Mol Cell Biol **21**(13): 4330-4336.

O'Shea, K. S., L. H. Liu, et al. (1990). "Role of the extracellular matrix protein thrombospondin in the early development of the mouse embryo." J Cell Biol **111**(6 Pt 1): 2713-2723.

Ogata, T., J. M. Wozney, et al. (1993). "Bone morphogenetic protein 2 transiently enhances expression of a gene, Id (inhibitor of differentiation), encoding a helix-loop-helix molecule in osteoblast-like cells." Proc Natl Acad Sci U S A **90**(19): 9219-9222.

Ott, M., U. M. Litzenburger, et al. (2012). "Promotion of glioblastoma cell motility by enhancer of zeste homolog 2 (EZH2) is mediated by AXL receptor kinase." PLoS One **7**(10): e47663.

Otte, A. P. and T. H. Kwaks (2003). "Gene repression by Polycomb group protein complexes: a distinct complex for every occasion?" Curr Opin Genet Dev **13**(5): 448-454.

Ozen, O., B. Krebs, et al. (2004). "Expression of matrix metalloproteinases and their inhibitors in medulloblastomas and their prognostic relevance." Clin Cancer Res **10**(14): 4746-4753.

Packer, R. J. (1999). "Brain tumors in children." Archives of Neurology **56**(4): 421-425.

Packer, R. J., P. Cogen, et al. (1999). "Medulloblastoma: clinical and biologic aspects." Neuro Oncol **1**(3): 232-250.

Packer, R. J., B. R. Rood, et al. (2003). "Medulloblastoma: present concepts of stratification into risk groups." Pediatr Neurosurg **39**(2): 60-67.

Palfi, S., K. R. Swanson, et al. (2004). "Correlation of in vitro infiltration with glioma histological type in organotypic brain slices." British Journal of Cancer **91**(4): 745-752.

Paraf, F., S. Jothy, et al. (1997). "Brain tumor-polyposis syndrome: two genetic diseases?" J Clin Oncol **15**(7): 2744-2758.

Park, I. K., D. Qian, et al. (2003). "Bmi-1 is required for maintenance of adult self-renewing haematopoietic stem cells." Nature **423**(6937): 302-305.

Park, T. S., H. J. Hoffman, et al. (1983). "Medulloblastoma: clinical presentation and management. Experience at the hospital for sick children, toronto, 1950-1980." J Neurosurg **58**(4): 543-552.

Parker, K. and G. J. Pilkington (2005). "Morphological, immunocytochemical and flow cytometric in vitro characterisation of a surface-adherent medulloblastoma." Anticancer Res **25**(6B): 3855-3863.

Parsons, D. W., M. Li, et al. (2011). "The genetic landscape of the childhood cancer medulloblastoma." Science **331**(6016): 435-439.

Patankar, T. F., D. Mitra, et al. (2005). "Dilatation of the Virchow-Robin space is a sensitive indicator of cerebral microvascular disease: Study in elderly patients with dementia." American Journal of Neuroradiology **26**(6): 1512-1520.

Pear, W. S., G. P. Nolan, et al. (1993). "Production of high-titer helper-free retroviruses by transient transfection." Proc Natl Acad Sci U S A **90**(18): 8392-8396.

Pearl, G. S. and Y. Takei (1981). "Cerebellar "neuroblastoma": nosology as it relates to medulloblastoma." Cancer **47**(4): 772-779.

Pei, Y., C. E. Moore, et al. (2012). "An animal model of MYC-driven medulloblastoma." Cancer Cell **21**(2): 155-167.

Peng, Y., Q. Kang, et al. (2004). "Inhibitor of DNA binding/differentiation helix-loop-helix proteins mediate bone morphogenetic protein-induced osteoblast differentiation of mesenchymal stem cells." J Biol Chem **279**(31): 32941-32949.

Pfister, S., M. Remke, et al. (2009). "Outcome prediction in pediatric medulloblastoma based on DNA copy-number aberrations of chromosomes 6q and 17q and the MYC and MYCN loci." J Clin Oncol **27**(10): 1627-1636.

Piccirillo, S. G., B. A. Reynolds, et al. (2006). "Bone morphogenetic proteins inhibit the tumorigenic potential of human brain tumour-initiating cells." Nature **444**(7120): 761-765.

Pilkington, G. J. (1994). "Tumor-Cell Migration in the Central-Nervous-System." Brain Pathology **4**(2): 157-166.

Polkinghorn, W. R. and N. J. Tarbell (2007). "Medulloblastoma: tumorigenesis, current clinical paradigm, and efforts to improve risk stratification." Nat Clin Pract Oncol **4**(5): 295-304.

Pollack, I. F., P. Polinko, et al. (1995). "Mutism and pseudobulbar symptoms after resection of posterior fossa tumors in children: incidence and pathophysiology." Neurosurgery **37**(5): 885-893.

Pomeroy, S. L., P. Tamayo, et al. (2002). "Prediction of central nervous system embryonal tumour outcome based on gene expression." Nature **415**(6870): 436-442.

Prados, M. D., R. E. Warnick, et al. (1995). "Medulloblastoma in adults." Int J Radiat Oncol Biol Phys **32**(4): 1145-1152.

Raetzman, L. T. and R. E. Siegel (1999). "Immature granule neurons from cerebella of different ages exhibit distinct developmental potentials." J Neurobiol **38**(4): 559-570.

Raida, M., J. H. Clement, et al. (2005). "Expression of bone morphogenetic protein 2 in breast cancer cells inhibits hypoxic cell death." Int J Oncol **26**(6): 1465-1470.

Ramaekers, V. T., G. Heimann, et al. (1997). "Genetic disorders and cerebellar structural abnormalities in childhood." Brain **120 (Pt 10)**: 1739-1751.

Rankin, J., J. Short, et al. (2013). "Medulloblastoma in a patient with the PTPN11 p.Thr468Met mutation." Am J Med Genet A **161A**(8): 2027-2029.

Rasheed, B. K., T. T. Stenzel, et al. (1997). "PTEN gene mutations are seen in high-grade but not in low-grade gliomas." Cancer Res **57**(19): 4187-4190.

Reardon, D. A., E. Michalkiewicz, et al. (1997). "Extensive genomic abnormalities in childhood medulloblastoma by comparative genomic hybridization." Cancer Res **57**(18): 4042-4047.

Reddi, A. H. (1981). "Cell biology and biochemistry of endochondral bone development." Coll Relat Res **1**(2): 209-226.

Reddy, A. T. and R. J. Packer (1999). "Medulloblastoma." Curr Opin Neurol **12**(6): 681-685.

Remke, M., T. Hielscher, et al. (2011). "FSTL5 is a marker of poor prognosis in non-WNT/non-SHH medulloblastoma." J Clin Oncol **29**(29): 3852-3861.

Remke, M., T. Hielscher, et al. (2011). "Adult medulloblastoma comprises three major molecular variants." J Clin Oncol **29**(19): 2717-2723.

Richie, E. R., A. Schumacher, et al. (2002). "The Polycomb-group gene eed regulates thymocyte differentiation and suppresses the development of carcinogen-induced T-cell lymphomas." Oncogene **21**(2): 299-306.

Riffaud, L., S. Saikali, et al. (2009). "Survival and prognostic factors in a series of adults with medulloblastomas Clinical article." Journal of Neurosurgery **111**(3): 478-487.

Ringrose, L. and R. Paro (2004). "Epigenetic regulation of cellular memory by the Polycomb and Trithorax group proteins." Annu Rev Genet **38**: 413-443.

Rios, I., R. Alvarez-Rodriguez, et al. (2004). "Bmp2 antagonizes sonic hedgehog-mediated proliferation of cerebellar granule neurones through Smad5 signalling." Development **131**(13): 3159-3168.

Ris, M. D., R. Packer, et al. (2001). "Intellectual outcome after reduced-dose radiation therapy plus adjuvant chemotherapy for medulloblastoma: a Children's Cancer Group study." J Clin Oncol **19**(15): 3470-3476.

Rodini, C. O., D. E. Suzuki, et al. (2010). "Aberrant signaling pathways in medulloblastomas A stem cell connection." Arquivos De Neuro-Psiquiatria **68**(6): 947-952.

Rodriguez-Leon, J., R. Merino, et al. (1999). "Retinoic acid regulates programmed cell death through BMP signalling." Nat Cell Biol **1**(2): 125-126.

Rodriguez, L. G., X. Wu, et al. (2005). "Wound-healing assay." Methods Mol Biol **294**: 23-29.

Roger E McLendon, M. K. R., Darell D Bigner, Ed. (2006). Russel & Rubinstein's Pathology of Tumours of the Nervous System, CRC Press.

Rorke, L. B. (1994). "Experimental production of primitive neuroectodermal tumors and its relevance to human neuro-oncology." Am J Pathol **144**(3): 444-448.

Rosenzweig, B. L., T. Imamura, et al. (1995). "Cloning and characterization of a human type II receptor for bone morphogenetic proteins." Proc Natl Acad Sci U S A **92**(17): 7632-7636.

Rossi, A., V. Caracciolo, et al. (2008). "Medulloblastoma: from molecular pathology to therapy." Clin Cancer Res **14**(4): 971-976.

Roussel, M. F. and M. E. Hatten (2011). "Cerebellum development and medulloblastoma." Curr Top Dev Biol **94**: 235-282.

Rubinson, D. A., C. P. Dillon, et al. (2003). "A lentivirus-based system to functionally silence genes in primary mammalian cells, stem cells and transgenic mice by RNA interference." Nat Genet **33**(3): 401-406.

Rudin, C. M., C. L. Hann, et al. (2009). "Treatment of medulloblastoma with hedgehog pathway inhibitor GDC-0449." N Engl J Med **361**(12): 1173-1178.

Rutkowski, S., K. von Hoff, et al. (2010). "Survival and prognostic factors of early childhood medulloblastoma: an international meta-analysis." J Clin Oncol **28**(33): 4961-4968.

Ruzinova, M. B. and R. Benezra (2003). "Id proteins in development, cell cycle and cancer." Trends Cell Biol **13**(8): 410-418.

Salinas, P. C., C. Fletcher, et al. (1994). "Maintenance of Wnt-3 expression in Purkinje cells of the mouse cerebellum depends on interactions with granule cells." Development **120**(5): 1277-1286.

Salinas, P. C. and Y. Zou (2008). "Wnt signaling in neural circuit assembly." Annu Rev Neurosci **31**: 339-358.

Sarkozy, A., M. C. Digilio, et al. (2008). "Leopard syndrome." Orphanet J Rare Dis **3**: 13.

Sato, T., A. L. Joyner, et al. (2004). "How does Fgf signaling from the isthmic organizer induce midbrain and cerebellum development?" Dev Growth Differ **46**(6): 487-494.

Scheurlen, W. G., G. C. Schwabe, et al. (1998). "Molecular analysis of childhood primitive neuroectodermal tumors defines markers associated with poor outcome." J Clin Oncol **16**(7): 2478-2485.

Schuller, U., V. M. Heine, et al. (2008). "Acquisition of granule neuron precursor identity is a critical determinant of progenitor cell competence to form Shh-induced medulloblastoma." Cancer Cell **14**(2): 123-134.

Schuller, U. and D. H. Rowitch (2007). "Beta-catenin function is required for cerebellar morphogenesis." Brain Res **1140**: 161-169.

Schumacher, A., C. Faust, et al. (1996). "Positional cloning of a global regulator of anterior-posterior patterning in mice." Nature **384**(6610): 648.

Schutze, N. (2004). "siRNA technology." Mol Cell Endocrinol **213**(2): 115-119.

Shakhova, O., C. Leung, et al. (2006). "Lack of Rb and p53 delays cerebellar development and predisposes to large cell anaplastic medulloblastoma through amplification of N-Myc and Ptch2." Cancer Res **66**(10): 5190-5200.

Sharpless, N. E. and R. A. DePinho (1999). "The INK4A/ARF locus and its two gene products." Curr Opin Genet Dev **9**(1): 22-30.

Shepherd, T. G., B. L. Theriault, et al. (2008). "Autocrine BMP4 signalling regulates ID3 proto-oncogene expression in human ovarian cancer cells." Gene **414**(1-2): 95-105.

Shu, Q., K. K. Wong, et al. (2008). "Direct orthotopic transplantation of fresh surgical specimen preserves CD133+ tumor cells in clinically relevant mouse models of medulloblastoma and glioma." Stem Cells **26**(6): 1414-1424.

Sikkema, A. H., W. F. A. den Dunnen, et al. (2012). "EphB2 activity plays a pivotal role in pediatric medulloblastoma cell adhesion and invasion." Neuro-Oncology **14**(9): 1125-1135.

Simpson, K. J., L. M. Selfors, et al. (2008). "Identification of genes that regulate epithelial cell migration using an siRNA screening approach." Nat Cell Biol **10**(9): 1027-1038.

Smith, T. W. and R. I. Davidson (1984). "Medullomyoblastoma. A histologic, immunohistochemical, and ultrastructural study." Cancer **54**(2): 323-332.

Smith, W. C. and R. M. Harland (1992). "Expression cloning of noggin, a new dorsalizing factor localized to the Spemann organizer in Xenopus embryos." Cell **70**(5): 829-840.

Smoll, N. R. (2012). "Relative survival of childhood and adult medulloblastomas and primitive neuroectodermal tumors (PNETs)." Cancer **118**(5): 1313-1322.

Snyder, A. D., A. N. Dulin-Smith, et al. (2013). "Expression pattern of id proteins in medulloblastoma." Pathol Oncol Res **19**(3): 437-446.

Soda, H., E. Raymond, et al. (1998). "Antiproliferative effects of recombinant human bone morphogenetic protein-2 on human tumor colony-forming units." Anticancer Drugs **9**(4): 327-331.

Solecki, D. J., X. L. Liu, et al. (2001). "Activated Notch2 signaling inhibits differentiation of cerebellar granule neuron precursors by maintaining proliferation." Neuron **31**(4): 557-568.

Song, L. B., J. Li, et al. (2009). "The polycomb group protein Bmi-1 represses the tumor suppressor PTEN and induces epithelial-mesenchymal transition in human nasopharyngeal epithelial cells." J Clin Invest **119**(12): 3626-3636.

Sparmann, A. and M. van Lohuizen (2006). "Polycomb silencers control cell fate, development and cancer." Nat Rev Cancer **6**(11): 846-856.

Spiller, S. E., S. H. Ditzler, et al. (2008). "Response of preclinical medulloblastoma models to combination therapy with 13-cis retinoic acid and suberoylanilide hydroxamic acid (SAHA)." J Neurooncol **87**(2): 133-141.

Spiller, S. E., A. C. Ravanpay, et al. (2006). "Suberoylanilide hydroxamic acid is effective in preclinical studies of medulloblastoma." J Neurooncol **79**(3): 259-270.

St Clair, W. H., J. A. Adams, et al. (2004). "Advantage of protons compared to conventional X-ray or IMRT in the treatment of a pediatric patient with medulloblastoma." Int J Radiat Oncol Biol Phys **58**(3): 727-734.

Stevens, M. C., A. H. Cameron, et al. (1991). "Descriptive epidemiology of primary central nervous system tumours in children: a population-based study." Clin Oncol (R Coll Radiol) **3**(6): 323-329.

Stoeckli, E. T. (2010). "Neural circuit formation in the cerebellum is controlled by cell adhesion molecules of the Contactin family." Cell Adh Migr **4**(4): 523-526.

Stoppini, L., P. A. Buchs, et al. (1991). "A Simple Method for Organotypic Cultures of Nervous-Tissue." Journal of Neuroscience Methods **37**(2): 173-182.

Strober, W. (2001). Trypan Blue Exclusion Test of Cell Viability. Current Protocols in Immunology**:** A.3B.1 - A.3B.2.

Su, I. H., M. W. Dobenecker, et al. (2005). "Polycomb group protein ezh2 controls actin polymerization and cell signaling." Cell **121**(3): 425-436.

Sun, X. H., N. G. Copeland, et al. (1991). "Id proteins Id1 and Id2 selectively inhibit DNA binding by one class of helix-loop-helix proteins." Mol Cell Biol **11**(11): 5603-5611.

Sutter, R., O. Shakhova, et al. (2010). "Cerebellar stem cells act as medulloblastoma-initiating cells in a mouse model and a neural stem cell signature characterizes a subset of human medulloblastomas." Oncogene **29**(12): 1845-1856.

Tabori, U., B. Baskin, et al. (2010). "Universal poor survival in children with medulloblastoma harboring somatic TP53 mutations." J Clin Oncol **28**(8): 1345-1350.

Tabori, U., L. Sung, et al. (2005). "Medulloblastoma in the second decade of life: a specific group with respect to toxicity and management: a Canadian Pediatric Brain Tumor Consortium Study." Cancer **103**(9): 1874-1880.

Tabori, U., L. Sung, et al. (2006). "Distinctive clinical course and pattern of relapse in adolescents with medulloblastoma." Int J Radiat Oncol Biol Phys **64**(2): 402-407.

Taelman, V. F., R. Dobrowolski, et al. (2010). "Wnt signaling requires sequestration of glycogen synthase kinase 3 inside multivesicular endosomes." Cell **143**(7): 1136-1148.

Tagawa, M., T. Sakamoto, et al. (1990). "Expression of novel DNA-binding protein with zinc finger structure in various tumor cells." J Biol Chem **265**(32): 20021-20026.

Tan, M. H. and T. M. Chu (1985). "Characterization of the Tumorigenic and Metastatic Properties of a Human Pancreatic Tumor-Cell Line (Aspc-1) Implanted Orthotopically into Nude-Mice." Tumour Biology **6**(1): 89-98.

Tanaka, M., A. Tomita, et al. (1994). "Observation of the highly organized development of granule cells in rat cerebellar organotypic cultures." Brain Res **641**(2): 319-327.

Taylor, M. D., L. Liu, et al. (2002). "Mutations in SUFU predispose to medulloblastoma." Nat Genet **31**(3): 306-310.

Taylor, M. D., P. A. Northcott, et al. (2012). "Molecular subgroups of medulloblastoma: the current consensus." Acta Neuropathol **123**(4): 465-472.

Taylor, R. E., C. C. Bailey, et al. (2004). "Impact of radiotherapy parameters on outcome in the International Society of Paediatric Oncology/United Kingdom Children's Cancer Study Group PNET-3 study of preradiotherapy chemotherapy for M0-M1 medulloblastoma." Int J Radiat Oncol Biol Phys **58**(4): 1184-1193.

ten Dijke, P., H. Yamashita, et al. (1994). "Identification of type I receptors for osteogenic protein-1 and bone morphogenetic protein-4." J Biol Chem **269**(25): 16985-16988.

ten Donkelaar, H. J., M. Lammens, et al. (2003). "Development and developmental disorders of the human cerebellum." J Neurol **250**(9): 1025-1036.

Thawani, J. P., A. C. Wang, et al. (2010). "Bone morphogenetic proteins and cancer: review of the literature." Neurosurgery **66**(2): 233-246; discussion 246.

Thompson, M. C., C. Fuller, et al. (2006). "Genomics identifies medulloblastoma subgroups that are enriched for specific genetic alterations." J Clin Oncol **24**(12): 1924-1931.

Timmann, D. and I. Daum (2007). "Cerebellar contributions to cognitive functions: a progress report after two decades of research." Cerebellum **6**(3): 159-162.

Tomlinson, F. H., R. B. Jenkins, et al. (1994). "Aggressive medulloblastoma with high-level N-myc amplification." Mayo Clin Proc **69**(4): 359-365.

Tortori-Donati, P., M. P. Fondelli, et al. (1996). "Medulloblastoma in children: CT and MRI findings." Neuroradiology **38**(4): 352-359.

Turcot, J., J. P. Despres, et al. (1959). "Malignant tumors of the central nervous system associated with familial polyposis of the colon: report of two cases." Dis Colon Rectum **2**: 465-468.

Urist, M. R. (1965). "Bone: formation by autoinduction." Science **150**(3698): 893-899.

Valk-Lingbeek, M. E., S. W. Bruggeman, et al. (2004). "Stem cells and cancer; the polycomb connection." Cell **118**(4): 409-418.

van der Lugt, N. M., J. Domen, et al. (1994). "Posterior transformation, neurological abnormalities, and severe hematopoietic defects in mice with a targeted deletion of the bmi-1 proto-oncogene." Genes Dev **8**(7): 757-769.

van Kemenade, F. J., F. M. Raaphorst, et al. (2001). "Coexpression of BMI-1 and EZH2 polycomb-group proteins is associated with cycling cells and degree of malignancy in B-cell non-Hodgkin lymphoma." Blood **97**(12): 3896-3901.

van Lohuizen, M., M. Frasch, et al. (1991). "Sequence similarity between the mammalian bmi-1 proto-oncogene and the Drosophila regulatory genes Psc and Su(z)2." Nature **353**(6342): 353-355.

van Lohuizen, M., S. Verbeek, et al. (1991). "Identification of cooperating oncogenes in E mu-myc transgenic mice by provirus tagging." Cell **65**(5): 737-752.

Varambally, S., S. M. Dhanasekaran, et al. (2002). "The polycomb group protein EZH2 is involved in progression of prostate cancer." Nature **419**(6907): 624-629.

Varga, A. C. and J. L. Wrana (2005). "The disparate role of BMP in stem cell biology." Oncogene **24**(37): 5713-5721.

Verlooy, J., V. Mosseri, et al. (2006). "Treatment of high risk medulloblastomas in children above the age of 3 years: a SFOP study." Eur J Cancer **42**(17): 3004-3014.

Vermes, I., C. Haanen, et al. (1995). "A novel assay for apoptosis. Flow cytometric detection of phosphatidylserine expression on early apoptotic cells using fluorescein labelled Annexin V." J Immunol Methods **184**(1): 39-51.

Villeneuve, J., P. Tremblay, et al. (2005). "Tumor necrosis factor reduces brain tumor growth by enhancing macrophage recruitment and microcyst formation." Cancer Res **65**(9): 3928-3936.

Vince, G. H., C. Herbold, et al. (2001). "Medulloblastoma displays distinct regional matrix metalloprotease expression." J Neurooncol **53**(2): 99-106.

von Bueren, A. O., K. von Hoff, et al. (2011). "Treatment of young children with localized medulloblastoma by chemotherapy alone: results of the prospective, multicenter trial HIT 2000 confirming the prognostic impact of histology." Neuro Oncol **13**(6): 669-679.

von Hoff, K., W. Hartmann, et al. (2010). "Large cell/anaplastic medulloblastoma: outcome according to myc status, histopathological, and clinical risk factors." Pediatr Blood Cancer **54**(3): 369-376.

Vrijens, K., W. W. Lin, et al. (2013). "Identification of Small Molecule Activators of BMP Signaling." PLoS One **8**(3).

Wan, W. H., M. B. Fortuna, et al. (1987). "A rapid and efficient method for testing immunohistochemical reactivity of monoclonal antibodies against multiple tissue samples simultaneously." J Immunol Methods **103**(1): 121-129.

Wang, H., L. Wang, et al. (2004). "Role of histone H2A ubiquitination in Polycomb silencing." Nature **431**(7010): 873-878.

Wang, J., X. J. Wang, et al. (2008). "Partial Biological Characterization of Cancer Stem-like Cell Line (WJ(2)) of Human Glioblastoma Multiforme." Cellular and Molecular Neurobiology **28**(7): 991-1003.

Wang, V. Y. and H. Y. Zoghbi (2001). "Genetic regulation of cerebellar development." Nat Rev Neurosci **2**(7): 484-491.

Wang, X., C. Venugopal, et al. (2012). "Sonic hedgehog regulates Bmi1 in human medulloblastoma brain tumor-initiating cells." Oncogene **31**(2): 187-199.

Wang, Z., S. S. Kim, et al. (2012). "E-cadherin upregulates expression of matrix macromolecules aggrecan and collagen II in the intervertebral disc cells through activation of the intracellular BMP-Smad1/5 pathway." J Orthop Res **30**(11): 1746-1752.

Watson, A., A. Eilers, et al. (1998). "Phosphorylation of c-Jun is necessary for apoptosis induced by survival signal withdrawal in cerebellar granule neurons." J Neurosci **18**(2): 751-762.

Wechsler-Reya, R. and M. P. Scott (2001). "The developmental biology of brain tumors." Annu Rev Neurosci **24**: 385-428.

Wechsler-Reya, R. J. and M. P. Scott (1999). "Control of neuronal precursor proliferation in the cerebellum by Sonic Hedgehog." Neuron **22**(1): 103-114.

Weggen, S., T. A. Bayer, et al. (2000). "Low frequency of SV40, JC and BK polyomavirus sequences in human medulloblastomas, meningiomas and ependymomas." Brain Pathol **10**(1): 85-92.

Wiederschain, D., L. Chen, et al. (2007). "Contribution of polycomb homologues Bmi-1 and Mel-18 to medulloblastoma pathogenesis." Mol Cell Biol **27**(13): 4968-4979.

Wikstrand, C. J., H. S. Friedman, et al. (1991). "Medulloblastoma cell-substrate interaction in vitro." Invasion Metastasis **11**(6): 310-324.

Wingate, R. J. (2001). "The rhombic lip and early cerebellar development." Curr Opin Neurobiol **11**(1): 82-88.

Wixon, S. a. S., KL (1997). Anesthesia and Analgesia in Rodents. Anesthesia and Analgesia in Laboratory Animals. S. W. DJ Kohn, WJ White, GJ Benson, Academic Press.

Wozney, J. M. and V. Rosen (1998). "Bone morphogenetic protein and bone morphogenetic protein gene family in bone formation and repair." Clin Orthop Relat Res(346): 26-37.

Wozney, J. M., V. Rosen, et al. (1988). "Novel regulators of bone formation: molecular clones and activities." Science **242**(4885): 1528-1534.

Wu, X., P. A. Northcott, et al. (2011). "Mouse models of medulloblastoma." Chin J Cancer **30**(7): 442-449.

Wu, X., P. A. Northcott, et al. (2012). "Clonal selection drives genetic divergence of metastatic medulloblastoma." Nature **482**(7386): 529-533.

Yang, J. and R. A. Weinberg (2008). "Epithelial-mesenchymal transition: at the crossroads of development and tumor metastasis." Dev Cell **14**(6): 818-829.

Yang, M. H., D. S. S. Hsu, et al. (2010). "Bmi1 is essential in Twist1-induced epithelial-mesenchymal transition." Nature Cell Biology **12**(10): 982-992.

Yao, X. B., X. X. Wang, et al. (2013). "Silencing Bmi-1 expression by RNA interference suppresses the growth of laryngeal carcinoma cells." Int J Mol Med **31**(5): 1262-1272.

Yauch, R. L., G. J. Dijkgraaf, et al. (2009). "Smoothened mutation confers resistance to a Hedgehog pathway inhibitor in medulloblastoma." Science **326**(5952): 572-574.

Ye, L., J. M. Lewis-Russell, et al. (2007). "Hepatocyte growth factor up-regulates the expression of the bone morphogenetic protein (BMP) receptors, BMPR-IB and BMPR-II, in human prostate cancer cells." Int J Oncol **30**(2): 521-529.

Yilmaz, M. and G. Christofori (2009). "EMT, the cytoskeleton, and cancer cell invasion." Cancer and Metastasis Reviews **28**(1-2): 15-33.

Yin, T., H. Wei, et al. (2011). "Bmi-1 promotes the chemoresistance, invasion and tumorigenesis of pancreatic cancer cells." Chemotherapy **57**(6): 488-496.

Yokota, N., S. Nishizawa, et al. (2002). "Role of Wnt pathway in medulloblastoma oncogenesis." Int J Cancer **101**(2): 198-201.

Yu, J. Y., S. L. DeRuiter, et al. (2002). "RNA interference by expression of short-interfering RNAs and hairpin RNAs in mammalian cells." Proc Natl Acad Sci U S A **99**(9): 6047-6052.

Zahm, S. H. and M. H. Ward (1998). "Pesticides and childhood cancer." Environ Health Perspect **106 Suppl 3**: 893-908.

Zavadil, J. and E. P. Bottinger (2005). "TGF-beta and epithelial-to-mesenchymal transitions." Oncogene **24**(37): 5764-5774.

Zeltzer, P. M., J. M. Boyett, et al. (1999). "Metastasis stage, adjuvant treatment, and residual tumor are prognostic factors for medulloblastoma in children: conclusions from the Children's Cancer Group 921 randomized phase III study." J Clin Oncol **17**(3): 832-845.

Zhang, R. and L. Zhou (1999). "Medulloblastoma." Chin Med J (Engl) **112**(4): 297-301.

Zhang, X., X. Li, et al. (2002). "Experiment and observation on invasion of brain glioma in vivo." Journal of Clinical Neuroscience **9**(6): 668-671.

Zhang, X., A. Santuccione, et al. (2011). "Differentiation of postnatal cerebellar glial progenitors is controlled by Bmi1 through BMP pathway inhibition." Glia **59**(7): 1118-1131.

Zhao, H., O. Ayrault, et al. (2008). "Post-transcriptional down-regulation of Atoh1/Math1 by bone morphogenic proteins suppresses medulloblastoma development." Genes Dev **22**(6): 722-727.

Zhao, X., Z. Liu, et al. (2012). "Global gene expression profiling confirms the molecular fidelity of primary tumor-based orthotopic xenograft mouse models of medulloblastoma." Neuro Oncol **14**(5): 574-583.

Zhou, L., D. Picard, et al. (2010). "Silencing of thrombospondin-1 is critical for myc-induced metastatic phenotypes in medulloblastoma." Cancer Res **70**(20): 8199-8210.

Zimmerman, L. B., J. M. De Jesus-Escobar, et al. (1996). "The Spemann organizer signal noggin binds and inactivates bone morphogenetic protein 4." Cell **86**(4): 599-606.

Zurawel, R. H., C. Allen, et al. (2000). "Analysis of PTCH/SMO/SHH pathway genes in medulloblastoma." Genes Chromosomes Cancer **27**(1): 44-51.

Zurawel, R. H., C. Allen, et al. (2000). "Evidence that haploinsufficiency of Ptch leads to medulloblastoma in mice." Genes Chromosomes Cancer **28**(1): 77-81.

Zurawel, R. H., S. A. Chiappa, et al. (1998). "Sporadic medulloblastomas contain oncogenic beta-catenin mutations." Cancer Res **58**(5): 896-899.